Application of Electrochemical Approach for *in situ* H_2O_2 Generation in Enzyme Catalysis

Vom Promotionsausschuss der
Technischen Universität Hamburg

zur Erlangung des akademischen Grades

Doktor-Ingenieur (Dr.-Ing.)

genehmigte Dissertation (Kumulativ)

von
Giovanni Vallian Sayoga

aus
Tasikmalaya, Indonesien

2025

Examination board

1st examiner : Prof. Dr. Andreas Liese
2nd examiner : Prof. Dr. Anna-Lena Heins
Chairperson : Prof. Dr. Stefan Heinrich

Examination date

02 October 2025

TORE identifiers

DOI: https://doi.org/10.15480/882.15986
Handle: https://hdl.handle.net/11420/57981

Creative Commons License Agreement

Acknowledgement

First and foremost, I would like to express my sincere gratitude to Prof. Andreas Liese for giving me the opportunity to pursue and continue my PhD research in his institute, as well as for his invaluable supervision and unwavering support.

I am also grateful to Prof. Anna-Lena Heins for reviewing my thesis as the second examiner and to Prof. Stefan Heinrich for chairing the examination.

Special thanks go to my project partners, Vici and Hubi, for the successful collaboration throughout the project.

I would like to express my heartfelt appreciation to the wonderful ITB and IBB teams I had the privilege to work with during my PhD. Your support, insightful discussions, and collaborative spirit have been essential to this work.

My sincere thanks to my group leader, Dr. Daniel Ohde, for his continuous guidance and for fostering such a supportive and motivating environment.

A big thank you to my amazing office colleagues—Luca, Leon, and Marlene—for your support, humor, and teamwork, which made every day enjoyable.

I am also especially thankful to Vici for her valuable feedback during the proofreading and correction phases of both the manuscripts and this dissertation.

Finally, I would like to express my deepest gratitude to my family and friends for their constant encouragement. To my wife Quita and my daughter Kimmy—your patience, love, and understanding gave me strength and balance throughout this journey.

Abstract

Hydrogen peroxide (H_2O_2) is an environmentally safe chemical and widely employed as a co-substrate in biocatalytic processes. Among various enzymes that are capable of utilizing H_2O_2 as a co-substrate, the recombinant unspecific peroxygenase from the fungus *Agrocybe aegerita* (r*Aae*UPO) stands out as the favorite due to its stability and versatility. Nevertheless, the technical application and combination of r*Aae*UPO and H_2O_2 in the biotechnological field remains challenging. This is due to the toxicity of H_2O_2 towards biocatalysts and the inactivation of r*Aae*UPO at an elevated concentration of H_2O_2. The precise dosing of H_2O_2 is of great importance, yet very challenging. A number of strategies have been explored to mitigate the deactivation effect of H_2O_2. Thus far, they have been largely deemed unsatisfactory due to the dilution effect or formation of complex by-products. An electrochemical approach represents an attractive method that provides controllable *in situ* generation of H_2O_2. The objective of this dissertation is to develop a fully controllable system for the electrochemical *in situ* generation of H_2O_2, designed as an optimizable platform for H_2O_2-dependent enzymatic reactions and to promote catalyst efficiency. To address these challenges, the All-in-One (AiO) electrode system was employed for the *in situ* generation of H_2O_2. This concept was integrated with the enzymatic hydroxylation, catalyzed by r*Aae*UPO, to establish a bioelectrochemical system (BES). The maximum H_2O_2 productivity and Faradaic efficiency achieved in the AiO electrode system were 0.87 μM min^{-1} cm^{-2} and 60%, respectively. The application of the AiO electrode within the BES yielded promising results, achieving a total turnover number (TTN) of 450,000 mol mol^{-1} and a turnover frequency (TOF) of 7.7 s^{-1}. By incorporating aeration and increasing the number of electrodes, the specific surface area was enhanced, resulting in an increase in both TTN and TOF up to 700,000 mol mol^{-1} and 20.1 s^{-1}, respectively, with a productivity of 1.3 g L^{-1} d^{-1}. Although H_2O_2 productivity was identified as the limiting factor, the system demonstrated considerable potential for optimization through surface modification of the electrode. Moreover, this dissertation compared two modes of *in situ* H_2O_2 electrogeneration: the conventional galvanostatic mode and the H_2O_2-stat mode. The two modes were tested within the gas diffusion electrode system, employing the identical enzymatic reaction. While the galvanostatic mode demonstrated a maximum H_2O_2 productivity of 5.5 μM min^{-1} cm^{-2} and a productivity of 10.5 g L^{-1} d^{-1} at 6.4 mA cm^{-2}, the H_2O_2-stat mode, particularly at a H_2O_2 concentration limit of 0.2 mM, yielded favorable outcomes with a TTN of 655,000 mol mol^{-1}, a TOF of 80.3 s^{-1}, and a productivity of 6.1 g L^{-1} d^{-1}. The successful application of the H_2O_2-stat mode highlights its potential as a more effective alternative to the galvanostatic approach, significantly enhancing the process performance of r*Aae*UPO and advancing the field of enzymatic electrosynthesis.

Kurzfassung

Wasserstoffperoxid (H_2O_2) findet häufig Verwendung als Co-Substrat in biokatalytischen Prozessen. Die rekombinante unspezifische Peroxygenase aus *Agrocybe aegerita* (r*Aae*UPO) weist eine hohe Stabilität sowie Vielseitigkeit auf und erscheint daher vielversprechend für technische Anwendungen in Kombination mit H_2O_2. Allerdings bleibt die technische Anwendung von r*Aae*UPO mit H_2O_2 bislang eine Herausforderung. Die Toxizität von H_2O_2 sowie die Inaktivierung von r*Aae*UPO bei höheren H_2O_2 Konzentrationen stellen wesentliche Herausforderungen dar. Bisherige Strategien zur Minderung dieser Effekte erweisen sich als unzureichend. Ein elektrochemischer Ansatz zur kontrollierten *in situ* Erzeugung von H_2O_2 könnte eine effektive Lösung bieten. Das Ziel dieser Dissertation ist es, ein vollständig kontrollierbares System zur elektrochemischen *in situ* Erzeugung von H_2O_2 zu entwickeln, das als optimierbare Plattform für H_2O_2-abhängige enzymatische Reaktionen konzipiert ist und die Katalysatoreffizienz steigern soll. Um die genannten Herausforderungen zu bewältigen, wurde das All-in-One (AiO) Elektroden-System für die *in situ* Erzeugung von H_2O_2 eingesetzt. Dieses Konzept wurde mit der enzymatischen Hydroxylierung, katalysiert durch die r*Aae*UPO, integriert, um ein bioelektrochemisches System (BES) zu etablieren. Die maximale H_2O_2-Produktivität und Faradaische Effizienz, die im AiO-Elektrodensystem erreicht wurden, betrugen 0,87 μM min^{-1} cm^{-2} und 60%. Der Einsatz der AiO-Elektrode im BES ergab vielversprechende Ergebnisse, mit einer total turnover number (TTN) von 450.000 mol mol^{-1} und einer turnover frequency (TOF) von 7,7 s^{-1}. Durch die Integration der Begasung und die Erhöhung der Anzahl der Elektroden wurde die spezifische Oberfläche vergrößert, was zu einer Steigerung von TTN und TOF auf bis zu 700.000 mol mol^{-1} und 20,1 s^{-1} führte, bei einer Produktivität von 1,3 g L^{-1} d^{-1}. Obwohl die H_2O_2-Produktivität als limitierender Faktor identifiziert wurde, zeigte das System ein beträchtliches Optimierungspotenzial durch Modifikation der Elektrodenoberfläche. Darüber hinaus verglich diese Dissertation zwei Modi der *in situ* H_2O_2-Elektrogenerierung: den konventionellen galvanostatischen Modus und den H_2O_2-stat Modus. Die beiden Modi wurden im Gasdiffusionselektrodensystem getestet, wobei die identische enzymatische Reaktion eingesetzt wurde. Während der galvanostatische Modus eine maximale H_2O_2-Produktivität von 5,5 μM min^{-1} cm^{-2} und eine Produktivität von 10,5 g L^{-1} d^{-1} bei 6,4 mA cm^{-2} aufwies, lieferte der H_2O_2-stat Modus, insbesondere bei einer H_2O_2-Konzentrationsgrenze von 0,2 mM, vorteilhaftere Ergebnisse mit einer TTN von 655.000 mol mol^{-1}, einer TOF von 80,3 s^{-1} und einer Produktivität von 6,1 g L^{-1} d^{-1}. Die erfolgreiche Anwendung des H_2O_2-stat Modus unterstreicht sein Potenzial als effektivere Alternative zum galvanostatischen Ansatz, was die Prozessleistung der r*Aae*UPO erheblich verbessert und das Feld der enzymatische Elektrosynthese voranbringt.

Table of Contents

Abstract i
Kurzfassung ii
Table of Contents iii
Abbreviations v
1. Introduction 1
2. Objective 4
3. Theoretical Background 5
3.1. H_2O_2 Synthesis Methods 5
3.2. *in situ* Generation of H_2O_2 6
3.3. *in situ* Electrosynthesis of H_2O_2 in Bioelectrochemical Systems 11
3.4. Recombinant Unspecific Peroxygenase from the Fungus *Agrocybe aegerita* 14
4. Overview of Publications 17
5. Quantitative and Non-Quantitative Assessments of Enzymatic Electrosynthesis: A Case Study of Parameter Requirements 21
5.1. Quantitative Analysis of Electroenzymatic Hydroxylation of Benzene 35
6. Application of the All-in-One Electrode for *in situ* H_2O_2 Generation in Hydroxylation Catalyzed by Unspecific Peroxygenase from *Agrocybe Aegerita* 41
6.1. Integration of Multiple All-in-One Electrodes 50
7. Electrochemical H_2O_2-Stat Mode as Reaction Concept to Improve the Process Performance of an Unspecific Peroxygenase 59
7.1. Electroenzymatic Hydroxylation of EBA under H_2O_2-Stat Mode and Fed-Batch Process 70
8. General Discussion and Outlook 73
9. Summary 89
10. References 92
11. Appendix 103
11.1. Supporting Information to Chapter 5 103
11.1.1. Determination of benzene, phenol, hydroquinone, resorcinol and catechol 103
11.1.2. Control experiment with manual feeding of H_2O_2 105
11.2. Supporting Information to Chapter 6 106
11.2.1. Determination of oxygen productivity at the anode 106
11.2.2. Determination of oxygen mass transfer coefficient in the bioelectrochemical system with an aeration 106
11.2.3. Determination of superoxide and hydroxyl radical concentration 107

11.3. Supporting Information to Chapter 7 115
11.4. Integration of the All-in-One Electrode in an Electrochemical Flow Cell for *in situ* Hydrogen Peroxide Supply in Hydroxylation Mediated by Immobilized Unspecific Peroxygenase 120
11.4.1. Abstract 120
11.4.2. Introduction 121
11.4.3. Experimental 123
11.4.4. Results and discussion 128
11.4.5. Conclusions 144
11.4.6. Supporting Information 145

Abbreviations

Abbreviation	Definition
A	Area [cm^2]
*Aae*UPO	Unspecific peroxygenase from *Agrocybe aegerita*
ABTS	2,2′-Azino-bis(3-ethylbenzothiazoline-6-sulfonic acid)
ACN	Acetonitrile
AiO	All-in-One
BES	Bioelectrochemical system
BNAH	1-Benzyl-1,4-dihydronicotinamide
CNT	Carbon nanotube
CPO	Chloroperoxidase
CV	Cyclic voltammetry
d	Diameter [cm]
EBA	4-Ethylbenzoic acid
EDTA	Ethylenediaminetetraacetate
F.E.	Faradaic efficiency
FMN	Flavin adenine mononucleotide
GDE	Gas diffusion electrode
GOx	Glucose oxidase
h	Hour
HEBA	4-(1-Hydroxyethyl)benzoic acid
HTA	2-Hydroxyterephthalic acid
KP_i	Potassium phosphate buffer
k_La	Volume specific mass transfer rate
K_M	Michaelis-Menten constant [mM]; affinity of a compound towards an enzyme
l	Length [cm]
min	Minute
NBT	Nitro blue tetrazolium
ORR	Oxygen reduction reaction
PIs	Performance indicators
r*Aae*UPO	Recombinant unspecific peroxygenase from *Agrocybe aegerita*
ROS	Reactive oxygen species
rpm	Revolution per minute
STY	Space time yield
TFA	Trifluoroacetic acid
TOF	Turnover frequency
TTN	Total turnover number
U_{ABTS}	Unit; unit of enzyme activity based on ABTS assay [µmol min^{-1}]
UPO	Unspecific peroxygenase
V	Volume [mL]
vvm	Volume air per volume of medium and minute

1. Introduction

The quantity of produced and commercially available chemicals on the global market is predicted to double from 2015 to 2035, with sales of nearly 3 trillion Euros [1,2]. Fossil resources such as oil and gas which are normally used to produce chemical-based products are currently available, but only in a limited quantity and are expected to become more expensive over time as they are finite resources. The chemicals, particularly those which are based on fossil resources have adverse effect on the environment and have changed earth considerably [2,3]. While the most used raw materials in the chemical industry are petrochemical, particularly crude oil, these finite raw materials need to be replaced by renewable and sustainable resources soon. Presently, bio-based and eco-friendly processes to produce chemical products are gaining relevance in industries. Still, the transition from fossil materials as main resources to renewable resources is a major challenge in the chemical industry. Nonetheless, the aforementioned transition presents not only a major challenge, but also an unprecedented opportunity in the future [2]. Apart from sustainability and renewability, the shift from fossil resources to renewable resources should also focus on the interlinking of (bio-)chemical transformations with the utilization of electric energy [2,4]. Combining the chemical and the energy sector can be achieved to a certain degree using the current technologies. However, the gap between the chemical and the energy sector can be narrowed or even bridged by electrobiotechnology [2,5]. Electrobiotechnology is a discipline which combines the field of biotechnology and electrochemistry [2,6]. The combination of biotechnology and the electrochemistry can create a new venue for the conversion of chemical and electric energy. The utilization of biocatalyst, such as enzymes, within the electrochemical system enhances its appeal and allows for the efficient and selective conversion of renewable raw materials. From a UN sustainable development goals perspective, this process contributes to the affordable and clean energy, as well as responsible consumption and production [7].

The notion of combining the advantages of biocatalysts and electrochemical processes has gained attention among researchers in the field of electrobiotechnology [5]. On the one hand, biocatalysts, particularly enzymes, exhibit remarkable characteristics such as high regio- and stereoselectivity, and exceptional catalytic performance. They operate under mild condition and catalyze organic syntheses typically without side reactions [2,8,9]. On the other hand, electrochemical processes offer distinct advantages in terms of energy efficiency, cost-effectiveness, and versatility [10,11]. Moreover, these processes are regarded as environmentally friendly as they can be operated in non-volatile media and utilize electrons as clean reagents, especially, if combined with renewable energy [10]. Considering the growing

importance of sustainability in industrial processes, the unique properties of enzymes and electrochemical processes make electrobiotechnology an attractive alternative to traditional catalysis [8,10]. The applications of electrobiotechnology have been documented in a number of fields including bio-photovoltaics [12], energy recovery [13], wastewater treatment [14], enzymatic biosensors [15], enzymatic synthesis of complex chemicals [16,17] and microbial electrosynthesis [18]. These examples illustrate the significant potential of integrating biotechnology and electrochemistry to enable more efficient industrial processes.

Hydrogen peroxide (H_2O_2), which is a strong oxidant, already finds its extensive application in diverse industrial sectors, particularly in chemical synthesis [19–21], environmental remediation [22,23] and energy conversion [24]. Despite its eco-friendly attributes, owing to its environmentally benign nature with water being its sole degradation product [25], current large-scale production methods, such as the anthraquinone oxidation (AO) process, pose sustainability challenges [25,26]. The AO process involves multistep-reactions, is energy-intensive and generates organic waste [26,27]. Moreover, the handling and storage of bulk H_2O_2 entail safety risks and significant costs [28], which is unjustifiable given that only certain industries, such as aerospace industry, require the use of high H_2O_2 concentration [25,29]. Furthermore, H_2O_2 also can be used as a co-substrate in variety of biocatalytic reactions [30] such as epoxidation [31], decarboxylation [32] and hydroxylation [33]. Nonetheless, the technical application of H_2O_2 in biotechnological field is still limited, mainly due to its deactivation effect towards biocatalysts at excess concentration [30,34].

One of the enzymes that utilizes H_2O_2 as the co-substrate is the unspecific peroxygenase (UPO). The UPO from the basidiomycete fungus *Agrocybe aegerita* (*Aae*UPO) - recently re-classified to *Cyclocybe aegerita* - (EC 1.11.2.1) was first documented in 2004 [35]. Ever since, the recombinant *Aae*UPO (r*Aae*UPO) has been regarded as the most versatile oxyfunctionalizing enzyme in terms of the substrate scope and the reaction variety [36]. Among its diverse catalytic activities, r*Aae*UPO is capable of catalyzing several important reactions, including the epoxidation of alkenes, hydroxylation of alkanes, oxidation of aromatics, *O*- and *N*-dealkylations and one-electron oxidation [37]. This feature has attracted the attention of organic chemists as well, since the oxyfunctionalization is one of the most challenging chemical reactions in organic synthesis, especially, the oxyfunctionalization of unactivated C-H bonds [38,39]. Additionally, r*Aae*UPO exhibits high stability and requires only H_2O_2 as the reducing equivalent, in comparison to other enzymes catalyzing the same type of reactions (*e.g.,* cytochrome P450 monooxygenases) [40,41]. Nevertheless, complications arise when r*Aae*UPO is confronted with elevated H_2O_2 concentrations. The presence of an elevated H_2O_2

concentration leads to an unproductive catalase reaction, which increases costs, and to a catalase malfunction reaction that causes heme bleaching and enzyme inactivation [36].

This is a main drawback for the heme-containing enzymes such as r*Aae*UPO, which, also similar to H_2O_2, hinders their technical application. The key to overcome the inactivating effect of H_2O_2 is to continuously supply H_2O_2 at a low but still sufficient catalytical level. In this regard, various approaches have been developed, including the feeding of diluted H_2O_2 or *in situ* H_2O_2 generation. The *in situ* generation of H_2O_2 can be accomplished through numerous methods, for example through the utilization of a chemical reductant [42], an enzyme [43,44], and piezocatalytic method [45]. Nevertheless, it should be noted that both the enzymatic and chemical reductant approaches have been reported to generate a stoichiometric amount of by-products [16,42]. A direct *in situ* electrosynthesis of H_2O_2 through the reduction of oxygen at an electrode presents an appealing approach to circumvent the irreversible deactivation of enzymes. This method provides a controlled and low generation of H_2O_2, without the aforementioned drawback [46]. Electrochemical reduction of O_2 is regarded as a clean process for the H_2O_2 generation, as it eliminates the need for additional chemicals, produces no complex by-products, and only requires electricity as the input, especially when combined with the application of abundant and inexpensive catalysts like carbon-based materials [8,47].

In this cumulative dissertation, the *in situ* and on-demand electrosynthesis of H_2O_2 is accomplished via the All-in-One (AiO) electrode system, equipped with the carbon felt cathode. The rod-shaped structure of the AiO electrode, which houses the membrane-less cathode and anode, allows for convenient integration into a conventional bioreactor, thereby transforming it into a bioelectrochemical system (BES). The *in situ* generation of H_2O_2 via the AiO electrode is combined with an enzymatic hydroxylation, catalyzed by r*Aae*UPO, to establish a proof of principle. To further enhance the biocatalyst's efficiency and to prevent excessive accumulation of H_2O_2, an automation system is developed. This system utilizes the input from the H_2O_2 sensor to maintain a constant low level of H_2O_2 concentration by regulating the electrical output of a power supply to the electrodes. The ability of the automation system to maintain a constant H_2O_2 concentration during an electroenzymatic reaction is demonstrated in a gas diffusion electrode (GDE) system. Additionally, in light of the recent increase in laboratory-scale enzymatic electrosynthesis reports, a summary of relevant studies is made. Following the evaluation of the reported parameter and performance indicators, a recommendation is proposed for reporting relevant performance indicators in electroenzymatic processes to enable both qualitative and quantitative comparisons between studies.

2. Objective

The primary objective of this dissertation is to develop and establish a fully controllable system for electrochemical *in situ* H_2O_2 generation. This system is designed to serve as an optimizable platform for H_2O_2-dependent enzymatic reactions, thereby realizing a decentralized and environmentally friendly generation of H_2O_2 and enhancing the stability of H_2O_2-dependent enzymes.

To achieve the primary objective, a comprehensive review of the relevant studies reported to date is necessary. This review includes the evaluation and summarization of performance indicators and process parameters from available examples in the field of bioelectrochemistry, with a specific focus on enzymatic electrosynthesis processes. Subsequently, these studies are compared based on both quantitative indicators and non-quantitative parameters. Based on the internal evaluation, the most important performance indicators for electroenzymatic processes that should be reported in all respective publications to allow for quantitative analysis, are proposed.

Furthermore, to develop a controllable *in situ* generation of H_2O_2 and construct an optimizable platform for H_2O_2-dependent enzymatic reactions in order to promote catalyst efficiency, the AiO electrode, previously developed for gas fermentation, is fitted with a carbon felt cathode to generate the H_2O_2 *in situ*. A characterization study of the AiO electrode system regarding its ability to generate H_2O_2 *in situ* will be conducted. The *in situ* electrogeneration of H_2O_2 using the AiO electrode will subsequently be combined with an enzymatic hydroxylation catalyzed by r*Aae*UPO as a proof of principle. Performance indicators such as analytical yield, total turnover number (TTN) and turnover frequency (TOF) from electroenzymatic processes will be analyzed and compared.

Finally, to enhance the efficiency of the electroenzymatic system and improve the operational stability of H_2O_2-dependent enzymes, an automated system will be developed. This system will enable precise control of a constant H_2O_2 concentration (H_2O_2-stat mode), independent of the enzyme activity. The proof of concept for the automation system will be demonstrated using the same model reaction, within a GDE system. The optimal H_2O_2 concentration limit under the H_2O_2-stat mode, which would enable a high TOF while maintaining a high TTN, will be investigated. Additionally, experiments under galvanostatic mode at constant current densities will be performed and serve as an internal benchmark.

3. Theoretical Background

This chapter presents an overview of the synthesis of H_2O_2, bioelectrochemical system (BES), and the recombinant unspecific peroxygenase from the fungus *Agrocybe aegerita* (r*Aae*UPO), with the objective of facilitating the reader's comprehension of the present project.

3.1. H_2O_2 Synthesis Methods

H_2O_2 is a powerful and efficient oxidizing agent, surpassing other oxidants like nitric acid and sodium hypochlorite [25]. Furthermore, it decomposes only into H_2O and O_2 [25], making it one of the cleanest and most versatile oxidants available [48]. Beyond its role as an oxidant in chemical synthesis [21,49], H_2O_2 is widely employed as a disinfectant [50], in bleaching industries [51] and in wastewater treatment [19]. Approximately 2 million metric tons of H_2O_2 are produced on annual basis [51], with 43% are being used in detergent applications and 41% in pulp and paper bleaching (**Fig. 3. 1**) [25].

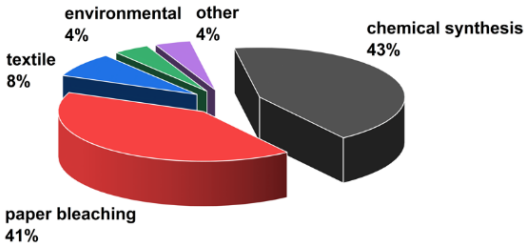

Fig. 3. 1. *Consumption of H_2O_2 in Europe.*

At industrial scale, H_2O_2 is primarily produced via the anthraquinone oxidation (AO) process [52,53]. This process starts with the catalytic hydrogenation of 2-alkylanthraquinone (AQ) to 2-alkylanthrahydroquinone (AHQ), which is then oxidized with air to regenerate AQ and produce H_2O_2 [52,53]. H_2O_2 is extracted from the organic phase using distilled water to yield a 30% w/v H_2O_2 solution, then followed by a distillation to produce 70% w/v H_2O_2 [25]. Although the AO process provides high H_2O_2 yield, it is not without its drawbacks. These include the use of toxic solvent system, occurrence of side reactions, multistep processes, production of organic waste, energy intensiveness and high production costs [25,54].

A direct synthesis of H_2O_2 can be achieved from molecular H_2 and O_2 gases either under plasma [55,56] or using catalysts from noble metals such as Pd [57,58] and Pd/Au [59,60], as well as halide ions like chlorides and bromides [61]. This method offers advantages such as

continuous production process and suitability for decentralized production. Nonetheless, this method suffers from a critical potential explosion of H_2/O_2 gas mixture over a wide range of concentrations (H_2/O_2 mixture is flammable at 4-94% v/v H_2) and poor selectivity [25,62,63].

An alternative method to synthesize H_2O_2 in a large-scale is through the oxidation of primary or secondary alcohols, generating aldehydes or ketones as by-products [64,65]. A notable example is the partial oxidation of 2-propanol, where 2-propanol/ water azeotrope is oxidized by an O_2-saturated gas stream at 140 °C and 20 bar (**Fig. 3. 2**). The mixture, containing unconverted 2-propanol, acetone and H_2O_2 is separated via evaporation. Subsequently, the concentrated H_2O_2 is diluted with water to a concentration below 50% w/v and purified. The downside of this process is that the purity of H_2O_2 is lower than the AO process due to the solubility of alcohol in the peroxide phase [25,64].

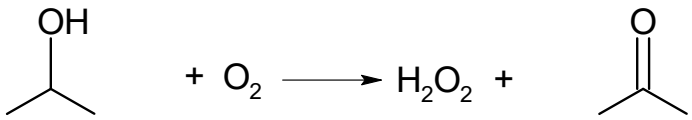

Fig. 3. 2. *H_2O_2 synthesis based on a secondary alcohol oxidation process.*

In regard to the utilization of H_2O_2 within the electroenzymatic reaction system in this dissertation, H_2O_2 is employed by r*Aae*UPO as an oxygen donor and electron acceptor to facilitate the conversion of the substrate 4-ethylbenzoic acid (EBA) and benzene to their respective products, 4-(1-hydroxyethyl)benzoic acid (HEBA) and hydroquinone.

3.2. *in situ* Generation of H_2O_2

The utilization of H_2O_2 as a co-substrate for enzymes like peroxygenases and peroxidases unlocks a variety of interesting biocatalytic reactions such as hydroxylation, epoxidation, Baeyer-Villiger oxidation and sulfoxidation [30]. Nonetheless, the oxidative inactivation of the heme moiety caused by the H_2O_2 reduces the operational stability of H_2O_2-dependent enzymes significantly [66]. Consequently, the stoichiometric addition of H_2O_2 into a reaction mixture at once is unfeasible, as it leads to enzyme inactivation [36,47]. To retain the enzyme activity and maintain the catalytic reaction, a continuous supply of H_2O_2 at low concentration is necessary. Typically, this is achieved through a combination of portion-wise addition of diluted H_2O_2 stock solution and rigorous mixing [67,68]. As a result, significant volume increase and dilution of the reaction mixture are unavoidable. Several studies reported an application of organic peroxide such as *tert*-butyl hydroperoxide [69,70]. However, organic peroxides are considered

as a weak oxidant compared to H_2O_2. Nowadays, the state of the art method in providing H_2O_2-dependent enzymes with a continuous supply of H_2O_2 at low concentration is to generate H_2O_2 *in situ* through a reduction of molecular oxygen. Examples of such methods include an enzymatic [44], a photochemical [66], a chemical [42] or an electrochemical [71] process.

The oxidative inactivation of biocatalysts, especially enzymes, presents a major challenge to the robustness of biochemical transformations, making a straightforward stoichiometric addition of H_2O_2 impractical [72]. The most prevalent method to generate H_2O_2 *in situ* is to use oxidases, such as glucose oxidase (GOx) [44] or amino acid oxidase [73]. GOx from *Aspergillus niger* is frequently used to oxidize glucose to gluconic acid and thereby generating H_2O_2 (**Fig. 3. 3. A**) [74]. One advantage of utilizing GOx as an auxiliary enzyme is that it is commercially available at an affordable price. The *in situ* generation of H_2O_2 using GOx has been proven to improve the lifetime of the biocatalyst, for example in a chloroperoxidase (CPO)-catalyzed oxygen-transfer reaction [74]. Nevertheless, the formation of gluconic acid leads to a pH shift, especially when the by-product accumulates in the medium. Consequently, the implementation of this method on a larger scale requires an additional pH control system. Furthermore, the high viscosity of concentrated glucose solution requires rigorous mixing, thus, increases the energy input. Moreover, the utilization of glucose as a two-electron donor is inefficient, as it generates 198 g by-product per 34 g of H_2O_2 [47], which is contrary to the principles of green chemistry [75]. Additionally, glucose is edible, which introduces a potential conflict of interest with the food industry [30]. Amino acid oxidases, while also available and affordable, have not been widely implemented for *in situ* H_2O_2 generation [47].

In addition to enzymatic methods, H_2O_2 can be generated *in situ* through a photochemical approach using a combination of visible light, a photocatalyst such as flavin adenine mononucleotide (FMN), and a sacrificial electron donor like ethylenediaminetetraacetate (EDTA) (**Fig. 3. 3. B**) [72,76,77]. The photocatalytic productivity of H_2O_2 has been identified as the limiting factor in the overall enzymatic reaction, with its productivity depending on the photocatalyst concentration, light intensity and the availability of oxygen in the medium [72,76]. Despite its successful laboratory-scale implementation and simplicity, the utilization of EDTA is undesirable from an environmental perspective due to the generation of unwanted and toxic by-products, namely ethylene diamine and formaldehyde [72]. Alternative electron donors such as methionine or nicotine are equally unattractive, as they also generate significant by-products. Formate, a simple and inexpensive sacrificial electron donor that generates CO_2 as a sole by-product, is more suitable substitute for EDTA. Nevertheless, reduced enantioselectivity was reported for CPO-catalyzed sulfoxidation [72] and epoxidation [78] when formate was used as the sacrificial electron donor, compared to EDTA.

A chemical strategy serves as another route for *in situ* H_2O_2 generation. Nicotinamide derivative, 1-benzyl-1,4-dihydronicotinamide (BNAH) [79], and organometallic complex, pentamethylcyclopentadienyl rhodium 2,2′-bipyridin [80], have been reported as chemical catalysts for the oxygen reduction. The use of BNAH is frequently accompanied by that of FMN (**Fig. 3. 3. C**), where BNAH acts as a reductant that facilitates FMN reduction. Subsequently, the reduced FMN reacts with molecular oxygen to generate H_2O_2 *in situ*. The productivity of H_2O_2 in this system depends on the concentrations of FMN, BNAH and oxygen in the medium. One study reported a 100% conversion and a TOF of 40 min^{-1} in a reaction involving cytochrome P450 monooxygenase (P450), BNAH and FMN for myristic acid hydroxylation [79]. Similar to the photochemical method, the H_2O_2 productivity remains the rate-limiting step.

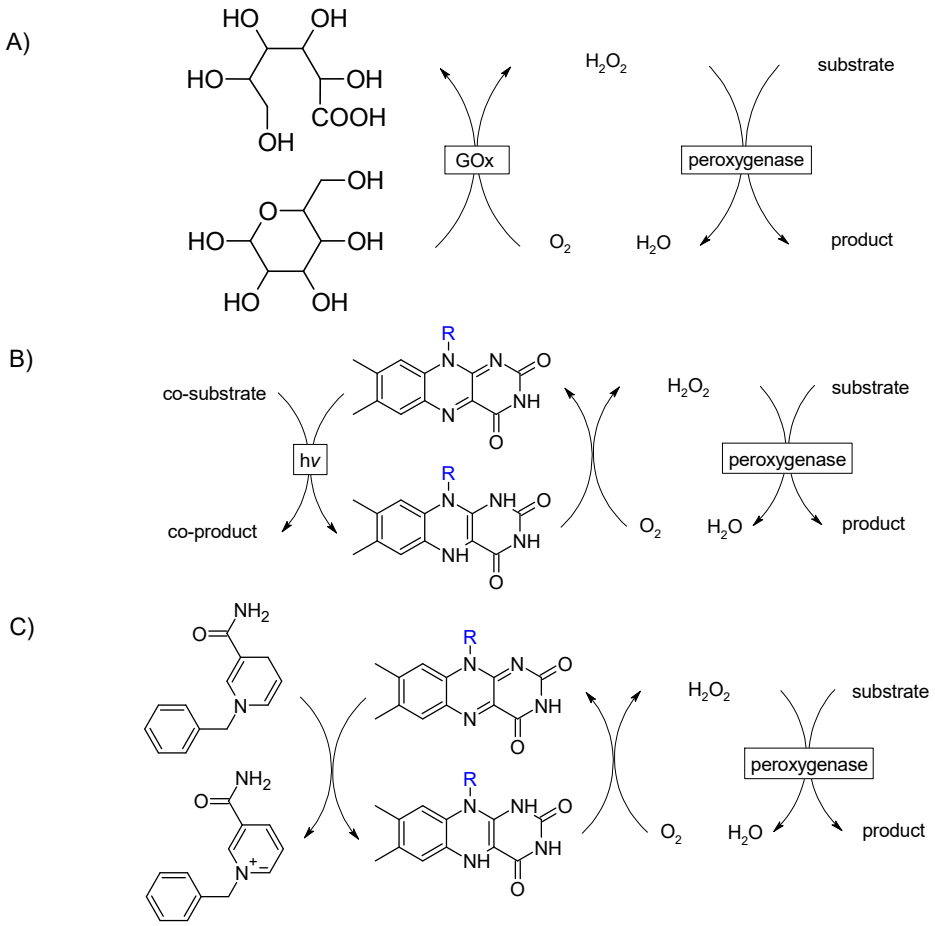

***Fig. 3. 3. A**) Glucose oxidase (GOx)-catalyzed in situ generation of H_2O_2 **B**) photochemical in situ generation of H_2O_2 and **C**) chemical in situ generation of H_2O_2 to facilitate peroxygenase-catalyzed reactions.*

Although the aforementioned methods are able to generate H_2O_2 *in situ*, they still have various drawbacks, such as the requirement of a second enzyme in biocatalytic systems, significant pH shifts, the need for rigorous mixing which can compromise enzyme stability, and the formation of undesirable by-products. In contrast, *in situ* electrosynthesis of H_2O_2 offers a more

sophisticated and environmentally-friendly approach, particularly when combined with a renewable energy. Moreover, no additional hazardous chemicals are required in the process.

In 1887, H_2O_2 was first synthesized from oxygen at a Hg-Au electrode, albeit with a lower efficiency than chemical methods [81]. Today, the laboratory-scale electrosynthesis of H_2O_2 is typically carried out in small-scale reactors. However, scaling up these experiments up to industrially relevant volumes is likely feasible, as demonstrated by pilot plants operating at intermediate scales [82]. In general, H_2O_2 can be electrochemically synthesized either at the anode through the two-electron oxidation of water (equation (**Eq.**) **3.1**) or at the cathode via two-electron reduction of oxygen (**Eq. 3.2**) [83]. The redox potential E is expressed in volts (V) and correlated to a reference electrode, the standard hydrogen electrode (SHE). During electrolysis, the concentration of H_2O_2 in an aqueous medium accumulates only up to a certain point before reaching a steady state [84]. The development of H_2O_2 electrosynthesis and its catalysts are complex due to common electrode materials' tendency to favor competing reactions [48]. Specifically, the full oxygen reduction reaction (ORR) via the four-electron mechanism (**Eq. 3.3**) and the hydrogen evolution reaction at the cathode (**Eq. 3.4**) [85]. Unlike other processes that target a single stable product, H_2O_2 electrosynthesis is challenging because it involves reversible redox reactions of the starting materials, intermediates and products [86]. The desired product H_2O_2 can undergo further oxidation (*e.g.* one-electron oxidation) to generate radicals (*e.g.,* $HO_2^{\bullet}$, $O_2^{\bullet -}$) (**Eq. 3.5**), be reduced via one-electron (**Eq. 3.6**) or two-electron (**Eq. 3.7**) mechanism to produce hydroxyl radical and water, or decompose to water and oxygen (**Eq. 3.8**) [85,87,88]. All of these competing and deleterious reactions lower the yield of H_2O_2 and that is also the reason why the concentration of H_2O_2 can only accumulate to a specific point before the rate of competing reactions surpass the formation rate of H_2O_2. Aside from the further oxidation and decomposition of H_2O_2, one other major challenge lies within the poor solubility of molecular oxygen in aqueous media, which is around 0.25 mM at room temperature (22 – 25 °C) and atmospheric pressure [47]. Thus, the dissolved oxygen is quickly depleted and the diffusion of oxygen into the reaction medium and towards the electrode becomes rate-limiting. It is also important to mention, that the intermediates from these redox reactions, especially radical species, decrease the stability of biocatalysts significantly if the electrosynthesis of H_2O_2 is combined with a biocatalytic reaction [45,66].

$$2H_2O \rightarrow H_2O_2 + 2H^+ + 2e^- \qquad \text{E = 1.760 V vs. SHE} \qquad (\mathbf{3.1})$$

$$O_2 + 2H^+ + 2e^- \rightarrow H_2O_2 \qquad \text{E = 0.670 V vs. SHE} \qquad (\mathbf{3.2})$$

$$O_2 + 4H^+ + 4e^- \rightarrow 2H_2O \qquad \text{E = 1.229 V vs. SHE} \qquad (\mathbf{3.3})$$

$$2H^+ + 2e^- \rightarrow H_2 \qquad \text{E = 0.0 V vs. SHE} \qquad (\mathbf{3.4})$$

$$H_2O_2 \rightarrow HO_2^{\bullet} + H^+ + e^- \quad \text{E = -1.461 V vs. SHE} \quad (\mathbf{3.5})$$

$$H_2O_2 + e^- \rightarrow HO^{\bullet} + OH^- \quad \text{E = 0.104 V vs. SHE} \quad (\mathbf{3.6})$$

$$H_2O_2 + 2H^+ + 2e^- \rightarrow 2H_2O \quad \text{E = 1.763 V vs. SHE} \quad (\mathbf{3.7})$$

$$H_2O_2 \rightarrow H_2O + \frac{1}{2}O_2 \quad \text{E = 1.096 V vs. SHE} \quad (\mathbf{3.8})$$

The evolution of electrode materials has progressed to include doped carbons [84], noble metal alloys [89], and metal oxides [90]. However, all materials exhibit an inverse relationship between current density/ potential and H_2O_2 selectivity. Pure metals like Hg, Au, Cu, Pt, and Pd can generate H_2O_2 at low overpotential during the ORR, but this results in low current densities [91]. To favor H_2O_2 generation, increasing the mass transfer rate is essential to prevent further decomposition, which is achievable by varying electrode parameters and dimensions, as well as flow rates [92,93]. Despite efforts, pure metals do not achieve 100% H_2O_2 selectivity, prompting research into alloys and composites. Pd/Au [28], Pt/Pd [94], W/Au [95] and Pt/Hg [96] are some examples based on metal alloys. In these alloys, one metal enhances the activity while the other stabilizes the reaction intermediates. For example, in the Pd/Au alloy, Pd facilitates the two-electron transfer to oxygen, while Au weakly binds oxygen and prevents bond cleavage, thereby improving selectivity [48,97]. The performance of alloy electrocatalysts depends on the spacing between active metal atoms and the ratio of inactive to active metal. However, increasing selectivity often reduces the reaction rate. Although metal alloys offer promising catalytic activity for H_2O_2 electrosynthesis, they often involve expensive metals [48]. Carbon materials, on the other hand, are abundant and cheaper. Carbon allotropes like graphite, graphene, carbon nanotubes (CNTs), porous carbon, and amorphous carbon, are utilized as electrocatalysts [62,98–100]. Porous carbon materials are advantageous due to their larger surface area, which enhances mass transport and provides more defect sites favorable for H_2O_2 electrosynthesis [100]. Nevertheless, materials with high defect density, due to smaller pores, can reduce H_2O_2 yield by trapping it and causing further reduction or decomposition [101]. While carbon catalysts perform similarly or better than commercial Pt catalysts in alkaline mediums, their activity in acidic conditions is low. Doping carbon materials with elements like boron, nitrogen, sulfur, and phosphorus can increase selectivity towards H_2O_2 [48]. For instance, nitrogen-doped graphite shows high selectivity for H_2O_2 [101], but nitrogen-doped CNTs reduce H_2O_2 selectivity due to increased electron transfer [102]. Due to its availability, price and surface area, carbon-based electrode such as carbon felt and carbon black in form of a GDE are utilized in this dissertation as working electrodes.

3.3. *in situ* Electrosynthesis of H_2O_2 in Bioelectrochemical Systems

The *in situ* electrosynthesis of H_2O_2 has been combined with several biocatalytic reactions, among others chlorination [71], oxidation [103], hydroxylation [104] and halogenation [105]. In these processes, H_2O_2 acts as a co-substrate for the enzymatic reaction, serving as both the oxygen donor and electron acceptor. The *in situ* electrosynthesis of the co-substrate H_2O_2 within the biocatalytic reaction is typically performed in a two-electrode configuration using various carbon-based materials as a working electrode (cathode), and under either a galvanostatic (constant current) or a potentiostatic (constant potential) operation mode [16,46,106,107], which results in a constant H_2O_2 productivity. The reactor concept for BES is fundamentally divided into two types, single-chamber systems and two-chamber systems. The H-cell is one of the most common two-chamber reactor setups frequently used in a laboratory-scale. This setup consists of two chambers connected by a glass tube, forming the “H” shape that gives it its name, and separated by a membrane (**Fig. 3. 4. A**) [108]. The simplicity of the setup makes this reactor advantageous for preliminary investigations and comparative studies. Nevertheless, the membrane creates an extra resistance for proton diffusion to the cathode, thus, increasing the internal resistance of the system [108,109]. In order to avoid this problem, single-chamber systems were developed. Regarding the scalability, single-chamber systems are often the better choice because membranes are normally prone to fouling (*e.g.* biofouling), high in maintenance and cost-intensive [108,109]. One example from the single-chamber systems is the bottle-type reactor. This system is suitable for screening and preliminary laboratory-scale investigations. Both electrodes are placed inside the bottle and an isolator also can be implemented between the electrode to avoid short circuit (**Fig. 3. 4. B**) [110].

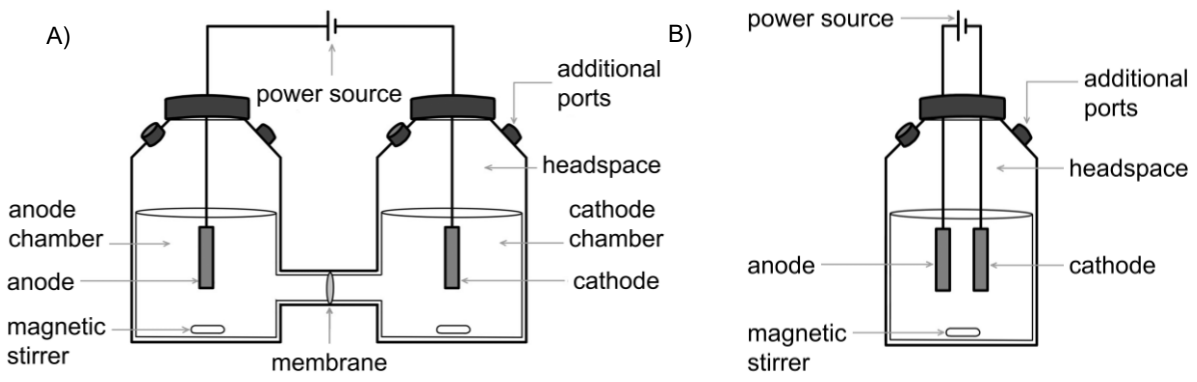

Fig. 3. 4. A*) The setup of the H-cell electrochemical system and* ***B****) the setup of the single-chamber bottle type electrochemical system.*

The GDE is a frequently utilized electrode in single-chamber systems. It is an electrode that is shaped like a thin sheet of paper and possesses a three-phase boundary consisting of a gas, liquid, and solid phase (**Fig. 3. 5**) [111,112]. This enables a direct and higher mass transport of oxygen from the atmosphere through the electrode and in contact with the electrolyte [111]. Thus, limitations due to low oxygen solubility and diffusivity in the liquid and towards the electrode are avoided [112]. A GDE possesses hydrophobic and hydrophilic regions. The hydrophobic region is created using materials such as polytetrafluoroethylene (PTFE). The PTFE enables the formation of a porous three-dimensional gas pathway throughout the GDE and acts at the same time as a barrier to prevent liquid leakage through the electrode [111]. The hydrophilic region, which is the electrocatalytic active region, is created using, for instance, carbon-based materials (*e.g.,* carbon black) and electrocatalysts, which are positioned facing the electrolyte solution. Additionally, a metal mesh, such as nickel mesh is typically employed to maintain the GDE's structural integrity and acts at the same time as a current collector [113].

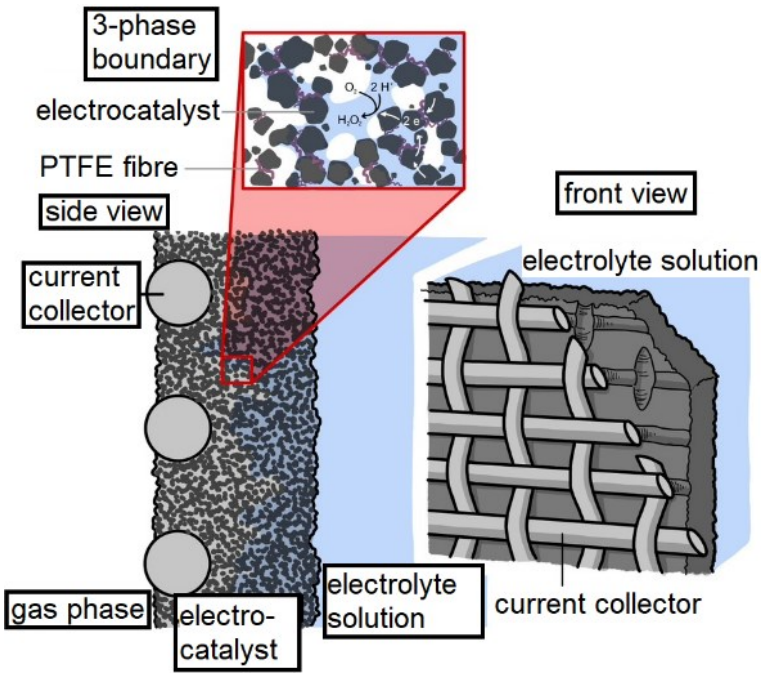

Fig. 3. 5. *Schematic representation of a gas diffusion electrode (GDE). Porous GDE system comprised of a current collector (illustrated as a single metal mesh fibers) and electrocatalyst particles. A curved pattern inside the GDE shows the vertical pattern of the three-phase boundary with gas phase at the left side and electrolyte solution at the right side of the GDE. Insert: the cathodic H_2O_2 synthesis from oxygen at the three-phase boundary.*

In this dissertation, the *in situ* and on-demand electrochemical generation of H_2O_2 will be realized and integrated with enzymatic hydroxylation not only in a BES equipped with a GDE, but also with the AiO electrode system (**Fig. 3. 6**; membrane-less, 2-electrode configuration). The rod-shaped structure of the AiO electrode enables a convenient integration into a conventional bioreactor such as a stirred tank reactor, and multiple electrodes also can be integrated into the bioreactor in different ports to ensure a higher electrochemically active

surface to volume ratio in a larger reactor. By carefully regulating the generation rate of H_2O_2 to match the H_2O_2-consuming rate through the biocatalytic reaction, a stable reaction system can be realized. The AiO electrode system was first developed to generate H_2 *in situ* in anaerobic fermentation processes [13,114]. Here, the AiO electrode is fitted with a carbon felt cathode to facilitate the electrosynthesis of H_2O_2. In contrast to other established electrochemical systems, such as the H-cell system, both electrodes are utilized to generate desired products: oxygen, hydrogen ion and H_2O_2. Typically, the counter electrode exerts no direct influence on the electrogenerative process and is merely employed to sustain the electric circuit. Frequently, the counter electrode even produces toxic by-products [115]. The H_2O_2 is synthesized *in situ* through water electrolysis. Principally, oxygen and hydrogen ion are generated at the anode (counter electrode) through oxidation of water (**Eq. 3.9**), and diffuse towards the cathode. Subsequently, oxygen is reduced at the cathode through the two-electron mechanism of ORR to generate H_2O_2 (**Eq. 3.2**).

$$H_2O \rightarrow \frac{1}{2}O_2 + 2H^+ + 2e^- \qquad \text{E = -1.229 V vs. SHE} \qquad (\mathbf{3.9})$$

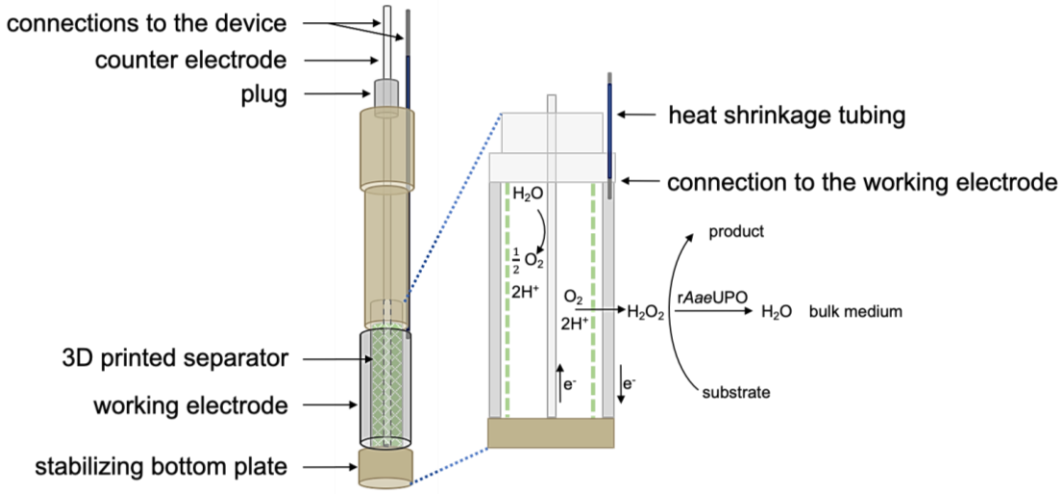

Fig. 3. 6. *Schematic representation of the All-in-One (AiO) electrode. The generated H_2O_2 is directly consumed by the enzyme recombinant unspecific peroxygenase from Agrocybe aegerita (rAaeUPO) for the conversion of the substrate to the product.*

The application of *in situ* electrosynthesis of H_2O_2 in biocatalytic reactions is primarily aimed to enhance the biocatalyst stability [8]. High enzyme stability can be achieved in a process with limited H_2O_2. Therefore, in any BES that combines *in situ* electrogeneration of H_2O_2 with H_2O_2-dependent enzymes, it is crucial to determine optimal parameters. These parameters must maintain H_2O_2 concentrations at levels that enable efficient catalytic turnover while minimizing undesired enzyme inactivation, in order to achieve the highest possible catalyst efficiency. For example, in the enzymatic chlorination [71], it was shown that the catalytic productivity

depends significantly on the generation rate of H_2O_2, which itself is highly influenced by electrochemical parameters such as current density and/ or potential. The efficiency of H_2O_2 electrogeneration is measured by the Faradaic efficiency (F.E.), which describes how much energy is consumed for the formation of H_2O_2 or the formation of side products (**Eq. 3.10**) [8].

$$Faradaic\ efficiency = \frac{n \cdot F \cdot [H_2O_2] \cdot V}{Q} \cdot 100\% \quad (\mathbf{3.10})$$

With:

n : number of transferred electrons (2)

F : Faradaic constant (96,500 [C mol^{-1}])

$[H_2O_2]$: H_2O_2 concentration [M]

V : reaction volume [L]

Q : total charge [C]

3.4. Recombinant Unspecific Peroxygenase from the Fungus *Agrocybe aegerita* (r*Aae*UPO)

r*Aae*UPO (EC 1.11.2.1) belongs to the peroxidase superfamily and able to incorporate oxygen into organic molecules [35]. It catalyzes, among others, hydroxylation, epoxidation, dealkylation, oxidation of organic hetero atoms and inorganic halides as well as one-electron oxidation [37]. Unlike P450s and CPO, r*Aae*UPO is more stable due to its extracellular occurrence, self-sufficient, does not require an expensive nicotinamide cofactor and can address oxyfunctionalizations of unactivated carbons [38].

In addition to its use as an electron acceptor and oxygen donor for a desired reaction, *e.g.* hydroxylation, r*Aae*UPO also catalyzes the dismutation of H_2O_2 via a catalase-like reaction [37]. This happens because, instead of reacting with the target substrate, the highly reactive species of r*Aae*UPO compound I (formed after reacting with the first H_2O_2 molecule) reacts with a second H_2O_2 molecule to form compound II before returning to its resting state (**Fig. 3. 7**). While the catalase activity could be advantageous, it poses a significant drawback for potential r*Aae*UPO applications. This unproductive catalytic cycle and consumption of the co-substrate H_2O_2 increases the costs, especially in industrial application [36]. Even more critical, this catalase-like reaction can lead to enzyme inactivation, known as the catalase malfunction reaction. This issue is common among heme-containing oxidoreductases and is

particularly severe when these enzymes are exposed to excess H_2O_2 [106]. The inactivation of r*Aae*UPO is frequently attributed to the reaction involving compound III, which is formed after the compound II reacted with a third H_2O_2 molecule. It is hypothesized that compound III may engage in a Haber-Weiss like reaction with an additional H_2O_2 molecule [36]. This reaction generates hydroxyl radicals, which can subsequently oxidize critical sites such as the C5 position of the porphyrin ring, leading to enzyme inactivation [30,36]. The resulting α-meso-hydroxyheme can react with oxygen to form verdoheme. Further oxidation leads to the production of biliverdin, accompanied by the release of iron (heme-bleaching). This process results in the irreversible inactivation of the enzyme [36]. Considering various TTNs reported for different r*Aae*UPO substrates [35,40,43,116], it is possible that their inactivation must be dependent also on the selectivity or affinity of r*Aae*UPO towards particular substrates. The catalase activity of r*Aae*UPO can be reduced by employing an appropriate target substrate at a suitable concentration. Typically, the stationary concentration of this substrate should be significantly higher than that of the H_2O_2, as long as no substrate inhibition is present. Specifically, for r*Aae*UPO, optimizing the ratio of H_2O_2 to the target substrate can help minimize catalase activity. This optimization will lead to higher product yields, increased residual r*Aae*UPO activities, and improved TTN [36].

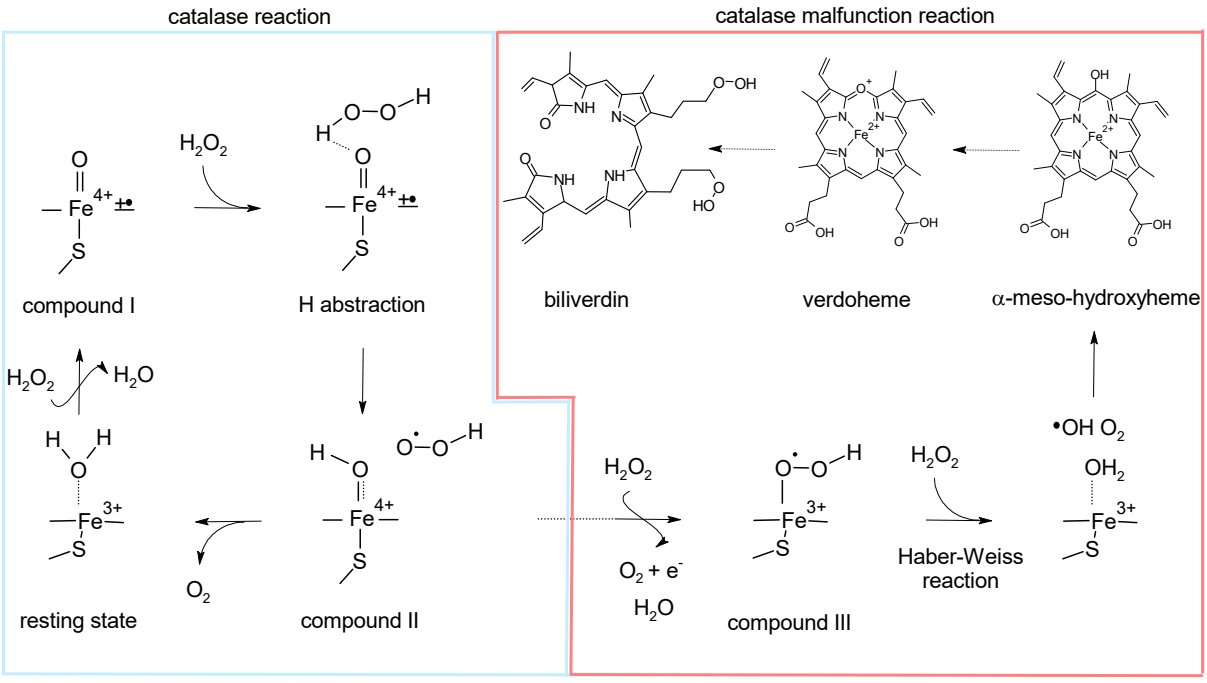

Fig. 3. 7. *Proposed catalytic cycle for the catalase-like reaction of rAaeUPO, divided in a catalase-like activity and a catalase malfunction leading to compound III, hydroxyl radical formation, finally resulting in enzyme inactivation with related verdoheme formation (heme bleaching) [36].*

To quantify the activity of r*Aae*UPO, the 2,2'-azino-bis(3-ethylbenzothiazoline-6-sulfonic acid) (ABTS) is employed as a substrate. ABTS is frequently employed as a substrate in conjunction

with H_2O_2 for the purpose of assessing peroxidase activity, and thus represents an established method of quantification (ABTS assay). In the presence of active r*Aae*UPO and H_2O_2, and under suitable conditions (*e.g.,* in 0.1 M citrate/ phosphate buffer pH 4.4), ABTS is oxidized and forms a dark green product, namely the ABTS radical cation. The *rAae*UPO activity is determined by monitoring the change in absorbance over time at 420 nm, which is indicative of the formation of the ABTS radical cation. The ABTS assay is one of the core methods to assess and optimize r*Aae*UPO-catalyzed reactions in the investigated BES.

4. Overview of Publications

This section provides an overview of the publications that form the foundation of this thesis. The publications are presented in a logical sequence and not necessarily in a chronological order. Between each main publication, presented in chapter **5**, **6** and **7**, additional results and discussions are outlined with the aim to elucidate the connections and transitions between these publications. These are outlined in subchapter **5.1**, **6.1**, and **7.1**. In general, this thesis addresses the following three main topics:

1) Identification and reporting of key performance indicators in electroenzymatic processes to facilitate objective comparisons between studies.
   [Sayoga GV, Abt M, Teetz N, Bueschler VS, Liese A, Franzreb M, Holtmann D. Quantitative and Non-Quantitative Assessments of Enzymatic Electrosynthesis: A Case Study of Parameter Requirements. ChemElectroChem 2023;10:e202300226. https://doi.org/10.1002/celc.202300226]
2) Development of a BES by integrating the AiO electrode system for the *in situ* H_2O_2 generation with an enzymatic hydroxylation.
   [Sayoga GV, Bueschler VS, Beisch H, Holtmann D, Zeng A-P, Fiedler B, Ohde D, Liese A. Application of the all-in-one electrode for *in situ* H_2O_2 generation in hydroxylation catalyzed by unspecific peroxygenase from *Agrocybe aegerita*. Mol Catal 2023;547:113325. https://doi.org/10.1016/j.mcat.2023.113325]
3) Optimization of an electroenzymatic hydroxylation reaction within a GDE system by employing a H_2O_2-stat mode.
   [Sayoga GV, Bueschler VS, Beisch H, Utesch T, Holtmann D, Fiedler B, Ohde D, Liese A. Electrochemical H_2O_2-stat mode as reaction concept to improve the process performance of an unspecific peroxygenase. New Biotechnol 2023;78:95–104. https://doi.org/10.1016/j.nbt.2023.10.007]

The first manuscript, "*Quantitative and Non-Quantitative Assessments of Enzymatic Electrosynthesis: A Case Study of Parameter Requirements*", addresses the integration of enzymatic and electrochemical processes, highlighting their potential to improve production processes as demonstrated by extraordinary laboratory-scale performance indicators. Nevertheless, it identifies a significant gap in the literature regarding the inconsistent reporting of essential process parameters, attributed to the varied metrics used by the experts in their respective fields. This manuscript summarizes key performance indicators and advocates for their consistent inclusion in all relevant publications to enable objective comparisons.

Additionally, it underscores the importance of non-quantitative assessments, such as sustainability and contributions to the UN Sustainable Development Goals. By using H_2O_2-dependent peroxygenases as a case study, the manuscript emphasizes the necessity of defining benchmarks for laboratory investigations to ensure successful scaling and application of electroenzymatic processes.

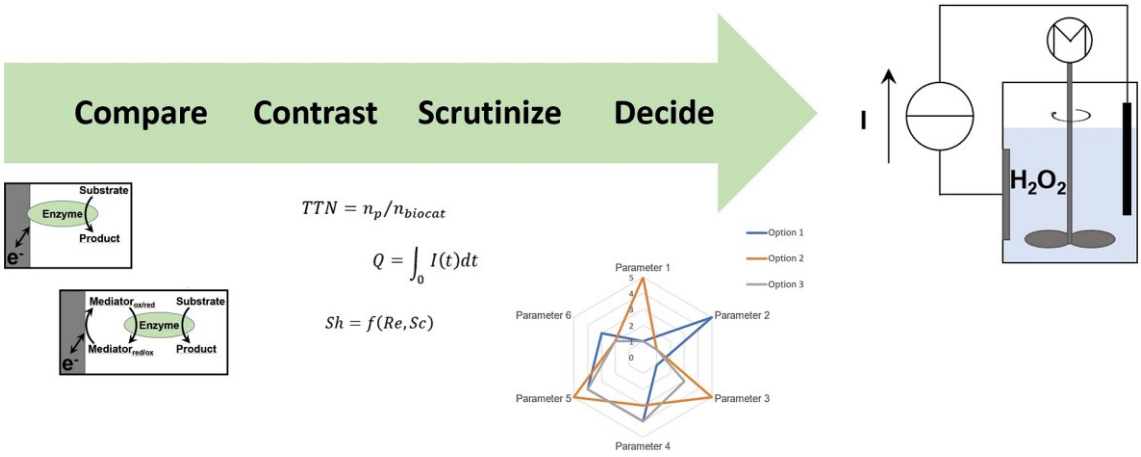

Fig. 4. 1. *The graphical abstract for the manuscript, "Quantitative and Non-Quantitative Assessments of Enzymatic Electrosynthesis: A Case Study of Parameter Requirements", illustrates the concept of "Compare, Contrast, Scrutinize and Decide". This concept advocates for the appropriate determination of process performance in order to quantitatively and non-quantitatively evaluate electroenzymatic processes [117].*

The second manuscript, "*Application of the All-in-One Electrode for in situ H_2O_2 Generation in Hydroxylation Catalyzed by Unspecific Peroxygenase from Agrocybe Aegerita*", addresses the technical limitations of the versatile r*Aae*UPO, particularly its instability towards the co-substrate H_2O_2. This study introduces the AiO electrode system for *in situ* H_2O_2 generation, integrating it with enzymatic hydroxylation for the first time. The AiO electrode's unique structure, combining the counter and working electrode, allows easy incorporation into conventional bioreactors, converting them into a BES. The hydroxylation of 4-ethylbenzoic acid catalyzed by r*Aae*UPO served as the model reaction. This work demonstrates the potential of the AiO electrode system as an optimizable platform for H_2O_2-dependent enzymatic reactions, highlighting its simplicity and effectiveness in minimizing enzyme deactivation and avoiding common drawbacks of other methods.

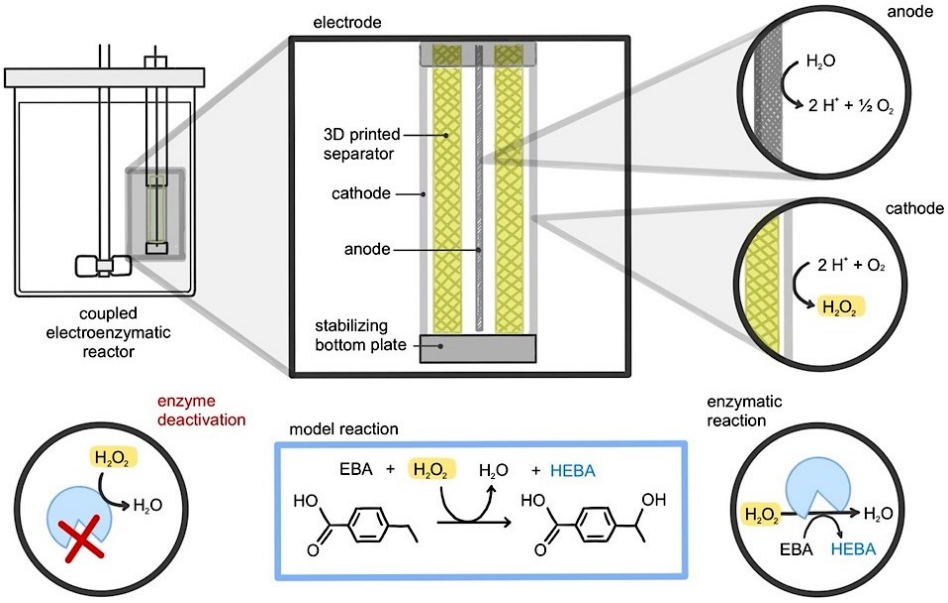

Fig. 4. 2. *The graphical abstract for the manuscript, "Application of the All-in-One Electrode for in situ H_2O_2 Generation in Hydroxylation Catalyzed by Unspecific Peroxygenase from Agrocybe Aegerita", illustrates the application and combination of the All-in-One electrode for in situ generation of H_2O_2 with an enzymatic hydroxylation of 4-ethylbenzoic acid (EBA) to 4-(1-hydroxyethyl)benzoic acid (HEBA) in a bioelectrochemical system [118].*

The third manuscript, "*Electrochemical H_2O_2-Stat Mode as Reaction Concept to Improve the Process Performance of an Unspecific Peroxygenase*", investigates the impact of different H_2O_2 electrogeneration modes on the performance of the r*Aae*UPO. Utilizing a GDE-based system, the study explores how the mode of H_2O_2 supply affects enzyme stability and productivity. Two modes were compared: the galvanostatic mode, which maintains constant productivity of H_2O_2, and the H_2O_2-stat mode, which maintains a constant H_2O_2 concentration. An automation system was exclusively developed to maintain a constant H_2O_2 concentration. The findings reveal that while the galvanostatic mode achieves higher productivity at higher current densities, it also leads to faster enzyme deactivation due to excess H_2O_2 accumulation as the enzyme activity decreases over time. Conversely, the H_2O_2-stat mode, though yielding lower productivity, allows for higher TTNs and TOFs by preventing H_2O_2 accumulation and thereby protecting the enzyme from rapid deactivation. This study demonstrates the potential of the H_2O_2-stat mode to enhance process performance in electroenzymatic applications and suggests its utility in further investigations of H_2O_2-dependent enzymes.

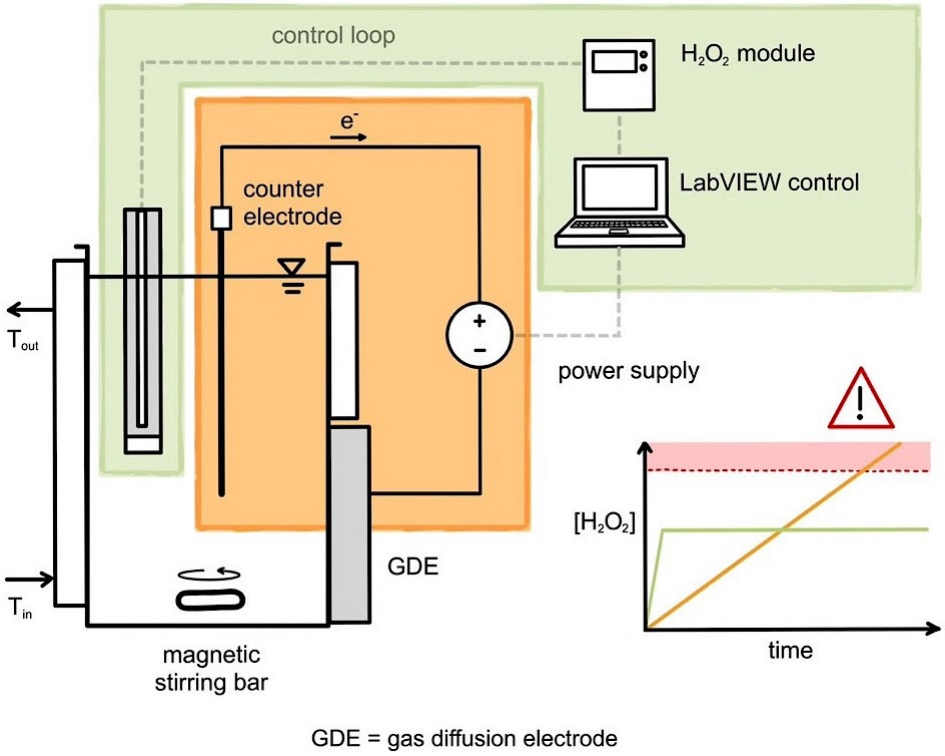

Fig. 4. 3. *The graphical abstract for the manuscript, "Electrochemical H_2O_2-Stat Mode as Reaction Concept to Improve the Process Performance of an Unspecific Peroxygenase", illustrates two distinct H_2O_2 electrogeneration methods and their respective H_2O_2 concentration over time in batch mode within the gas diffusion electrode (GDE)-system. Green: H_2O_2-stat mode with the automation, orange: galvanostatic mode [119].*

5. Quantitative and Non-Quantitative Assessments of Enzymatic Electrosynthesis: A Case Study of Parameter Requirements

Giovanni V. Sayoga[a], Michael Abt[b], Niklas Teetz[c], Victoria S. Bueschler[a], Andreas Liese[a], Matthias Franzreb[b], Dirk Holtmann[c,d]

[a]Institute of Technical Biocatalysis, Hamburg University of Technology, Denickestraße 15, 21073 - Hamburg, Germany
[b]Institute of Functional Interfaces, Karlsruhe Institute of Technology, Hermann-von-Helmholtz-Platz 1, 76344 - Eggenstein-Leopoldshafen, Germany
[c]Institute of Bioprocess Engineering and Pharmaceutical Technology, University of Applied Sciences Mittelhessen, Wiesenstrasse 14, 35390 - Giessen, Germany
[d]Institute of Process Engineering in Life Sciences, Karlsruhe Institute of Technology, Fritz-Haber-Weg 4, 76131 - Karlsruhe, Germany

Bibliographic details
published September 2023, Volume 10, Issue 24
ChemElectroChem (Wiley-VCH GmbH)
DOI: 10.1002/celc.202300226

Check for updates

ChemElectroChem

Concept
doi.org/10.1002/celc.202300226

Chemistry Europe
European Chemical Societies Publishing

www.chemelectrochem.org

Quantitative and Non-Quantitative Assessments of Enzymatic Electrosynthesis: A Case Study of Parameter Requirements

Giovanni Sayoga[+],[a] Michael Abt[+],[b] Niklas Teetz[+],[c, d] Victoria Bueschler[+],[a] Andreas Liese,[a] Matthias Franzreb,[b] and Dirk Holtmann*[c, d]

The integration of enzymatic and electrochemical reactions offers a unique opportunity to optimize production processes. Recently, an increasing number of laboratory-scale enzymatic electrosyntheses have shown impressive performance indicators, leading to scientific interest in technical implementation. However, important process parameters are missing in most of the relevant literature. On one hand, this is due to the large variety of relevant performance indicators. On the other hand, enzyme technologists and electrochemists use different parameters to describe a process. In this article, we review the most important performance indicators in electroenzymatic processes and suggest that in order to allow quantitative comparison, these indicators should be reported in all respective publications. In addition to quantitative parameters, non-quantitative assessments often need to be included in a final evaluation. Examples of such parameters are sustainability, contribution to the UN Sustainable Development Goals or interactions with the overall process. We demonstrate the evaluation of processes using hydrogen peroxide-dependent peroxygenases. The strength of the proposed evaluation system lies in its ability to identify weaknesses in a process at an early stage of development. Finally, it can be concluded that all evaluated enzymatic electrosynthesis do not yet meet typical industrial requirements for an enzyme-based process.

1. Introduction

The importance of energy- and material-efficient industrial processes is increasing with the current challenges of a growing world population, unstable availability and costs of raw materials and energy, and environmental requirements. The combination of biotechnology and electrochemistry can contribute to the realization of efficient industrial processes. The general motivation for studying electro-biotechnological processes is to combine the advantages of electrochemistry (high energetic and atomic efficiencies) with the advantages enzymes or whole-cell catalysts (high regio- and enantioselectivity), thus electro-biotechnological processes are considered as one of the emerging techniques to combine biochemical transformations with the storage and utilization of electrical energy from renewable sources.

The applications of electro-biotechnology mainly comprise sensory aspects (biosensors), the conversion of chemical energy into electrical energy in enzymatic or microbial fuel cells and electro-biotechnological production processes. Among these applications, the synthesis of chemicals and energy carriers has gained the greatest interest so far.[1] Electro-biotechnological production processes can be divided in microbial and enzymatic electrosynthesis (MES or EES). In MES, the metabolic pathways of organisms are used to produce complex molecules such as bioplastics or terpenes as well as bulk chemicals such as acetate, methane and isopropanol.[2–8] In contrast, EES addresses mostly single reaction steps or small cascades up to 3 enzymatic reactions. EES has gained prominence because of its use of renewable energy inputs as well as highly specific enzyme biocatalysts and its capability of performing reactions with high yields.[9] Most enzymes used in EES are members of the group of oxidoreductases (Enzyme Commission number 1). Oxidoreductases are enzymes that catalyse the transfer of electrons from one molecule (the reductant or electron donor) to another molecule (the oxidant or electron acceptor). A large number of the oxidoreductases are using oxidised or reduced cofactors (such as nicotinamide adenine dinucleotides or flavins) as electron carriers. In whole-cell catalysts, these cofactors are regenerated intracellularly; when using isolated enzymes, this regeneration must be technologically solved. One option is the use of electrochemical regeneration or substitution processes. Figure 1 schematically shows the different

[a] G. Sayoga,[+] V. Bueschler,[+] Prof. Dr. A. Liese
Institute of Technical Biocatalysis, Hamburg University of Technology
Denickestraße 15, 21073 Hamburg, Germany

[b] M. Abt,[+] Prof. Dr. M. Franzreb
Institute of Functional Interfaces, Karlsruhe Institute of Technology
Hermann-von-Helmholtz-Platz 1, 76344 Eggenstein-Leopoldshafen, Germany

[c] N. Teetz,[+] Prof. Dr. D. Holtmann
Institute of Bioprocess Engineering and Pharmaceutical Technology,
University of Applied Sciences Mittelhessen
Wiesenstrasse 14, 35390 Giessen, Germany

[d] N. Teetz,[+] Prof. Dr. D. Holtmann
Institute of Process Engineering in Life Sciences, Karlsruhe Institute of Technology
Fritz-Haber-Weg 4, 76131 Karlsruhe, Germany
E-mail: dirk.holtmann@kit.edu

[+] contributed equally

ChemElectroChem
Concept
doi.org/10.1002/celc.202300226
Chemistry Europe
European Chemical Societies Publishing

modes of electron transfer between electrodes and enzymes. The direct electron transfer (DET) is based on the interaction between a redox-active motive of the enzyme and an electrode (Figure 1 A). However, because the redox cofactors are typically deeply embedded in the protein matrix of the enzymes, electrons cannot easily be transferred between the electrode and enzyme.[10] Different types of mediated electron transfer (MET) can be used to overcome this limitation (Figure 1 B–D). Mediators hereby acts as an electron shuttle between electrode and biocatalysts or cofactors.[11] In MET the electron shuttle is used to transfer electrons between the electrode and the natural cofactor. The enzyme reaction is comparable to the natural reaction. A mediated electron transfer between the electrode and an enzyme can be used to drive an enzymatic reaction or to regenerate a cofactor for a second enzymatic reaction. The use of direct electron transfer between the cofactor and the electrode minimizes the complexity of the reaction system caused by the addition of a mediator (Figure 1 E). EES often uses either cofactor-dependent enzymes or

Giovanni Sayoga was born in Tasikmalaya, Indonesia in 1992. He obtained his Bachelor's degree in 2018 and Master's degree in 2020, both in the field of Bioprocess Engineering from the Hamburg University of Technology (TUHH), Germany. Currently, he is pursuing his PhD at the Institute of Technical Biocatalysis of TUHH, under the supervision of Prof. Andreas Liese. His current PhD research revolves around in situ electrochemical generation of H_2O_2 as a co-substrate for biocatalytic reactions.

Michael Abt received his MSc degree in chemical engineering from the Technical University of Munich in 2020, where he investigated key performance indicators for the operation of a high-gradient magnetic separator for protein purification. He is currently working on his PhD project at the Karlsruhe Institute of Technology, under the supervision of Prof. Dr.-Ing. Matthias Franzreb. His research focuses on the development, the exemplary application, and the process characterization of novel electrochemical fluidized bed reactors for electroenzymatic syntheses including gaseous phase.

Niklas Teetz received his M. Sc. degree in molecular biology from the Goethe University of Frankfurt a. M. in 2021 after investigating a paired electrolysis cell combining Kolbe electrosynthesis and biosynthesis via Cupriavidus necator at DECHEMA Research Institute. He started his PhD studies at University of Applied Sciences Mittelhessen at the Institute of Bioprocess Intensification and is currently concluding this work at the Institute of Electrobiotechnology at the Karlsruhe Institute of Technology. His research focuses on reaction and enzyme engineering of unspecific peroxygenases.

Victoria Bueschler completed their Bachelors's and Masters's degrees in Bioprocess Engineering at Hamburg University of Technology (TUHH) in Hamburg, Germany. Focussing on heterogeneous enzyme biocatalysis and inline analytical methods in their Bachelors's and Masters's thesis, they began their Ph.D. research project on an enzymatic bioelectrochemical system in early 2021. Since 2023 they are the research group leader for the Process Analytical Technologies group at the Institute of Technical Biocatalysis at the Hamburg University of Technology.

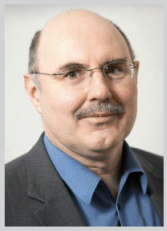

Matthias Franzreb (1963) received his Ph.D. in chemical engineering from the University of Karlsruhe. Afterwards he entered the Karlsruhe Institute of Technology and started his work on magnetic micro-adsorbents and their application in protein purification and enzyme immobilization. In 2002, he finished his Habilitation and in 2009, he was awarded an Extraordinary Professorship by the Karlsruhe Institute of Technology (KIT). His research focuses on device development and modelling for novel bioseparations and electroenzymatic reactions.

Andreas Liese studied chemistry and carried out his doctoral research at the Research Center Jülich, Germany. He received his Ph.D. from the University of Bonn in 1998. From 1998 to 2003, Liese was an assistant professor at the University of Bonn and head of the Enzyme Group within the Research Center Jülich. After a sabbatical in 2000 at Pfizer Global Research & Development, San Diego, USA, he worked as associate professor at the University of Münster from 2003 to 2004. In 2004 he became a full professor of the Institute of Technical Biocatalysis at the Hamburg University of Technology (TUHH), Germany.

Dirk Holtmann completed his diploma in chemical engineering/biotechnology in 1999. He received his PhD at the Otto-von-Guericke University Magdeburg on the electrochemical measurement of microbial activities. Until September 2019 he was head of the Industrial Biotechnology Group at the DECHEMA Research Institute. After that he was professor for Intensification of Bioprocesses at THM (Gießen, Germany). In 2023 he became full professor for Electrobiotechnology at the Karlsruhe Institute of Technology. His current research activities focus on biocatalysis, bioprocess engineering and bioelectrochemical synthesis.

ChemElectroChem
Concept
doi.org/10.1002/celc.202300226
Chemistry Europe
European Chemical Societies Publishing

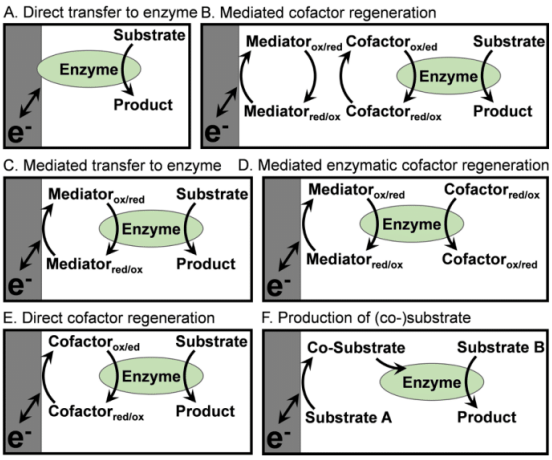

Figure 1. Scheme of electroenzymatic processes.

enzymes whose substrates can be generated electrochemically (especially H_2O_2-dependent enzymes, Figure 1 F).

Interest in enzymatic electrosynthesis has increased significantly in recent years, as evidenced by the growing number of publications in the field. Unfortunately, many of the studies are difficult to compare or evaluate. Proof-of-principle studies often do not report any metrics at all. Other publications use a wide variety of metrics. The aim of this paper is to describe the most important performance indicators and to compare the current examples in the field of EES using these indicators. Finally, different options will be compared based on these indicators and other non-quantitative parameters.

2. Overview of Important Performance Indicators

Understanding and overcoming the limiting factors of electroenzymatic systems is a challenging task that requires a parameter-based approach using standardized performance indicators (PIs). These PIs help to understand the system, enable comparability between different systems and allow benchmarking with more conventional processes. Table 1 provides an overview of the key performance indicators for enzymatic electrosynthesis. The table assumes that the geometry and volume of the reactor and the surface area of the electrodes are known. In addition, we assume that the kinetics of the enzyme reaction of interest have been studied in small, well-mixed batch studies that provide the traditional indicators V_{max}, k_{cat} and K_m. During the electroenzymatic process in the reactor, the applied potential and the resulting current should be monitored. In 3-electrode setups, the cell potential U_{cell} between the anode and cathode should be recorded in addition to the adjusted potential of the working electrode versus the reference electrode. In the following, it is assumed that a cofactor or co-substrate is electrochemically produced at the working electrode and simultaneously consumed by an enzymatic reaction involving an additional substrate in the reactor volume. However, other types of electroenzymatic processes can be treated analogously.

The first section of Table 1 lists the most important general reaction engineering PIs which can be calculated from the experimental data. It is always recommended to report the space-time-yield (STY) and achievable product titre for comparison with traditional processes.[12] The product titre also allows for an estimation of the effort required for product recovery in downstream processing. In case of an electrochemical co-factor regeneration or co-substrate generation, it can be useful to correlate the electroenzymatic STY of the product to the purely electrochemical STY of the intermediate to determine how much of the electrochemical generated substance is used in the combined system.[13] Together with the known amount of applied enzyme the total turnover number (TTN) and the turnover frequency (TOF) can be calculated as two of the key PIs of enzymatic as well as electroenzymatic systems.[14]

Important electrochemical PIs, such as the current efficiency (CE), the current density, and the specific energy consumption per kg of product can be calculated together with the data monitored by the potentiostat. To understand the relation of CE and applied potential, laboratory-scale experimental setups need to include a reference electrode to investigate the resulting overpotential of the electrode configuration. Besides the potential, the CE should always be paired with the current density. In many publications, the current density is referred to the projected electrode area. This is correct in the case of flat electrode types, like polished electrodes, meshes, and plates, when the geometric electrode area is equal to the electrode active surface area.[15] However, to calculate the correct electrode surface of porous electrodes with rougher surfaces such as carbon foam, carbon felt and diffusion electrodes, it is advised to determine the electrochemically active surface area via chronoamperometry or cyclic voltammetry.[15]

Most enzymatic electrosynthesis are adjusted to enzyme performance and suffer from comparable low concentrations and low electrolyte conductivity,[16] which can make it necessary to improve electrolyte-electrode mass transfer and to reduce ohmic resistance.[17] One simple beneficial way of improvement is to increase the surface-to-volume ratio.[18,19] Another often missing PI for reactor characterization is the mass transfer coefficient (k_{film}) at the electrode. For defined electrode geometries k_{film} can be calculated by the respective correlation between the Sherwood, Reynolds, and Schmidt number. In other cases, k_{film} can be estimated from well-defined electrochemical model reactions conducted in the same reactor.[20] The listed indicators deliver a comprehensive overview of the performance indicators of an electroenzymatic process and help to comprehend the system, to determine bottlenecks and to facilitate a scale-up of the process for industrial application.

ChemElectroChem | Concept doi.org/10.1002/celc.202300226 | Chemistry Europe European Chemical Societies Publishing

Table 1. Performance indicators to characterize electroenzymatic processes.

Symbol	Name	Formula	Meaning	Remarks
General reaction engineering performance indicators				
σ_p, $\dot{q}_{p,v}$	Space time yield (STY), volumetric productivity	$\sigma_p = m_p/(V \cdot \tau)$ $\dot{q}_{p,v} = m_p/(V \cdot t)$	Mass of a product formed per time and volume in batch and continuous process	Reported to compare different reactors. Ideally, use the liquid volume of the compartment with the working electrode for calculation
Y_p	Reaction yield	$Y_p = n_p/n_{r,0} \cdot \lvert v_r/v_p \rvert$ $Y_p = (\dot{n}_{p,out} - \dot{n}_{p,in})/\dot{n}_{r,in} \cdot \lvert v_r/v_p \rvert$	Yield of batch and of continuous electroenzymatic reaction	Specify components (products and reactants: co-factor, co-substrate or substrate) and clarify system boundary as well as process step.
X_r	Conversion	$X_r = 1 - n_r/n_{r,0}$ $X_r = 1 - \dot{n}_{r,out}/\dot{n}_{r,in}$	Conversion of batch and of continuous electroenzymatic reaction	Specify components (products and reactants: co-factor, co-substrate, substrate) and clarify system boundary as well as process step
S_p	Selectivity	$S_p = n_p/\Delta n_r \cdot \lvert v_r/v_p \rvert$ $S_p = (\dot{n}_{p,out} - \dot{n}_{p,in})/(\dot{n}_{r,in} - \dot{n}_{r,out}) \cdot \lvert v_r/v_p \rvert$	Selectivity of batch and of continuous electroenzymatic reaction	Specify components (products and reactants: co-factor, co-substrate or substrate) and clarify system boundary as well as process step.
E − factor	Environmental factor	$E - factor = c_{waste}/c_p$	Ratio of waste to product	The amount of waste is difficult to quantify, we recommend excluding water and normalize the waste generation to the reactor volume[21,22]
c_p, c_s	Product titer and substrate loading		Concentration of product/substrate	Declare concentrations to benchmark against conventional processes and to estimate costs[23]
Enzymatic performance indicators				
TTN / $TTN_{co-factor}$	Total turnover number	$TTN = n_p/n_{biocat}$ $TTN = n_{co-factor}/n_{biocat}$	Stability of the biocatalyst under process conditions	Reported for the product and the co-factor
TOF	Turnover frequency	$TOF = n_p/(n_{biocat} \cdot t)$	Turnover per unit time	Disregards enzyme stability in the process and should be paired with the total turnover number
$t_{0.5}$	Half-life time		Half-life time of enzyme	Gives information on enzyme stability under process conditions (time of the process when the residual activity ofthe enzyme is 50%)
c_{biocat}	Biocatalyst load		Concentration of enzyme	Declare the biocatalyst concentration for comparability and for cost estimation (i.e. ratio of deployed enzyme to product)[23]
ee	Enantiomeric excess (ee)	$ee = \lvert n_R - n_S \rvert/(n_R + n_S)$	Purity of chiral substance	Highlights enantioselectivity of biocatalyst
Electrochemical performance indicators[24–26]				
Φ_p^e	Current efficiency (CE)	$\Phi_p^e = n_p \cdot z/v_p \cdot F/Q$ $Q = \int_0^t I(t)dt$	Ratio between the amount of product and total amount of consumed electrons	Important for economic analysis and can be calculated for the electrochemical product or entire electroenzymatic reaction
Φ_G	Energy efficiency	$\Phi_G = (\Delta G \cdot n_p)/(Q \cdot U_{cell})$ $= v_p/Z \cdot (\Delta G \cdot \Phi_p^e)/(F \cdot U_{cell})$ $= \Delta E_{cell,eq}/U_{cell} \cdot \Phi_p^e$	Fraction of applied energy which is thermodynamically stored in the product of the electrochemical reaction	The energy efficiency for the applied electric energy combines voltage and current efficiency of the electrochemical cell
j, j_v	Current density, volumetric current density	$j = I/A_e$ $j_v = I/V$	Current per active electrode area or volume	Determine correct active electrode area or use liquid volume of compartment with working electrode for calculation
η_{WE}	Overpotential	$\eta_{WE} = E_{WE} - E_{eq,WE}$	Extra potential than thermodynamically expected from the equilibrium potential to drive a reaction	Overpotential at the working electrode
w	Specific electric energy consumption (sEEC)	$w = U_{cell} \cdot Q/m_p$	Electric energy consumption per mass of product	Reports the specific energy consumption of the production process
ETY	Electrode surface time yield	$ETY = m_p/(A_e \cdot t)$	Mass of product formed per time and electrode surface	Reported to determine scalability

ChemElectroChem | Concept doi.org/10.1002/celc.202300226 | Chemistry Europe European Chemical Societies Publishing

Table 1. continued

Symbol	Name	Formula	Meaning	Remarks
$Y_{p/e}$	Product yield per electron[18]	$Y_{p/e} = F \cdot n_p/Q$	Product yield per electron	Characterization and benchmarking
Reactor performance indicators				
A_e/V	Electrode surface per reactor volume	A_e/V	Ratio of electrode surface to volume	Determine active electrode surface and use liquid volume of compartment with working electrode for calculation
k_{film}	Film mass transfer coefficient	$k_{film} = Sh \cdot D_m/L$ $Sh = f(Re,\ Sc)$	Correlates diffusion rate with convective mass transfer rate	Defines the rate by which the educts can pass the Nernst film which surrounds the electrode

3. Examples of Electroenzymatic Processes

Numerous enzymes have been used for enzymatic electrosynthesis and the four most prominent electroenzymatic processes utilize the unspecific peroxygenase from the fungus *Agrocybe aegerita* (*Aae*UPO) for the hydroxylation of non-activated carbon,[27] chloroperoxidase (CPO) for the oxidation of thioanisole,[28,29] glucose oxidase (GOx) for the oxidation of glucose,[22,30] and formate dehydrogenase (FDH) for the reduction of the greenhouse gas CO_2.[31,32] To overcome the major enzyme instabilities at excess co-substrate H_2O_2 concentration, Lütz and co-workers combined the electrochemical H_2O_2 supply with CPO for the first time. The electrochemical system contained a cylindrical carbon felt working electrode and the oxidation of thioanisole to (*R*)-methylphenylsulfoxide was used as the model reaction system. Using this setup, a productivity up to 30 $g\,L^{-1}\,d^{-1}$ and a TTN as high as 95,000 $mol\,mol^{-1}$ were reported.[28] In electroenzymatic processes, high selectivity and sustainability are usually only being assumed. Varničić studied both of these aspects in more detail within an electroenzymatic process for the oxidation of the renewable feedstock glucose to gluconic acid in a membrane-less flow reactor using immobilized GOx at the anode and co-immobilized GOx and horseradish peroxidase (HRP) (catalase reaction) at the cathode (Vulcan carbon nanomaterials as support for biocatalysts). With the help of nuclear magnetic resonance (NMR) spectroscopy, a product selectivity of 97% was reported. Additionally, glucose conversion of 80% and E-factor of 9 were obtained.[22] A further distinctive result of the application of an electroenzymatic process was reported by Sokol et al. They mimicked the biological formate hydrogen lyase (FHL) complex and performed a reversible conversion of formate to H_2 and CO_2 under ambient conditions, which is normally realized via mixed-acid fermentation in *Escherichia coli*. It was achieved by employing a semiartificial system consisting of FDH and hydrogenase (H_2ase) (from *Desulfovibrio vulgaris*) immobilised on indium tin oxide (ITO). A TON of 23,000 $mol\,mol^{-1}$ and a TOF of 6.4 s^{-1} were achieved.[33]

In addition to the already mentioned processes, further recent and noteworthy examples of electroenzymatic processes are presented in Table 2, along with key performance indicators, electron transfer mechanisms, and process conditions used to perform the experiments. Among these examples, peroxidases (e.g., CPO and horseradish peroxidase (HRP)) have been implemented into various electroenzymatic processes such as chlorination, sulfoxidation and demethylation, and within different setups. With such a diverse set of processes, a comparison of the results is challenging even for comparable reaction systems, as different or unrelated parameters and performance indicators are reported. Firstly, this may be due to a broad range of available relevant performance indicators that can be used. Secondly, the background of researchers might be responsible as different indicators to describe a process are used in different academic disciplines. To better facilitate comparisons in the field of electrobiotechnology, a standardized reporting on electroenzymatic processes should be implemented.

The numerous listed examples demonstrate that electrobiotechnology has come a long way since its first inception in 1911.[1,48] Moreover, it is expected that electroenzymatic processes gain even more relevance in the near future. It can also be noted that developed and established processes on a lab scale have been reported in the literature quite progressively.[9] Several processes even show remarkable performance indicators, which is promising for future pilot scale processes.

4. Non-quantitative Parameter

Natural scientists, engineers as well as economists usually decide on the base of performance indicators (see above). However, there are also some evaluation criteria that cannot be directly linked to key indicators. Examples in this context are the contribution of a technology or product to the achievement of the United Nations Sustainable Development Goals (SDGs), the effort required to train employees on new processes, the flexibility of the application, the availability of necessary materials, or the acceptance of new products or processes by customers and the general public. Non-quantitative properties may also include non-detectable fluctuations in raw materials. In electroenzymatic processes, these can be, for example, typical variations in the composition or purity of the natural substrates or in the specific activity or stability of the enzymes. It should be noted that some key figures can only be calculated/estimated on an industrial scale. Our considerations (see below) refer to the early stages of process development.

ChemElectroChem | Concept doi.org/10.1002/celc.202300226 | Chemistry Europe European Chemical Societies Publishing

Table 2. Examples of electroenzymatic processes.[a]

Process types	e⁻ transfer mechanism	Enzyme, co-factors, substrate and product	Type of working electrode	Process condition	Key performance indicators	Ref.
Hydroxylation	F (2e⁻)	Enzyme: UPO, co-substrate: H_2O_2, substrate: ethylbenzene, product: 1-phenethyl alcohol	CB GDE, *A*: 2 cm^2	30 mL 0.1 M KP_i pH 7, 900 μL acetone, 500 μL substrate, 50 nM (0.3 U mL^{-1}) UPO, applied currents: −5 to −30 mA cm^{-2}	TTN: 400,000, productivity: 25 g L^{-1} d^{-1}, loss of enzyme activity: 0.33 U mL^{-1} h^{-1}, CE: 78%, H_2O_2 productivity [a]: 225 μM min^{-1} cm^{-2}	[27]
Flow-through reactor, hydroxylation	F (2e⁻)	Enzyme: UPO, co-substrate: H_2O_2, substrate: 4-ethylbenzoic acid, product: 4-(1-hydroxyethyl)benzoic acid	CB GDE, *A*: 5.5 cm^2	100 mL 100 mM KP_i pH 7, 10 mM substrate, 12.5 nM UPO, flow rate: 40 mL min^{-1}, 250 mL reservoir, applied currents: −10 to −80 mA, room temperature	TTN: 400,000; TOF: 150 s^{-1}, H_2O_2 productivity [a]: 32 μM min^{-1} cm^{-2}, kinetic parameter (*e.g.* K_m)	[34]
Flow-through reactor, chlorination	F (2e⁻)	Enzyme: CPO, co-substrate: H_2O_2, substrate: monochlorodimedone (MCD), product: dichlorodimedone (DMD)	GDE, *A*: 5.5 cm^2	8 mL 100 mM citrate pH 3.5/ 2.8 + 10 mM NaCl, flow rate: 50 mL min^{-1}, 50 mL reservoir, 5–30 nM CPO, applied currents: 5–30 mA, T: 30 °C	TTN: 1,150,000, productivity: 52 g L^{-1} d^{-1}, H_2O_2 productivity [a]: 10 μM min^{-1} cm^{-2}, CE: 50%, A_e/V: 0.11–0.32 cm^2 mL^{-1}, H_2O_2 / CPO productivity: 0.2 μmol H_2O_2 min^{-1} U_{CPO}^{-1}, ETY: 0.16 g cm^{-2} d^{-1}	[13]
Batch & fed-batch, flow-through packed bed reactor, sulfoxidation	F (2e⁻)	Enzyme: CPO, co-substrate: H_2O_2, substrate: thioanisole, product: (*R*)-methylphenylsulfoxide	Graphite grains, *d*: 0.6-1 mm, *A*: 1,350 cm^2	Cathode chamber: 40 mL 100 mM NaOAc pH 5 + 50 mM Na_2SO_4 + 10% (v/v) *t*-butanol, anode chamber: 0.05 M H_2SO_4, 11 U mL^{-1} CPO, total volume: 70–100 mL, flow rate: 100 mL min^{-1}, O_2-saturated, applied potential: 1.95 V	TTN: 145,000, medium conductivity: 13.4 mS cm^{-1}, productivity: 104 g L^{-1} d^{-1}, mass of isolated product: 1.2 g, purity: > 98%, ee: > 98.5%, CE: 75%	[29]
2-compartments reactor, sulfoxidation, 3- electrode configuration	F (2e⁻)	Enzyme: CPO, co-substrate: H_2O_2, substrate: thioanisole, product: (*R*)-methylphenylsulfoxide	GF (cylindrical), *A*: 74 cm^2	300 mL 0.1 M potassium citrate pH 5 + *t*-BuOH, 6 mmol substrate, O_2-saturated; T: 20 °C, 70 nmol CPO, applied potential: −0.5 V vs Ag/AgCl	TTN: 95,000, productivity: 30 g L^{-1} d^{-1}, ee: 98.5%, CE: 65.6%, current: 170 mA, H_2O_2 productivity [a]: 0.002 μM min^{-1} cm^{-2}, conversion: 100%, 23% CPO residual activity	[28]
H-cell, halogenation, 3- electrode configuration	F (2e⁻)	Enzyme: CPO, co-substrate: H_2O_2, substrate: 4-pentanoic acid, KBr, product: bromolactone	GDE with oCNT coating, *A*: 25 cm^2	Cathode chamber: 100 mL 100 mM Na citrate pH 5, 100 mM KBr, 50 mM substrate, 100 nM CPO, applied potential: −0.35 V vs Ag/AgCl or 25 nM at −0.25 V vs Ag/AgCl, anode chamber: 100 mL 100 mM Na citrate pH 5	Formation rate: 4.5 mM h^{-1}, CE: 80%, H_2O_2 productivity [a]: 4.7 μM min^{-1} cm^{-2}	[35]
Flow-through reactor, chlorination, sulfoxidation, oxidation	F (2e⁻)	Enzyme: CPO, co-substrate: H_2O_2, substrate: MCD, thioanisole, indole, product: DMD, methylphenylsulfoxide, oxindole	GDE, *A*: 5.5 cm^2 or 16.5 cm^2	8 mL 0.1 M citrate pH 2.75 + 10 mM NaCl or 0.1 M NaOAc pH 5 + 50 mM Na_sSO_4, reservoir: 50 mL, flow rate: 63 mL min^{-1}, 5 mM substrate, 10–600 nM CPO	TTN: 203,100 (MCD), productivity: 23 g L^{-1} d^{-1} (thioanisole), ETY: 0.87 g cm^{-2} d^{-1} (MCD), CE: 88%, H_2O_2 productivity [a]: 1.5 μM min^{-1} cm^{-2}, initial conversion rate [a]: 43.4 mM h^{-1}	[36]
2-compartments reactor, sulfoxidation, 3- electrode configuration	F (2e⁻)	Enzyme: CPO, co-substrate: H_2O_2, substrate: methyl p-tolyl sulfide, 1-methoxy-4-(methylthio)-benzene (**1**), *N*-MOC–L-methionine methyl ester, product: methyl p-tolyl sulfoxide, methoxypehnylmethylsulfoxide	CF (cylindrical), *A*: 74 cm^2	Cathode chamber: 290 mL 90 vol.–% 100 mM NaOAc + 50 mM Na_2SO_4 pH 5 and 10 vol.–% *tert*-butanol + 6 mmol substrate, T: 20 °C, anode chamber: 10 mL buffer, O_2-	TTN: 64,400 (**1**), isolated yield: 74.3% (**2**), CPO residual activity, conversion: 83% (**1**), K_m and V_{max}, ee: 99% (**1**), enzyme purity: 63%	[37]

ChemElectroChem | Concept doi.org/10.1002/celc.202300226 | Chemistry Europe European Chemical Societies Publishing

Table 2. continued

Process types	e⁻ transfer mechanism	Enzyme, co-factors, substrate and product	Type of working electrode	Process condition	Key performance indicators	Ref.
		(**2**), *N*-MOC–L-methionine methyl ester sulfoxide		saturated, 300 μL or 3.5 mL (22,700–36,500 U mL^{-1} stock solution) CPO, applied potential: −0.5 V vs. Ag/AgCl		
Oxidation, 3-electrode configuration	F ($2e^-$)	Enzyme: CPO, co-substrate: H_2O_2, substrate: cinnamyl alcohol, product: cinnamic aldehyde	Composite film-modified GC comprising chitosan, CPO, DDAB, and Nafion	2 mL 50 mM Phos. pH 4.5, T: 25 °C, O_2-saturated, immo. CPO ($2.9x10^{-4}$ mol L^{-1}) on the electrode surface, 0.05 mmol substrate, applied potential: −0.6 V vs. SCE	analytical yield: 51.8%, TTN: 80,500, formation rate [a]: 1.5 mM h^{-1}, turnover rate: 3.2 μmol h^{-1}, current density: 0.87 mA cm^{-2}, e^- transfer rate: 2.3 s^{-1}	[38]
H-cell, demethylation, 3-electrode configuration	F ($2e^-$)	Enzyme: HRP, co-substrate: H_2O_2, substrate: *N,N*-dimethylaniline, product: *N*-methylaniline, formaldehyde	GC disk, *d*: 5 mm	30 mL (both chamber) 0.2 M Phos. pH 5.5, 0.04 μg mL^{-1} HRP, 2 mM substrate, room temperature, air-saturated, applied current: 0.08 mA	K_m: 0.19 mM, V_{max} 2000 mol min^{-1} mol $enzyme^{-1}$, H_2O_2 productivity [a]: 1.3 μM min^{-1} cm^{-2}, formation rate [a]: 0.1 mM h^{-1}, ratio of formed product to theoretical H_2O_2 generated: 1.75	[39]
Packed-bed flow reactor, 2 compartments, demethylation, 3-electrode configuration	F ($2e^-$)	Enzyme: HRP, co-substrate: H_2O_2, substrate: *N,N*-dimethylaniline, product: *N*-methylaniline, formaldehyde	GF (*V*: 2 cm^3) & RVC (*V*: 8.2 cm^3)	Working volume, [a]: 12.29 mL, 0.2 M Phos. pH 5.5, reservoir: 200 mL, flow rate: 50 mL min^{-1}, O_2-saturated, 2 mM substrate, immo. HRP: 5.4 mg mL^{-1}, applied current: 20 mA	CE: 45%, formation rate [a]: 7.8 mM h^{-1}, K_m: 0.52 mM (substrate) and 0.034 mM (H_2O_2)	[40]
H-cell flow-reactor, oxidation, 3-electrode configuration	F ($2e^-$)	Enzyme: HRP, co-substrate: H_2O_2, substrate: 2,4,6-trimethylphenol, product: 3,5-dimethyl-4-hydroxybenzyl alcohol, 3,5-dimethyl-4-hydroxybenzaldehyde, 2,6-dimethylbenzoquinone	RVC disk (60 ppi), *V*: 0.8 cm^3 −1.96 cm^3	15–120 mL 0.1 M pH 7 Phos., 5 mM substrate, 10 U mL^{-1} HRP, O_2-saturated, electrode rotation: 500 rpm, applied potential: −0.5 V vs. SCE, room temperature, reservoir: 500 mL, flow rate: 200 mL min^{-1}	Total yield: 95%, CE: 62%, charge: 3.7 F, current: 5 mA cm^{-3}	[41]
H-cell, conversion of CO_2 to methanol, 3-electrode configuration	E ($1e^-$)	Enzyme: FDH, FalDH, ADH, co-factor: NADH, substrate: CO_2, product: methanol	Rh complex-grafted CF	10 mL 50 mM Tris-HCl pH 7.4 (Serine Glycerol), N_2-saturated, 1 mg FDH, 1 mg FaldDH, 1 mg ADH, and 1 mM NADH, applied potential: 0.62 V vs. Ag/AgCl/KCL (3 M)	Enzyme activity: 384.6 U mL^{-1}, current density: −0.23 mA cm^{-2}, charge transfer resistance: 48 Ω, co-factor yield: 60%, formation rate: 0.48 mM h^{-1}	[31]
H-cell, conversion of CO_2 to formate, 3- electrode configuration	E ($1e^-$)	Enzyme: FDH, co-factor: NADH, substrate: CO_2, product: formate	Cu foam, *A*: 2.66 cm^2	Both chamber 15 mL 0.2 M PBS pH 7, 1 mg mL^{-1} FDH (free), 1 mg mL^{-1} cm^{-2} immo. FDH on EPSNF, NAD^+: 0.85 (free FDH) & 0.95 mM (immo. FDH), applied potential: −1.1 V vs. Ag/AgCl/KCL (3 M), CO_2 flow rate: 30 mL min^{-1}	Immo. FDH stability: 41% after 20 d, immo. FDH relative activity: 43%, reusability of immo. FDH: 8 cycles, immo. efficiency: 57%, optimum co-factor concentration: 0.45 mM (free FDH) & 0.51 mM (immo. FDH), product concentration: 0.61 mM (free FDH) & 0.31 mM (immo. FDH), yield of co-factor: 96%	[42]
Semi-continuous, H-cell with *in situ* product removal, conversion of CO_2 to	E ($1e^-$)	Enzyme: FDH, co-factor: NADH, substrate: CO_2, product: formate	Cu foam, *A*: 2.66 cm^2	Both chamber 20 mL 0.2 M PBS pH 7, 1 mg mL^{-1} cm^{-2} immo. FDH on EPSNF, NAD^+: 0.95 mM, applied po-	Regenerated co-factor concentration: 0.5 mM, immo. FDH relative activity: 43%, immo. FDH activity: 1.6 U mg^{-1}, immo.	[43]

ChemElectroChem | Concept doi.org/10.1002/celc.202300226 | Chemistry Europe European Chemical Societies Publishing

Table 2. continued

Process types	e^- transfer mechanism	Enzyme, co-factors, substrate and product	Type of working electrode	Process condition	Key performance indicators	Ref.
formate, 3- electrode configuration				tential: −1.1 V vs. Ag/AgCl/KCL (3 M), CO_2 flow rate: 30 mL min^{-1}, ethyl acetate as extraction phase, half of the reaction volume was replaced with fresh NAD^+ solution every hour	efficiency: 57%, loading capacity of immo. FDH: 90 μg cm^{-2}, reusability of immo. FDH: 8 cycles, immo. FDH stability: 41% after 20 d, product concentration: 0.44 mM	
Oxidation & reversible and interconversion of H_2 and CO_2 into formate, 3-electrode configuration	A ($1e^-$)	Enzyme: FDH, H_2ase, substrate: formate, CO_2, H_2, product: formate, H_2	Macro-mesoporous inverse opal ITO, thickness: 25 μm, *A*: 0.25 cm^2	2 mL 100 mM CO_2/$NaHCO_3$ pH 6.5–6.7, 50 mM KCl, 1 bar CO_2 or 0.4/0.6 bar H_2/CO_2, formate:10 or 20 mM, T: 23 or 25 °C, FDH: 2 μL, 19 μM, H_2ase: 2 μL, 5 μM, co-assembled: FDH: 19 nM, H_2ase: 3.4 nM, scan rate: 5 mV s^{-1}	current density: 0.25 mA cm^{-2}, CE: 81%, product concentration [a]: 2.91 mM H_2 & 18 mM formate, formation rate [a]: 0.12 mM H_2 h^{-1} & 0.67 mM formate h^{-1}, TON: 23,000, TOF: 6.4 s^{-1}	[33]
Flow- and membrane-less reactor, oxidation, 2- and 3-electrode configuration	C ($1e^-$)	Enzyme: GOx, HRP, BOD, mediator: tetrathiafulvalene, O_2, substrate: glucose, product: gluconic acid, side products: D-arabinose, formic acid	Vulcan carbon nanomaterials, *A*: 0.28 cm^2 or 1 cm^2	70 mL 0.1 M Phos. pH 6, 20 mM substrate, flow rates: 2–14 mL min^{-1}, O_2 supply: 500 mL min^{-1}, T: 22 °C, 10 mg mL^{-1} immo. GOx (anode) and 6 mg mL^{-1} and 18 mg mL^{-1} immo. GOx-HRP or 6 mg mL^{-1} and 10 mg mL^{-1} immo. GOx-BOD (cathode), applied cell potential: 0.0 V vs. SCE	Selectivity: 97%, conversion: 80%, productivity [a]: 864 g L^{-1} d^{-1}, product concentration [a]: 15.8 mM, yield: 75%, E-factor: 9, atom efficiency: 100%, CE: 100% (anode) & 16% (cathode), current density: 0.6 mA cm^{-2}	[22]
Oxidation, 3-electrode configuration	C ($2e^-$)	Enzyme: GOx, co-substrate: O_2, substrate: glucose, product: gluconic acid, H_2O_2	Polypyrole (film)-GOx-modified Pt, film thickness: 500 nm	2.5 mL 0.1 M Phos. pH 7, 20 mM substrate, 0.565 U GOx, air-saturated, room temperature, applied potential: 0.4 V vs. SCE	Thiele modulus, effectiveness factor, conversion: 62%, productivity [a]: 4.8 g L^{-1} d^{-1}, initial conversion rate: 1.6 mM h^{-1}	[44]
Packed-bed reactor, oxidation, 3-electrode configuration	B ($1e^-$)	Enzyme: GDH, co-factor: NADH, mediator: ABTS, methylene blue, substrate: glucose, product: lactone	GC particles, *A*: 24 m^2, m: 7.8 g, splintered: 1000–2000 μm	15 mL 50 mM TRIS/HCl pH 8, 2 U GDH, 10 mM substrate, 0.1 mM NADH, 0.01 mM ABTS, flow rate 2.5 mL min^{-1}, applied potential: 0.7 V vs. Ag/AgCl/KCL (3 M)	TTN of mediator: 1,860, TTN of co-factor: 93, productivity [a]: 33.6 g L^{-1} d^{-1}, conversion: 93%, TOF of mediator [a]: 33.3 s^{-1}, CE: 87%	[45]
Reduction, 3-electrode configuration	E ($1e^-$)	Enzyme: DSDH, co-factors: NADH, substrate: D-Fructose, product: D-Sorbitol	Multi-layer bio-electrode consisted of Rh-complex and glassy fibre on Bucky-Paper, *A*: 4 cm^2	30 mL 50 mM PBS pH 6.5, 1 mM NADH, 1 mM substrate, 1 mM NADH, immo. DSDH on the electrode, N_2-saturated, applied potential: −0.72 V vs. Ag/AgCl	TTN: 12,000, TTN of-co-factor: 2.61, TOF: 0.19 s^{-1}, TOF of co-factor: 1.3 s^{-1}, CE: 83%, conversion: 87%, current density: 0.037 mA cm^{-2}	[46]

ChemElectroChem | Concept doi.org/10.1002/celc.202300226 | Chemistry Europe European Chemical Societies Publishing

Table 2. continued

Process types	e^- transfer mechanism	Enzyme, co-factors, substrate and product	Type of working electrode	Process condition	Key performance indicators	Ref.
Hydroxylation, 3- electrode configuration	C ($1e^-$)	Enzyme: cytochrome P450 monooxygenases (P450cin), mediator: CoSep, PSF, SAF, FAD, FMN, substrate: 1,8-cineole, product: 2β-hydroxy-1,8-cineole	Pt, *A*: 2 cm^2	50 mM KP_i pH 7.5, 1 μM CinA, 3 μM CinC, 6 mM substrate, 1500 U mL^{-1} catalase, 5 mM CoSep, 1.2 mM PSF, 1.2 mM SAF, 0.6 mM FAD, 0.6 mM FMN, 0.8 mM potassium ferrocyanide, 0.8 mM ethyl-/methyl viologen, room temperature, applied potential: −0.75 V vs. Ag/AgCl	TTN: 2,600, formation rate: 6.5 nmol(product)-$nmol^{-1}$ (P450) min^{-1} cm^{-2} (electrode), CE: 10%,	[47]

[a] Unless stated otherwise, batch reaction process in a standard one chamber reactor using 2-electrode configuration are described. **e^- transfer mechanism**, each alphabet refers to the electroenzymatic process depicted in Figure 1. **Enzyme**, ADH: alcohol dehydrogenase, BOD: bilirubin oxidase, CPO: chloroperoxidase, DSDH: D-sorbitol dehydrogenase, FalDH: formaldehyde dehydrogenase, FDH: formate dehydrogenase, GDH: glucose dehydrogenase, GOx: glucose oxidase, H_2ase: hydrogenase, HRP: horseradish peroxidase, UPO: unspecific peroxygenase. **Co-factor/ mediator**, ABTS: 2,2′-azino-bis(3-ethylbenzothiazoline-6-sulfonic acid), CoSep: cobalt sepulchrate, FAD: flavin adenine dinucleotide, FMN: flavin mononucleotide, NAD^+: oxidized nicotinamide adenine dinucleotide, NADH: reduced nicotinamide adenine dinucleotide, PSF: phenosafranine, SAF: safranine. **Type of working electrode**, *A*: geometric surface area, CB: carbon black, CF/ GF: carbon/ graphite felt, oCNT: oxidized carbon nanotubes, Cu: copper, *d*: diameter, DDAB: didodecylmethylammonium bromide, GC: glassy carbon, GDE: gas diffusion electrode, ITO: indium tin oxide, ppi: pores per linear inch, Pt: platinum, Rh: rhodium, RVC: reticulated vitreous carbon, *V*: volume. **Process condition**, Ag/AgCl: silver/silver chloride, EPSNF: electrospun polystyrene nanofiber, Immo.: immobilized, KBr: potassium bromide, KCl: potassium chloride, KP_i: potassium phosphate, Na_2SO_4: sodium sulfate, NaCl: sodium chloride, NaOAc: sodium acetate, PBS: phosphate-buffered saline, Phos.: Phosphate buffer, SCE: saturated calomel electrode, TRIS/HCl: TRIS-hydrochloride. **Key performance indicator**, A_e/V: ratio of apparent electrode surface area to reaction volume, CE: current efficiency, d: days, ee: enantiomeric excess, ETY: electrode-time yield, K_m: Michaelis-Menten constant, STY: space-time yield, TOF: turnover frequency, TON: turnover number, TTN: total turnover number, V_{max} : maximum reaction rate. [a)] parameter and key performance indicators were recalculated/ converted from the actual reported value and its unit using the available information from the corresponding publication to have the same consistent unit with the other references.

Finally, in the case of electrochemical and electroenzymatic processes, electricity prices can be subject to very strong fluctuations due to political decisions, although they are quantitative values.

5. Case Study: Hydrogen Peroxide-Driven Bio-Catalysis – Using Quantitative and Non-quantitative Parameters To Compare Different Processes

As shown above, both quantitative and non-quantitative parameters must be considered to characterise or to compare processes. The following case study illustrates how these parameters can be applied. Here, we compare different enzymatic processes for the enzyme catalysed synthesis of (*R*)-1-phenylethanol from ethylbenzene with an unspecific peroxygenase (UPO, Scheme 1).

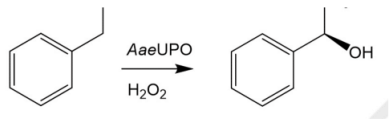

Scheme 1. Hydroxylation of ethylbenzene to (*R*)-1-phenylethanol using an unspecific peroxygenase (UPO)

In general, the chemical oxyfunctionalization of C–H bonds requires elevated temperatures and large amounts of organic solvents. However, there are biocatalysts that allow the conversion of non-activated C–H bonds under mild conditions. A prominent and emerging example is the unspecific peroxygenase from the fungus *Agrocybe aegerita* (*Aae*UPO), which can be exploited for regio- and stereospecific oxyfunctionalization of various substrates.[49,50] UPOs have emerged as "dream biocatalysts" of great industrial interest because of their tremendous potential to catalyse this oxyfunctionalization. For this reason, and because of the availability of several well-described processes, these enzymes were used in this case study. A major drawback of *Aae*UPO, which prevents its application on a technical scale, is its inactivation at excess concentrations of the co-substrate H_2O_2. Therefore, several approaches to supply hydrogen peroxide at low but sufficient levels have been investigated in combination with the UPO (Figure 2):

- Feeding of H_2O_2: Kluge *et al.* used a combined H_2O_2 and substrate solution feeding.[51,52]
- Immobilised enzymes and feeding of H_2O_2: Hobisch et al. used a covalently immobilized UPO variant in a rotating bed reactor two-liquid-phase system.[53]
- Enzyme cascades: An enzymatic methanol oxidizing cascade was used to provide sufficient hydrogen peroxide concentrations for *Aae*UPO. Here the complete oxidation of 1 equivalent of methanol resulted in the generation of 3 equivalents of hydrogen peroxide.[54]

ChemElectroChem
Concept
doi.org/10.1002/celc.202300226
Chemistry Europe
European Chemical Societies Publishing

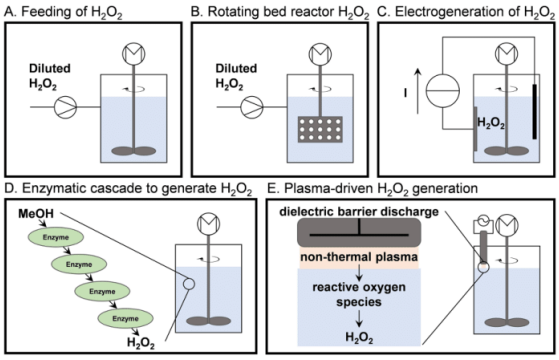

Figure 2. Schematic representation of the different approaches for the hydroxylation of ethylbenzene to (*R*)-1-phenylethanol using the unspecific peroxygenase from the fungus *Agrocybe aegerita* (*Aae*UPO, description in the main text)

- Plasma driven system: The *in-situ* production of H_2O_2 by dielectric barrier discharge plasma was coupled with the peroxygenase reaction.[55]
- Electrochemistry: The electrochemical reduction of molecular oxygen to H_2O_2 using a gas diffusion electrode in combination with the peroxygenase was investigated by Horst et al.[27]

For comparison of these processes, 5 parameters were used as examples. Three of them are of quantitative nature and are listed in Table 1 (final product concentration, space-time yield, total turnover number). For comparison, the highest value is defined to be 100%. All values between 100% and 90% are assigned a value of 5, values between 75 and 90% are assigned a value of 4, values between 50 and 75% are assigned a value of 3, and values between 20 and 50% are assigned a value of 2. Finally, values between 0 and 20% are assigned a value of 1. In addition, two non-quantitative parameters are considered. The "simplicity of the system" means how close a process is to common enzyme technology processes and is therefore related to the estimated investment costs for new technology deployment and staff training. This parameter can also be referred to as the hurdle for implementing an "unusual" technology in an enzyme process. Scalability describes the challenges of transferring laboratory processes to large-scale applications. At this early stage of the process, the variable costs cannot be definitively determined, so they are estimated here (parameter estimated flexible cost to operate). The fewer chemicals required for the process, the better the process is evaluated. Again, the processes were assigned values from 5 (best) to 1 (worst). This assignment was made after extensive discussion among the team of authors; it can be assumed that other teams of experts will come to slightly different conclusions, but most probably the tendency will remain the same (Table 3 and Figure 3).

A number of conclusions can be drawn from this comparison, e.g. (i) there is no perfect procedure yet, (ii) the process in the rotating bed-reactor with immobilized enzymes and feeding of diluted H_2O_2 shows the best overall performance so far and (iii) the electrochemical system needs to be improved with respect to the product concentration and thus the substrate concentration used, as well as the space-time yield.

Although the evaluation of each parameter can be different, as described above, this principle seems to be the only way to compare different processes. Only focusing on single variables such as TTN or productivity or only using quantitative data would lead to an incomplete evaluation. The strength of this evaluation system also lies in its ability to identify weaknesses in a process at an early stage of development. The following two comments are especially important. First, we are comparing published performance indicator, not technologies. In some cases, the technology is still in the early stages of development and significant improvements in performance indicators can be expected. Second, all of the processes described do not yet meet the typical industrial requirements for an enzyme-based process.[23] Here, the following values are given as examples for the production of a prochiral ketone: substrate loading $>160\ g\,L^{-1}$, reaction time $<10\ h$, catalyst loading $<1\ g\,L^{-1}$, isolated yield $>90\%$, and space-time yield/productivity $>16\ g\,L^{-1}\,h^{-1}$. Processes with comparably high metrics should also be the objective for process development when using UPO as enzyme. Since typical electroenzymatic processes (Table 2) are usually also aimed at the production of bulk chemicals, comparable performance indicators should be realized.

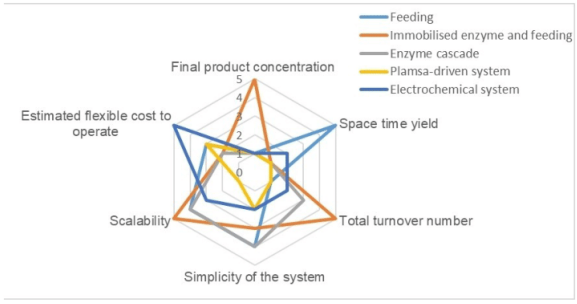

Figure 3. Example of the use of quantitative and non-quantitative parameters to compare different approaches to hydroxylate ethylbenzene to (*R*)-1-phenylethanol using an unspecific peroxygenase.

ChemElectroChem | Concept doi.org/10.1002/celc.202300226 | Chemistry Europe European Chemical Societies Publishing

Table 3. Evaluation of different approaches to provide H_2O_2 for the hydroxylation of ethylbenzene to (*R*)-1-phenylethanol using the unspecific peroxygenase from the fungus *Agrocybe aegerita* (*Aae*UPO).

	Feeding	Immobilized enzyme and feeding	Enzyme cascade	Plasma-driven	Electro-chemical system
Final product concentration	0.4 g L^{-1}	50.6 g L^{-1}	3.8 g L^{-1}	0.2 g L^{-1}	2.2 g L^{-1}
	0.8 %	100.0 %	7.5 %	0.3 %	4.3 %
	1	5	1	1	1
Productivity	2.50 g L^{-1} h^{-1}	0.41 g L^{-1} h^{-1}	0.03 g L^{-1} h^{-1}	0.34 g L^{-1} h^{-1}	0.55 g L^{-1} h^{-1}
	100.0 %	16.4 %	1.3 %	13.5 %	22.0 %
	5	1	1	1	2
Total turnover number	43,000	909,000	468,500	13,787	400,000
	4.7 %	100.0 %	51.5 %	1.5 %	44.0 %
	1	5	3	1	2
Simplicity of the system	4	3	4	2	2
	Installing a pumping system can be regarded as straightforward. Reaction volume increases when diluted solutions are used.	Using a specialized type of reactor and immobilisation plus losses during enzyme immobilisation (not regarded).	For an enzyme technician, the threshold for using an enzyme cascade is quite low. The product isolation can be a challenge.	For the introduction of a completely different technology, there is a high threshold.	For the introduction of a completely different technology, there is a high threshold.
Scalability	4	5	4	1	3
	On a larger scale, there may be problems with heterogeneity.	Scale-up was shown in chemical engineering.	On a larger scale, there may be problems with heterogeneity.	Up-scaling has not been the subject of much research so far.	Up-scaling has been demonstrated in process engineering, not for enzyme processes.
Estimated flexible cost to operate	3	2	2	3	5
	Here, only H_2O_2 has to be added, and the authors have developed a recycling concept for the solvent. However, enzymatic stability is very low.	Enzyme immobilization and high losses during the immobilization process result in high costs.	High costs for the different enzymes and cofactors.	Only small amounts of reagents are required. The energy consumption has not yet been evaluated.	No additional reagents are required and energy efficiency is very high.

6. Summary and Outlook

The integration of enzymatic and electrochemical processes offers a unique opportunity to optimize production processes. Recently, more and more electroenzymatic processes have shown impressive performance indicators at laboratory scale, which has led to scientific interest in their technical implementation. For this transfer of processes from laboratory scale to technical applications, different options for electroenzymatic processes have to be considered on the one hand, but also in contrast to alternative processes. A large number of relevant parameters can be used for this purpose, and it must be decided in each case which parameters are relevant. However, it is important to define benchmarks or key performance indicators for all laboratory investigations - only in this way can promising laboratory results be transferred to applications.

Abbreviations

Symbols and descriptions used in formulas.

A_e	Electrode surface (m^2)
c_i	Concentration with indices *i*: p = product, s = substrate, waste = waste, r = reactants (co-factor, co-substrate or substrate), biocat = biocatalyst (mol L^{-1})
D_m	Diffusion coefficient (m^2 s^{-1})
$\Delta E_{cell,eq}$	Difference of working and counter electrode potentials in a reversible equilibrium (V)
ee	Enantiomeric excess (–)
$E_{eq,WE}$	Equilibrium working electrode potential (V)
E_{WE}	Electrode potential working electrode (V)
ETY	Electrode surface time yield (kg m^{-2} s^{-1})
F	Faraday constant (A s mol^{-1})
ΔG	Theoretical Gibbs energy change (J mol^{-1})
I	Current (A)
j	Current density (A m^{-2})
j_v	Volumetric current density (A m^{-3})
k_{cat}	Catalytic rate constant (s^{-1})
k_{film}	Film mass transfer coefficient (m s^{-1})
K_m	Michaelis-Menten-constant (mol L^{-1})
L	Characteristic length (m)
m_p	Mass of product (kg)

ChemElectroChem | Concept | doi.org/10.1002/celc.202300226 | Chemistry Europe European Chemical Societies Publishing

n_i	Mole amount with Indices *i*: p = product, r = reactants (co-factor, co-substrate or substrate), biocat = biocatalyst, R = (R)-enantiomer, S = (S)-enantiomer (mol)
Q	Electric charge (A s)
$\dot{q}_{p,v}$	Volumetric productivity (kg m^{-3} s^{-1})
Re	Reynolds number (–)
S_r	Selectivity (–)
Sc	Schmidt number (–)
Sh	Sherwood number (–)
t	Time (s)
$t_{0.5}$	Half-life time (s)
TOF	Turnover frequency (mol$_p$ mol$_{biocat}^{-1}$ s^{-1})
TTN/TTN$_{cofactor}$	Total turnover number (mol$_p$ mol$_{biocat/cofactor}^{-1}$)
U_{cell}	Cell voltage (V)
V	Liquid volume of compartment with working electrode (m^3)
V_{max}	Maximum rate at substrate saturation (mol L^{-1} s^{-1})
w	Specific electric energy consumption (sEEC) (J kg^{-1})
X	Conversion (–)
Y	Reaction yield (–)
$Y_{p/e}$	Product yield per electron[18] (–)
Z	Charge number (–)
σ_p	Space time yield (STY) (kg m^{-3} s^{-1})
η_{WE}	Overpotential (V)
Φ_G	Energy efficiency (–)
Φ_p^e	Current efficiency (–)
v_i	Stochiometric number with indices *i*: p = product, r = reactants (co-factor, co-substrate or substrate) (–)
τ	Residence time (s)

Acknowledgements

This work was performed within the project "Bioelectrochemical and engineering fundamentals to establish electro-biotechnology for biosynthesis - Power to value-added products (eBiotech)" funded by the Deutsche Forschungsgemeinschaft (DFG) - project number 422694804. NT, AL and DH thank the Deutsche Forschungsgemeinschaft for funding the project "Enzyme and reaction engineering of unspecific peroxygenase driven hydroxylation of butane (BUPOx)" (project number 465474720). Open Access funding enabled and organized by ProjektDEAL.

Conflict of Interests

The authors declare no conflict of interest.

Data Availability Statement

Data sharing is not applicable to this article as no new data were created or analyzed in this study.

Keywords: Biocatalysis · Electrobiotechnology · Enzymatic electrosynthesis · Performance indicators · Unspecific peroxidases

[1] F. Harnisch, D. Holtmann in *Bioelectrosynthesis* (Eds.: F. Harnisch, D. Holtmann), Springer International Publishing, Cham, **2019**, pp. 1–14.
[2] Q. Liang, Y. Gao, Z. Li, J. Cai, N. Chu, W. Hao, Y. Jiang, R. J. Zeng, *Front. Environ. Sci. Eng.* **2022**, *16*, 42.
[3] J. S. Deutzmann, F. Kracke, W. Gu, A. M. Spormann, *Environ. Sci. Technol.* **2022**, *56*, 16073.
[4] Q. Fu, Y. He, Z. Li, J. Li, L. Zhang, X. Zhu, Q. Liao, *Energy Convers. Manage.* **2022**, *268*, 116018.
[5] W. Cai, K. Cui, Z. Liu, X. Jin, Q. Chen, K. Guo, Y. Wang, *Chem. Eng. J.* **2022**, *428*, 132093.
[6] N. Teetz, D. Holtmann, F. Harnisch, M. Stöckl, *Angew. Chem. Int. Ed.* **2022**, *134*, e202210596.
[7] M. Stöckl, S. Harms, I. Dinges, S. Dimitrova, D. Holtmann, *ChemSusChem* **2020**, *13*, 4086.
[8] F. Mayer, F. Enzmann, A. M. Lopez, D. Holtmann, *Bioresour. Technol.* **2019**, *289*, 121706.
[9] R. Wu, C. Ma, Z. Zhu, *Curr. Opin. Electrochem.* **2020**, *19*, 1.
[10] S. Yu, N. V. Myung, *Front. Chem.* **2020**, *8*, 620153.
[11] A. Gemünde, B. Lai, L. Pause, J. Krömer, D. Holtmann, *ChemElectroChem* **2022**, *9*, e202200216.
[12] M. Dias Gomes, J. M. Woodley, *Molecules* **2019**, *24*.
[13] D. Holtmann, T. Krieg, L. Getrey, J. Schrader, *Catal. Commun.* **2014**, *51*, 82.
[14] T. Krieg, A. Sydow, U. Schröder, J. Schrader, D. Holtmann, *Trends Biotechnol.* **2014**, *32*, 645.
[15] M. Sharma, S. Bajracharya, S. Gildemyn, S. A. Patil, Y. Alvarez-Gallego, D. Pant, K. Rabaey, X. Dominguez-Benetton, *Electrochim. Acta* **2014**, *140*, 191.
[16] C. Kohlmann, W. Märkle, S. Lütz, *J. Mol. Catal. B* **2008**, *51*, 57.
[17] L. M. Schmitz, K. Rosenthal, S. Lütz, *Adv. Biochem. Eng./Biotechnol.* **2019**, *167*, 87.
[18] T. Krieg, J. Madjarov, L. F. M. Rosa, F. Enzmann, F. Harnisch, D. Holtmann, K. Rabaey, *Adv. Biochem. Eng./Biotechnol.* **2019**, *167*, 231.
[19] S. Arshi, M. Nozari-Asbemarz, E. Magner, *Catalysts* **2020**, *10*, 1232.
[20] A. H. Sulaymon, A. H. Abbar in *Electrolysis* **2012**.
[21] R. A. Sheldon, *Green Chem.* **2007**, *9*, 1273.
[22] M. Varničić, I. N. Zasheva, E. Haak, K. Sundmacher, T. Vidaković-Koch, *Catalysts* **2020**, *10*, 269.
[23] S. Wu, R. Snajdrova, J. C. Moore, K. Baldenius, U. T. Bornscheuer, *Angew. Chem. Int. Ed.* **2021**, *60*, 88.
[24] J. M. Pingarrón, J. Labuda, J. Barek, C. M. A. Brett, M. F. Camões, M. Fojta, D. B. Hibbert, *Pure Appl. Chem.* **2020**, *92*, 641.
[25] G. Gritzner, G. Kreysa, *IUPAC Standards Online*, De Gruyter, **2016**.
[26] *Quantities, units and symbols in physical chemistry*, Royal Soc. of Chemistry, Cambridge, **2007**.
[27] A. Horst, S. Bormann, J. Meyer, M. Steinhagen, R. Ludwig, A. Drews, M. Ansorge-Schumacher, D. Holtmann, *J. Mol. Catal. B: Enzym* **2016**, *133*, 137–142.
[28] S. Lütz, E. Steckhan, A. Liese, *Electrochem. Commun.* **2004**, *6*, 583.
[29] S. Lütz, K. Vuorilehto, A. Liese, *Biotechnol. Bioeng.* **2007**, *98*, 525.
[30] M. Varničić, T. Vidaković-Koch, K. Sundmacher, *Electrochim. Acta* **2015**, *174*, 480.
[31] Z. Zhang, H. Wang, Y. Nie, X. Zhang, X. Ji, *Front. Chem.* **2022**, *10*, 894106.
[32] P. Chiranjeevi, M. Bulut, T. Breugelmans, S. A. Patil, D. Pant, *Curr. Opin. Green Sustain. Chem.* **2019**, *16*, 65.
[33] K. P. Sokol, W. E. Robinson, A. R. Oliveira, S. Zacarias, C.-Y. Lee, C. Madden, A. Bassegoda, J. Hirst, I. A. C. Pereira, E. Reisner, *J. Am. Chem. Soc.* **2019**, *141*, 17498.
[34] S. Bormann, D. Hertweck, S. Schneider, J. Z. Bloh, R. Ulber, A. C. Spiess, D. Holtmann, *Biotechnol. Bioeng.* **2021**, *118*, 7.
[35] S. Bormann, M. M. C. H. van Schie, T. P. de Almeida, W. Zhang, M. Stöckl, R. Ulber, F. Hollmann, D. Holtmann, *ChemSusChem* **2019**, *12*, 4759.
[36] T. Krieg, S. Hüttmann, K.-M. Mangold, J. Schrader, D. Holtmann, *Green Chem.* **2011**, *13*, 2686.
[37] C. Kohlmann, S. Lütz, *Eng. Life Sci.* **2006**, *6*, 170.
[38] H. Tian, S. Mu, H. Li, X. Wu, Z. Lu, *ChemCatChem* **2012**, *4*, 1850.
[39] J. K. Chen, K. Nobe, *J. Electrochem. Soc.* **1993**, *140*, 299.
[40] J. K. Chen, K. Nobe, *J. Electrochem. Soc.* **1993**, *140*, 304.
[41] P. N. Bartlett, D. Pletcher, J. Zeng, *J. Electrochem. Soc.* **1999**, *146*, 1088.

ChemElectroChem
Concept
doi.org/10.1002/celc.202300226
Chemistry Europe
European Chemical Societies Publishing

[42] R. Barin, D. Biria, S. Rashid-Nadimi, M. A. Asadollahi, *J. CO_2 Util.* **2018**, *28*, 117.
[43] R. Barin, D. Biria, S. Rashid-Nadimi, M. A. Asadollahi, *Chem. Eng. Process.* **2019**, *140*, 78.
[44] P. Gros, A. Bergel, *AIChE J.* **2005**, *51*, 989.
[45] S. Kochius, J. B. Park, C. Ley, P. Könst, F. Hollmann, J. Schrader, D. Holtmann, *J. Mol. Catal. B: Enzym* **2014**, *103*, 94.
[46] L. Zhang, M. Etienne, N. Vilà, T. X. H. Le, G.-W. Kohring, A. Walcarius, *ChemCatChem* **2018**, *10*, 4067.
[47] S. Z. Çekiç, D. Holtmann, G. Güven, K.-M. Mangold, U. Schwaneberg, J. Schrader, *Electrochem. Commun.* **2010**, *12*, 1547.
[48] M. C. Potter, *Proc. R. Soc. Lond. B.* **1911**, *84*, 260.
[49] M. Hobisch, D. Holtmann, P. Gomez de Santos, M. Alcalde, F. Hollmann, S. Kara, *Biotechnol. Adv.* **2021**, *51*, 107615.
[50] B. O. Burek, S. Bormann, F. Hollmann, J. Z. Bloh, D. Holtmann, *Green Chem.* **2019**, *21*, 3232.
[51] S. Friedrich, G. Gröbe, M. Kluge, T. Brinkmann, M. Hofrichter, K. Scheibner, *J. Mol. Catal. B: Enzym* **2014**, *103*, 36.
[52] M. Kluge, R. Ullrich, K. Scheibner, M. Hofrichter, *Green Chem.* **2012**, *14*, 440.
[53] M. Hobisch, P. de Santis, S. Serban, A. Basso, E. Byström, S. Kara, *Org. Process Res. Dev.* **2022**, *26*, 2761.
[54] Y. Ni, E. Fernández-Fueyo, A. Gomez Baraibar, R. Ullrich, M. Hofrichter, H. Yanase, M. Alcalde, W. J. H. van Berkel, F. Hollmann, *Angew. Chem. Int. Ed.* **2016**, *55*, 798.
[55] A. Yayci, Á. G. Baraibar, M. Krewing, E. F. Fueyo, F. Hollmann, M. Alcalde, R. Kourist, J. E. Bandow, *ChemSusChem* **2020**, *13*, 2072.

Manuscript received: May 22, 2023
Revised manuscript received: July 26, 2023
Version of record online: September 29, 2023

5.1. Quantitative Analysis of Electroenzymatic Hydroxylation of Benzene

After summarizing and evaluating process parameters and PIs from various literature in the field of bioelectrochemistry, particularly in electroenzymatic processes, it is evident that there are numerous ways to characterize and describe different processes, or even a specific process. To enable objective comparisons between studies, both quantitatively and qualitatively, it is suggested that certain PIs and process parameters be reported in respective publications. These parameters and PIs can be summarized into four groups: general reaction engineering PIs, enzymatic PIs, electrochemical PIs, and reactor indicators. Essential PIs for electroenzymatic processes from these groups include, but not limited to: productivity, final product concentration, co-substrate productivity, F.E., current density, cell potential, TTN and TOF. Furthermore, process parameters like starting substrate and product concentration, applied current, geometrical area of working electrode, biocatalyst loading and activity, experiment duration and reaction volume are as equally important since they enable the calculation of aforementioned PIs and additionally the calculation of conversion, yield, electrode surface to volume ratio, enzyme half-lime time and electrode-time yield.

Building upon the comprehensive evaluation of process parameters and PIs, the knowledge gained regarding the standardized reporting of these metrics was systematically implemented within the electroenzymatic system studied in this dissertation. The electrobiotechnological processes investigated herein belong to the group of enzymatic electrosynthesis, where the co-substrate H_2O_2 is electrochemically generated *in situ* and subsequently utilized by the H_2O_2-dependent enzyme for biocatalytic reactions.

In order to develop an optimizable platform for H_2O_2-dependent enzymatic reactions and at the same time enhance the biocatalyst's stability, a controllable *in situ* electrogeneration of H_2O_2 needed to be established first. The *in situ* electrogeneration of H_2O_2 was realized via the application of the AiO electrode system. Preliminary experiments were conducted to gather initial information. Unless otherwise indicated, experiments were performed as biological duplicates. That is to say, the identical experiments were repeated twice under the same reaction conditions. Methods utilized to conduct experiments in this subchapter are specified in the appendix **11.1. Supporting Information to Chapter 5**. Before combining the AiO electrode with a biocatalytic reaction, its ability to generate H_2O_2 *in situ* was characterized. Due to its physical flexibility, carbon felt was utilized as the cathode, as it could be suitably wrapped

around the AiO electrode scaffold. The AiO electrode characterization was performed in an abiotic condition, initially in 0.05 M citrate/ sodium phosphate buffer pH 5, as this was found to be the best buffer for r*Aae*UPO in terms of its activity and stability. The H_2O_2 specific productivity, the F.E. and the cell potential from the preliminary study are shown in figure **Fig. 5. 1. A**.

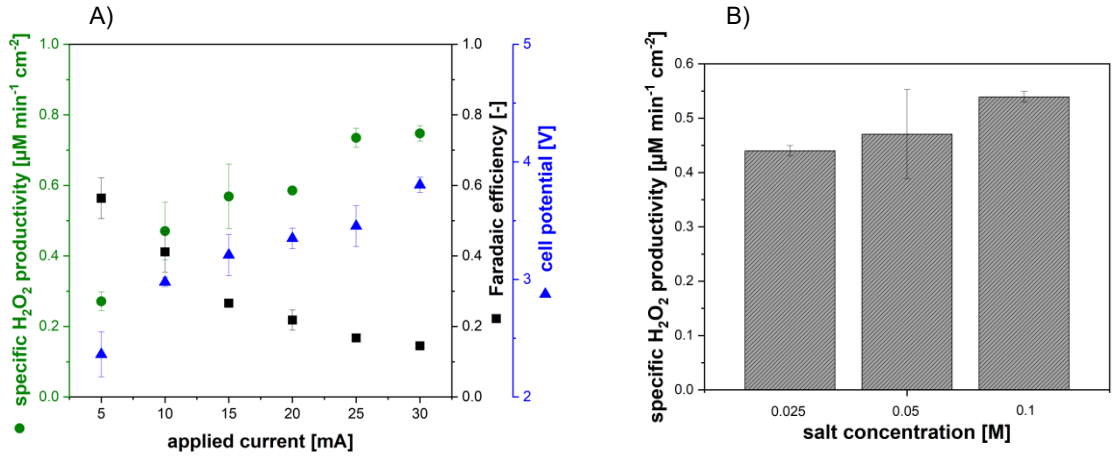

Fig. 5. 1. A) *Specific H_2O_2 productivity, Faradaic efficiency (F.E.) and resulting cell potential as a function of applied current.* ***B)*** *Specific H_2O_2 productivity at different citrate/ sodium phosphate concentrations. Reaction condition: carbon felt working electrode (11 cm^2), platinized titanium counter electrode (4.24 cm^2), 200 mL 0.05 M citrate/ sodium phosphate pH 5, 22 ± 1 °C, 250 rpm. Applied potential of 3 V in the experiment performed at various citrate/ sodium phosphate concentrations. F.E. was determined after 30 min. Biological duplicates were performed.*

The H_2O_2 productivity increased with increasing applied current up to 0.75 µM min^{-1} cm^{-2} at 30 mA. In parallel, the F.E. decreased, while the resulting cell potential showed an almost linear increase. The decrease in the F.E. could potentially be attributed to the occurrence of undesirable side reactions, such as the evolution of hydrogen, the complete reduction of oxygen to water, as well as further redox reactions of H_2O_2 to radicals and water. The formation of bubbles on the cathode surface, which was observed particularly at high current, may indicate the occurrence of the hydrogen evolution reaction. The rate of competing reactions is reported to depend on the current and potential applied during the electrochemical process [84,85], which is consistent with the observed results. In regard to the impact of salt concentration on H_2O_2 productivity, experiments conducted at a constant potential of 3 V revealed a notable enhancement in H_2O_2 productivity with increasing citrate/ sodium phosphate concentrations (**Fig. 5. 1. B**). This phenomenon can be ascribed to the enhanced conductivity provided by the added salt, which facilitates a higher current flow and consequently a higher rate of H_2O_2 formation at the same applied potential (**Table 5. 1**). In conclusion, the preliminary results demonstrated that the combination of a carbon felt cathode within the AiO electrode system is effective for the *in situ* generation of H_2O_2.

Table 5. 1. *Medium conductivity, resulting current and H_2O_2 productivity at different citrate/ sodium phosphate concentrations and at 3 V.*

Salt concentration [M]	Conductivity [mS cm^{-1}]	Current [mA]	H_2O_2 productivity [µM min^{-1} cm^{-2}]
0.025	3.01	11.5	0.45
0.05	6.57	16.2	0.47
0.1	12.05	26.2	0.54

The integration of the electrochemical and biocatalytic systems enabled the establishment of a BES for r*Aae*UPO-catalyzed hydroxylation. This integration facilitated the simultaneous generation and consumption of H_2O_2 in a batch operation mode, enabling the electroenzymatic hydroxylation to occur. The electroenzymatic reaction was performed at electrical currents between 5 mA and 30 mA, identical to the previously tested range. In the preliminary model reaction system, r*Aae*UPO catalyzed the hydroxylation of benzene in two steps to dihydroxybenzene isomers (**Fig. 5. 2**). Phenol was formed as an intermediate, which was then further hydroxylated by the same enzyme to catechol, hydroquinone, and resorcinol.

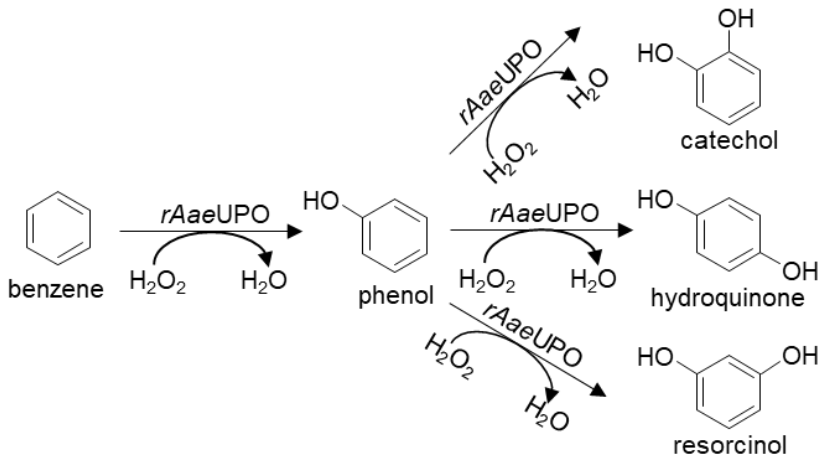

Fig. 5. 2. *Two-step hydroxylation of benzene catalyzed by the recombinant unspecific peroxygenase from Agrocybe aegerita (rAaeUPO).*

In **Fig. 5. 3. A**, the electroenzymatic hydroxylation performed at 30 mA is shown. No accumulation of H_2O_2 was detected during the active phase of the enzyme. However, it is possible that H_2O_2 was present in the medium at a concentration lower than the detection limit of 15 µM. During the course of the experiment, it was observed that the enzyme relative activity gradually decreased over time. In the initial stage of the reaction, the concentration of phenol, which is an intermediate product, increased and then remained constant at 40 µM. This can be attributed to the balanced rates of phenol formation and its subsequent conversion. The concentration of hydroquinone exhibited a steady increase over time with a formation rate of

0.57 µM min^{-1}. In parallel, the concentration of catechol also increased, albeit at a slower rate of 0.14 µM min^{-1}. With regard to resorcinol, the concentration exhibited an initial increase. However, as the reaction proceeded, the concentration began to decline. This decline can be explained by further oxidation of resorcinol to, *e.g.,* 1,2,4-trihydroxybenzene. In this specific reaction system, hydroquinone was identified as the primary product formed from benzene.

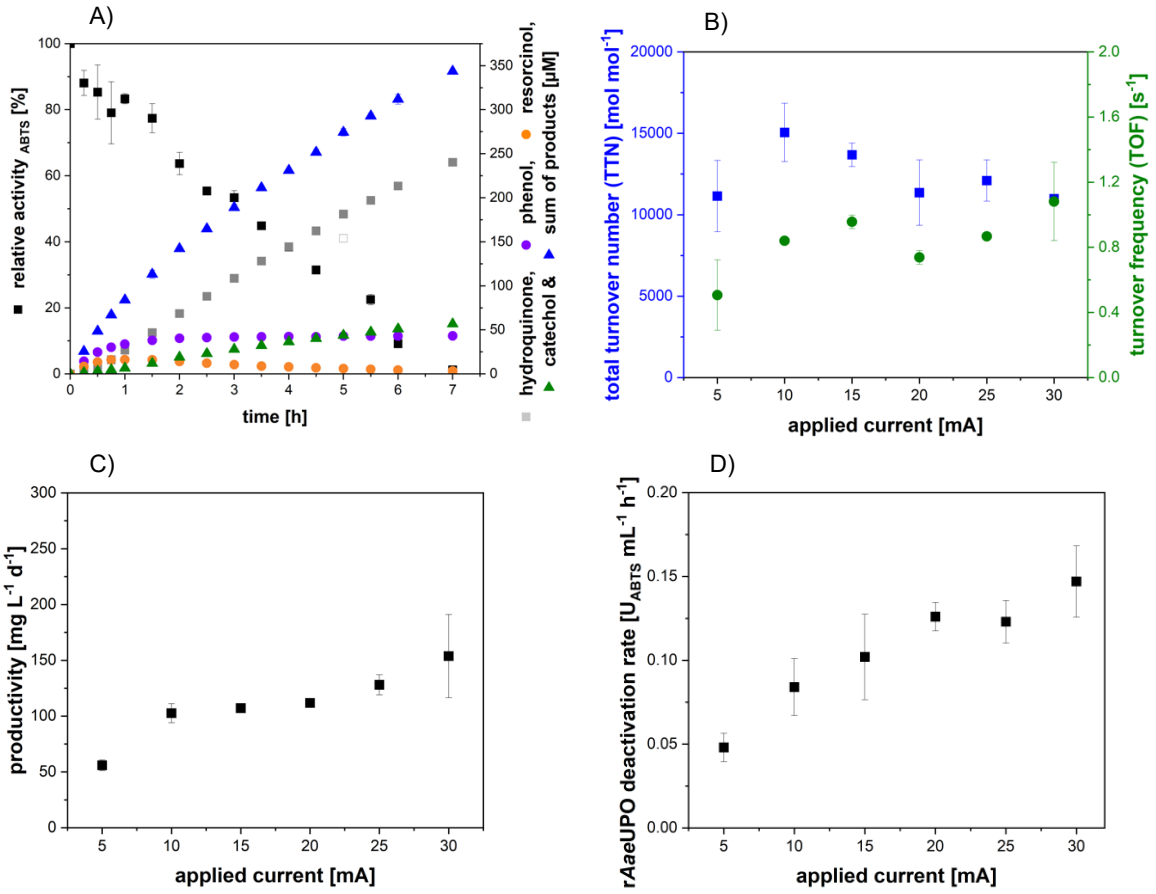

***Fig. 5. 3. A**) Hydroxylation of benzene catalyzed by rAaeUPO in an All-in-One electrode system with in situ H_2O_2 generation at 30 mA. **B**) The corresponding total turnover number (TTN), turnover frequency (TOF), **C**) productivity and **D**) rAaeUPO deactivation rate at different applied currents. Reaction condition: carbon felt working electrode (5.5 cm^2), platinized titanium counter electrode (4.24 cm^2), 200 mL 0.05 M citrate/ sodium phosphate pH 5, 20 mM benzene, 1 U_{ABTS} mL^{-1} (30 nM) rAaeUPO, 250 rpm, 22 ± 1 °C. Biological duplicates were performed.*

The TTN and the TOF were determined for each applied current (**Fig. 5. 3. B**), calculated from the sum of the products catechol, hydroquinone and resorcinol. The highest TOF of 1.1 s^{-1} was obtained at 30 mA, while the highest TTN of 15,000 mol mol^{-1} was obtained at 10 mA. As the applied current was increased, the TTN declined, although the productivity continued to increase (**Fig. 5. 3. C**). The stability of the enzyme remains a pivotal factor influencing the TTN. It can be postulated that the stability of the enzyme might be influenced by the presence of H_2O_2 and the adsorption of the enzyme on the electrode surface. Although enzyme adsorption on the electrode surface did not inevitably result in enzyme deactivation, there was a potential for enzyme destabilization. The deactivation effect of the electrical field or pulsed electric field

on the enzyme has been documented. It is hypothesized that alterations in the enzyme's secondary, tertiary, and quaternary structures might be induced by the electric field, consequently affecting enzyme activity and stability [120]. Therefore, it is important to carefully evaluate the impact of enzyme adsorption on the electrode surface and consider strategies to minimize any potential destabilization that may occur. Furthermore, the electrogeneration of H_2O_2 is closely linked to the formation of radicals. The formation rate of these radicals are influenced by the applied current and cell potential. This is displayed from the increasing enzyme activity loss with increasing applied current (**Fig. 5. 3. D**). Thus, increasing the current beyond 10 mA might favor the formation of radicals, prompting faster enzyme deactivation and decreasing the TTN.

Following the establishment of the BES, a control experiment with manual addition of H_2O_2 solution was conducted (**Fig. 5. 4. A**). The experiment was performed identical to the previous electroenzymatic experiment, without the electrical current and the H_2O_2 feed was manually adjusted every 30 min. The concentration of H_2O_2 was kept between 100 – 300 µM to make sure that the reaction was not limited by the H_2O_2, yet sufficiently low to prevent fast r*Aae*UPO deactivation [106]. Although the H_2O_2 concentration during the experiment was below 400 µM, the enzyme activity declined rapidly within the initial hour, resulting in a 60% loss of its initial activity. This decline continued, leading to complete deactivation after 4.5 h. Given that the total H_2O_2 introduced was circa 1.72 mM and the total measured product concentration was 222 µM, it can be assumed that the remaining H_2O_2 went to the catalase and catalase malfunction reactions. In the control experiment, resorcinol was identified as the main product, whereas in the BES, hydroquinone was identified as such. It has been reported that the main product resulting from the hydroxylation of benzene catalyzed by UPO is the *p*-benzoquinone, which is the product from further oxidation of hydroquinone [33]. The discrepancy observed herein could be attributed to the H_2O_2 concentration in the medium. In the BES, the accumulation of H_2O_2 was lower than that observed in the control experiment, which resulted in a limitation of the catalytic reaction. At an excess H_2O_2 concentration, the reaction proceeded at a higher rate, allowing for a faster consecutive hydroxylation of hydroquinone to *p*-benzoquinone. Therefore, the concentration of hydroquinone present in the medium was found to be relatively low, even lower than that of resorcinol. A higher catalytic reaction rate led to a higher productivity compared to that obtained in the BES at 10 mA (**Fig. 5. 4. B**). However, due to a higher H_2O_2 accumulation in the medium the enzyme stability was lower and the TTN was around 3 times lower than that achieved in the BES. This results confirmed that the application of *in situ* electrochemical generation of H_2O_2 could enhance the biocatalyst's stability by providing continuously low concentration of H_2O_2.

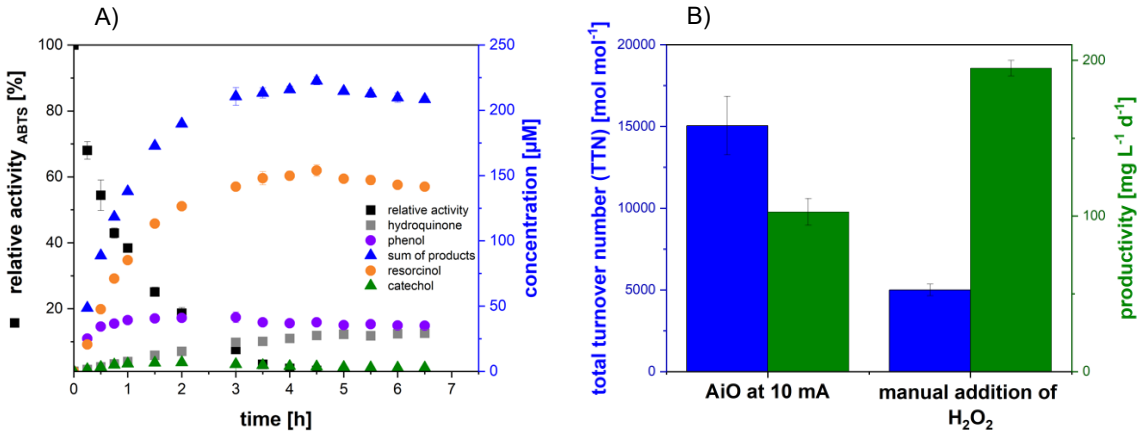

***Fig. 5. 4. A**) Hydroxylation of benzene catalyzed by rAaeUPO with manual addition of H_2O_2. **B**) Total turnover number (TTN) and productivity from BES at 10 mA and control experiment. Reaction condition: All-in-One electrode, 200 mL 0.05 M citrate/ sodium phosphate pH 5, 20 mM benzene, H_2O_2: 100-300 µM (1.72 mM total H_2O_2 added), 1 U_{ABTS} mL^{-1} (30 nM) rAaeUPO, 250 rpm, 22 ± 1 °C.*

Nevertheless, a comprehensive quantification of the substrate and the products was not feasible. Benzene is highly volatile and has a low solubility in aqueous solutions. In addition, benzene adsorbs on the reactor wall and subsequently disappear out of the solution. Therefore, it was not possible to rely on the quantification of benzene alone. Meanwhile, catechol, hydroquinone and resorcinol could undergo a third hydroxylation yielding *o*-benzoquinone, *p*-benzoquinone and 1,2,4-trihydroxybenzene (or hydroxy-*p*-benzoquinone), respectively [33]. Quantifying all possible products presented a significant challenge. As a result, the mole balance of the reactions could not be closed and as not all the products could be quantified the TTN obtained from this reaction system is also lower compared to that of other r*Aae*UPO-catalyzed reactions [66,104,121]. As the main objective of this dissertation was to develop a controllable *in situ* electrosynthesis of H_2O_2 and its utilization in a biocatalytic reaction to enhance the enzyme stability, further investigations were conducted using a second model reaction system: the hydroxylation of 4-ethylbenzoic acid (EBA) to 4-(1-hydroxyethyl)benzoic acid (HEBA). The absence of by-products in this model reaction system simplifies the analytical quantification process, making it suitable for an in-depth characterization of the BES. Since EBA is insoluble in acidic conditions, potassium phosphate (KP_i) buffer at pH 7 was selected as the medium. Additionally, the H_2O_2 sensor, intended to be used in the later stage of the study, exhibits cross-sensitivity to carboxylic acids. Hence, the change of the buffer system was necessary for further course of the project. The characterization and quantitative analysis of the BES using the second model reaction system are presented in the following chapter.

6. Application of the All-in-One Electrode for *in situ* H_2O_2 Generation in Hydroxylation Catalyzed by Unspecific Peroxygenase from *Agrocybe Aegerita*

Giovanni V. Sayoga[a], Victoria S. Bueschler[a], Hubert Beisch[b], Dirk Holtmann[c], An-Ping Zeng[d,e], Bodo Fiedler[b], Daniel Ohde[a], Andreas Liese[a]

[a]Institute of Technical Biocatalysis, Hamburg University of Technology, Denickestraße 15, 21073 - Hamburg, Germany
[b]Institute of Polymers and Composites, Hamburg University of Technology, Denickestraße 15, 21073 - Hamburg, Germany
[c]Institute of Process Engineering in Life Sciences, Karlsruhe Institute of Technology, Fritz-Haber-Weg 4, 76131 - Karlsruhe, Germany
[d]Institute of Bioprocess and Biosystems Engineering, Hamburg University of Technology, Denickestraße 15, 21073 - Hamburg, Germany
[e]Center of Synthetic Biology and Integrated Bioengineering, School of Engineering, Westlake University, Hangzhou, Zhejiang 310024, China

Bibliographic details
published August 2023, Volume 547, 113325
Molecular Catalysis (Elsevier)
DOI: 10.1016/j.mcat.2023.113325

Molecular Catalysis 547 (2023) 113325

Contents lists available at ScienceDirect

Molecular Catalysis

journal homepage: www.journals.elsevier.com/molecular-catalysis

Application of the all-in-one electrode for *in situ* H_2O_2 generation in hydroxylation catalyzed by unspecific peroxygenase from *Agrocybe aegerita*

Giovanni V. Sayoga [a], Victoria S. Bueschler [a], Hubert Beisch [b], Dirk Holtmann [c], An-Ping Zeng [d,e], Bodo Fiedler [b], Daniel Ohde [a], Andreas Liese [a,*]

[a] Institute of Technical Biocatalysis, Hamburg University of Technology, Denickestraße 15, 21073, Hamburg, Germany
[b] Institute of Polymers and Composites, Hamburg University of Technology, Denickestraße 15, 21073, Hamburg, Germany
[c] Institute of Process Engineering in Life Sciences, Karlsruhe Institute of Technology, Fritz-Haber-Weg 4, 76131, Karlsruhe, Germany
[d] Institute of Bioprocess and Biosystems Engineering, Hamburg University of Technology, Denickestraße 15, 21073, Hamburg, Germany
[e] Center of Synthetic Biology and Integrated Bioengineering, School of Engineering, Westlake University, Hangzhou, Zhejiang, 310024, China

ARTICLE INFO

Keywords:
Biocatalysis
Bioelectrochemical system
Electroenzymatic
Electrosynthesis
Hydrogen peroxide

ABSTRACT

The versatile unspecific peroxygenase from the fungus *Agrocybe aegerita* (*Aae*UPO) is capable to perform hydroxylation of various substrates, even unactivated C—H bonds. The technical application of *Aae*UPO is still limited due to an instability towards its co-substrate hydrogen peroxide (H_2O_2). Electrochemical synthesis of H_2O_2 is an attractive approach that provides controllable *in situ* generation of H_2O_2. The aims of this study are to promote catalyst efficiency and develop an individually tailored system for H_2O_2-dependent reactions. Herein, an All-in-One electrode (AiO) system with a carbon felt cathode is used to generate H_2O_2 *in situ* and combined for the first time with an enzymatic hydroxylation. The AiO electrode combines the counter and working electrode in a single rod structure. This shape provides convenient integration into conventional bioreactors, thus, converting them into bioelectrochemical systems (BES). Hydroxylation of 4-ethylbenzoic acid (EBA) catalyzed by the recombinant *Aae*UPO (r*Aae*UPO) was chosen as the model reaction. Total turnover number (TTN) up to 450,000 mol mol^{-1} and turnover frequency (TOF) up to 7.7 s^{-1} were achieved using the AiO electrode system. The H_2O_2 productivity was identified as the limiting factor in the hydroxylation of EBA. However, with numbering-up or surface enlargement, this process could have great potential as an optimizable platform for H_2O_2-dependent enzymatic reactions.

1. Introduction

As a mild and stable oxidant with high oxidation power, H_2O_2 is an important chemical with wide-range applications on an industrial scale [1]. This environmentally-friendly chemical is mainly applied as an oxidizer in the chemical industry and water treatment processes, as a disinfectant, and as a bleaching agent [2–4]. Furthermore, there are a variety of biocatalytic reactions that can utilize H_2O_2 as a co-substrate, for example hydroxylation, epoxidation, sulfoxidation, and halogenation [5]. Nevertheless, the established methods to produce H_2O_2 are commonly associated with safety concerns, are cost-intensive, and generate organic waste [2,6–8]. Most importantly, the full industrial application of H_2O_2 in the biotechnological field is still very limited [9,10]. This is because of enzymes inactivation by the H_2O_2 [5,11,12].

Numerous approaches to minimize the deactivation effect of H_2O_2 have been evaluated. As the stoichiometric addition of H_2O_2 is not practical, the key to increasing the enzyme stability is to work with constantly low H_2O_2 concentration [13]. In general, a low concentration of H_2O_2 can be achieved either by feeding diluted H_2O_2 or generating H_2O_2 *in situ* [14]. Feeding diluted H_2O_2 solution leads to an increase in the reaction volume and a high local H_2O_2 concentration [13,15]. The commonly used method to generate H_2O_2 *in situ* is by using glucose oxidase to oxidize glucose and thereby forming H_2O_2 [15–17]. The main drawback of this method is the accumulation of the undesired co-product gluconic acid which also shifts the pH of the reaction medium. Consequently, the application of this method at a large scale may require additional pH-control. Moreover, feeding highly concentrated glucose affects the viscosity of the reaction medium as the solution has a high viscosity [13,15]. Another approach to generate H_2O_2 *in situ* in a controlled manner is by employing a chemical reductant to reduce

* Corresponding author at: Institute of Technical Biocatalysis, Hamburg University of Technology, Denickestraße 15, 20173, Hamburg, Germany.
E-mail address: liese@tuhh.de (A. Liese).

https://doi.org/10.1016/j.mcat.2023.113325
Received 1 May 2023; Received in revised form 15 June 2023; Accepted 16 June 2023
Available online 19 June 2023

oxygen (O_2) [18]. However, both approaches (enzymatic and chemical reductant) are reported to produce a stoichiometric amount of by-product (*e.g.* gluconic acid and 2-indoxyl/ or 3-oxindole in oxidation of indole to 2-oxindole), thus, decreasing the reaction selectivity [11, 18].

Direct *in situ* electrosynthesis of H_2O_2 via reduction of O_2 at an electrode offers an attractive approach to avoid the irreversible deactivation of enzymes by providing a low and controllable generation of H_2O_2, without having the drawbacks mentioned earlier [19]. Electrochemical reduction of O_2 is considered as one of the cleanest processes to generate H_2O_2 since it requires no additional chemicals, generates no by-product and otherwise, only electricity is required [11,12,15]. Recently, *in situ* generation of H_2O_2 at gas diffusion electrodes (GDEs) has gained attention [20]. GDEs have been combined with H_2O_2-dependent enzymes in a BES, such as the vanadium chloroperoxidase (CPO) from *Curvularia inaequalis* [21], CPO from *Caldariomyces fumago* [12], and r*Aae*UPO [13]. The conventional H-cell BES also has been linked with a H_2O_2-dependent enzyme for demethylation reaction catalyzed by horseradish peroxidase [22]. Nonetheless, H-cell systems have poorly mixed zones near the separator, require a pH control, have "unused" volume in the counter electrode chamber [23] and generally not scalable. A production plant (20,000 tons year^{-1}) based on the GDE system for chlorine production is already established [24]. Still, the risk associated with the scaling-up of GDEs such as pressure difference across the porous gas diffusion layer, potentially causing flooding and electrolyte breakthrough and decrease in performance, has to be considered [25].

In 2018, Utesch introduced the AiO electrode concept, which combines both counter and working electrode into a single structure [23]. The rod shape structure of the AiO electrode enables a convenient integration into conventional bioreactors, thus converting them into BES [23,26]. Moreover, enlarging the surface area of the AiO electrode and numbering-up of these could offer a better distribution of electrochemically active surface areas in a larger bioreactor [23]. The AiO electrode system for generation of H_2 has already shown promising potential during the implementation in anaerobic fermentations [23, 26–28]. So far it has not been implemented in electroenzymatic processes [23,26–28].

The aims of this study are to develop a controllable *in situ* generation of H_2O_2 and construct an optimizable platform for H_2O_2-dependent reaction to promote catalyst efficiency. Herein, the AiO electrode, previously developed by Utesch, was modified and fitted with a carbon felt working electrode to generate the H_2O_2 *in situ* (Fig. 1) [23]. The *in situ* electrogeneration of H_2O_2 using the AiO electrode was combined with the hydroxylation of EBA to 4-(1-hydroxyethyl)benzoic acid (HEBA) catalyzed by the r*Aae*UPO. r*Aae*UPO is of interest due to its ability to catalyze the hydroxylation of unactivated C—H bonds, its high stability and it does not require an expensive nicotinamide cofactor [5,29,30]. Characterization of the AiO electrode regarding its ability to generate H_2O_2 was performed. We demonstrated, as a proof of concept, the combination of modified AiO electrode with the hydroxylation of EBA catalyzed by r*Aae*UPO at different applied currents. The analytical yield, TTN and TOF from electroenzymatic processes were analyzed and compared.

2. Experimental

2.1. Materials

Unless otherwise stated, all chemicals were purchased from Carl Roth (Karlsruhe, Germany) or Sigma Aldrich (Steinheim, Germany) in a purity ≥98%. HEBA (≥97%) was purchased from BLD Pharm (China). Carbon felt electrode (area weight: 250 g m^{-2}, thickness: 2.5 mm, surface area (Brunnauer-Emmet-Teller method): 0.4 m^2 g^{-1}) was purchased from SGL Carbon (Sigracell®, Wiesbaden, Germany). 2,2′-azino-bis(3-ethylbenzothiazoline-6-sulfonic acid) (ABTS) (≥98%) was purchased from TCI (Eschborn, Germany).

2.2. Production of his-tagged rAaeUPO

The pre-culture containing *Pichia pastoris* (X33) able to express recombinant protein r*Aae*UPO-PaDa-I-C6His was inoculated overnight in 50 mL BMGY medium with 25 μg mL^{-1} Zeocin at 200 rpm, 30 °C [31]. The inoculum was cultivated in a 1 L DASGIP bioreactor system (Eppendorf, Hamburg, Germany) with an initial working volume of 500 mL basal salt medium containing 40 g L^{-1} glycerol. The fermentation was conducted first in a glycerol batch mode and then in a fed-batch mode, with glycerol (50% v/v glycerol with 12 mL L^{-1} of PTM1 trace salts) being used as the initial feed and methanol (with 12 mL L^{-1} of PTM1 trace salts) being used later as the feed. The dissolved oxygen (DO) content and temperature were set at 30% and 30 °C, respectively. To maintain these values, the stirring rate (400 to 1200 rpm) and aeration rate (30 to 60 L h^{-1} ≙ *ca.* 1 vvm) were regulated automatically by the system. Further, a 25% v/v ammonia solution was used to maintain the pH at 5. Once the initial glycerol was consumed, the glycerol fed-batch was started and maintained for 24 h. Afterwards, the glycerol feed was stopped and the methanol fed-batch phase was started to induce the overexpression of r*Aae*UPO. The feeding rates of both glycerol and methanol in the fed-batch phase were controlled based on DO levels. The feeding profiles were set according to Cino *et al.,* [32]. Following the fermentation, the fermentation broth was centrifuged (Beckmann J2HS, Beckmann Coulter, California, USA) at 5000 rpm for 2 h at 4 °C. The supernatant was sterile-filtered (0.22 μm, DURAPORE, Merck Millipore, Massachusetts, USA) and concentrated by

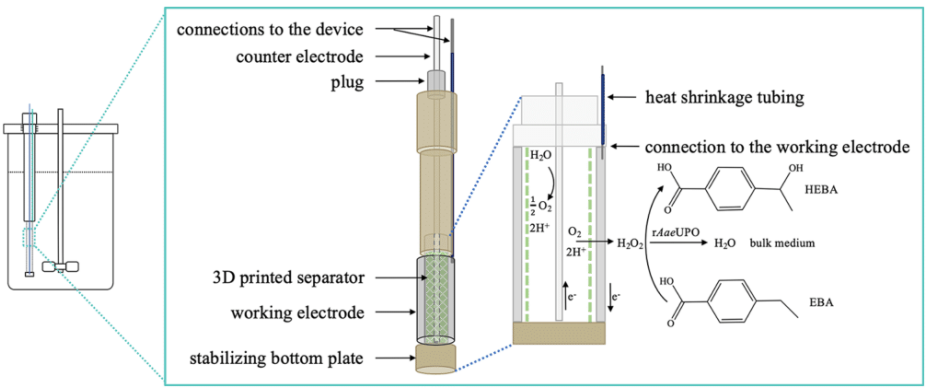

Fig. 1. Schematic representation of the All-in-One electrode with a carbon felt working electrode for the electroenzymatic hydroxylation of 4-ethylbenzoic acid (EBA) to 4-(1-hydroxyethyl)benzoic acid (HEBA) catalyzed by the recombinant unspecific peroxygenase from *Agrocybe aegerita* (r*Aae*UPO).

ultrafiltration (10 kDa molecular weight cut off, Minimate TFF Capsule, Pall, New York, USA). r*Aae*UPOs were diafiltrated and concentrated in 0.1 M potassium phosphate (KP_i) buffer, pH 7.

2.3. Analytical methods

2.3.1. Determination of enzyme activity

The enzyme activity was determined with an ABTS assay. The assay was performed photometrically (Genesys 180, Thermo Scientific, Massachusetts, USA) at 420 nm for 1 min (ε_{ABTS} = 36,000 M^{-1} cm^{-1}) as technical duplicates. The assay consisted of 750 µL 0.1 M Na_2HPO_4/ 0.1 M citric acid buffer pH 4.4, 100 µL 3 mM ABTS, 50 µL 40 mM H_2O_2 and 100 µL sample. The sample was added last as it starts the reaction. The measurement was started after properly mixing the completed reaction mixture by pipetting up and down 5 times. The r*Aae*UPO activity and concentration were calculated as shown in the following [33]:

$$v = \frac{slope\ of\ the\ absorbance\ [min^{-1}] \cdot 10}{36\ [mM^{-1}\ cm^{-1}] \cdot 1\ cm} \quad (1)$$

$$c_{rAaeUPO} = v \cdot \frac{(k_m + S)}{k_{cat} \cdot S} = v \cdot df \cdot (k_m + S) \cdot \frac{1}{k_{cat} \cdot S} \quad (2)$$

Where v is the r*Aae*UPO activity [U mL^{-1}], S is the final substrate (ABTS) concentration in the assay [mM], $c_{rAaeUPO}$ is the concentration of r*Aae*UPO [µM], k_m is the Michaelis-Menten parameter (50 µM) [34], k_{cat} is the catalytic rate constant (546 s^{-1}) [34] and *df* is the dilution factor (20, 10 or 1).

2.3.2. Determination of H_2O_2 concentration

H_2O_2 concentrations were determined photometrically by an iodide method (lower detection limit of 10 µM) described in [35]. The assay (1 mL) contained the sample from the reaction system, iodide reagent (0.4 M potassium iodide, 0.05 M NaOH, 10^{-4} M ammonium molybdate) and 0.5 M potassium hydrogen phthalate in a ratio of 4:3:3 and was measured at 351 nm in technical duplicates. Calibration curves (10 µM to 100 µM) were prepared using diluted H_2O_2 solution. H_2O_2 concentrations were also determined using QUANTOFIX Peroxide 25 (lower detection limit of 15 µM) (Macherey-Nagel, Düren, Germany) in conjunction with the reflectometer QUANTOFIX Relax (Macherey-Nagel, Düren, Germany).

2.3.3. Determination of 4-ethylbenzoic acid (EBA) and 4-(1-hydroxyethyl) benzoic acid (HEBA) concentrations

EBA and HEBA concentrations were determined using a Nexera LC-40 HPLC system (Shimadzu, Kyoto, Japan) equipped with a UV–Vis SPD-40 detector (Shimadzu, Kyoto, Japan) and an Inertsil ODS-P, C18-RP, 5 µm, 100 Å column (GL Science, Japan). The chromatography analysis was carried out at 35 °C using a binary gradient of 0.1% v/v of trifluoroacetic acid (TFA) in H_2O and 0.095% v/v TFA in acetonitrile (ACN) at a flow rate of 0.5 mL min^{-1}. A gradient for ACN was applied as follow: 0 min: 35%, to 7 min: 80%, to 9 min: 35%, to 10 min: 35%. EBA and HEBA were detected at 237 nm and had retention times of 8.3 min and 4.2 min, respectively. For the sample preparation, a 20 µL sample was taken out from the reactor and mixed with 80 µL 3% v/v TFA in H_2O, followed by a centrifugation (Biofuge Fresco, Heraeus, Hanau, Germany) at 13,000 rpm and 4 °C for 4 min. The supernatant was transferred to an HPLC-vial and measured as described above. Calibration curves (0.5 mM to 10 mM) were prepared using authentic standards. All measurements were done in technical duplicates.

2.4. Electrochemical investigation

A cyclic voltammetry (CV) analysis was conducted to investigate the electrochemical processes taking place at the interface between the electrode surface and the surrounding medium. The CV was controlled and recorded using a computer-controlled potentiostat (Gamry Interface 1000, Philadelphia, USA) in a three-electrode system (200 mL). Carbon felt (A: 1 cm^2) (titanium wire 99.8% as the electrical connector), platinum wire (99.9%, A: 1.13 cm^2) (Chempur, Karlsruhe, Germany) and Ag/AgCl 3 M NaCl (RE-1B, ALS, Tokyo, Japan) were used as working, counter and reference electrode, respectively. The CV was recorded in a 0.1 M KP_i buffer pH 7 saturated with air or N_2 at room temperature (21–23 °C) with a scan rate of 100 mV s^{-1}. The distance between working and counter electrode was 2.5 cm. No iR compensation was applied.

2.5. Electrochemical setup

Electrochemical and electroenzymatic experiments were conducted in a 250 mL DASGIP reactor. Investigations were performed using the modified AiO electrode (total length: 145 mm, length of the scaffold within the reactor: 115 mm, d (within the reactor): 12 mm, M20 × 1.5 thread) with the carbon felt working electrode (A: 11 cm^2) wrapped around the AiO electrode scaffold to get an overall cylindrical geometry. Platinized titanium (A: 4.24 cm^2) (METAKEM, Usingen, Germany) was used as the counter electrode and located inside the AiO electrode scaffold. Water electrolysis takes place at the counter electrode (anode) generating the required O_2 and H^+molecules *in situ*. Formed O_2 and H^+ then diffuse from the anode towards the working electrode (cathode), where they are reduced at the surface of the working electrode to H_2O_2 which is subsequently used as co-substrate for the enzymatic hydroxylation (Fig. 1).

2.6. Electroenzymatic experiments

The BES utilized the AiO electrode with carbon felt and contained 200 mL 0.1 M KP_i pH 7, 8 mM EBA and 1 U_{ABTS} mL^{-1} (30 nM) of r*Aae*UPO. Amperostatic experiments were performed at electrical currents between 5 and 30 mA. The electrical currents were held constant using a power supply (Keithley 2231a-30–3 DC, Tektronix, Oregon, USA). The stirrer (magnetic bar, d: 0.5 cm, l: 3 cm) speed was set to 250 rpm and experiments were performed at room temperature (21–23 °C). Samples for the measurement of EBA, HEBA, H_2O_2 concentration, and r*Aae*UPO activity were taken periodically from the system. Each experiment was stopped when there was no measurable r*Aae*UPO activity (slope of the absorbance < 0.01 min^{-1}). Electroenzymatic experiments were performed as biological duplicates. TTN is defined as the quotient of the final product concentration once the enzyme was deactivated and the applied enzyme concentration. The turnover number (TON) is described as the quotient of the product concentration at a specific time before the enzyme was deactivated and the applied enzyme concentration. The TOF refers to the TON per unit time. TOFs were calculated from the initial part of the experiment where the product formation was linear.

The H_2O_2 productivity was determined between 5 and 30 mA applied currents, using the same setup without the enzyme and EBA. The H_2O_2 concentration was measured periodically over the course of 30 min. Biological duplicates were performed for each electrical current. The Faradaic efficiency (F.E.) is an electrochemical parameter that describes how much energy is consumed for the formation of H_2O_2 or the formation of side products. The F.E. of H_2O_2 formation is calculated using the equation given elsewhere [12].

Two types of control experiments were performed. 1) The individual component was incubated in the previously described BES without applying any current. This was primarily done to investigate if adsorption of the substrate, product, and r*Aae*UPO on the electrode surface occurs. 2) Electroenzymatic experiments were performed as previously described at 10 mA for 5 h, but without addition of the enzyme. This investigation aimed to assess the stability of the substrate and product in the electrochemical environment.

3. Results and discussion

To promote catalyst efficiency and develop a customizable system for H_2O_2-dependent reactions, the AiO electrode system with a carbon felt cathode was employed in a hydroxylation reaction for *in situ* and on-demand H_2O_2 generation. To achieve this objective, it was essential to conduct a CV study to analyze redox processes of electroactive species occurring on the electrode surface. Additionally, the AiO electrode was characterized to determine its H_2O_2 generation capabilities. Finally, the electrochemical and biocatalytical systems were integrated to create and validate a BES for the electroenzymatic hydroxylation.

3.1. Electrochemical investigation and characterization

CV analysis was performed to investigate possible oxidation and reduction processes of electroactive species at the surface of carbon felt working electrode. The CV measurement was done either in an N_2-saturated or air-saturated medium. The potential was swept with a scan rate of 100 mV s^{-1} between −2.5 V and 3 V going into the negative region first. The curves obtained from the CV study (Fig. 2) resemble typical curves that are described in the literature for carbon-based materials [36–38]. An apparent current response is observed at a cathodic potential of −1 V *vs.* Ag/AgCl with a peak current of −0.015 A. The iR compensation to correct the iR drop caused by the distance between the working- and the reference electrode and the solution resistance was not applied. In this case, the cathodic peak could be observed at a more negative potential than it would be otherwise observed with the iR compensation. The current response is observable in the air-saturated medium, and less pronounce in the N_2-saturated medium. This peak response is attributed to the O_2 reduction reaction (ORR) on the surface of the working electrode and potentially generation of H_2O_2 (Equation (Eq.) 3). In several publications, similar potentials for ORR are reported [7,19,35,37]. The existence of the peak in the N_2-saturated medium could be explained by the remaining O_2 in the system. The peak for the reduction of O_2 to H_2O is absent in this voltammogram. A higher overpotential or lower scan rate might be required to be able to see the reaction.

$$O_2 + 2H^+ + 2e^- \rightarrow H_2O_2 \; E = 0.670 \text{ V } vs.\text{SHE} \quad (3)$$

The CV analysis provided evidence of the carbon felt material's capacity to reduce oxygen molecules, indicating its potential for generating H_2O_2. Subsequently, the carbon felt cathode was incorporated into the AiO electrode, and a characterization study was conducted to assess its ability to generate H_2O_2 *in situ*. This evaluation was performed prior to initiating the hydroxylation reaction. The generation of H_2O_2 *in situ* was determined in the absence of the enzyme and the substrate. Specific productivities, Faradaic efficiencies (F.Es.) and resulting cell potentials as a function of applied current are shown in Fig. 3A.

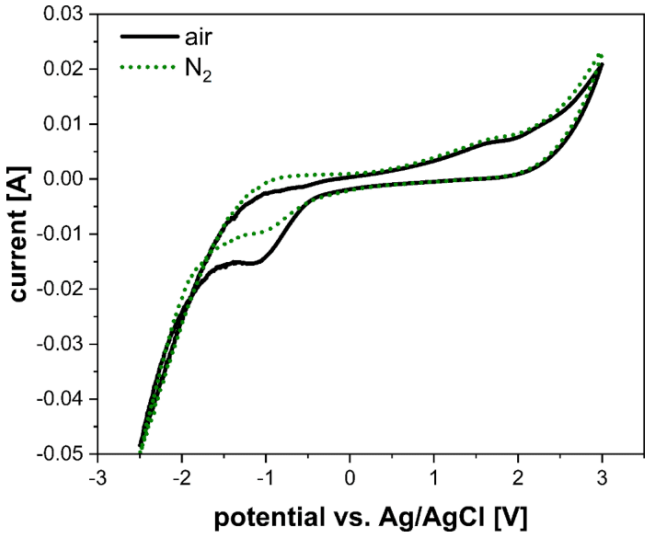

Fig. 2. Cyclic voltammogram of the carbon felt electrode. Parameter: 200 mL 0.1 M KP_i pH 7, room temperature (21–23 °C), scan rate: 100 mV s^{-1}, carbon felt working electrode (1 cm^2), platinum counter electrode (1.13 cm^2), Ag/AgCl 3 M NaCl reference electrode, saturated with air or N_2.

The H_2O_2 specific productivity is increasing from 0.29 μM min^{-1} cm^{-2} to 0.87 μM min^{-1} cm^{-2} with increasing applied current from 5 mA to 25 mA. However, as the applied current is further increased to 30 mA, the H_2O_2 specific productivity is decreasing to 0.49 μM min^{-1} cm^{-2}. Consequently, the highest H_2O_2 specific productivity acquired in this study was 0.87 μM min^{-1} cm^{-2} at 25 mA. Compared to the productivities obtained from GDE-based systems from literature, the highest productivity achieved in this study is 2 to 37 times lower [10,12]. However, compared to productivities obtained using conventional 3D carbon-based electrodes, the here reported productivities are comparable [11,22,35,37,38]. In GDEs, the mass transfer of O_2 towards the electrode is enhanced because O_2 from the atmosphere diffuses directly into the GDE through its gas-facing side. Hence, an O_2 limitation can be prevented enabling higher H_2O_2 productivities [20]. Meanwhile, O_2 solubility and diffusivity towards the electrode were the limiting factors not only in this study, but also in other conventional electrochemical systems. The resulting potential shows a linear increase from 1.7 V to 3 V as the applied current is increased from 5 mA to 30 mA. An opposite behavior is observed for the F.E. of the H_2O_2. As the applied current is increased from 5 mA to 30 mA, the F.E. is decreasing from 60% to 3%. The decrease in the F.E. can be attributed to the occurrence of undesired side reactions. The main side reactions are the evolution of hydrogen Eq. (4)) at the cathode and the complete reduction of O_2 to H_2O (Eq. (5)) through the 4-electron mechanism. Due to its lower solubility compared to O_2, H_2 diffuses out of the solution faster and O_2 is reduced at the electrode. Thus, the possibility of knallgas reaction is avoided. Moreover, H_2O_2 molecules which were already generated inside the medium can be further reduced to H_2O (Eq. (6)), oxidized to generate intermediate radicals ($HO_2^{\bullet}$, $O_2^{\bullet -}$) (Eq. (7) & (8) at the anode, or decomposed to form O_2 (Eq. (9)) both at the anode and in the medium [13,35,37,39]. The rate of competing reactions is reported to depend on the applied current or potential [35,37]. The combination of all these effects leads to a decreased accumulation of H_2O_2 concentration, resulting in a lower F.E. as the applied current increases. This effect could also explain why the specific productivity was decreasing at the highest applied current. In Fig. 3B, it is observed that the formation of H_2O_2 is only linear in the first 5 min, except at 5 mA. At applied current higher than 15 mA, after 5 min, the rates of the competing reactions are analogous or even higher than the H_2O_2 formation rate, which reduces the accumulated H_2O_2 concentration. The F.Es. obtained in this study are within the reported F.E. values in literature which range from 50% to 89% [10,13,14,37]. Implementing an ion-selective membrane around the separator to divide the anodic and cathodic compartment could increase the F.E.. Nonetheless, this approach would increase the complexity of the setup due to the necessity to install the membrane and it hinders the O_2 transfer towards the cathode. This is not necessary because in the ideal case, the generated H_2O_2 should be consumed by the r*Aae*UPO instantaneously.

$$2H^+ + 2e^- \rightarrow H_2 \; E = 0.0 \text{ V } vs. \text{ SHE} \quad (4)$$

$$O_2 + 4H^+ + 4e^- \rightarrow 2H_2O \; E = 1.229 \text{ V } vs. \text{ SHE} \quad (5)$$

$$H_2O_2 + 2H^+ + 2e^- \rightarrow 2H_2O \; E = 1.763 \text{ V } vs. \text{ SHE} \quad (6)$$

$$H_2O_2 \rightarrow HO_2^{\bullet} + H^+ + e^- \; E = -1.461 \text{ V } vs. \text{ SHE} \quad (7)$$

$$HO_2^{\bullet} \rightarrow O_2 + H^+ + e^- \; E = -0.102 \text{ V } vs. \text{ SHE} \quad (8)$$

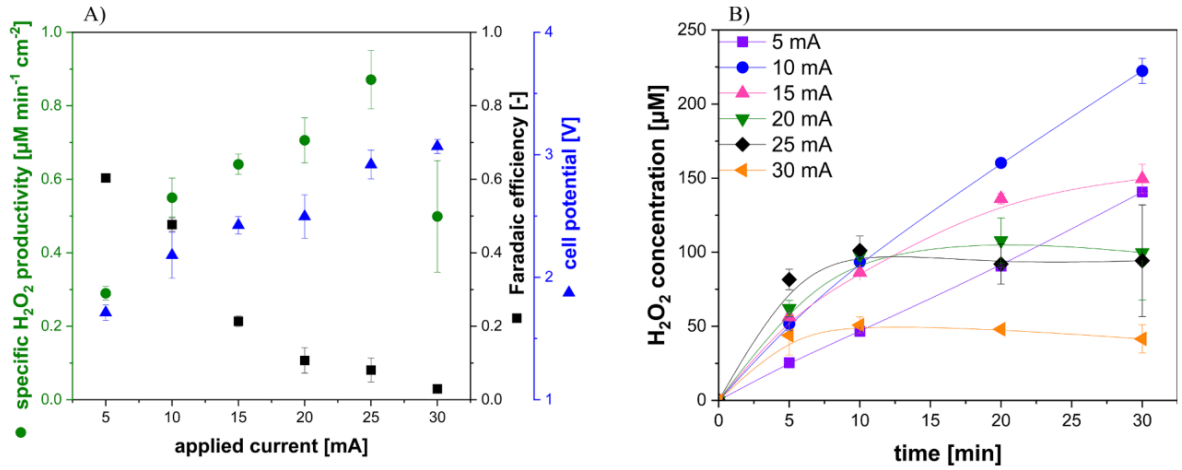

Fig. 3. A) Specific H_2O_2 productivity, Faradaic efficiency (F.E.) and resulting cell potential as a function of applied current. B) H_2O_2 concentration as a function of the time at different applied currents. Parameter: carbon felt working electrode (11 cm^2), platinized titanium counter electrode (4.24 cm^2), 200 mL 0.1 M KP_i pH 7, room temperature (21–23 °C), 250 rpm. F.E. was determined after 30 min. Biological duplicates were performed. The depicted lines serve as a visual aid.

$$H_2O_2 \rightarrow H_2O + \frac{1}{2}O_2 \quad E = 1.096\ \text{V}\ vs.\ \text{SHE} \tag{9}$$

For a further electrochemical characterization, the operational stability of the substrate and product were investigated in the reaction system at 10 mA for 5 h without the enzyme. It was found that the concentrations of both components remained constant (Fig. S5).

3.2. Electroenzymatic hydroxylation of 4-ethylbenzoic acid (EBA)

After the CV analysis and the characterization of the AiO electrode, the electrochemical and the biocatalytical systems were combined to form a BES for the hydroxylation of EBA to HEBA, catalyzed by r*Aae*UPO (Fig. 4). In this study, EBA was selected as the model substrate instead of benzene or ethylbenzene, which are commonly used as model substrates for the r*Aae*UPO due to its higher solubility in aqueous solution [30]. Additionally, issues with miscibility and evaporation, which hinder the use of benzene and ethylbenzene, can be avoided as EBA is solid at room temperature [40]. Moreover, there are no by-products or subsequent reactions that could affect the reaction selectivity.

The electroenzymatic hydroxylation reactions were conducted at different applied currents ranging from 5 mA to 30 mA. The reaction mixture contained 8 mM EBA and 1 U_{ABTS} mL^{-1} (30 nM) r*Aae*UPO. H_2O_2 was generated *in situ* by the AiO electrode. Exemplarily, the results of processes performed at 10 and 30 mA are shown in Fig. 5A & B.

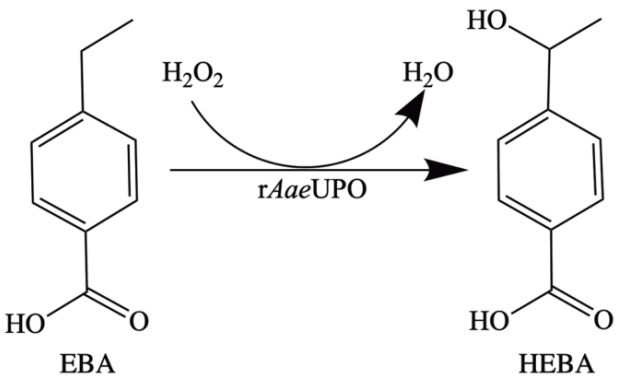

Fig. 4. Hydroxylation of 4-ethylbenzoic acid (EBA) to 4-(1-hydroxyethyl)benzoic acid (HEBA) catalyzed by the recombinant unspecific peroxygenase from *Agrocybe aegerita* (r*Aae*UPO).

Before the experiment was initiated, r*Aae*UPO was added to the mixture, and a sample was withdrawn to determine the initial activity using the ABTS assay. The initial activity was defined as "100%" activity. Enzyme activities determined during the experiment are related to the initial activity and expressed as the apparent ABTS-activity due to the simultaneous presence of ABTS and EBA in the sample (absolute activity could not be determined). In general, although the H_2O_2 was generated continuously *in situ*, there was no H_2O_2 accumulation observed (lower detection limit of 15 µM) within the system while the enzyme was still active. This evidently points towards a lower H_2O_2 generation rate by the AiO electrode compared to the consumption rate through the catalytic reaction. Despite H_2O_2 being generated at a moderate rate and no apparent H_2O_2 accumulation occurs, the relative enzyme activity was still decreasing linearly up to 7 h. This phenomenon has been described before and it is known that in a heme-containing enzyme like *Aae*UPO, a highly reactive intermediate compound I can react with a second H_2O_2 molecule to undergo a catalase reaction instead of reacting with an organic substrate to form compound II [41]. Compound II can further react with a H_2O_2 molecule to forms compound III, which causes a heme bleaching, also called catalase malfunction, and overall protein damage (compound I-III: different states of the enzyme; the catalytic cycle is illustrated in [41]) [13,41]. Additionally, the deactivation due to the degradation of heme is inevitable and correlated directly with the product formation, and is independent of the H_2O_2 supply [14]. Similar linear trends of a decreasing enzyme activity were reported in a different reaction system with *in situ* generation of H_2O_2 for heme-enzymes as well [11,14,19]. On this note, it can be observed that the residual enzyme activity decreases at a faster rate with increasing applied current. For example, a 20% loss of activity occurred at 10 mA after 7 h. Meanwhile, a higher activity loss of 30% was observed at 30 mA at the same time point. After 24 h, 10% of the initial enzyme activity remained at 10 mA and less than 5% at 30 mA. Because of a faster deactivation rate at higher applied currents, less active enzyme was present to carry out the catalytic conversion (Fig. 5C). This decreased the productivity and the final product concentration that was obtained before all (or near all) enzyme was deactivated. The highest product formation rate occurred within 7 h (Fig. 5A & B). In the aforementioned time frame, formation rates of 4.3 µM min^{-1} and 3.4 µM min^{-1} were determined for 10 mA and 30 mA, respectively. The product formation and substrate conversion were linear within this range. The linearity can be explained by the constant generation rate of H_2O_2 at a fixed current, combined with an excess of enzyme causing the H_2O_2 generation rate to be the limiting factor for the reaction rate. Afterwards, both formation and conversion rates were decreasing as the residual enzyme activity

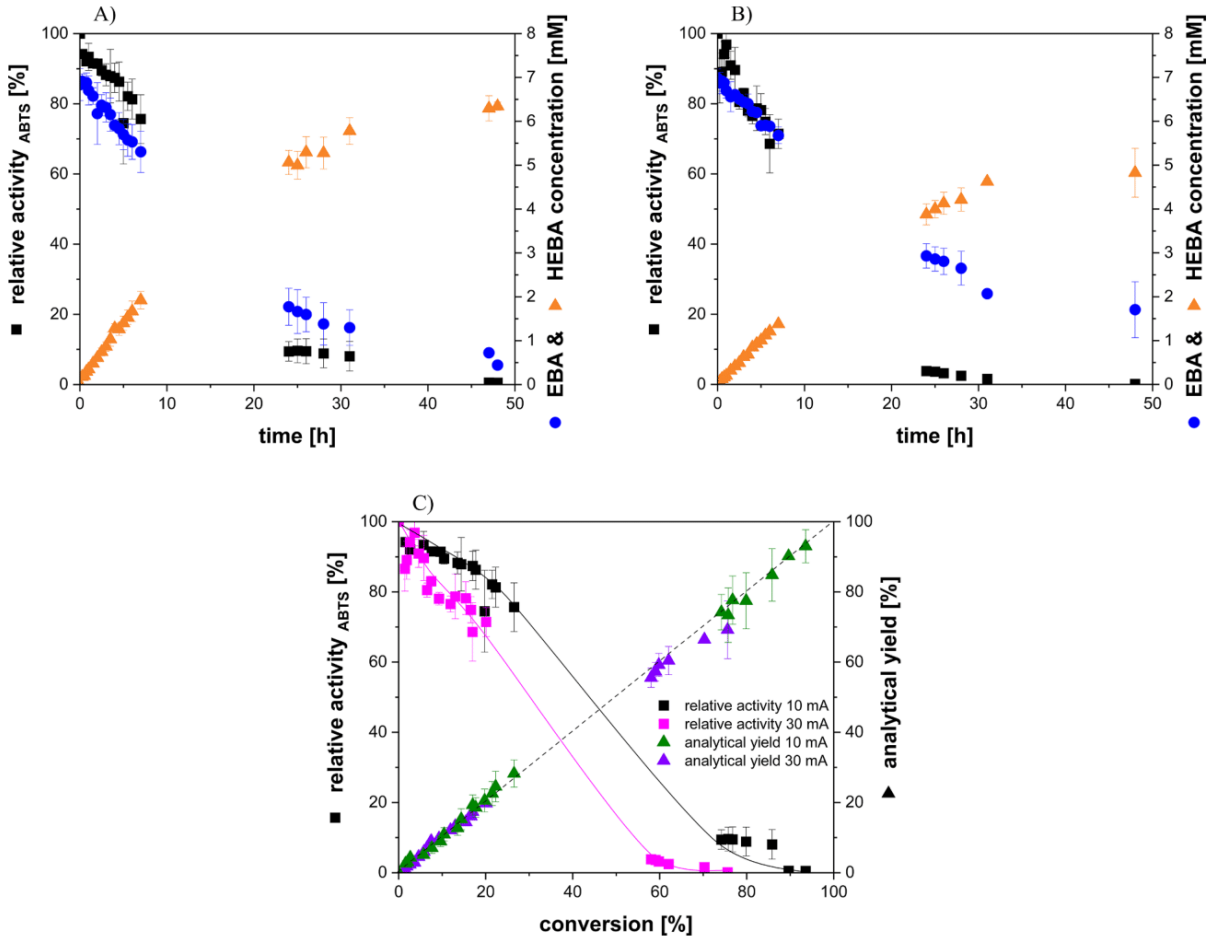

Fig. 5. Hydroxylation of EBA catalyzed by r*Aae*UPO in an All-in-One electrode system with *in situ* H_2O_2 generation at A) 10 mA and B) at 30 mA. Parameter: 200 mL 0.1 M KP_i pH 7, 8 mM EBA, 1 U_{ABTS} mL^{-1} (30 nM) r*Aae*UPO, 250 rpm, room temperature (21–23 °C). EBA: 4-ethylbenzoic acid, HEBA: 4-(1-hydroxyethyl)benzoic acid. Biological duplicates were performed. See Fig. S7 A-D for the full data set. C) the corresponding analytical yield and enzyme relative activity as a function of the conversion for the experiment performed at 10 mA and 30 mA. The depicted lines serve as a visual aid.

declined below 20%. Due to the enzyme deactivation, the reaction was limited by the enzyme activity rather than the availability of H_2O_2. Based on additional control experiments, no significant substrate and product adsorption on electrode surface were observed (Fig. S4).

3.3. Evaluation of key performance indicators from the electroenzymatic hydroxylation

Once the feasibility of the bioelectrochemical system has been established, the subsequent step was the assessment of the overall efficiency. This evaluation was accomplished by employing key

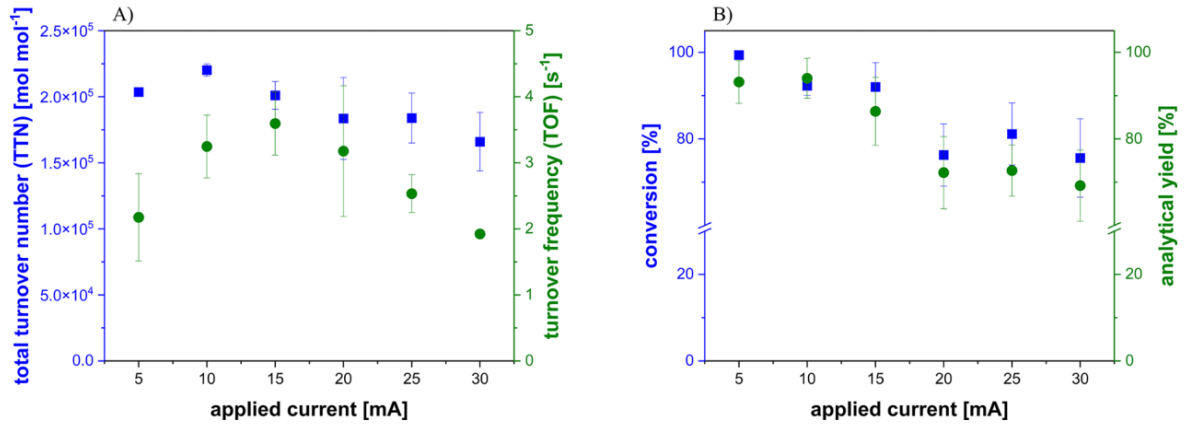

Fig. 6. A) Total turnover number (TTN), turnover frequency (TOF), B) analytical yield and conversion determined for the hydroxylation of EBA catalyzed by the r*Aae*UPO in the AiO electrode system with *in situ* generation of H_2O_2 as a function of applied current. Biological duplicates were performed.

performance indicators such as TTN, TOF, analytical yield, and conversion. The calculated results of the key performance indicators for each applied electrical current are shown in Fig. 6.

The TTN increases from 200,000 mol mol^{-1} at 5 mA to 220,000 mol mol^{-1} at 10 mA. However, as the applied current was further increased beyond 10 mA, the TTN decreased. It implies that there is a correlation between the stability of the enzyme and the applied current. There are several factors that could influence the stability of the enzyme. Other than the presence of H_2O_2 (in a concentration lower than the detection limit) and the elongated exposure to process conditions such as pH, temperature and ionic strength, the adsorption of the enzyme on the electrode surface was observed (Fig. S6). After 7 h, a loss of 15% of enzyme activity (initial activity: 1 U_{ABTS} mL^{-1}) was observed in the liquid phase, attributed to adsorption on the electrode surface. More importantly, the electrogeneration of H_2O_2 through ORR is highly associated with the formation of radicals like superoxide and hydroperoxide [39,42]. The intensity and the formation rate of these radicals are dependent on the applied current and cell potential, generally increasing at higher potential and current [13,39,42]. Increasing the current beyond 10 mA might lead to a higher formation of radicals, prompting greater enzyme deactivation and decreasing the final product concentration, thus, also decreasing the TTN. Similarly, a maximum was observed for TOF at 15 mA with up to 3.6 s^{-1}. The highest analytical yields of 98% were achieved at 5 mA and 10 mA (Fig. 6B). However, the substrate conversion was higher with there being a difference of up to 0.4 mM between the measured product and the residual substrate concentration. Thus, there is a disparity between conversions and analytical yields.

Since the reaction is limited by the generation of H_2O_2 and not by the enzymatic conversion, the enzyme concentration was reduced from 30 nM (Fig. 5) to 10 nM (Fig. S7 E) to increase the catalyst efficiency. By decreasing the added enzyme concentration (at 10 mA), the formation rate decreased slightly to 4 μM min^{-1} and a total deactivation occurred within 24 h. A total of 4.5 mM product was formed using three times lower enzyme concentration, and this resulted in an increase of TTN and TOF to 450,000 mol mol^{-1} and 7.7 s^{-1}, respectively. Further decreasing the enzyme concentration (at the same applied current) may not necessarily result in an even higher TTN, as the H_2O_2 productivity may exceed the enzymatic conversion. Additionally, it has been indicated in the literature that there could be a H_2O_2 concentration-independent limit for UPOs which exhibit an inherent "maximum" of TTN [43]. Hence, decreasing the H_2O_2 productivity to an infinitely low production rate would not result in a significantly higher TTN [43].

Several TTNs are reported in literatures. Bormann achieved a TTN of 164,000 mol mol^{-1} with manual addition of H_2O_2 and up to 400,000 mol mol^{-1} with *in situ* generation of H_2O_2 in a GDE-system, both using the same substrate and enzyme as in this study [30,43]. Ni and coworker reported a TTN of 470,000 mol mol^{-1}, using r*Aae*UPO and *n*-ethylbenzene as the substrate, while H_2O_2 was generated *in situ* using an enzymatic cascade that used 5 different enzymes, NAD^+ as cofactor and methanol as sacrificial electron donor [44]. Horst *et al.* achieved a maximum TTN of 400,000 mol mol^{-1} also using a GDE-based system for the r*Aae*UPO-catalyzed hydroxylation of *n*-ethylbenzene [13]. Seelbach *et al.*, compared the oxidation of indole catalyzed by the CPO in different operation modes and with different H_2O_2 addition methods. He showed that the application of the sensor-controlled H_2O_2 addition in a fed-batch mode yielded higher enzyme stability and TTN (866,000 mol mol^{-1}), compared to the step-wise or continuous addition of H_2O_2 in a batch mode [45]. Brummund *et al.*, reported a TTN of 4100 mol mol^{-1} for the oxidation of α-ionone catalyzed by the cytochrome P450 monooxygenase with NADPH regeneration system, employing glucose dehydrogenase and glucose as the second enzyme and substrate [46]. Although the P450 monooxygenases can catalyze the oxidation of various substrates, they are unstable, require expensive NADPH cofactor and have low coupling efficiency [46].

The highest TTN value obtained in this study is comparable to those found in literatures using electrochemical generation of H_2O_2, and exceeds the TTN from the system with manual addition of H_2O_2. Compared to the TTN reported by Ni, the TTN achieved in this study is around 10% lower, but the system used herein is far less complex, inexpensive and utilized only one enzyme [44]. In terms of TOFs, the highest TOF (7.7 s^{-1}) obtained here is currently 18 times lower than the TOF reported for the GDE-based system. This is because of lower H_2O_2 productivities achieved in this system compared to the GDE-based systems [43].

4. Conclusions

For the first time, the AiO electrode was applied in an electroenzymatic process to provide H_2O_2 *in situ* for the enzymatic hydroxylation. A TTN comparable to the best values found in literatures was achieved. The H_2O_2 productivity was identified as the limitation in this system. Optimization of the modified AiO electrode in terms of design, H_2O_2 productivity and F.E. is still ongoing. The productivity could be potentially enhanced by increasing the electrode surface, such as using a larger geometry, porous materials (*e.g.* Globugraphite) or coating with carbon nanotubes. Due to its simplicity, electrochemical *in situ* generation of H_2O_2 still remains an attractive method to minimize enzyme deactivation by reducing the contact with the co-substrate H_2O_2. By using the proposed system, drawbacks of other methods such as volume increase, formation of by-products and pH-shift can be avoided. This study shows that the AiO electrode system has the potential to be integrated into further electroenzymatic processes and could serve as an optimizable platform for H_2O_2-dependent enzymatic reactions.

CRediT authorship contribution statement

Giovanni V. Sayoga: Investigation, Validation, Visualization, Data curation, Writing – original draft. **Victoria S. Bueschler:** Investigation, Validation, Writing – review & editing. **Hubert Beisch:** Writing – review & editing. **Dirk Holtmann:** Writing – review & editing. **An-Ping Zeng:** Conceptualization, Funding acquisition, Writing – review & editing. **Bodo Fiedler:** Funding acquisition, Writing – review & editing. **Daniel Ohde:** Supervision, Project administration, Writing – review & editing. **Andreas Liese:** Conceptualization, Data curation, Funding acquisition, Resources, Supervision, Writing – review & editing.

Declaration of Competing Interest

The authors declare that they have no known competing financial interests or personal relationships that could have appeared to influence the work reported in this paper.

Data availability

Data will be made available on request.

Acknowledgement

The work was supported by the Deutsche Forschungsgemeinschaft (DFG, German Research Foundation, e-Biotech SPP 2240) (Project number: 445947004). The author(s) thank Leon Klose and Fernando Lopez Haro from TUHH for the preparation of graphical abstract.

Supplementary materials

Supplementary material associated with this article can be found, in the online version, at doi:10.1016/j.mcat.2023.113325.

References

[1] Y. Jiang, P. Ni, C. Chen, Y. Lu, P. Yang, B. Kong, A. Fisher, X. Wang, Selective electrochemical H2O2 production through two-electron oxygen electrochemistry, Adv. Energy Mater. 8 (2018), 1801909, https://doi.org/10.1002/aenm.201801909.

[2] J.M. Campos-Martin, G. Blanco-Brieva, J.L. Fierro, Hydrogen peroxide synthesis: an outlook beyond the anthraquinone process, Angew. Chem. Int. Ed. 45 (2006) 6962–6984.

[3] Z. Chen, S. Chen, S. Siahrostami, P. Chakthranont, C. Hahn, D. Nordlund, S. Dimosthenis, J.K. Nørskov, Z. Bao, T.F. Jaramillo, Development of a reactor with carbon catalysts for modular-scale, low-cost electrochemical generation of H_2O_2, React. Chem. Eng. 2 (2017) 239–245, https://doi.org/10.1039/C6RE00195E.

[4] A. Hasanzadeh, A. Khataee, M. Zarei, Y. Zhang, Two-electron oxygen reduction on fullerene C60-carbon nanotubes covalent hybrid as a metal-free electrocatalyst, Sci. Rep. 9 (2019) 13780.

[5] B.O. Burek, S. Bormann, F. Hollmann, J.Z. Bloh, D. Holtmann, Hydrogen peroxide driven biocatalysis, Green Chem. 21 (2019) 3232–3249, https://doi.org/10.1039/C9GC00633H.

[6] I. Yamanaka, T. Murayama, Neutral H2O2 synthesis by electrolysis of water and O2, Angew. Chem. 120 (2008) 1926–1928.

[7] T. Murayama, I. Yamanaka, Electrosynthesis of neutral H2O2 solution from O2 and water at a mixed carbon cathode using an exposed solid-polymer-electrolyte electrolysis cell, J. Phys. Chem. C. 115 (2011) 5792–5799.

[8] C.H. Choi, H.C. Kwon, S. Yook, H. Shin, H. Kim, M. Choi, Hydrogen peroxide synthesis via enhanced two-electron oxygen reduction pathway on carbon-coated Pt surface, J. Phys. Chem. C. 118 (2014) 30063–30070, https://doi.org/10.1021/jp5113894.

[9] J.-B. Park, D.S. Clark, Deactivation mechanisms of chloroperoxidase during biotransformations, Biotechnol. Bioeng. 93 (2006) 1190–1195, https://doi.org/10.1002/bit.20825.

[10] D. Holtmann, T. Krieg, L. Getrey, J. Schrader, Electroenzymatic process to overcome enzyme instabilities, Catal. Commun. 51 (2014) 82–85.

[11] S. Lütz, E. Steckhan, A. Liese, First asymmetric electroenzymatic oxidation catalyzed by a peroxidase, Electrochem. Commun. 6 (2004) 583–587, https://doi.org/10.1016/j.elecom.2004.04.009.

[12] T. Krieg, S. Hüttmann, K.-M. Mangold, J. Schrader, D. Holtmann, Gas diffusion electrode as novel reaction system for an electro-enzymatic process with chloroperoxidase, Green Chem 13 (2011) 2686–2689, https://doi.org/10.1039/C1GC15391A.

[13] A.E.W. Horst, S. Bormann, J. Meyer, M. Steinhagen, R. Ludwig, A. Drews, M. Ansorge-Schumacher, D. Holtmann, Electro-enzymatic hydroxylation of ethylbenzene by the evolved unspecific peroxygenase of Agrocybe aegerita, J. Mol. Catal. B Enzym. 133 (2016) S137–S142, https://doi.org/10.1016/j.molcatb.2016.12.008.

[14] S. Lütz, K. Vuorilehto, A. Liese, Process development for the electroenzymatic synthesis of (R)-methylphenylsulfoxide by use of a 3-dimensional electrode, Biotechnol. Bioeng. 98 (2007) 525–534, https://doi.org/10.1002/bit.21434.

[15] S. Bormann, A.G. Baraibar, Y. Ni, D. Holtmann, F. Hollmann, Specific oxyfunctionalisations catalysed by peroxygenases: opportunities, challenges and solutions, Catal. Sci. Technol. 5 (2015) 2038–2052, https://doi.org/10.1039/C4CY01477D.

[16] F. van de Velde, N.D. Lourenço, M. Bakker, F. van Rantwijk, R.A. Sheldon, Improved operational stability of peroxidases by coimmobilization with glucose oxidase, Biotechnol. Bioeng. 69 (2000) 286–291, https://doi.org/10.1002/1097-0290(20000805)69:3<286::AID-BIT6>3.0.CO;2-R.

[17] F. van Rantwijk, R.A. Sheldon, Selective oxygen transfer catalysed by heme peroxidases: synthetic and mechanistic aspects, Curr. Opin. Biotechnol. 11 (2000) 554–564, https://doi.org/10.1016/S0958-1669(00)00143-9.

[18] F. van de Velde, F. van Rantwijk, R.A. Sheldon, Selective oxidations with molecular oxygen, catalyzed by chloroperoxidase in the presence of a reductant, J. Mol. Catal. B Enzym. 6 (1999) 453–461, https://doi.org/10.1016/S1381-1169(99)00059-X.

[19] C. Kohlmann, S. Lütz, Electroenzymatic synthesis of chiral sulfoxides, Eng. Life Sci. 6 (2006) 170–174, https://doi.org/10.1002/elsc.200620907.

[20] M. Stöckl, T. Lange, P. Izadi, S. Bolat, N. Teetz, F. Harnisch, D. Holtmann, Application of gas diffusion electrodes in bioeconomy–an update, Biotechnol. Bioeng. (2023).

[21] S. Bormann, M.M. van Schie, T.P. De Almeida, W. Zhang, M. Stöckl, R. Ulber, F. Hollmann, D. Holtmann, H2O2 production at low overpotentials for electroenzymatic halogenation reactions, ChemSusChem 12 (2019) 4759–4763.

[22] J.K. Chen, K. Nobe, Oxidation of Dimethylaniline by Horseradish Peroxidase and Electrogenerated Peroxide: I. Free Enzyme Studies, J. Electrochem. Soc. 140 (1993) 299, https://doi.org/10.1149/1.2221041.

[23] T. Utesch, A.-P. Zeng, A novel All-in-One electrolysis electrode and bioreactor enable better study of electrochemical effects and electricity-aided bioprocesses, Eng. Life Sci. 18 (2018) 600–610.

[24] Energieeinsparung bei der Chlorproduktion, Covestro AG. (n.d.). https://www.covestro.com/de/sustainability/flagship-solutions/oxygen-depolarized-cathode (accessed April 18, 2023).

[25] L.M. Baumgartner, C.I. Koopman, A. Forner-Cuenca, D.A. Vermaas, Narrow pressure stability window of gas diffusion electrodes limits the scale-up of CO2 electrolyzers, ACS Sustain. Chem. Eng. 10 (2022) 4683–4693, https://doi.org/10.1021/acssuschemeng.2c00195.

[26] J. Herzog, A. Mook, L. Guhl, M. Bäumler, M.H. Beck, D. Weuster-Botz, F. R. Bengelsdorf, A.-P. Zeng, Novel synthetic co-culture of Acetobacterium woodii and Clostridium drakei using CO2 and *in situ* generated H2 for the production of caproic acid via lactic acid, Eng. Life Sci 23 (2022), e2100169, https://doi.org/10.1002/elsc.202100169.

[27] P. Arbter, A. Sinha, J. Troesch, T. Utesch, A.-P. Zeng, Redox governed electro-fermentation improves lipid production by the oleaginous yeast Rhodosporidium toruloides, Bioresour. Technol. 294 (2019), 122122, https://doi.org/10.1016/j.biortech.2019.122122.

[28] P. Arbter, W. Sabra, T. Utesch, Y. Hong, A.-P. Zeng, Metabolomic and kinetic investigations on the electricity-aided production of butanol by Clostridium pasteurianum strains, Eng. Life Sci. 21 (2021) 181–195.

[29] M. Hofrichter, R. Ullrich, Oxidations catalyzed by fungal peroxygenases, Curr. Opin. Chem. Biol. 19 (2014) 116–125, https://doi.org/10.1016/j.cbpa.2014.01.015.

[30] S. Bormann, B.O. Burek, R. Ulber, D. Holtmann, Immobilization of unspecific peroxygenase expressed in Pichia pastoris by metal affinity binding, Mol. Catal. 492 (2020), 110999, https://doi.org/10.1016/j.mcat.2020.110999.

[31] P. Molina-Espeja, E. Garcia-Ruiz, D. Gonzalez-Perez, R. Ullrich, M. Hofrichter, M. Alcalde, Directed evolution of unspecific peroxygenase from Agrocybe aegerita, Appl. Environ. Microbiol. 80 (2014) 3496–3507.

[32] J. Cino, High-yield protein production from Pichia pastoris yeast: a protocol for benchtop fermentation, Am. Biotechnol. Lab. 17 (1999) 10–13.

[33] F. Perz, S. Bormann, R. Ulber, M. Alcalde, P. Bubenheim, F. Hollmann, D. Holtmann, A. Liese, Enzymatic oxidation of butane to 2-butanol in a bubble column, ChemCatChem 12 (2020) 3666–3669.

[34] P. Molina-Espeja, S. Ma, D.M. Mate, R. Ludwig, M. Alcalde, Tandem-yeast expression system for engineering and producing unspecific peroxygenase, Enzyme Microb. Technol. 73–74 (2015) 29–33, https://doi.org/10.1016/j.enzmictec.2015.03.004.

[35] A.R. Khataee, M. Safarpour, M. Zarei, S. Aber, Electrochemical generation of H2O2 using immobilized carbon nanotubes on graphite electrode fed with air: investigation of operational parameters, J. Electroanal. Chem. 659 (2011) 63–68, https://doi.org/10.1016/j.jelechem.2011.05.002.

[36] M. Zhou, Q. Yu, L. Lei, The preparation and characterization of a graphite–PTFE cathode system for the decolorization of C.I. Acid Red 2, Dyes Pigment. 77 (2008) 129–136, https://doi.org/10.1016/j.dyepig.2007.04.002.

[37] E. Peralta, R. Natividad, G. Roa, R. Marin, R. Romero, T. Pavon, A comparative study on the electrochemical production of H2O2 between BDD and graphite cathodes, Sustain. Environ. Res. 23 (2013) 259–266.

[38] K. Wang, Z. Zhu, D. Xu, M. Li, S. Yuan, H. Wang, Highly active and cheap graphite/polytetrafluoroethylene composite coating cathodes for electrogeneration of hydrogen peroxide, Clean Technol. Environ. Policy. 24 (2022) 2407–2417, https://doi.org/10.1007/s10098-022-02323-z.

[39] A.D. Pozzo, L.D. Palma, C. Merli, E. Petrucci, An experimental comparison of a graphite electrode and a gas diffusion electrode for the cathodic production of hydrogen peroxide, J. Appl. Electrochem. 35 (2005) 413–419, https://doi.org/10.1007/s10800-005-0800-2.

[40] A. Karich, M. Kluge, R. Ullrich, M. Hofrichter, Benzene oxygenation and oxidation by the peroxygenase of Agrocybe aegerita, AMB Express 3 (2013) 5, https://doi.org/10.1186/2191-0855-3-5.

[41] A. Karich, K. Scheibner, R. Ullrich, M. Hofrichter, Exploring the catalase activity of unspecific peroxygenases and the mechanism of peroxide-dependent heme destruction, J. Mol. Catal. B Enzym. 134 (2016) 238–246, https://doi.org/10.1016/j.molcatb.2016.10.014.

[42] J.-M. Noël, A. Latus, C. Lagrost, E. Volanschi, P. Hapiot, Evidence for OH radical production during electrocatalysis of oxygen reduction on Pt surfaces: consequences and application, J. Am. Chem. Soc. 134 (2012) 2835–2841, https://doi.org/10.1021/ja211663t.

[43] S. Bormann, D. Hertweck, S. Schneider, J.Z. Bloh, R. Ulber, A.C. Spiess, D. Holtmann, Modeling and simulation-based design of electroenzymatic batch processes catalyzed by unspecific peroxygenase from A. aegerita, Biotechnol. Bioeng. 118 (2021) 7–16.

[44] Y. Ni, E. Fernández-Fueyo, A.G. Baraibar, R. Ullrich, M. Hofrichter, H. Yanase, M. Alcalde, W.J.H. van Berkel, F. Hollmann, Peroxygenase-catalyzed oxyfunctionalization reactions promoted by the complete oxidation of methanol, Angew. Chem. Int. Ed. 55 (2016) 798–801, https://doi.org/10.1002/anie.201507881.

[45] K. Seelbach, M.P.J. van Deurzen, F. van Rantwijk, R.A. Sheldon, U. Kragl, Improvement of the total turnover number and space-time yield for chloroperoxidase catalyzed oxidation, Biotechnol. Bioeng. 55 (1997) 283–288, https://doi.org/10.1002/(SICI)1097-0290(19970720)55:2<283::AID-BIT6>3.0.CO;2-E.

[46] J. Brummund, M. Müller, T. Schmitges, I. Kaluzna, D. Mink, L. Hilterhaus, A. Liese, Process development for oxidations of hydrophobic compounds applying cytochrome P450 monooxygenases in-vitro, J. Biotechnol. 233 (2016) 143–150, https://doi.org/10.1016/j.jbiotec.2016.07.002.

6.1. Integration of Multiple All-in-One Electrodes

Following the successful combination of the *in situ* electrosynthesis of H_2O_2 with enzymatic hydroxylation catalyzed by r*Aae*UPO to establish a BES, further optimization of the AiO electrode system was conducted. It was identified that the productivity of the co-substrate H_2O_2 represented a significant limitation of the system, which subsequently resulted in a lower TOF compared to values reported in the literature. In the AiO electrode system, both the anode and cathode are utilized for the simultaneous *in situ* generation of oxygen and H_2O_2, respectively. A potential limitation in H_2O_2 productivity within the AiO electrode system might arise due to the restricted oxygen availability. It is also crucial to consider the electron balance during the electrolysis. For each H_2O_2 molecule synthesized at the cathode (**Eq. 3.2**), only half an oxygen molecule is generated at the anode (**Eq. 3.9**). This imbalance might intensify the oxygen limitation. To investigate this, experiments were conducted to quantify oxygen productivity at the anode. Methods utilized to conduct experiments in this subchapter are specified in the appendix **11.2. Supporting Information to Chapter 6**.

The results confirmed that oxygen productivity (**Fig. 6. 1**) was consistently lower than the measured H_2O_2 productivity (**Fig. 3. A**; publication). For example, at 10 mA, the oxygen productivity was 0.32 µM min^{-1} cm^{-2}, while the H_2O_2 productivity was 0.55 µM min^{-1} cm^{-2}. At 20 mA, the oxygen productivity increased to 0.50 µM min^{-1} cm^{-2}, whereas the H_2O_2 productivity reached 0.70 µM min^{-1} cm^{-2}. This comparison reveals a 30 – 42% discrepancy between the amounts of generated oxygen and H_2O_2, indicating that the additional oxygen needed for the H_2O_2 formation might originated from dissolved atmospheric oxygen diffusing into the system and stored oxygen in the medium at the start of the experiment. In addition to competing side reactions, limited oxygen availability also provides an explanation for the plateau observed in H_2O_2 concentration after approximately 5 min at higher applied currents (**Fig. 3. B**; publication). Despite increasing the current, oxygen productivity could not match the rate of H_2O_2 generation, thus limiting further H_2O_2 accumulation. Therefore, oxygen supply becomes a rate-limiting factor, particularly at higher currents, where competing side reactions become most pronounced.

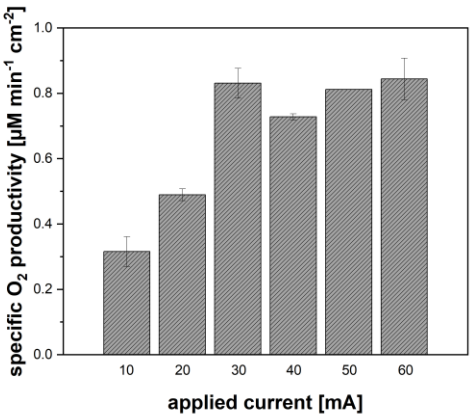

Fig. 6. 1. *Specific oxygen productivity at the anode of the All-in-One electrode system as a function of applied current. Reaction condition: 200 mL 0.1 M KP_i buffer pH 7, 250 rpm, temperature: 22 ± 1 °C, 5 min. Carbon felt working electrode was replaced by titanium wire to reduce the possibility of oxygen reduction reaction. Biological duplicates were performed.*

To maintain a consistent supply of oxygen within the medium, aeration was introduced into the system. The aeration source was strategically positioned directly beneath the electrode and above the stirrer (high shear force) to ensure optimal dispersion of bubbles and enhance the oxygen transfer. The influence of various airflow rates on H_2O_2 productivity was subsequently investigated to determine the optimal condition.

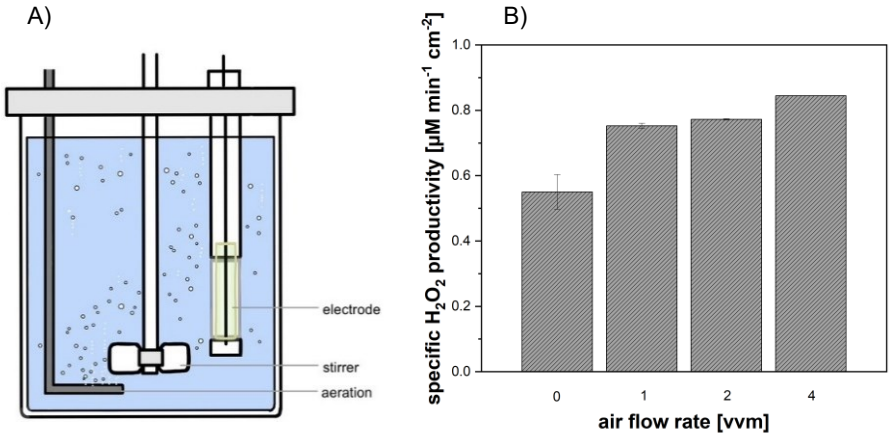

Fig. 6. 2. A*) Schematic representation of the All-in-One electrode system with the aeration.* ***B****) Specific H_2O_2 productivity as a function of air flow rate. Reaction condition: 200 mL 0.1 M KP_i buffer pH 7, 10 mA, 250 rpm, temperature: 22 ± 1 °C, 30 min. Biological duplicates were performed.*

The H_2O_2 productivity increased proportionally with the air flow rate at a constant applied current of 10 mA (**Fig 6. 2. B**). The highest observed productivity reached 0.84 µM min^{-1} cm^{-2} at an aeration rate of 4 vvm, representing a 53% improvement compared to the system without aeration. The enhanced H_2O_2 productivity can be primarily attributed to the increased oxygen availability in the medium, which supports the electrochemical ORR responsible for the H_2O_2 generation. This hypothesis was further supported by the observed increase in dissolved

oxygen concentration and its mass transfer rate (k_La) in the medium, which correlated with both higher air flow rates and increased stirring rates (**Fig. 6. 3**). The k_La value rose almost linearly from 0.028 min^{-1} to 0.1 min^{-1} at 1 vvm as the stirring rate increased from 250 rpm to 1000 rpm. This improvement is likely due to the smaller bubble diameters produced at higher stirring rates, which increased the bubble residence time in the medium and the mass transfer. In contrast, the k_La value showed no significant increase when the air flow rate was raised from 2 vvm to 4 vvm, as higher air flow rates tend to generate larger air bubbles (due to bubble coalescence) with greater buoyancy, leading to a shorter residence times. Consequently, increasing the stirring rate proves to be more efficient in enhancing the oxygen mass transfer than simply increasing the air flow rate. Another contributing factor to the increased H_2O_2 productivity, besides the enhanced oxygen availability, was the turbulent flow at the electrode interface introduced by the aeration. This turbulent flow likely reduced the thickness of the electrochemical double layer, thereby improving the mass transfer of oxygen to the cathode. This aspect is supported by the decrease of the cell potential from 2.3 V in non-aerated condition to 2.1 V at 4 vvm, at the same applied current of 10 mA. Additionally, the turbulence facilitated faster desorption of the formed H_2O_2 from the electrode surface, minimizing the potential of further redox reactions of the formed H_2O_2 that would otherwise reduce the H_2O_2 yield. Notably, the F.E. of the system at 10 mA, increased from 48% without aeration to 52%, 63% and 68% at air flow rates of 1, 2 and 4 vvm, respectively.

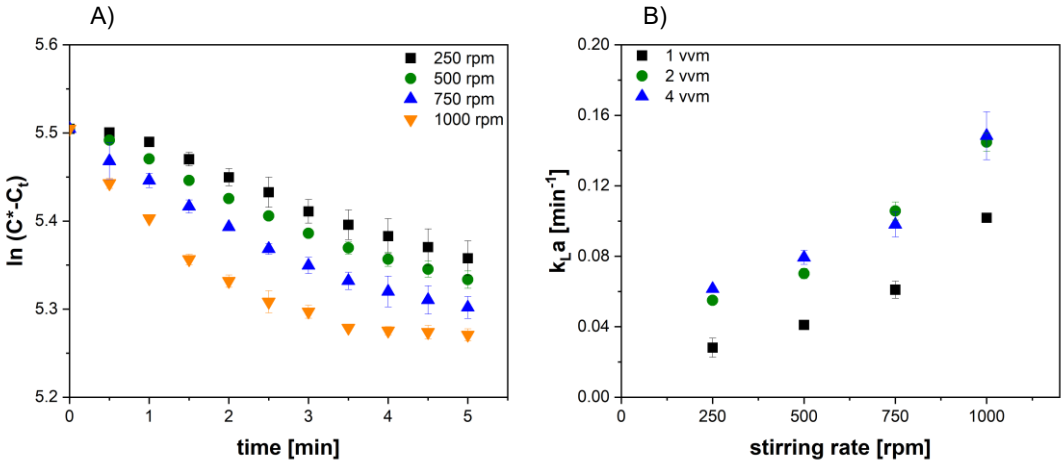

Fig. 6. 3. A*) Oxygen concentration as a function of time at 1 vvm and various stirring rates.* ***B****) Oxygen mass transfer coefficient (k_La) as a function of stirring rate at various aeration rates. Reaction condition: 200 mL 0.1 M KP_i pH 7, temperature: 22 ± 1 °C. k_La was determined through the slope of the difference in the natural logarithm of theoretical maximum dissolved oxygen concentration (C^*) and the concentration of dissolved oxygen (C_t) over time ($k_La = \frac{ln(C^*-C_t)}{t_2-t_1}$) [122]. Theoretical maximum dissolved oxygen concentration in the medium was 245 µM.*

Although the oxygen mass transfer in the medium was improved and the mixing time reduced by a factor of 2.8 from 18.67 s to 6.67 s with increased stirring rate (**Fig. S6. 8**, see **Appendix** supporting information), a stirring rate of 250 rpm was retained for subsequent experiments.

This decision was made to ensure consistent and comparable reaction conditions with previous experiments. The next step was determining whether the increase in H_2O_2 productivity, following the introduction of aeration into the system, could directly be translated to an improvement in biocatalytic productivity within the BES. To explore this, experiments were conducted at an applied current of 10 mA and using 10 nM (0.3 U_{ABTS} mL^{-1}) r*Aae*UPO with air flow rates of 1 vvm and 4 vvm (representing the lowest and highest aeration rates tested). The results are displayed in **Fig. 6. 4**. Herein, TON are plotted as a function of time instead of the product concentration, as both product concentration and TON follow the same progression over time.

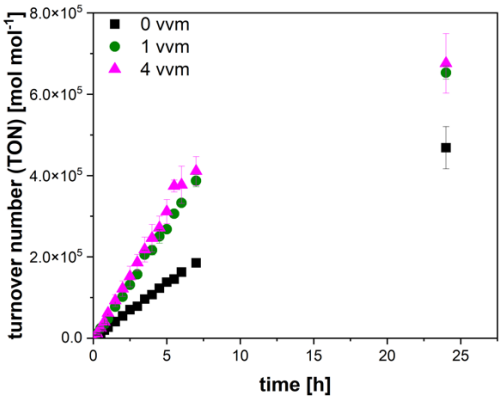

Fig. 6. 4. *Turnover number (TON) as a function of time from the electroenzymatic hydroxylation in the All-in-One electrode system at various aeration rates. Reaction condition: 200 mL 0.1 M KP_i buffer pH 7, 8 mM EBA, 10 nM rAaeUPO, 250 rpm, temperature: 22 ± 1 °C, 24 h, 10 mA, sparged with air. Biological duplicates were performed.*

In comparison to experiments conducted without aeration, moderate accumulations of H_2O_2 were observed even while the enzyme was still active. Specifically, H_2O_2 concentration reached approximately 35 µM at 1 vvm and 60 µM at 4 vvm air flow rates. This accumulation increased progressively as the enzyme activity declined over time. The observed accumulation indicated that the H_2O_2 productivity exceeded the enzyme's catalytic capacity to convert H_2O_2. As a result, the saturation of the enzyme by the co-substrate increased, leading to an enhanced biocatalytic product formation rate, which rose from 4 µM min^{-1} to 11.5 µM min^{-1} at 4 vvm. Correspondingly, the TOF increased from 7.7 s^{-1} to 17.1 s^{-1}, and the TTN increased from 450,000 mol mol^{-1} to 670,000 mol mol^{-1} (**Table 6. 1**). This suggests that the aeration facilitated a higher rate of H_2O_2 generation and potentially reduced the rate of competing reactions, especially the formation of radicals. Thus, promoting an overall increase in biocatalytic efficiency. A 48% increase in the TTN can be directly linked to the aforementioned enhanced biocatalytic productivity due to higher saturation by the co-substrate, particularly during the initial phase of the reaction when enzyme activity was at its peak. Thus, leading to a higher final product concentration upon complete enzyme deactivation, which was 7.97 mM.

However, it is important to note that further increasing the aeration rate from 1 vvm to 4 vvm did not result in a proportionate enhancement of the biocatalytic product formation rate, indicating that the effect of aeration on productivity plateaus beyond a certain threshold. The comparable results observed in experiments conducted at 1 vvm and 4 vvm, with respect to the product formation rate, TTN, and TOF (**Table 6. 1**), can be attributed to the comparable H_2O_2 productivities, which were 0.75 µM min^{-1} cm^{-2} at 1 vvm and 0.84 µM min^{-1} cm^{-2} at 4 vvm, and the similar accumulation of H_2O_2 in the medium. Although the oxygen mass transfer rate increased from 0.028 min^{-1} to 0.06 min^{-1} as the aeration rate increased from 1 vvm to 4 vvm, the absence of a significant increase in H_2O_2 productivity and accumulation suggests that the electrochemically active surface area capable of facilitating ORR might have become a limiting factor.

Table 6. 1. *Total turnover number (TTN) and turnover frequency (TOF) obtained from the hydroxylation of 4-ethylbenzoicacid (EBA) catalyzed by the recombinant unspecific peroxygenase from Agrocybe aegerita (rAaeUPO) in the All-in-One (AiO) electrode system with in situ H_2O_2 generation at 10 mA.*

Configuration	Initial formation rate [µM min^{-1}]	TTN [mol mol^{-1}]	TOF [s^{-1}]
1 AiO electrode, 0 vvm	4.0	450,000	7.7
1 AiO electrode, 1 vvm	11.0	650,000	13.2
1 AiO electrode, 4 vvm	11.5	670,000	17.1
2 AiO electrodes, 0 vvm	12.2	480,000	15.8
2 AiO electrodes, 1 vvm	13.6	660,000	20.1

To address the limitation posed by the restricted electrochemical surface area, a strategy of electrode numbering-up was employed as part of a surface enlargement approach. This was achieved by incorporating two AiO electrodes within a single reactor.

By incorporating two AiO electrodes into the system, the surface-to-volume ratio doubled from 0.055 cm^{-1} to 0.11 cm^{-1}, thereby increasing the available electrochemical surface area. With the power supply featuring multiple channels, each electrode was controlled independently. To maintain consistency with previous experiments involving a single AiO electrode, the same current density was applied to each electrode. The electroenzymatic hydroxylation reaction was subsequently repeated to evaluate the effectiveness of this multi-electrode configuration. The integration of two AiO electrodes in the electroenzymatic hydroxylation at 10 mA, without aeration, resulted in a TOF of 15.8 s^{-1}, an increase by a factor of 2 compared to the TOF observed in experiments with a single AiO electrode under identical conditions (**Table 6. 1**). This increase in TOF can be attributed to the higher surface-to-volume ratio provided by the dual-electrode setup. Supporting this hypothesis, the surface-specific H_2O_2 productivity in the dual-electrode system was 0.45 µM min^{-1} cm^{-2}, approximately 18% lower than that of the single-electrode system with 0.55 µM min^{-1} cm^{-2}. However, this slight reduction in surface-

specific productivity was compensated by the increased surface-to-volume ratio in the multiple-electrode configuration.

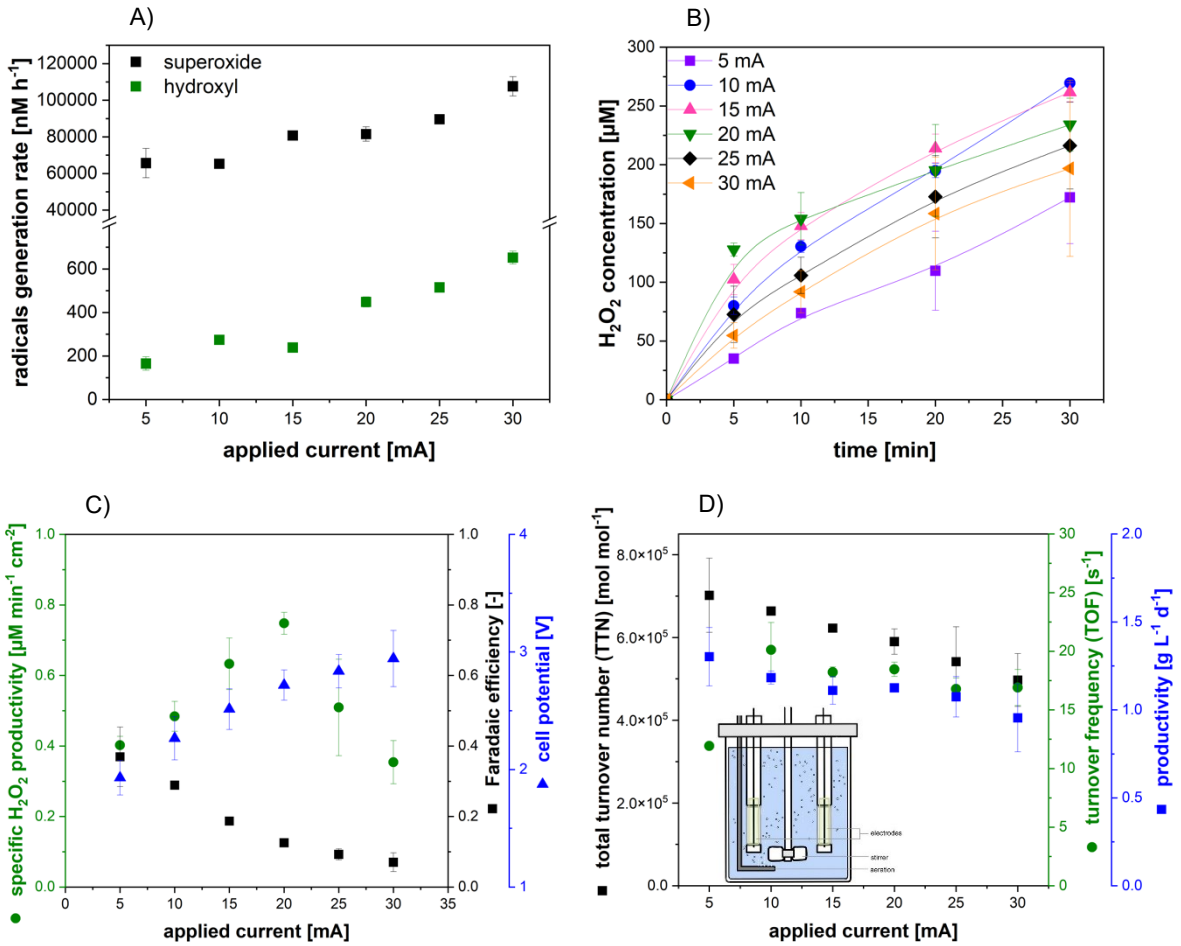

***Fig. 6. 5. A**) Formation rate of superoxide and hydroxyl radicals as a function of applied current in the two All-in-One (AiO) electrodes system. Reaction condition: 200 mL nitro blue tetrazolium or terephthalic acid assay in 0.1 M KP_i pH 7, 250 rpm, temperature: 22 ± 1 °C. **B**) H_2O_2 concentration as a function of the time at different applied currents in the two AiO electrodes system with 1 vvm aeration. **C**) Specific H_2O_2 productivity, Faradaic efficiency (F.E.) and resulting cell potential as a function of applied current in the two AiO electrodes system with 1 vvm aeration. **D**) Total turnover number (TTN), Turnover frequency (TOF) and productivity as a function of applied current from the electroenzymatic hydroxylation with in situ generation of H_2O_2 in the two AiO electrodes system with 1 vvm aeration. Insert: schematic representation of the two All-in-One electrodes system with an aeration. Reaction condition: each AiO electrode equipped with carbon felt cathode (11 cm^2) and platinized titanium anode (4.24 cm^2), 200 mL 0.1 M KP_i pH 7, 8 mM EBA, 10 nM rAaeUPO, temperature: 22 ± 1 °C, 250 rpm. F.E. was determined after 30 min. The "applied current" displayed on the graph represents the current applied to each of the AiO electrode within the system. Biological duplicates were performed. The depicted lines serve as a visual aid.*

During the electroenzymatic reaction, approximately 40 µM of H_2O_2 was accumulated (**Fig. S6. 9**), a phenomenon that was absent in experiments with a single AiO electrode without aeration. While the TOF was significantly improved, the TTN only showed an increase from 450,000 mol mol^{-1} to 480,000 mol mol^{-1} (**Table 6. 1**). The increased surface-to-volume ratio not only led to higher H_2O_2 accumulation but also further accelerated radical generation rates (**Fig. 6. 5. A**) (data containing the formation rate of radicals in the two-electrode system with aeration is not available). Electrons and holes (h^+) reacted with oxygen and water, forming

superoxide and hydroxyl radicals, with the one-electron reduction of H_2O_2 contributing to hydroxyl radical formation (**Eq. 3.6**) [66]. The hydroxyl radical formation rate doubled in the dual-electrode system compared to the single electrode system (**Fig. S6. 10**), ranging from 100 to 600 nM h^{-1}, while the superoxide formation increased by 40 – 50%. This elevated radical production compromised the enzyme stability, increasing the deactivation rate from 0.03 U_{ABTS} mL^{-1} h^{-1} to 0.036 U_{ABTS} mL^{-1} h^{-1} at 10 mA. As a result, despite the doubled TOF, the TTN improvement was marginal compared to the single-electrode system. Again, this outcome can be attributed to the fact that, while the initial product formation rate and TOF increased, a much higher final product concentration was not achieved (around 6.2 mM) due to a higher enzyme deactivation rate. Additionally, hydroxyl radicals not only destabilized r*Aae*UPO stability but also interfered with the H_2O_2 formation by slowing the oxygen reduction kinetics [45]. Introducing radical scavengers like ethylbenzene or isopropanol for hydroxyl radicals, and benzoquinone or superoxide dismutase for superoxide, could potentially enhance the r*Aae*UPO stability [45].

Given the minimal differences in the TTN between the single-electrode experiments conducted at 1 vvm and 4 vvm aeration rates (**Table 6. 1**), and also to avoid excessive aeration of the system, 1 vvm aeration rate was selected as the optimal condition for the multiple-electrodes system. The overall trends of the specific H_2O_2 productivity, cell potential and F.E. in the multiple AiO electrodes system (**Fig. 6. 5. C**) closely mirrored those observed in the single-electrode system (**Fig. 3. A**; publication). Compared to the non-aerated setup with two AiO electrodes, the specific H_2O_2 productivity increased by approximately 11%. Moreover, the integration of two AiO electrodes with aeration resulted in an increase in specific H_2O_2 productivity ranging from 7% to 33% across various currents, except at 25 mA and 30 mA, when compared to the single-electrode system. However, the enhancement effect of the aeration on the specific H_2O_2 productivity in the dual-electrode setup was less pronounced than that observed in the single-electrode system with 1 vvm aeration, which saw a 36% increase (**Fig. 6. 2. B**). This reduced effect can likely be attributed to the placement of the sparger which was located between the two AiO electrodes, in contrast to its position in the single-electrode system where it was located directly beneath the electrode. The different positioning of the sparger likely reduced the impact of the turbulent flow on the oxygen mass transfer and the H_2O_2 desorption from the electrode. Additionally, the doubling of the electrochemical surface area may have increased the rates of competing reactions, such as the full reduction of oxygen to water (**Eq. 3.3**), the reduction of H_2O_2 to hydroxyl radicals or water (**Eq. 3.6**, **Eq. 3.7**), and the oxidation of H_2O_2 (**Eq. 3.5**). These factors likely contributed to the relatively moderate increase in surface-specific H_2O_2 productivity in the dual-electrodes system. The F.E. in the dual AiO electrodes system ranged from 15% to 133% higher (**Fig. 6.**

5. C) than that of the single-electrode system (**Fig. 3. A**; publication), particularly at higher applied currents between 20 – 30 mA. At these currents, H_2O_2 accumulation continued without reaching a plateau, at least up to 30 min of reaction time (**Fig. 6. 5. B**). On the contrary, at lower applied currents between 5 mA and 15 mA, the F.E. decreased by as much as 38%. Although the accumulation of H_2O_2 in the medium after 30 minutes was higher, the accumulated H_2O_2 did not double within the same timeframe, despite the doubling of the total applied current, resulting in a decreased F.E.. The performance indicators from the electroenzymatic hydroxylation within dual AiO electrodes system are summarized in **Fig. 6. 5. D**. Notably, during the initial seven hours of the reaction, H_2O_2 accumulation reached approximately 49 µM (**Fig. S6. 11**). As the enzyme's stability gradually declined, H_2O_2 accumulation further increased, eventually reaching 1.7 mM after 24 h, when no enzyme activity remained. The utilization of multiple AiO electrodes provided a significant enhancement in the system's performance, with the TOF reaching up to 20.1 s^{-1}, a 52% improvement over the TOF observed in the single electrode system with 1 vvm aeration and a 27% increase compared to the multiple electrodes system without aeration (**Table 6. 1**). It is worth mentioning that the highest TTN achieved within this configuration was 700,000 mol mol^{-1} at 5 mA. The maximum productivity of 1.30 g L^{-1} d^{-1} was achieved at the lowest applied current, with a declining trend observed as the current increased. This decrease in productivity correlates with the reduction in enzyme stability at higher currents, which subsequently led to a lower final product concentration. The productivity was determined based on the final product concentration over a fixed experimental duration of 24 h, as the exact point of complete enzyme deactivation was unknown (likely occurring overnight). Consequently, the reduction in final product concentration at higher currents resulted in a proportional decrease in productivity. Similar to the single electrode system (**Fig. 6. A**; publication), both TTN and TOF showed a decreasing trend with increasing applied current. This reduction is attributed to factors such as the destabilization of r*Aae*UPO, driven by the catalase malfunction reaction and the presence of radicals, which adversely affect the enzyme activity and stability.

After establishing the multiple AiO electrodes system to enhance the electrochemical surface area, optimization was pursued to further improve the enzyme stability and productivity. The aim was to develop a BES capable of maintaining a constant H_2O_2 concentration, thereby preventing its excessive accumulation, which could compromise the enzyme stability and accelerate H_2O_2 buildup — issues that were previously observed in the BES operated under galvanostatic condition [16,103] and in the AiO electrode system. Although there have been reports on sensor-controlled H_2O_2 dosing to regulate H_2O_2 concentrations in biocatalytic systems [67,123], detailed studies on sensor-controlled electrogeneration of H_2O_2 in BES remain limited. To address this knowledge gap and assess the feasibility of such a system,

modifications to the existing setup were required. An automated system incorporating a H_2O_2 sensor and an *in situ* H_2O_2 generation was developed to maintain a predefined concentration of H_2O_2 (H_2O_2-stat mode), independent of the enzyme activity and the progress of the reaction. Additionally, it was important to investigate the influence of various H_2O_2 threshold concentrations on the stability of r*Aae*UPO and the overall performance of the BES. However, the AiO electrode system, utilizing a carbon felt cathode, was unable to sustain H_2O_2 concentrations above 60 µM during the electroenzymatic reaction without undergoing further redox conversion, particularly given the simultaneous consumption of H_2O_2 by the enzyme. Furthermore, no linear correlation was observed between the applied current and specific H_2O_2 productivity in the AiO electrode system. While H_2O_2 productivity initially increased with increasing applied current, it declined at currents above 20 mA. This non-linear behavior posed a significant challenge in the development of the automation system. To address this issue, a GDE was implemented as an alternative cathode in the BES. Given the extensive application of GDE in BES [8,104,112], the GDE was also utilized as a reference system to benchmark the performance of the AiO electrode system. The development and comprehensive characterization of the GDE system for the electroenzymatic hydroxylation, incorporating an automation program at various H_2O_2-stat concentrations, will be discussed in detail in the subsequent chapter.

7. Electrochemical H_2O_2-Stat Mode as Reaction Concept to Improve the Process Performance of an Unspecific Peroxygenase

Giovanni V. Sayoga[a], Victoria S. Bueschler[a], Hubert Beisch[b], Tyll Utesch[c], Dirk Holtmann[d], Bodo Fiedler[b], Daniel Ohde[a], Andreas Liese[a]

[a]Institute of Technical Biocatalysis, Hamburg University of Technology, Denickestraße 15, 21073 - Hamburg, Germany
[b]Institute of Polymers and Composites, Hamburg University of Technology, Denickestraße 15, 21073 - Hamburg, Germany
[c]Institute of Bioprocess and Biosystems Engineering, Hamburg University of Technology, Denickestraße 15, 21073 - Hamburg, Germany
[d]Institute of Process Engineering in Life Sciences, Karlsruhe Institute of Technology, Fritz-Haber-Weg 4, 76131 - Karlsruhe, Germany

Bibliographic details
published October 2023, Volume 78, pages 95-104
New Biotechnology (Elsevier)
DOI: 10.1016/j.nbt.2023.10.007

New BIOTECHNOLOGY 78 (2023) 95–104

Contents lists available at ScienceDirect

New BIOTECHNOLOGY

journal homepage: www.elsevier.com/locate/nbt

Electrochemical H_2O_2 - stat mode as reaction concept to improve the process performance of an unspecific peroxygenase

Giovanni V. Sayoga [a,*], Victoria S. Bueschler [a], Hubert Beisch [b], Tyll Utesch [c], Dirk Holtmann [d], Bodo Fiedler [b], Daniel Ohde [a], Andreas Liese [a,*]

[a] Institute of Technical Biocatalysis, Hamburg University of Technology, Denickestraße 15, 21073 Hamburg, Germany
[b] Institute of Polymers and Composites, Hamburg University of Technology, Denickestraße 15, 21073 Hamburg, Germany
[c] Institute of Bioprocess and Biosystems Engineering, Hamburg University of Technology, Denickestraße 15, 21073 Hamburg, Germany
[d] Institute of Process Engineering in Life Sciences, Karlsruhe Institute of Technology, Fritz-Haber-Weg 4, 76131 Karlsruhe, Germany

ARTICLE INFO

Keywords:
Biocatalysis
Bioelectrochemical system
Bioelectrocatalysis
Electrosynthesis
Hydrogen peroxide

ABSTRACT

The electroenzymatic hydroxylation of 4-ethylbenzoic acid catalyzed by the recombinant unspecific peroxygenase from the fungus *Agrocybe aegerita* (r*Aae*UPO) was performed in a gas diffusion electrode (GDE)-based system. Enzyme stability and productivity are significantly affected by the way the co-substrate hydrogen peroxide (H_2O_2) is supplied. In this study, two *in-situ* electrogeneration modes of H_2O_2 were established and compared. Experiments under galvanostatic conditions (constant productivity of H_2O_2) were conducted at current densities spanning from 0.8 mA cm^{-2} to 6.4 mA cm^{-2}. For comparison, experiments under H_2O_2-stat mode (constant H_2O_2 concentration) were performed. Here, four H_2O_2 concentrations between 0.06 mM and 0.28 mM were tested. A maximum H_2O_2 productivity of 5.5 μM min^{-1} cm^{-2} and productivity of 10.5 g L^{-1} d^{-1} were achieved under the galvanostatic condition at 6.4 mA cm^{-2}. Meanwhile, the highest total turnover number (TTN) of 710,000 mol mol^{-1} and turnover frequency (TOF) of 87.5 s^{-1} were obtained under the H_2O_2-stat mode at concentration limits of 0.15 mM and 0.28 mM, respectively. The most favorable outcome in terms of maximum achievable TTN, TOF and productivity was found under the H_2O_2-stat mode at concentration limit of 0.2 mM. Here, a TTN of 655,000 mol mol^{-1}, a TOF of 80.3 s^{-1} and a productivity of 6.1 g L^{-1} d^{-1} were achieved. The electrochemical H_2O_2-stat mode not only offers a promising alternative reaction concept to the well-established galvanostatic mode but also enhances the process performance of unspecific peroxygenases.

Introduction

The unspecific peroxygenase (UPO) from the basidiomycete fungus *Agrocybe aegerita* (*Aae*UPO) (EC 1.11.2.1) was first discovered and documented in 2004 [1]. Since then, UPO has attracted a lot of interest due to its ability to selectively introduce oxygen atoms into various organic molecules such as benzene, pyridine and cyclohexane and derivatives thereof [2]. UPO catalyzes, among others, epoxidation of alkenes, hydroxylation of alkanes, oxidation of aromatics and *N*-dealkylations [3]. This feature has also drawn the attention of organic chemists, since oxyfunctionalization is one of the most challenging chemical reactions in organic synthesis, especially, the oxyfunctionalization of unactivated C-H bonds [2,4]. Until recently, research on cytochrome P450 monooxygenases was mainly in focus for the enzymatic selective introduction of oxygen functionalities [5,6]. While P450 monooxygenases are able to incorporate oxygen into organic substrates, these enzymes are relatively unstable, dependent on an expensive cofactor and have low catalytic activity [5–7]. In comparison, UPOs are fairly stable and require only hydrogen peroxide (H_2O_2), acting simultaneously as the oxygen donor and the electron acceptor [5].

Despite their relative high stability, UPOs still suffer from

Abbreviations: *Aae*UPO, unspecific peroxygenase from *Agrocybe aegerita*; ABTS, 2,2′-azino-bis(3-ethylbenzothiazoline-6-sulfonic acid); CPO, chloroperoxidase; EBA, 4-ethylbenzoic acid; F.E., Faradaic efficiency; GDE, gas diffusion electrode; GOx, glucose oxidase; HEBA, 4-(1-hydroxyethyl)benzoic acid; KP_i, potassium phosphate buffer; r*Aae*UPO, recombinant unspecific peroxygenase from *Agrocybe aegerita*; TOF, turnover frequency; TON, turnover number; TTN, total turnover number; UPO, unspecific peroxygenase.

* Corresponding authors.
E-mail addresses: giovanni.sayoga@tuhh.de (G.V. Sayoga), liese@tuhh.de (A. Liese).

https://doi.org/10.1016/j.nbt.2023.10.007
Received 16 September 2023; Received in revised form 10 October 2023; Accepted 15 October 2023
Available online 16 October 2023

inactivation at an elevated concentration of its co-substrate H_2O_2 [8]. This is one reason why the full technical application of UPOs is still limited [8]. There are several established methods already reported to mitigate the inactivating effect of H_2O_2. The approaches mainly focus on the adjustment of reaction conditions, especially to keep a constantly low H_2O_2 concentration. Feeding a diluted H_2O_2 solution into a reaction medium has been shown to be able to increase the total turnover number (TTN) [9], which is defined as the quotient of moles of the product generated after the enzyme was deactivated and the moles of the used enzyme. However, this approach leads to a volume increase and high local H_2O_2 concentrations [10]. As a result, several *in-situ* H_2O_2 generation methods have been investigated. *In-situ* generation of H_2O_2 can be accomplished through various approaches, including the utilization of a chemical reductant such as dihydroxyfumaric acid [11], an enzyme *e.g.,* glucose oxidase (GOx) [12], a piezocatalytic method [13], photocatalysis [14] or an electrochemical method [15].

Lately, the application of a specific electrode type called gas diffusion electrode (GDE) has been expanded, particularly in the electrochemical reduction of O_2 to H_2O_2 [16]. The GDE possesses a three-phase boundary consisting of a gas, liquid and solid phase [16]. This enables a direct and higher mass transport of O_2 from the atmosphere through the electrode and in contact with the electrolyte [16]. Thus, limitations due to low O_2 solubility and diffusivity in the liquid and towards the electrode are avoided [17]. The combination of the *in-situ* generation of H_2O_2 and the subsequent biocatalytic reaction has been reported. Examples are the oxidation of thioanisole catalyzed by the chloroperoxidase (CPO) from *Caldariomyces fumago* [10,15], the halogenation of 4-pentenoic acid catalyzed by the vanadium CPO from *Curvularia inaequalis* [18], and the hydroxylation of ethylbenzene catalyzed by the recombinant *Aae*UPO (r*Aae*UPO) [19]. The electrochemical *in-situ* H_2O_2 generation method does not increase the reaction volume and avoids the formation of by-products (*e.g.,* gluconic acid), which may occur when using diluted H_2O_2 solution or enzymatic *in-situ* H_2O_2 generation with GOx, respectively [10].

Usually, H_2O_2 is generated *in-situ* at a constant rate (galvanostatic) [10,15,18–20]. However, this approach leads to an accumulation of H_2O_2 in the medium as the enzyme activity constantly decreases due to H_2O_2-dependent enzyme deactivation, the so-called catalase malfunction reaction [8]. In turn, accumulation of H_2O_2 further increases the enzyme deactivation rate. It has been demonstrated that by keeping the H_2O_2 concentration constant (H_2O_2-stat mode), by adjusting the feeding rate of H_2O_2 to a set H_2O_2 concentration of 50 μM, the enzyme operational stability could be increased, compared to the continuous addition of H_2O_2 [9]. Moreover, the H_2O_2-stat mode was implemented within the bioelectrochemical system, with H_2O_2 concentration limits set at 0.5 mM and 1.2 mM [21]. Nevertheless, due to relative high H_2O_2 concentration thresholds the enzyme operational stability and the final obtained product concentration were low compared to the galvanostatic mode [21].

In this study, the hydroxylation of 4-ethlybenzoic acid (EBA) catalyzed by r*Aae*UPO was performed in a GDE system. Two electrogeneration modes were employed to supply the H_2O_2 *in-situ*. 1) A H_2O_2-stat mode at a concentration limit set between 0.06 mM and 0.28 mM. A custom automation program was developed to regulate the current output of the power supply to the GDE. This program utilized the input from the H_2O_2 sensor to ensure a constant H_2O_2 concentration (Fig. 1). 2) A galvanostatic mode at a constant current density between 0.8 mA cm^{-2} and 6.4 mA cm^{-2}, which served as an internal benchmark. The TTN, turnover frequency (TOF) and the productivity were determined and compared. The objective is to find the optimal H_2O_2 concentration limit under the H_2O_2-stat mode, which would enable a high TOF while maintaining a high TTN.

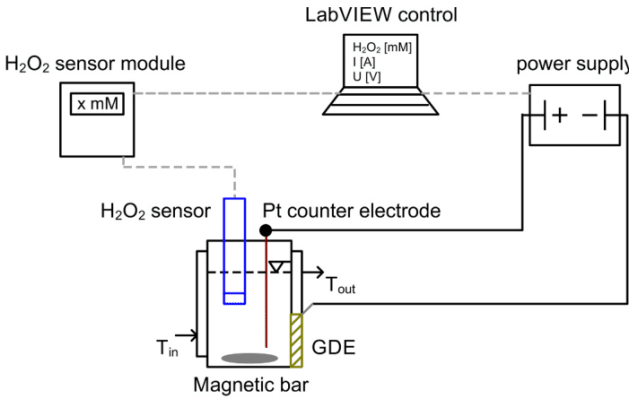

Fig. 1. Schematic representation of the complete electroenzymatic reaction system, including the H_2O_2 sensor, H_2O_2 sensor module, power supply and Lab VIEW control unit. The control unit is used to regulate the current output sent to the electrodes and to maintain a constant H_2O_2 concentration. GDE: gas diffusion electrode (working electrode), Pt: platinum (counter electrode). Dashed line: working cycle of the automation system. Solid line: electric circuit between the power supply and the electrodes.

Material and methods

Materials

Unless otherwise stated, all chemicals were purchased from Carl Roth (Karlsruhe, Germany) or Sigma Aldrich (Steinheim, Germany) in a purity ≥ 98%. HEBA (≥97%) was purchased from BLD Pharm (China). 2,2′-azino-bis(3-ethylbenzothiazoline-6-sulfonic acid) (ABTS) (≥98%) was purchased from TCI (Eschborn, Germany).

Production of his-tagged rAaeUPO

The inoculum seed of *Pichia pastoris* (X33), which expresses the recombinant protein r*Aae*UPO-PaDa-I-C6His was prepared as described in [22], in a 50 mL buffered complex glycerol medium (BMGY) containing 25 μg mL^{-1} Zeocin. The main fermentation was conducted in a 1 L DASGIP bioreactor system (Eppendorf, Hamburg, Germany) and performed as stated in [22]. Modifications to the fermentation process are described in the following. The glycerol batch phase was started by cultivating the inoculum in a 500 mL basal salt medium containing 40 g L^{-1} glycerol. Once the initial glycerol was consumed as indicated by the spike of the dissolved oxygen (DO) signal, the glycerol fed-batch phase was started and maintained for 24 h. Afterwards, the glycerol feed was stopped and the methanol fed-batch phase was started to induce the overexpression of r*Aae*UPO. The DO content and temperature were set at 30% and 30 °C, respectively. To maintain these values, the stirring rate (400–1200 rpm) and aeration rate (30–60 L h^{-1} ≙ *ca.* 1 vvm) were regulated automatically by the system. A 25% v/v ammonia solution was used to maintain the pH at 5. The feeding profiles of glycerol and methanol in the fed-batch phase were set as stated in [23]. The biomass was separated from the fermentation broth *via* centrifugation (Beckmann J2HS, Beckmann Coulter, California, USA) at 5000 rpm for 2 h at 4 °C. The supernatant was sterile-filtered (0.22 μm, DURAPORE, Merck Millipore, Massachusetts, USA) and concentrated by ultrafiltration (10 kDa molecular weight cut off, Minimate TFF Capsule, Pall, New York, USA). r*Aae*UPOs were dialyzed and concentrated in 0.1 M potassium phosphate (KP_i) buffer, pH 7.

Determination of enzyme activity and concentration

The enzyme activity was quantified using an ABTS assay. The activity assay was conducted spectrophotometrically (Genesys 180, Thermo Scientific, Massachusetts, USA) at 420 nm for 1 min as technical duplicates. The assay consisted of 750 µL 0.1 M Na_2HPO_4/ 0.1 M citric acid buffer pH 4.4, 100 µL 3 mM ABTS, 50 µL 40 mM H_2O_2 and 100 µL sample. The sample was added last as it starts the reaction. Directly after adding the sample, the reaction mixture was mixed by pipetting up and down 5 times using the sample pipette tip. The r*Aae*UPO activity and concentration were calculated as shown below, using equations described previously in [24].

$$v = \frac{slope \quad of \quad the \quad absorbance \quad [\min^{-1}] \bullet 10}{36\left[mM^{-1} \quad cm^{-1}\right] \bullet 1cm} \tag{1}$$

$$c_{rAaeUPO} = v \bullet \frac{(k_m + S)}{k_{cat} \bullet S} = v \bullet df \bullet (k_m + S) \bullet \frac{1}{k_{cat} \bullet S} \tag{2}$$

Where v is the r*Aae*UPO volumetric activity in U mL^{-1}, S is the substrate ABTS concentration in the assay in mM, $c_{rAaeUPO}$ is the r*Aae*UPO concentration in µM, k_m is the Michaelis-Menten parameter (50 µM) [5], k_{cat} is the catalytic rate constant (546 s^{-1}) [5] and df is the dilution factor (10, 5 or 1).

Offline H_2O_2 determination

H_2O_2 concentrations were determined photometrically (lower detection limit of 10 µM) [25]. The assay (1 mL) contained the sample, iodide reagent (0.4 M potassium iodide, 0.05 M NaOH, 10^{-4} M ammonium molybdate) and 0.5 M potassium hydrogen phthalate in a ratio of 4:3:3. The treated sample was measured directly at 351 nm in technical duplicates. Calibration curves (10–100 µM) were prepared using diluted H_2O_2 solution.

Determination of 4-ethylbenzoic acid (EBA) and 4-(1-hydroxyethyl) benzoic acid (HEBA)

EBA and HEBA concentrations were quantified using a Nexera LC-40 HPLC system (Shimadzu, Kyoto, Japan) equipped with a UV-Vis SPD-40 detector (Shimadzu, Kyoto, Japan) and an Inertsil ODS-P, C18-RP, 5 µm, 100 Å column (GL Science, Japan). Sample preparation and chromatography analysis were carried out following the procedures described in [26]. Calibration curves (0.5–10 mM) were prepared using authentic standards (Suppl. Fig. S1, Fig. S2). All measurements were conducted in technical duplicates.

Electrochemical setup

Electrochemical and electroenzymatic experiments were conducted in an undivided reactor. Carbon black GDE (PerOx with PTFE layer, Gaskatel, Kassel, Germany) (A: 12.56 cm^2, thickness: 250 µm) served as the working electrode and was fixed at the side of the reactor. One side of the GDE faced the liquid phase, while the other side faced the ambient air. A platinum (Pt) wire (Chempur, Karlsruhe, Germany) (99.9%, A: 1.5 cm^2) served as the counter electrode. Galvanostatic and dynamic electrical currents were generated by a Keithley 2231a-30–3 DC (Tektronix, Oregon, USA) power supply. Stainless steel crocodile clips were used as connectors. The reactor was equipped with a DULCOTEST PEROX H3 E H_2O_2 sensor (ProMinent, Heidelberg, Germany), a DULCOMETER dialog DACb H_2O_2 sensor module (ProMinent, Heidelberg, Germany) and an NI LabVIEW 2021 SP1 virtual instrumentation program (National Instruments, Texas, USA) (Fig. 1). The H_2O_2 sensor has a response time of 45 s with a lower and an upper detection limit of 0.006 mM and 0.294 mM, respectively. A constant H_2O_2 concentration (H_2O_2-stat mode) in the medium was maintained by employing an automation program designed in- and controlled by the LabVIEW software (Suppl. Fig. S5). The H_2O_2 concentration was measured by the H_2O_2 sensor and the concentration was transmitted to LabVIEW. LabVIEW controlled the current output of the power supply and based on the set H_2O_2 concentration limit, the electrical current sent to the electrode was adjusted to control the H_2O_2 productivity. For the automation program, the maximum potential, proportional gain and integral time were set to 6 V, 0.01, and 2 min, respectively. The H_2O_2 concentration limit was set either to 0.06 mM, 0.15 mM, 0.2 mM or 0.28 mM. These values were selected to ensure a relatively balanced distribution across the H_2O_2 sensor's limit.

Electroenzymatic experiments

The reaction medium contained 200 mL 0.1 M KP_i pH 7, 8 mM EBA and 10 nM of r*Aae*UPO. The medium was stirred at 250 rpm by a magnetic bar (d: 0.5 cm, l: 3 cm). The experiments were conducted at 22 ± 1 °C to minimize thermal deactivation of the enzyme. Galvanostatic experiments were performed at electrical current densities between 0.8 mA cm^{-2} and 6.4 mA cm^{-2}. In the H_2O_2-stat mode, the automation system was engaged. Thus, a dynamic current was applied to the electrodes. Experiments were initiated by either starting the power supply or the automation program. Samples for the quantification of EBA, 4-(1-hydroxyethyl)benzoic acid (HEBA) (20 µL), H_2O_2 concentration (100–800 µL), and r*Aae*UPO activity (65–200 µL) were taken periodically from the system. Each experiment was stopped when there was no measurable r*Aae*UPO activity (slope of the absorbance < 0.01 cm^{-1} min^{-1}). Unless otherwise stated, electroenzymatic experiments were performed as duplicates. The TOF refers to the turnover number (TON) per unit time (60 min). The TON is described as the quotient of moles of the product generated at a specific time before the enzyme was deactivated and the moles of the used enzyme. The productivity is defined as the mass of product (derived from the final product concentration) per used reactor volume and time.

The H_2O_2 productivity was determined in an abiotic environment (without EBA and r*Aae*UPO) and in galvanostatic mode (0.8 mA cm^{-2} - 6.4 mA cm^{-2}). The H_2O_2 concentration was measured periodically over the course of 30 min. Duplicates were performed for each current density. The Faradaic efficiency (F.E.) describes how much energy in form of electrons is consumed for the formation of H_2O_2 and the formation of side products. The H_2O_2 F.E. was calculated using the equation given elsewhere [27].

Results and discussion

To determine the optimal H_2O_2 concentration limit for the r*Aae*UPO-catalyzed hydroxylation of EBA under the H_2O_2-stat mode in the GDE system, several steps were taken. Initially, the electrochemical characterization of the system was conducted to assess the H_2O_2 productivity. Thereafter, the electroenzymatic hydroxylation of EBA was performed under galvanostatic mode to establish a reference for TOF, TTN, and productivity. Subsequently, electroenzymatic experiments were repeated under H_2O_2-stat mode. Finally, the TOF, TTN, and productivity obtained from both H_2O_2 electrogeneration methods were compared to identify the most efficient approach and eventually the optimal H_2O_2 concentration limit.

Electroenzymatic hydroxylation of EBA under galvanostatic mode

As a part of the system's electrochemical characterization process in regards to its H_2O_2 generation capabilities, the H_2O_2 productivity was determined at various current densities. The electrochemical characterization was conducted in an abiotic environment, without the enzyme and the substrate.

In Fig. 2A, the accumulated H_2O_2 concentration increased linearly over time for all tested current densities within the 30 min running time.

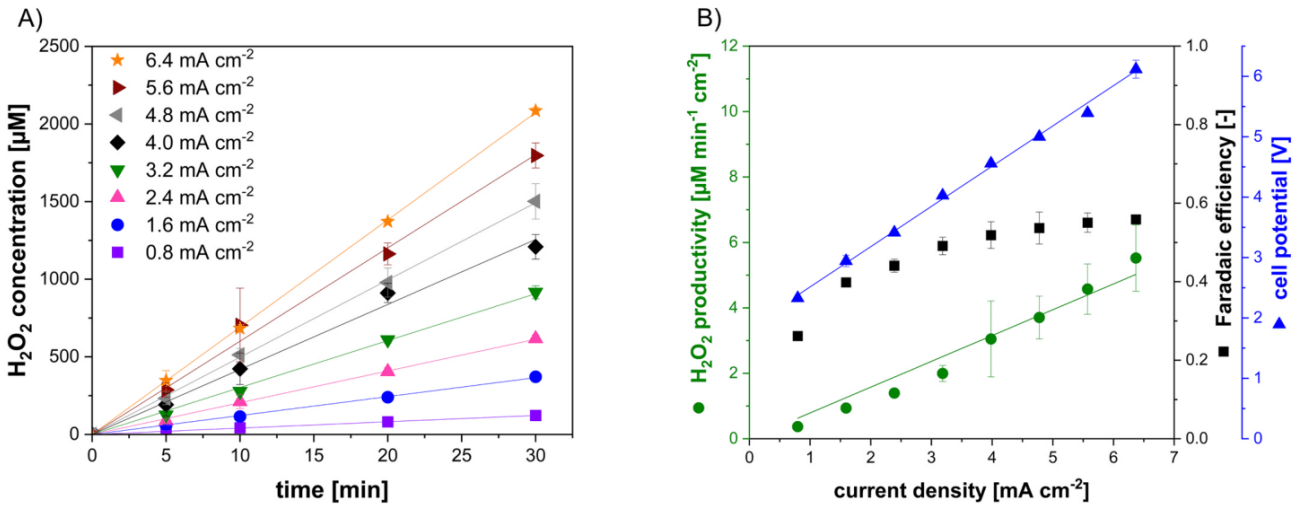

Fig. 2. A) H_2O_2 concentration as a function of time at various current densities. B) H_2O_2 productivity, Faradaic efficiency (F.E.) and resulting cell potential as a function of current density. Reaction conditions: GDE (12.56 cm^2), Pt counter electrode (1.5 cm^2), 200 mL 0.1 M KP_i pH 7, temperature: 22 ± 1 °C, 250 rpm. F.E. was determined after 30 min. Duplicates were performed. Depicted lines are linear regression fits with $R^2 \geq 0.99$.

Based on these results, it can be concluded that there is no indication of O_2 diffusion and mass transfer limitation at the GDE within the tested range. Additionally, as depicted in the Fig. 2B, H_2O_2 productivities, resulting cell potentials and the F.Es. are shown as a function of the current density. The H_2O_2 productivity (y [µM min^{-1} cm^{-2}] = 0.79 [µM min^{-1} mA^{-1}] • J [mA cm^{-2}]) and the resulting cell potential (y [V] = 0.67 [V cm^2 mA^{-1}] • J [mA cm^{-2}] + 1.85 [V]) show a linear increase with increasing current density. The maximum H_2O_2 productivity of 5.5 µM min^{-1} cm^{-2} was achieved at 6.4 mA cm^{-2}, the highest tested current density. The highest H_2O_2 productivity reported here is comparable to those reported in literature for GDE-based systems [18,20,27]. It is also observed in Fig. 2B that the F.E. increases from 0.26 at 0.8 mA cm^{-2} to 0.50 at 3.2 mA cm^{-2}. Upon further increasing the current density, the F.E. shows only minimal improvement and reaches an apparent plateau, with a maximum of 0.55 at 6.4 mA cm^{-2}. A similar behavior was reported, where the F.E. increased from 0.60 to 0.78 as the current density was increased from 5 mA cm^{-2} to 30 mA cm^{-2} [19]. A F.E. below 1 means that not all electrons were efficiently used to generate H_2O_2, or the resulting concentration of accumulated H_2O_2 was lower than the theoretical concentration calculated based on the total consumed electrons. Competing reactions such as hydrogen evolution and direct reduction of O_2 to H_2O are known to reduce the F.E. [25,28]. Furthermore, within the electrochemical system the formed H_2O_2 could be further reduced to H_2O, oxidized to radicals or decomposed to O_2 and H_2O, thus reduced the accumulated H_2O_2 concentration [25,26,28]. Surface modification approaches such as thermal oxidation (*e.g.,* using KOH) and coating with carbon nanotubes offer promising ways to enhance the performance of carbon-based electrodes [18,29]. These modifications provide a more active surface with O or OH groups and higher current density, respectively [18,29]. As a result, H_2O_2 generation is effectively promoted, leading to an increase in the F.E. [18,29]. Additionally, minimizing the contact between the formed H_2O_2 and counter electrode by placing the counter electrode in a separate compartment is expected also to increase the F.E. of the system. Overall, obtained F.Es. in this study are comparable to the reported values in literature for GDE systems and 3D carbon-based electrodes [10,20,27,30,31].

Following the electrochemical characterization, the electroenzymatic hydroxylation of EBA was performed. The electroenzymatic experiments were conducted initially under the galvanostatic mode by applying various current densities between 0.8 mA cm^{-2} and 6.4 mA cm^{-2}. The hydroxylation of EBA was catalyzed by r*Aae*UPO and yielded HEBA as the product. Before starting the experiment, r*Aae*UPO was added to the reaction mixture. A sample was taken to determine the initial activity using the ABTS assay, which was set as 100% relative activity. Throughout the experiment, enzyme activities were measured relative to the initial activity and expressed as the apparent ABTS-activity due to the coexistence of ABTS and EBA in the sample. Fig. 3A-D show the results of electroenzymatic experiments performed at 0.8 mA cm^{-2}, 2.4 mA cm^{-2}, 4.0 mA cm^{-2} and 5.6 mA cm^{-2}, respectively. As the current density is increased, the H_2O_2 productivity increases correspondingly from 0.37 to 4.6 µM min^{-1} cm^{-2}. In general, it can be observed that for a period of time the reactions reach an apparent equilibrium in terms of the measured H_2O_2 concentration, with higher H_2O_2 concentrations being maintained at increased current densities (Fig. 3E). At the same time, the duration, in which the H_2O_2 concentration remains constant (termed as apparent equilibrium time) shortens (Fig. 3E). This phenomenon occurred because the relative enzyme activity and the catalytic consumption rate of the H_2O_2 decreased over the course of the experiment, while the H_2O_2 productivity remained constant. The apparent equilibrium time was determined using a threshold of 30%, which represents the minimum acceptable deviation from the apparent H_2O_2 equilibrium concentration. This choice was made considering the generally low H_2O_2 concentrations observed during the experiment. Opting for a lower threshold, such as 10%, would have resulted in the inability to differentiate deviations from a lower apparent equilibrium H_2O_2 concentration *e.g.,* 0.13 mM at 2.4 mA cm^{-2}, or lower. Consequently, deviations below 30% were considered to be minor fluctuations. At low current density, such as 0.8 mA cm^{-2}, the H_2O_2 generation rate becomes the rate-limiting step of the reaction. As a result, the apparent equilibrium H_2O_2 concentration is among the lowest compared to other current densities, and the apparent equilibrium time is longer (Fig. 3E) due to higher enzyme stability (71 h). However, at current densities ≥ 2.4 mA cm^{-2}, the catalytic consumption rate of H_2O_2 becomes lower than the H_2O_2 productivity, making the H_2O_2 consumption rate the limiting factor of the reaction and leading to a higher apparent equilibrium H_2O_2 concentration. As more substrate is converted and the enzyme activity gradually decreases, less H_2O_2 is consumed, resulting in its accumulation in the medium. This accumulation triggers a catalase malfunction reaction, causing even faster enzyme deactivation and resulting in a rapid loss of enzyme activity. Consequently, the apparent equilibrium time decreases with increasing current density (Fig. 3E). In the initial phase of the reaction, the product formation exhibits a linearity for all applied current densities.

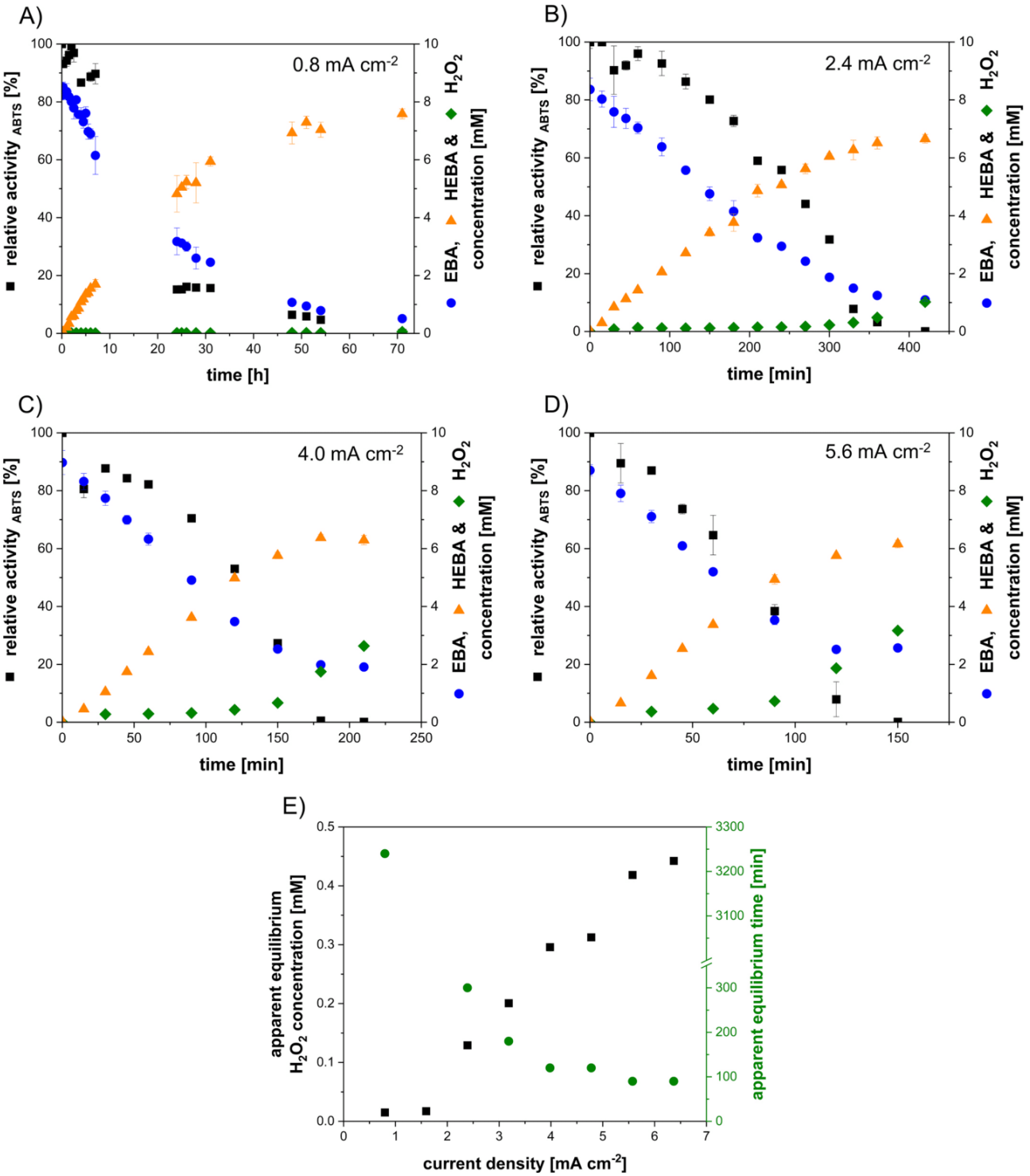

Fig. 3. Hydroxylation of EBA catalyzed by r*Aae*UPO in a GDE system with *in-situ* H_2O_2 generation at A) 0.8 mA cm^{-2}, B) at 2.4 mA cm^{-2}, C) at 4.0 mA cm^{-2} and D) at 5.6 mA cm^{-2}. Reaction conditions: 200 mL 0.1 M KP_i pH 7, 8 mM EBA, 10 nM r*Aae*UPO, 250 rpm, temperature: 22 ± 1 °C. EBA: 4-ethylbenzoic acid, HEBA: 4-(1-hydroxyethyl)benzoic acid. See Fig. S4. A-D for the full data set. E) Apparent equilibrium H_2O_2 concentration and apparent equilibrium time as a function of current density. The apparent equilibrium time describes the duration, in which the H_2O_2 concentration remains relatively constant during the experiment. The apparent equilibrium time is the duration until the H_2O_2 concentration deviates from the apparent equilibrium H_2O_2 concentration by 30%. The threshold of 30% was chosen due to overall low H_2O_2 concentrations during the experiment. Deviations below 30% were interpreted as minor fluctuations. Data shown are average from technical duplicates.

Nonetheless, the duration of linearity for the product formation differs for each current density. At lower applied current density such as 2.4 mA cm^{-2}, the formation rate stays within the linear range for a longer duration (210 min, Fig. 3B), whereas at higher current densities *e.g.,* 5.6 mA cm^{-2}, the formation rate deviates from the linear range more quickly (90 min, Fig. 3D) due to higher substrate conversion rate and faster enzyme deactivation.

It is observable in Fig. 4 that the productivity and the TOF are increasing with increasing current density. The highest productivity and TOF obtained under the galvanostatic mode are 10.5 g L^{-1} d^{-1} and 76.7 s^{-1}, respectively. Both are achieved at the highest current density, 6.4 mA cm^{-2}. Meanwhile, the TTN reaches its maximum of approximately 650,000 mol mol^{-1} at around 2.4 mA cm^{-2} and 3.2 mA cm^{-2}. An inverse behavior is observed as the current density is increased beyond 3.2 mA cm^{-2}. The TTN decreases to 500,000 mol mol^{-1} at 6.4 mA cm^{-2}. The increasing productivity and TOF could not compensate the faster enzyme deactivation as the current density was increased above 3.2 mA cm^{-2}. A faster enzyme deactivation resulted in a reduced final product concentration before all enzyme was deactivated, leading to a decrease in the TTN. A fluctuation in TOF is observed, decreases from 66 s^{-1} to 55 s^{-1} at 4.8 mA cm^{-2} and increases again to 73 s^{-1} at 5.6 mA cm^{-2}. This observed trend could potentially represent an isolated deviation. Furthermore, other literatures have reported a trend of TOF either remaining stagnant or decreasing with increasing current density, without exhibiting fluctuations [21,26]. The maximum TTN obtained under the galvanostatic mode is higher compared to those reported in literatures (400,000 mol mol^{-1}) using a GDE-based system [19,21]. A higher TTN obtained here can be explained by a higher enzyme stability due to comparably lower H_2O_2 productivity. The maximum H_2O_2 productivity achieved in this study is between 5.8 and 41 times lower [19,21]. The relatively small ratio of 0.12 between the counter electrode and the working electrode surface area may restrict the electron flow, potentially diminishing the overall efficiency of the working electrode. This could be an explanation for the observed low H_2O_2 productivity, especially when considering that other literatures have reported ratios of 0.8 and 1, which could lead to improved performance [19,21]. Due to lower H_2O_2 productivity, the obtained TOF and the productivity are 1.7 and 2.4 times lower, respectively [19,21].

Electroenzymatic hydroxylation of EBA under H_2O_2-stat mode

The results from the electroenzymatic hydroxylation of EBA conducted under the galvanostatic mode, discussed in the previous section, served as a reference in this study. Herein, electroenzymatic

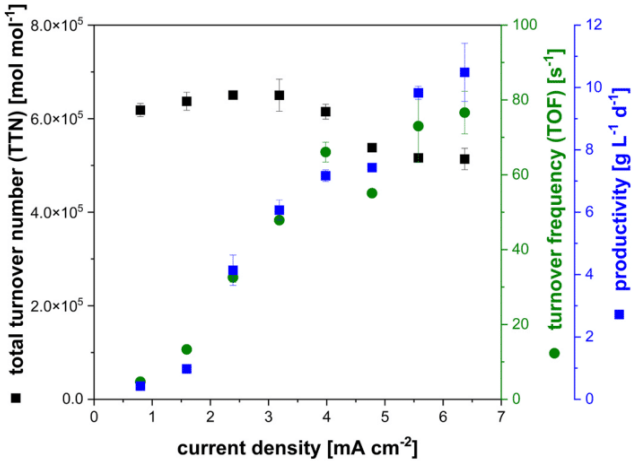

Fig. 4. Corresponding TTN, TOF and productivity as a function of current density. Data shown are average from technical duplicates.

experiments were conducted once again, this time utilizing the H_2O_2-stat mode at a concentration limit set between 0.06 mM and 0.28 mM, with the intention to increase the enzyme stability and the TTN.

In the H_2O_2–stat mode, the H_2O_2 concentration increases to a predetermined concentration and a steady concentration is maintained throughout the experiment. This is automated *via* LabVIEW by regulating the electrical current output of the power supply, therefore delivering a dynamic current to the electrodes based on the input from the H_2O_2 sensor, which measures the H_2O_2 concentration in the medium. Fig. 5A-D illustrate the results from the hydroxylation of EBA performed under the H_2O_2-stat mode with the H_2O_2 concentration limit set to 0.06 mM, 0.15 mM, 0.2 mM and 0.28 mM, respectively. As soon as the experiment is initiated by engaging the automation system, the power supply increases the current output towards the electrodes to increase the H_2O_2 productivity and to reach its respective H_2O_2 concentration limit.

Moreover, in Fig. 6A, the resulting current density, measured H_2O_2 concentrations, and enzyme relative activity over time obtained from the experiment performed under the H_2O_2–stat mode with the H_2O_2 limit set to 0.15 mM are plotted together. This assessment is performed for the set concentration of 0.15 mM solely for the purpose of exemplifying the automation system and thus, the changes in the current density throughout the experiment, allowing for adjustments of H_2O_2 productivity. It is apparent from Fig. 6A that the current density is increased to 4 mA cm^{-2} within the first 15 min and remains relatively constant up to 60 min. Correspondingly, the H_2O_2 concentration increases to its limit of 0.15 mM. The measured H_2O_2 concentration is stable for the whole duration of the experiment. Parallel to the online quantification using the H_2O_2 sensor, the H_2O_2 concentrations were also quantified using an offline photometrical method (indicated as H_2O_2 offline) as a validation of the H_2O_2 sensor values. In this regard, a maximum deviation of 0.03 mM was observed between the offline and online H_2O_2 quantification. The observed deviation could be attributed to the use of different calibration systems for each method. The online quantification method, utilizing the H_2O_2 sensor, employs an internal 2-points calibration (set by the manufacturer) with calibration points set at 0 mM and 0.294 mM, which correspond to the theoretical zero value and upper detection limit, respectively. On the other hand, the offline quantification method utilizes a 9-points calibration, with calibration points ranging from 0 mM to 0.1 mM (Suppl. Fig. S3). The observed deviation during the experiment was likely due to reaching the practical lower quantification limit of the online method. This is due to the utilization of a 2-points calibration, which provides fewer reference points. Especially, at lower concentration ranges, resulting in less precise detection of H_2O_2. This is reflected in the fact that the highest deviation between the offline and online H_2O_2 quantification was found in the experiment performed at the H_2O_2-stat concentration of 0.06 mM (Fig. 5A). This highlights the importance of performing an offline quantification as a control to an online quantification. After 60 min (Fig. 6A), the current density is steadily decreasing and starts to mimic the declining trend of the relative enzyme activity and the substrate concentration (Fig. 5B). The current output and thus, the current density is reduced to lower the H_2O_2 productivity since the enzymatic H_2O_2 consumption is also declining as the enzyme activity decreases. In this way, the amount of generated H_2O_2 is adjusted to stay equal to the amount of consumed H_2O_2 keeping the H_2O_2 concentration constant in the reaction medium.

In general, the final product concentration obtained and the duration of the reaction decrease when the H_2O_2-stat concentration limit is increased. By raising the H_2O_2 concentration limit, the availability of the co-substrate increases, leading to a higher reaction rate ($K_{M,\ H2O2}$: 1.3–1.8 mM [5,21,32]). Correspondingly, both TOF and the productivity increase, reaching a maximum of 87.5 s^{-1} and 6.9 g L^{-1} d^{-1}, respectively (Fig. 6B). Additionally, reaching a high TOF and reaction rate at a higher H_2O_2-stat concentration limit also increases the possibility of r*Aae*UPO undergoing catalase and catalase malfunction

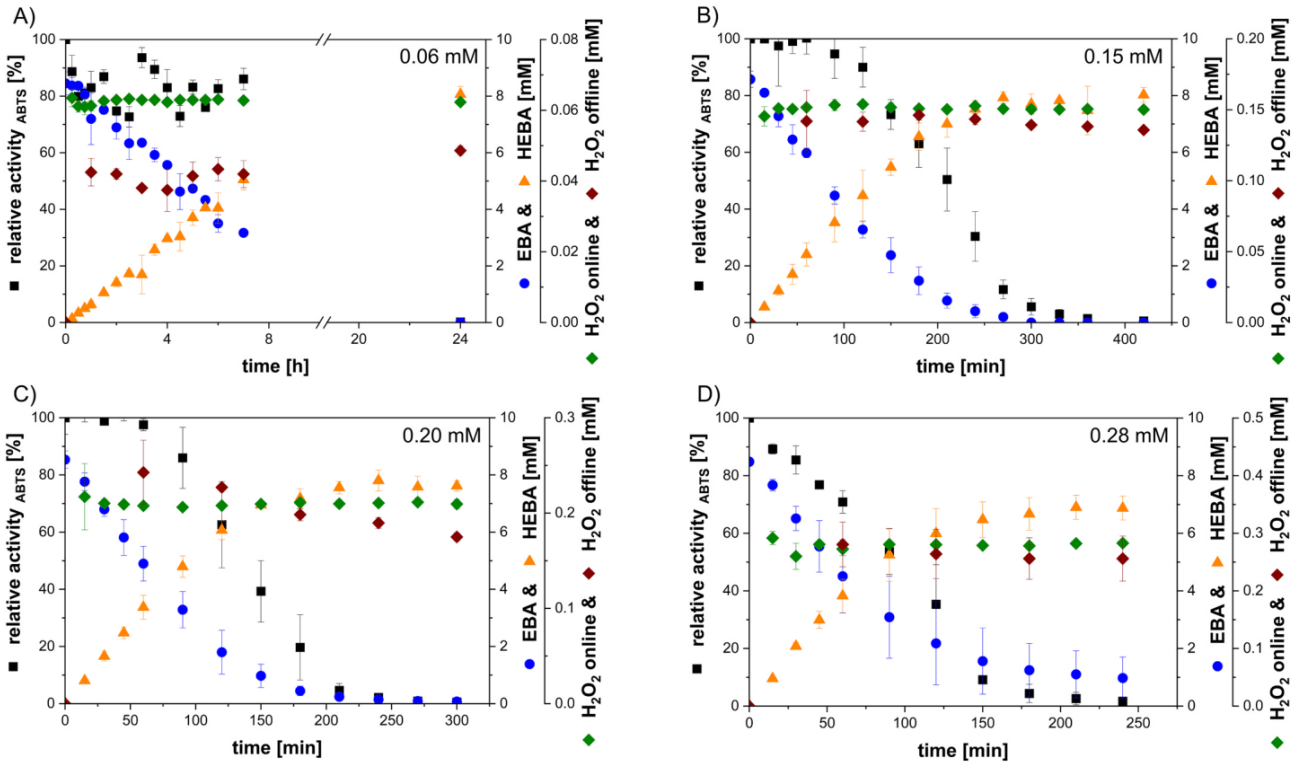

Fig. 5. Hydroxylation of EBA catalyzed by r*Aae*UPO in a GDE system operating in H_2O_2-stat mode with the H_2O_2 limit set to A) 0.06 mM, B) 0.15 mM, C) 0.2 mM and D) 0.28 mM. Reaction conditions: 200 mL 0.1 M KP_i pH 7, 8 mM EBA, 10 nM r*Aae*UPO, 250 rpm, temperature: 22 ± 1 °C. EBA: 4-ethylbenzoic acid, HEBA: 4-(1-hydroxyethyl)benzoic acid. H_2O_2 offline: an offline H_2O_2 quantification *via* a photometrical method serves as a control for the online quantification. Duplicates were performed.

reactions [8,21]. The reason for the aforementioned reactions is that the highly reactive species of r*Aae*UPO (termed as compound I) formed after binding with the first H_2O_2 molecule, can react not only with the substrate EBA to yield the product HEBA, but also with a second and third H_2O_2 molecule [8,21]. The reaction of compound I with the second H_2O_2 molecule yields compound II. Compound II can further react with H_2O_2, yielding compound III. The formation of compound III would eventually lead to a heme-bleaching and irreversible enzyme deactivation [8,21]. Moreover, the catalase and catalase malfunction reactions become more pronounced at lower substrate concentrations [15]. For EBA, a K_M of 2.3 mM was reported [21]. In this case, reaching EBA concentrations below its K_M leads not only to a reduced reaction rate but also prompting the catalase malfunction reaction due to constant availability of H_2O_2 in the medium, leading to a faster enzyme deactivation with increasing H_2O_2-stat concentration limit (Fig. 6C). This also decreases the obtained final product concentration. The final sampling point for the experiment conducted at the H_2O_2-stat limit of 0.06 mM (Fig. 5A) was taken after 24 h. By this time, the enzyme had already been deactivated. Therefore, the enzyme operational lifetime was determined based on the point where the current density was reduced and stabilized (by the automation system) at around 0.16 mA cm^{-2}. At this current density, the H_2O_2 productivity had ceased, effectively preventing its accumulation, due to the absence of H_2O_2 consumption by the enzyme. Regarding the product HEBA, no product inhibition was observed, at least up to 8 mM.

Overall, the highest analytical yield achieved in this study was 95%. The TTN decreases from the maximum of 710,000 mol mol^{-1} at a H_2O_2-stat setting of 0.15 mM to 570,000 mol mol^{-1} at 0.28 mM (Fig. 6B). Although the highest TTN is obtained at a set concentration of 0.15 mM, the corresponding TOF (58.0 s^{-1}) and productivity (4.6 g L^{-1} d^{-1}) are far from the maximum. As the H_2O_2 concentration limit is increased from 0.15 mM to 0.2 mM, the TOF increases to 80.3 s^{-1} and the productivity increases to 6.1 g L^{-1} d^{-1}. Nevertheless, further increasing the H_2O_2-stat concentration from 0.2 mM to 0.28 mM does not significantly increase the TOF and productivity anymore. Therefore, under these circumstances and in this specific system, it is recommended to set the H_2O_2-stat concentration to 0.2 mM as this concentration limit allows not only the achievement of comparably high TOF and productivity, but also a competitive TTN (655,000 mol mol^{-1}), compared to other reported TTNs from comparable reaction systems in a lab-scale (Table 1).

Comparing the key performance indicators from the electroenzymatic experiments conducted under the galvanostatic mode and under H_2O_2-stat operation, the maximum TOF achieved using both methods are comparable (Fig. 4, Fig. 6B). However, the highest productivity achieved under the galvanostatic method (10.5 g L^{-1} d^{-1}) is higher compared to the one obtained under the H_2O_2-stat mode (6.9 g L^{-1} d^{-1}). A higher productivity under the galvanostatic method can be explained by a higher H_2O_2 productivity and a higher accumulation of H_2O_2 in the medium. However, due to a higher and an ever-increasing accumulation of H_2O_2 under the galvanostatic method, leading to a faster enzyme deactivation, the obtained final product concentration and the TTN decrease. In this regard, the maximum TTN acquired under the H_2O_2-stat mode is 10% higher compared to the maximum TTN acquired under the galvanostatic method. Under an optimum condition (H_2O_2-stat mode: 0.2 mM, galvanostatic mode: 3.2 mA cm^{-2}), the experiment conducted under H_2O_2-stat mode still has a higher TTN (655,000 mol mol^{-1}) and TOF (80.3 s^{-1}), as well as a similar productivity (6.1 g L^{-1} d^{-1}). In Table 1, the impact of various H_2O_2 supply methods on the enzyme stability and thus, also on the TTN for H_2O_2-dependent enzymatic reactions are listed. The TTN serves as an important metric to assess the suitability of a biocatalyst for a specific process. It also effectively correlates the yield of the product to the input

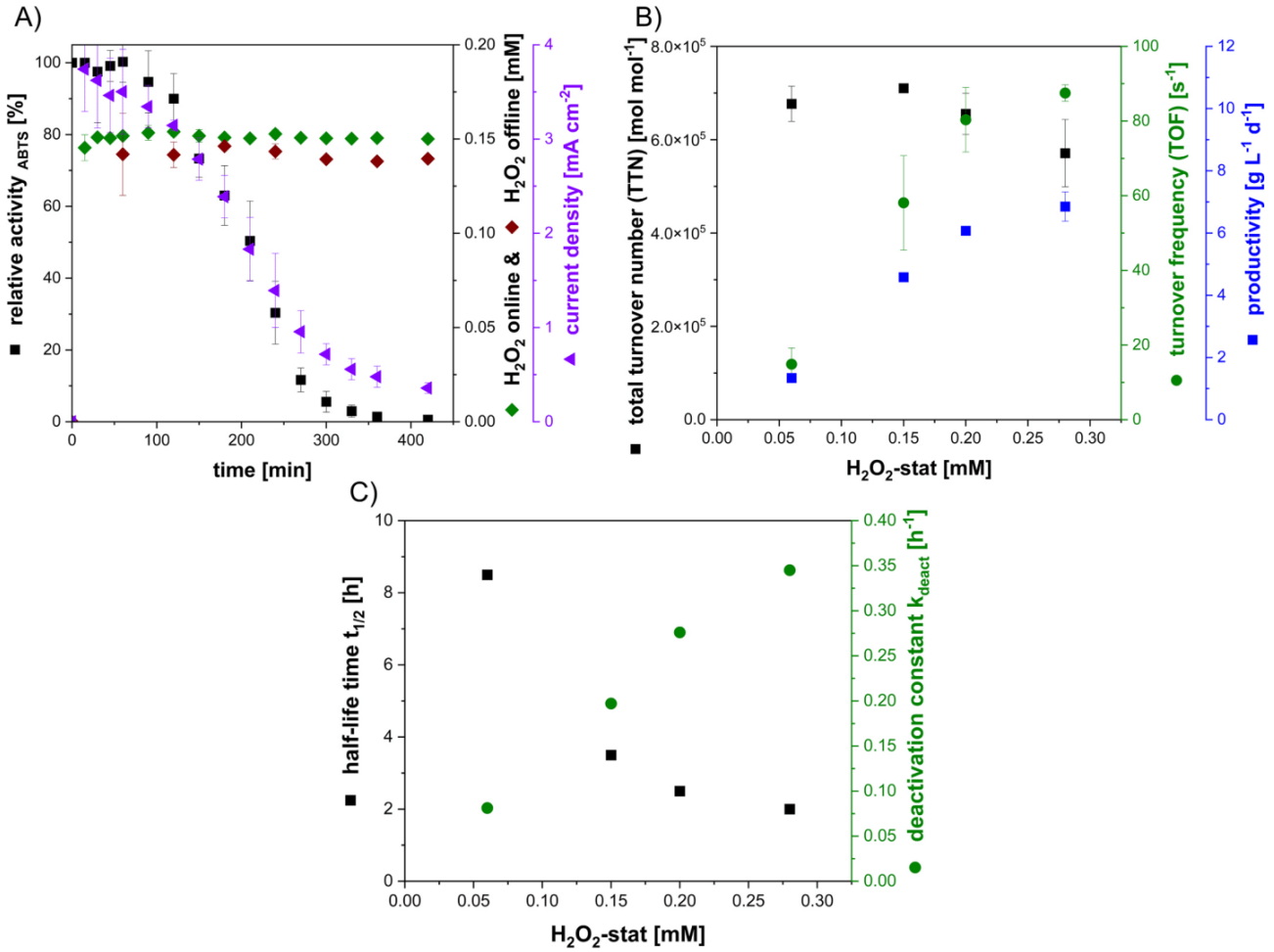

Fig. 6. A) Time-dependent relative enzyme activity, current density and H_2O_2 concentrations for the hydroxylation of EBA operated under H_2O_2-stat mode with the H_2O_2 limit set to 0.15 mM. H_2O_2 offline: an offline H_2O_2 quantification *via* a photometrical method serves as a control for the online quantification. B) Corresponding TTN, TOF and productivity as a function of the set H_2O_2-stat concentration. C) Half-life time ($t_{1/2}$) and deactivation constant (k_{deact}) of r*Aae*UPO at different H_2O_2-stat concentrations. The half-life time of r*Aae*UPO was determined by dividing the actual enzyme operational lifetime observed during the experiment (experiments shown in Fig. 5. A-D) by two. Deactivation constant was determined from the half-life time ($t_{1/2}$). $k_{deact} = \frac{\ln(2)}{t_{1/2}}$. Duplicates were performed.

Table 1
Comparison of the impact of different H_2O_2 supply method on the total turnover number (TTN) of H_2O_2–dependent enzymatic reactions.

Substrate, enzyme	Reaction system	TTN [mol mol^{-1}]	Literature
Indole, CPO	Batch, sensor-controlled feeding of H_2O_2	644,000	[9]
Thioanisole, CPO	Batch, *in-situ* electrogeneration of H_2O_2 (galvanostatic)	145,000	[15]
Ethylbenzene, r*Aae*UPO	Batch, immobilized enzyme, manual feeding of H_2O_2	900,000	[33]
Ethylbenzene, r*Aae*UPO	Batch, enzymatic *in-situ* generation of H_2O_2	470,000	[34]
Ethylbenzene, r*Aae*UPO	Batch, GDE-based system (galvanostatic)	400,000	[19]
EBA, r*Aae*UPO	Batch, GDE-based system, H_2O_2-stat mode (0.5 mM)	360,000	[21]
EBA, r*Aae*UPO	Batch, GDE-based system, H_2O_2-stat mode (0.15 mM)	710,000	This study

of the catalyst, providing valuable insights in cost valuation of a reaction system. The highest TTN (900,000 mol mol^{-1}) for r*Aae*UPO-catalyzed hydroxylation reaction was found in a batch system with manual feeding of H_2O_2 and immobilized enzyme [33]. Compared to the highest TTN reported in literature, the highest TTN in this study is around 20% lower. However, the electrogeneration of H_2O_2 eliminates the need for a second enzyme or volume increase. Additionally, the GDE system offers key advantages, including easy technical set-up and elimination of O_2 mass transfer limitations. The higher TTN reported in the literature previously can be attributed to enhanced enzyme operational stability resulting from the enzyme immobilization. Enzyme immobilization has been recognized as a significant approach to enhance the performance of bioelectrochemical systems, as also indicated in other literature [20,27]. This aspect could serve as an optimization point for the system presented in this study. Furthermore, while the current productivity is low, there is potential for future commercial applications with optimization. An optimization of the productivity under the H_2O_2-stat mode could potentially be achieved by employing a fed-batch or continuous process

in order to ensure a constant substrate concentration above the K_M value and the application of immobilization technique to increase the enzyme stability.

Conclusion

It is clear that the mode of H_2O_2 electrogeneration impacts the enzyme's operational stability and the overall productivity. The presented results demonstrate that each mode has its own advantages and disadvantages. On the one hand, galvanostatic mode offers a higher productivity at a higher current density but suffers from a faster enzyme deactivation due to a continuously increasing concentration of H_2O_2 and, therefore, excess of H_2O_2. As a result, the final product concentration and the TTN are reduced. On the other hand, operation under H_2O_2-stat condition provides the possibility to achieve high TOF and TTN, albeit at a lower productivity. The advantage of the H_2O_2-stat mode lies in its ability to adapt to the changes of the H_2O_2 consumption rate over time, in accordance to the progress of the reaction. Therefore, an excess of H_2O_2 is prevented protecting the enzyme from rapid deactivation. The key performance indicators such as productivity and TOF obtained under the H_2O_2-stat mode are comparable to those reported in literature. Notably, the TTN obtained in this study is higher than all reported values for r*Aae*UPO-catalyzed reaction in bioelectrochemical systems, to the best of our knowledge. Furthermore, in order to gain a comprehensive understanding of the inactivation mechanism in different H_2O_2-dependent enzymes, the H_2O_2-stat method introduced here can be applied in the study of these enzymes.

Declaration of Generative AI and AI-assisted technologies in the writing process

During the preparation of this work the author(s) used ChatGPT in order to improve the readability. After using this tool, the author(s) reviewed and edited the content as needed and take(s) full responsibility for the content of the publication.

Declaration of Competing Interest

The authors declare that they have no known competing financial interests or personal relationships that could have appeared to influence the work reported in this paper.

Data availability

Data will be made available on request.

Acknowledgements

This work was supported by the Deutsche Forschungsgemeinschaft (DFG, German Research Foundation, e-Biotech SPP 2240) (Project number: 445947004). Publishing fees supported by Funding Program Open Access Publishing of Hamburg University of Technology (TUHH). The authors thank Fernando Lopez Haro from the TUHH for the preparation of the graphical abstract.

Appendix A. Supporting information

Supplementary data associated with this article can be found in the online version at doi:10.1016/j.nbt.2023.10.007.

References

[1] Ullrich R, Nüske J, Scheibner K, Spantzel J, Hofrichter M. Novel haloperoxidase from the agaric basidiomycete *Agrocybe aegerita* oxidizes aryl alcohols and aldehydes. Appl Environ Microbiol 2004;70:4575–81.
[2] Hofrichter M, Ullrich R. Oxidations catalyzed by fungal peroxygenases. Curr Opin Chem Biol 2014;19:116–25. https://doi.org/10.1016/j.cbpa.2014.01.015.
[3] Hofrichter M, Kellner H, Pecyna MJ, Ullrich R. Fungal Unspecific Peroxygenases: Heme-thiolate proteins that combine peroxidase and cytochrome P450 Properties. In: Hrycay EG, Bandiera SM, editors. Monooxygenase Peroxidase Peroxygenase Prop. Mech. Cytochrome P450, vol. 851. Cham: Springer International Publishing; 2015. p. 341–68. https://doi.org/10.1007/978-3-319-16009-2_13.
[4] Godula K, Sames D. C-H bond functionalization in complex organic synthesis. Science 2006;312:67–72. https://doi.org/10.1126/science.1114731.
[5] Molina-Espeja P, Ma S, Mate DM, Ludwig R, Alcalde M. Tandem-yeast expression system for engineering and producing unspecific peroxygenase. Enzym Micro Technol 2015;73–74:29–33. https://doi.org/10.1016/j.enzmictec.2015.03.004.
[6] Brummund J, Müller M, Schmitges T, Kaluzna I, Mink D, Hilterhaus L, et al. Process development for oxidations of hydrophobic compounds applying cytochrome P450 monooxygenases *in-vitro*. J Biotechnol 2016;233:143–50. https://doi.org/10.1016/j.jbiotec.2016.07.002.
[7] Bernhardt R. Cytochromes P450 as versatile biocatalysts. J Biotechnol 2006;124:128–45. https://doi.org/10.1016/j.jbiotec.2006.01.026.
[8] Karich A, Scheibner K, Ullrich R, Hofrichter M. Exploring the catalase activity of unspecific peroxygenases and the mechanism of peroxide-dependent heme destruction. J Mol Catal B Enzym 2016;134:238–46. https://doi.org/10.1016/j.molcatb.2016.10.014.
[9] Seelbach K, van Deurzen MPJ, van Rantwijk F, Sheldon RA, Kragl U. Improvement of the total turnover number and space-time yield for chloroperoxidase catalyzed oxidation. Biotechnol Bioeng 1997;55:283–8. https://doi.org/10.1002/(SICI)1097-0290(19970720)55:2<283::AID-BIT6>3.0.CO;2-E.
[10] Lütz S, Steckhan E, Liese A. First asymmetric electroenzymatic oxidation catalyzed by a peroxidase. Electrochem Commun 2004;6:583–7. https://doi.org/10.1016/j.elecom.2004.04.009.
[11] van de Velde F, van Rantwijk F, Sheldon RA. Selective oxidations with molecular oxygen, catalyzed by chloroperoxidase in the presence of a reductant. J Mol Catal B Enzym 1999;6:453–61. https://doi.org/10.1016/S1381-1169(99)00059-X.
[12] van de Velde F, Lourenço ND, Bakker M, van Rantwijk F, Sheldon RA. Improved operational stability of peroxidases by coimmobilization with glucose oxidase. Biotechnol Bioeng 2000;69:286–91. https://doi.org/10.1002/1097-0290(20000805)69:3<286::AID-BIT6>3.0.CO;2-R.
[13] Yoon J, Kim J, Tieves F, Zhang W, Alcalde M, Hollmann F, et al. Piezobiocatalysis: ultrasound-driven enzymatic oxyfunctionalization of C–H bonds. ACS Catal 2020;10:5236–42. https://doi.org/10.1021/acscatal.0c00188.
[14] Burek BO, de Boer SR, Tieves F, Zhang W, van Schie M, Bormann S, et al. Photoenzymatic hydroxylation of ethylbenzene catalyzed by unspecific peroxygenase: origin of enzyme inactivation and the impact of light intensity and temperature. ChemCatChem 2019;11:3093–100. https://doi.org/10.1002/cctc.201900610.
[15] Lütz S, Vuorilehto K, Liese A. Process development for the electroenzymatic synthesis of (*R*)-methylphenylsulfoxide by use of a 3-dimensional electrode. Biotechnol Bioeng 2007;98:525–34. https://doi.org/10.1002/bit.21434.
[16] Stöckl M, Lange T, Izadi P, Bolat S, Teetz N, Harnisch F, et al. Application of gas diffusion electrodes in bioeconomy–an update. Biotechnol Bioeng 2023.
[17] Horst AEW, Mangold K-M, Holtmann D. Application of gas diffusion electrodes in bioelectrochemical syntheses and energy conversion. Biotechnol Bioeng 2016;113:260–7. https://doi.org/10.1002/bit.25698.
[18] Bormann S, van Schie MM, De Almeida TP, Zhang W, Stöckl M, Ulber R, et al. H_2O_2 production at low overpotentials for electroenzymatic halogenation reactions. ChemSusChem 2019;12:4759–63.
[19] Horst AEW, Bormann S, Meyer J, Steinhagen M, Ludwig R, Drews A, et al. Electroenzymatic hydroxylation of ethylbenzene by the evolved unspecific peroxygenase of *Agrocybe aegerita*. J Mol Catal B Enzym 2016;133:S137–42. https://doi.org/10.1016/j.molcatb.2016.12.008.
[20] Holtmann D, Krieg T, Getrey L, Schrader J. Electroenzymatic process to overcome enzyme instabilities. Catal Commun 2014;51:82–5.
[21] Bormann S, Hertweck D, Schneider S, Bloh JZ, Ulber R, Spiess AC, et al. Modeling and simulation-based design of electroenzymatic batch processes catalyzed by unspecific peroxygenase from *A. aegerita*. Biotechnol Bioeng 2021;118:7–16.
[22] Invitrogen. Pichia Fermentation Process Guidelines 2002.
[23] Cino J. High-yield protein production from *Pichia pastoris yeast*: A protocol for benchtop fermentation. Am Biotechnol Lab 1999;17:10–3.
[24] Perz F, Bormann S, Ulber R, Alcalde M, Bubenheim P, Hollmann F, et al. Enzymatic oxidation of butane to 2-butanol in a bubble column. ChemCatChem 2020;12:3666–9.
[25] Khataee AR, Safarpour M, Zarei M, Aber S. Electrochemical generation of H_2O_2 using immobilized carbon nanotubes on graphite electrode fed with air: investigation of operational parameters. J Electro Chem 2011;659:63–8. https://doi.org/10.1016/j.jelechem.2011.05.002.
[26] Sayoga GV, Bueschler VS, Beisch H, Holtmann D, Zeng A-P, Fiedler B, et al. Application of the all-in-one electrode for *in situ* H_2O_2 generation in hydroxylation

catalyzed by unspecific peroxygenase from *Agrocybe aegerita*. Mol Catal 2023;547:113325. https://doi.org/10.1016/j.mcat.2023.113325.

[27] Krieg T, Hüttmann S, Mangold K-M, Schrader J, Holtmann D. Gas diffusion electrode as novel reaction system for an electro-enzymatic process with chloroperoxidase. Green Chem 2011;13:2686–9. https://doi.org/10.1039/C1GC15391A.

[28] Peralta E, Natividad R, Roa G, Marin R, Romero R, Pavon T. A comparative study on the electrochemical production of H_2O_2 between BDD and graphite cathodes. Sustain Environ Res 2013;23:259–66.

[29] Wang Y, Liu Y, Wang K, Song S, Tsiakaras P, Liu H. Preparation and characterization of a novel KOH activated graphite felt cathode for the electro-Fenton process. Appl Catal B Environ 2015;165:360–8. https://doi.org/10.1016/j.apcatb.2014.09.074.

[30] Panizza M, Cerisola G. Electrochemical generation of H_2O_2 in low ionic strength media on gas diffusion cathode fed with air. Electrochim Acta 2008;54:876–8.

[31] Kim G-Y, Lee K-B, Cho S-H, Shim J, Moon S-H. Electroenzymatic degradation of azo dye using an immobilized peroxidase enzyme. J Hazard Mater 2005;126:183–8.

[32] Kluge MG, Ullrich R, Scheibner K, Hofrichter M. Spectrophotometric assay for detection of aromatic hydroxylation catalyzed by fungal haloperoxidase–peroxygenase. Appl Microbiol Biotechnol 2007;75:1473–8.

[33] Hobisch M, De Santis P, Serban S, Basso A, Byström E, Kara S. Peroxygenase-driven ethylbenzene hydroxylation in a rotating bed reactor. Org Process Res Dev 2022;26:2761–5.

[34] Ni Y, Fernández-Fueyo E, Baraibar AG, Ullrich R, Hofrichter M, Yanase H, et al. Peroxygenase-catalyzed oxyfunctionalization reactions promoted by the complete oxidation of methanol. Angew Chem Int Ed 2016;55:798–801. https://doi.org/10.1002/anie.201507881.

7.1. Electroenzymatic Hydroxylation of EBA under H_2O_2-Stat Mode and Fed-Batch Process

In a BES, particularly one that employs the combination of *in situ* generation of H_2O_2 and its further consumption in an enzymatic reaction, such as the application of H_2O_2-dependent enzyme r*Aae*UPO, a compromise between H_2O_2 productivity, biocatalytic productivity, enzymatic stability, and electrochemical efficiency must be made to improve the overall performance. An increase in both the productivity and accumulation of H_2O_2 has the potential to enhance enzymatic productivity. However, this may also result in a decreased r*Aae*UPO stability. This is particularly the case when the concentration of the target substrate is lower than its own K_M value and lower than the H_2O_2 concentration present in the medium. This condition typically leads to a more pronounced *rAae*UPO inactivation due to the catalase malfunction reaction. To avoid this situation, it is beneficial to maintain an excess substrate concentration and an adequate supply of H_2O_2 in the system.

To enhance the overall efficiency of the electroenzymatic hydroxylation process within the GDE system, a comparable methodology could be employed, wherein the concentration of the substrate EBA is consistently maintained at a level exceeding its K_M value of 2.3 mM [106]. One potential approach to achieve a concentration higher than the K_M value would be to initiate the reaction with a higher substrate concentration. However, the activity of r*Aae*UPO was reduced by 25% when the EBA concentration was increased to 12.5 mM, which was attributed to the presence of substrate surplus inhibition (**Fig. S7. 6**). As a result, it was not feasible to initiate the reaction with an EBA concentration exceeding 8 mM. To circumvent the issue of substrate surplus inhibition, a fed-batch operation mode was employed. Based on the initial activity of r*Aae*UPO in the BES the concentration of EBA within the medium was maintained at approximately 8 mM. This approach ensured that r*Aae*UPO was saturated with the substrate, thereby reducing the likelihood of a catalase malfunction reaction due to multiple reactions with H_2O_2 molecules. To test this hypothesis, the electroenzymatic hydroxylation of EBA in the GDE system at a H_2O_2-stat concentration of 0.2 mM was conducted under a fed-batch operation mode for EBA. The 0.2 mM H_2O_2 concentration threshold was selected on the basis of the preceding results, which demonstrated that this level of H_2O_2 delivered a comparatively high TOF, productivity, and competitive TTN (**Fig. 5. C**, **Fig. 6. B**; publication).

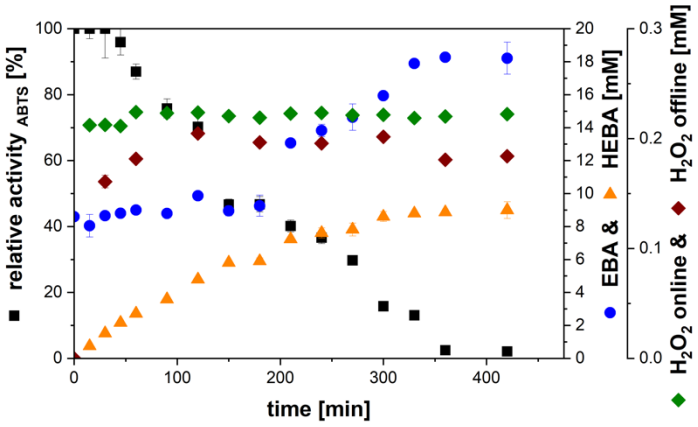

Fig. 7. 1. *Hydroxylation of EBA catalyzed by rAaeUPO in a GDE system under fed-batch process and in H_2O_2-stat mode with the H_2O_2 limit set to 0.2 mM. Reaction condition: 200 mL 0.1 M KP_i pH 7, 8 mM starting EBA concentration, 200 mM EBA stock solution, 10 nM rAaeUPO, 250 rpm, temperature: 22 ± 1 °C. EBA: 4-ethylbenzoic acid, HEBA: 4-(1-hydroxyethyl)benzoic acid. H_2O_2 offline: an offline H_2O_2 quantification via a photometrical method serves as a control for the online quantification. Data shown are average from technical duplicates.*

An EBA stock solution of 200 mM was prepared and introduced into the reaction system at an initial feeding rate of 0.06 mM min^{-1} (0.012 mmol min^{-1}) to prevent the accumulation of EBA in the medium. Given that the activity of r*Aae*UPO would decline over time, the feeding rate of EBA was progressively reduced until it was entirely stopped after 300 min (**Fig. 7. 1**). However, it appeared that the pre-calculated catalytic productivity from the preceding experiment (**Fig. 5. C**; publication) at the identical H_2O_2 threshold was slightly higher. Consequently, the substrate concentration gradually increased and accumulated up to 18 mM. Nevertheless, the fed-batch operation mode evidently enhanced the stability of r*Aae*UPO. The electroenzymatic hydroxylation of EBA conducted at the same H_2O_2 threshold under batch operation mode lasted for 300 min before the enzyme was totally deactivated, yielding a total product concentration of 7.6 mM. Concurrently, maintaining EBA concentrations above its K_M value and exceeding the H_2O_2 concentration could mitigate the probability of r*Aae*UPO being susceptible to catalase and catalase malfunction reactions. As a consequence, in this particular instance, the reaction persisted for up to 420 min, after which the enzyme demonstrated a residual activity of approximately 2%. During this time, a total product concentration of 9 mM was achieved. It should be noted that the accumulation of EBA in the medium could potentially suppress the biocatalytic activity. An accumulation of EBA above 15 mM has been demonstrated to reduce r*Aae*UPO activity by 65% (**Fig. S7. 6**). It is thus conceivable that maintaining the concentration of EBA at around 8 mM could facilitate a higher enzymatic conversion rate. In this instance, it was assumed that the enzyme was fully deactivated after 420 min to facilitate the calculation of the TTN. The TTN was determined to be 850,000 mol mol^{-1}, representing a notable increase of approximately 200,000 mol mol^{-1} in comparison to the batch operation mode. Additionally, the TTN was accompanied by a TOF of

67 s^{-1} and a productivity of 5.12 g L^{-1} d^{-1}, which are comparable to the TOF and productivity achieved in the batch mode. Based on these findings and obtained performance indicators, particularly the TTN, it can be postulated that the application of the fed-batch operation mode to maintain a stable substrate concentration, preferably above its K_M value (but below the K_i value) and higher than the co-substrate concentration, within the system is beneficial and could enhance the stability of r*Aae*UPO or even H_2O_2-dependent enzymes in general.

8. General Discussion and Outlook

Laboratory-scale electroenzymatic processes have shown promising performance indicators (PIs), sparking scientific interest in their potential for industrial application. However, a significant gap persists in the literature, as many studies do not report critical process parameters and PIs such as product titer, (analytical-) yield, biocatalyst loading, total turnover number (TTN), turnover frequency (TOF), Faradaic efficiency (F.E.), cell potential, and electrode surface area. This inconsistency hinders meaningful comparisons and identification of process limitations. To advance the field, it is crucial to adopt a parameter-driven approach for electroenzymatic systems, ensuring consistent reporting and comparability.

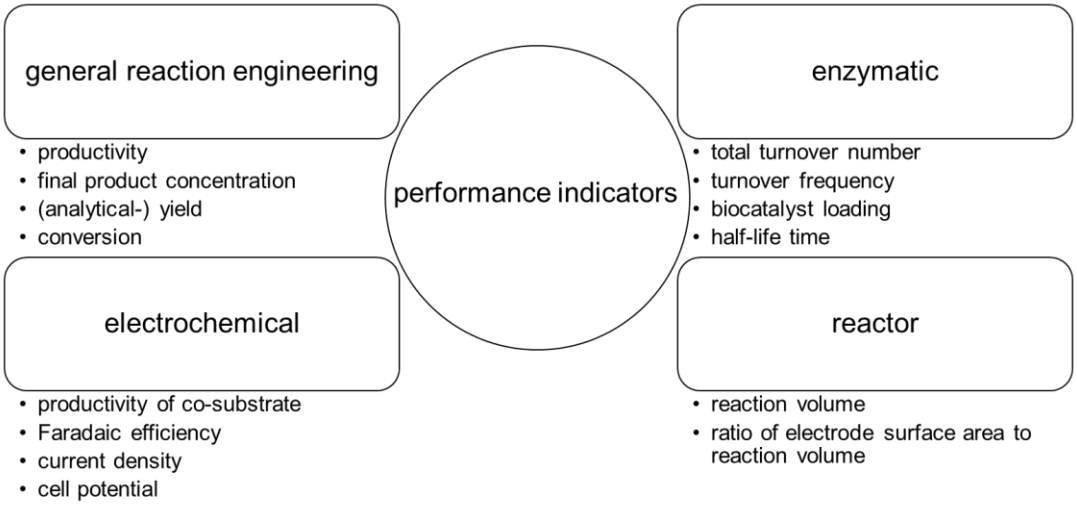

Fig. 8. 1. *Four categories of essential performance indicators in the field of electroenzymatic processes.*

To address this, the most significant PIs in the field of bioelectrochemistry, which should be included in every study, can be classified into four categories (**Fig. 8 .1**). General reaction engineering PIs are fundamental for evaluating and comparing the efficiency of electroenzymatic processes with traditional chemical processes. They also provide a critical foundation for assessing the overall effectiveness of different reaction systems. Electrochemical PIs offer insights into the efficiency of the co-substrate/ co-factor generation, which is vital for optimizing the process and reducing costs. Moreover, the F.E., current density, and cell potential are essential metrics for the comprehensive evaluation and comparison of various electrochemical systems, regardless of the scale or the nature of the product being generated. Furthermore, the catalytic efficiency, longevity of the biocatalyst, and the suitability of an enzyme in a specific system can be determined using enzymatic PIs. Finally, reactor indicators like the electrode surface area per reaction volume is of importance, as electrochemical reactions predominantly occur at the interface between the electrode and

the bulk medium. Understanding and optimizing this interface is the key to improve the overall efficiency of electroenzymatic processes, making it an essential parameter to report in related studies. Therefore, it is strongly advised that future studies report these PIs to enhance the robustness of the data and to facilitate meaningful comparisons between different systems.

In addition, it is recommended to provide relevant reaction parameters that would allow these PIs to be estimated retrospectively. For instance, in cases where current density is not stated, it is suggested to report the applied current along with the geometrical area of the working electrode. Similarly, if metrics such as TTN, TOF, enzyme half-life time and electrode-time yield are not provided, it is critical to include details such as the biocatalyst loading, the reaction time, the product concentration and the enzyme activity over time. Such practices improve data quality and facilitate precise comparisons.

It is also essential to acknowledge that certain evaluation criteria cannot be directly correlated with conventional PIs. Factors such as the alignment with the United Nations Sustainable Development Goals, system simplicity, scalability, application flexibility, material availability, and public acceptance are critical considerations that extend beyond standard PIs. These additional factors underscore the multifaceted nature of evaluating various processes and technologies, where both quantitative and qualitative assessments are essential for fully understanding their potential impact and enabling objective comparisons.

Subsequently, the knowledge gained was systematically applied to the electroenzymatic system studied in this dissertation. The research focuses on the *in situ* electrochemical generation of H_2O_2 as a co-substrate in a bioelectrochemical system (BES). Although H_2O_2 can be used in several biocatalytic reactions, such as hydroxylation, epoxidation, and sulfoxidation, its application in enzymatic processes remains relatively limited. This limitation primarily arises from the toxic and deactivating effects of H_2O_2 on enzymes, which has traditionally impeded its broader use in enzymatic systems. However, employing an electrochemical approach to continuously generate H_2O_2 *in situ* in a controllable manner and at low concentrations offers a viable solution to these challenges. By preventing the excessive accumulation of H_2O_2, this method significantly reduces enzyme deactivation and enhances the efficiency of H_2O_2-dependent enzymes. The advantages of *in situ* electrochemical H_2O_2 generation over alternative methods such as enzymatic or chemical generation and manual feeding of H_2O_2 are manifold. These include the elimination of the need for additional chemicals, the absence of complex by-product formation, no increase in reaction volume, and preserve consistent reaction conditions.

One of the most challenging chemical reactions is the oxyfunctionalization of unactivated carbon atoms, which typically necessitates high temperatures and the extensive use of organic solvents. However, certain biocatalysts facilitate the oxyfunctionalization of unactivated C-C and C-H bonds under mild conditions. A promising example is the recombinant unspecific peroxygenase from the fungus *Agrocybe aegerita* (r*Aae*UPO), which has demonstrated the ability to effectively catalyze the oxyfunctionalization of a wide range of substrates. Due to its high stability and reliance only on H_2O_2 as a co-substrate, r*Aae*UPO represents an ideal candidate for the integration into the BES.

To develop a customizable platform for H_2O_2-dependent reactions and enhance biocatalyst efficiency, the All-in-One (AiO) electrode system, featuring a carbon felt cathode, was utilized in the electroenzymatic hydroxylation. The physical flexibility of carbon felt made it an ideal choice for the cathode material in the AiO electrode system, as it could be easily wrapped around the AiO electrode scaffold, ensuring seamless integration. Although carbon felt electrodes have been previously employed in microbial fuel cells [124,125], their ability to perform an oxygen reduction reaction (ORR) remains to be validated. To investigate potential redox reactions on the surface of the cathode, a cyclic voltammetry (CV) study was conducted.

A current response was detected at a cathodic potential of -1 V vs. Ag/AgCl with a peak current of -0.015 A. This peak response was attributed to the ORR and potentially the generation of H_2O_2. It is worth mentioning that the iR compensation, which accounts for the iR drop, caused by the electrode's distance and the solution resistance was not applied. As a result, the observed cathodic peak appeared at a more negative potential than would be expected if iR compensation had been used. The CV analysis confirmed that the carbon felt electrode material is capable of reducing oxygen, indicating its potential for the *in situ* H_2O_2 generation. Based on these findings, carbon felt was incorporated into the AiO electrode, and a subsequent characterization study was performed to assess its *in situ* H_2O_2 generation ability, a fundamental step before initiating the electroenzymatic hydroxylation in the BES.

The characterization study was conducted using a single AiO electrode with a geometrical area of 11 cm^2, resulting in a surface-to-reaction volume of 0.055 cm^{-1}. The productivity of H_2O_2 was found to be influenced by the applied current, with an increase observed and a maximum productivity of 0.87 µM min^{-1} cm^{-2} was reached when the applied current was increased from 5 mA to 25 mA (**Fig. 3. A**; publication chapter 6). Despite the increase in the productivity with increasing applied current, the accumulation of H_2O_2 within the system did not exhibit a linear correlation with the reaction time, particularly at an applied current above 15 mA. The formation rate of H_2O_2 steadily declined and reached a plateau after 15 min (**Fig.**

3. B; publication chapter 6). This, in turn, resulted in a lower H_2O_2 accumulation at higher applied currents. The observed plateau can be attributed to the rates of deleterious reactions that were analogous or even higher than the formation rate of H_2O_2, particularly after 10 min at a current above 15 mA. These deleterious reactions were the further reduction of H_2O_2 to hydroxyl radical (**Eq. 3.6**) or water (**Eq. 3.7**) at the cathode, oxidation of H_2O_2 to hydroperoxyl radicals (**Eq. 3.5**) at the anode and the decomposition to water and oxygen (**Eq. 3.8**). Additional competing reactions, such as the complete reduction of oxygen to water (**Eq. 3.3**) and hydrogen evolution (**Eq. 3.4**) at the cathode, further hindered the formation of H_2O_2. It is crucial to acknowledge that these deleterious and competing reactions are dependent on the applied current and cell potential, and exceptionally prominent at higher applied current/ or cell potential [84,85]. These competing and deleterious reactions collectively reduce the yield of H_2O_2, ultimately limiting the accumulation of H_2O_2 to a specific point, in this case around 250 µM at 5 mA after 30 min. Similarly, the F.E. decreased with increasing current, reaching a maximum of 60%. When compared to PIs reported in literature, the F.E. of 60% and a H_2O_2 productivity of 0.87 µM min^{-1} cm^{-2} were comparable to those reported in gas diffusion electrode (GDE) systems and conventional graphite-based electrode systems [16,71,84,85,104].

The resulting surface-to-volume ratio is comparable to the specific electrode area found in Chloralkali cells [10]. In this study, the geometrical area of carbon felt was employed for the calculation of the surface-to-volume ratio and the H_2O_2 productivity, rather than the electrochemical surface area or the surface area provided by the manufacturer, which was determined via the Brunnauer-Emmet-Teller (BET) method. The BET method is a well-defined technique that, in most cases, provides an accurate estimation of total surface area. However, it also typically overestimates the electrochemically active surface area by a factor up to 100, given that only a fraction of the total surface area is electrochemically active [126]. As a result, the application of the BET surface area would underestimate the H_2O_2 productivity and overestimate the surface-to-volume ratio. The electrochemical surface area of porous materials, such as carbon felt, can be determined via a CV method, by analyzing the variation in peak current responses at different applied potentials. The actual electrochemical surface area is estimated by comparing the observed peak current to that of an electrode with a known surface area, in a manner analogous to constructing a calibration curve. Here, the CV method was employed in conjunction with the Fe^{2+}/Fe^{3+} redox reaction to ascertain the electrochemical surface area of the carbon felt. While peak currents were detected in the case of polished graphite electrodes with surface areas ranging from 0.085 cm^2 to 5.1 cm^2 (serving as a calibration standard), no discernible peak response was observed for the carbon felt. This suggests that the utilized carbon felt, with a geometrical area of 1 cm^2, may have had an actual electrochemical surface area too small to produce a detectable signal. The limited geometrical

surface area of the carbon felt resulted in an insufficient number of active sites for the regeneration of Fe^{2+}/Fe^{3+}, or alternatively, the current response may have been below the detection threshold. To improve the sensitivity of this method in the future, increasing the concentration of Fe^{2+}/Fe^{3+} or using carbon felt with a larger geometrical surface area could provide more accurate results. However, these approaches were not further explored in this dissertation.

Afterwards, to develop and validate the concept of a BES, the electrochemical *in situ* generation of H_2O_2 via the AiO electrode system was coupled with the enzymatic hydroxylation catalyzed by r*Aae*UPO. The initial model reaction system selected for this study was the two step hydroxylation of benzene, yielding resorcinol, hydroquinone and catechol as main products, as well as several by-products (**Fig. 5. 2**). Challenges with the analytical method led to the incomplete quantification of these products resulting in an incomplete evaluation of the system's performance. Consequently, critical PIs such as TTN, TOF, productivity and yield could not be fully quantified due to an incomplete molar balance of reactants and products, leading to low-value PIs. In this regard, a TTN of 15,000 mol mol^{-1}, a TOF of 0.84 s^{-1} and a productivity of 0.1 g L^{-1} d^{-1} were obtained, respectively (**Fig. 8. 2**).

Knowing that the main goal of the dissertation was to establish the concept of BES using the AiO electrode system and to enhance the efficiency of H_2O_2-dependent enzymes, a second model reaction system was selected: the hydroxylation of 4-ethylbenzoic acid (EBA). This reaction offered a simplified system for analysis, as only one product, 4-(1-hydroxyethyl)benzoic acid (HEBA), was generated from EBA. Using a starting concentration of 8 mM EBA and 30 nM (1 U_{ABTS} mL^{-1}) r*Aae*UPO, electroenzymatic experiments were conducted at applied currents ranging between 5 mA to 30 mA. A trend was observed, showing that the enzyme activity decreased at a faster rate as the applied current increased (**Fig. 5**; publication chapter 6). Despite no apparent accumulation of H_2O_2 during the reaction, it is possible that H_2O_2 concentrations remained below the detection threshold, leading to r*Aae*UPO deactivation due to multiple reactions with the co-substrate H_2O_2 rather than the target substrate EBA. This phenomenon is known as the catalase malfunction reaction and leads to a heme bleaching in heme-containing enzymes (**Fig. 3. 7**). The heme degradation and the subsequent enzyme deactivation are inevitable in such reactions and are directly associated with product formation [103]. An absent of H_2O_2 accumulation indicated that the consumption rate of H_2O_2 by r*Aae*UPO exceeded the rate of its electrochemical generation by the electrode. Moreover, radicals such as superoxide, hydroxyl radical, and hydroperoxyl radical were electrochemically generated *in situ* through water oxidation and H_2O_2 redox reactions. The generation rate of these radicals is directly influenced by the applied current,

with higher currents promoting increased radical formation [71]. Notably, the radical generation significantly increased when the applied current exceeded 10 mA (**Fig. S6. 10**), leading to a greater enzyme deactivation. As a consequence, a faster enzyme deactivation rate decreased not only the initial product formation rate (**Table 8. 1**) but also led to a decrease in the final product concentration, productivity, TTN and TOF. In this regard, the highest TTN and TOF achieved using the AiO electrode system were 220,000 mol mol^{-1} and 3.6 s^{-1}, respectively (**Fig. 6. A**; publication chapter 6). In this dissertation, the productivity was determined by quantifying the final product mass, calculated from the final product concentration obtained after 48 h. After 48 h, the enzyme was fully deactivated, however, the precise time point at which this occurred was unknown, since there was no overnight sampling in the period between 31 h to 48 h. Given that the experiment time was constant and that the enzyme deactivation rate increased in proportion to the applied current (**Fig. S6. 10**), it was also the case that the final product concentration obtained decreased. Consequently, the productivity exhibited a corresponding decline with increasing applied current. As the highest TTN was achieved at an applied current of 10 mA and that the obtained TOF and productivity were comparably high, this point was identified as the optimal current for subsequent experiments.

Table 8. 1. *The initial product formation rate and the productivity from the electroenzymatic hydroxylation of EBA catalyzed by rAaeUPO with in situ generation of H_2O_2 in the AiO electrode system. (results from chapter 6)*

Applied current [mA]	Initial formation rate [µM min^{-1}]	Productivity [g L^{-1} d^{-1}]
5	3.9	0.515
10	4.3	0.526
15	4.5	0.495
20	3.2	0.416
25	3.5	0.418
30	3.4	0.401

In light of the fact that the BES was constrained by the productivity of H_2O_2 and not by the enzymatic productivity, the applied biocatalyst loading was reduced by a factor of three to 10 nM (0.3 U_{ABTS} mL^{-1}). The reduction in catalyst loading at an applied current of 10 mA resulted in a slight decline in the initial product formation rate to 4 µM min^{-1} and a complete enzyme deactivation after 24 h (**Fig. S6. 7. E**). Nevertheless, the reduction in the catalyst loading resulted in enhanced catalyst efficiency, as demonstrated by the increase in both TOF and TTN to 7.7 s^{-1} and to 450,000 mol mol^{-1}, respectively (**Fig. 8. 2**). Simultaneously, the productivity after 24 h reached 0.8 g L^{-1} d^{-1}. With a maximum TTN of 450,000 mol mol^{-1}, this TTN exceeds those obtained in a system with manual addition of H_2O_2 [33,121], and is comparable to those reported in a system with electrochemical generation of H_2O_2 [8,106,112] and to that reported in a system with enzymatic generation of H_2O_2 [43]. It is important to note that the system employed in this study is markedly more straightforward and relies only on a

single enzyme compared to the aforementioned systems. With regard to TOFs, the highest value observed so far, with 7.7 s^{-1}, is 18 times lower than those obtained in GDE-based systems. This difference is largely attributable to the lower H_2O_2 productivity achieved in the current system.

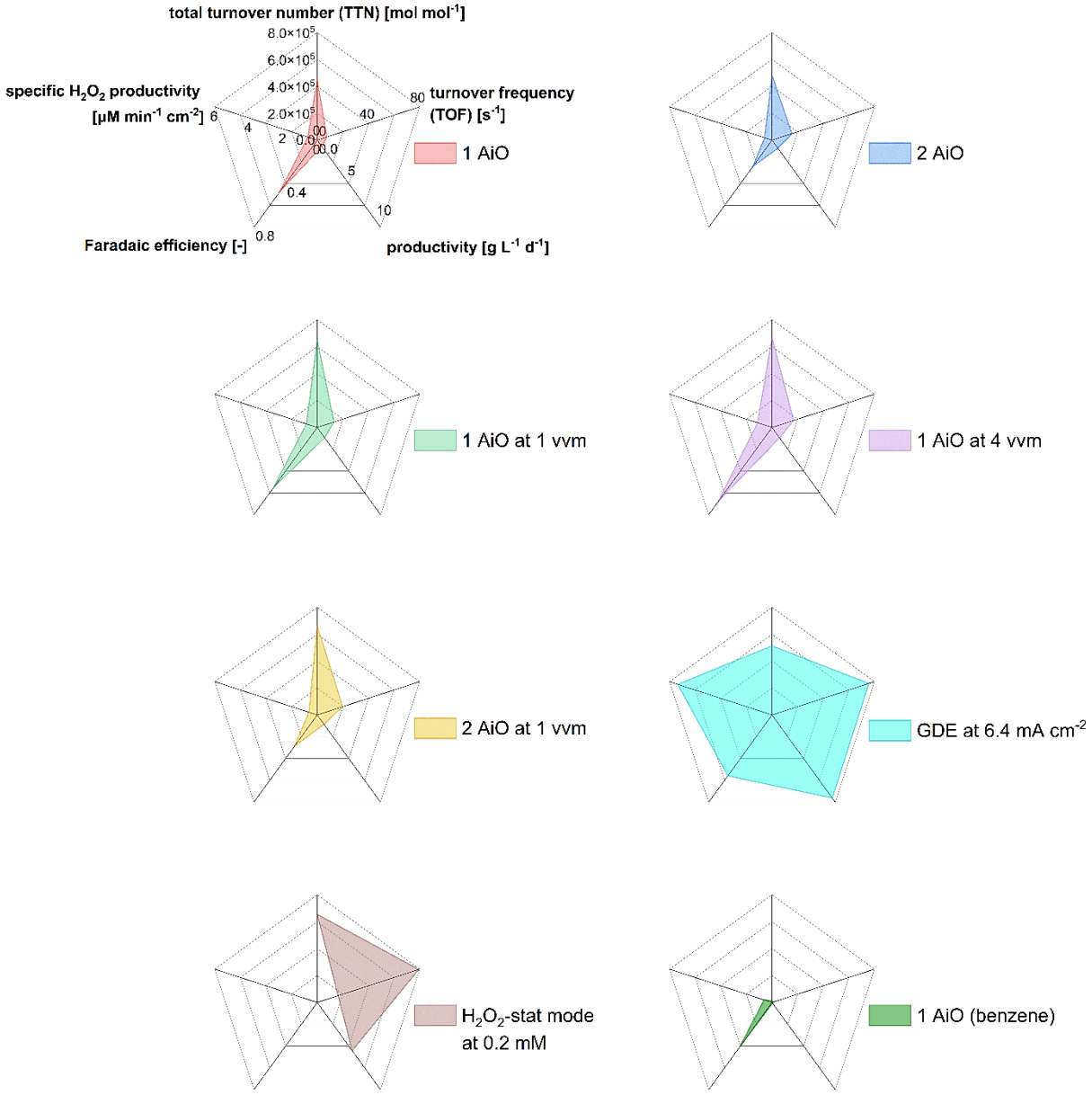

Fig. 8. 2. *Performance indicators of electroenzymatic hydroxylation of 4-ethylbenzoic acid (EBA) and benzene catalyzed by rAaeUPO within the All-in-One electrode (AiO) system and gas diffusion electrode (GDE) system, under various configurations. Experiments conducted at 10 mA (0.9 mA cm^{-2}) in the AiO electrode system. All experiments, except 1 AiO (benzene), were performed using 10 nM rAaeUPO (0.3 U_{ABTS} mL^{-1}).*

To improve the H_2O_2 productivity, aeration was introduced into the system. This measure was critical to ensure a sufficient supply of oxygen in the medium, as the availability of oxygen directly impacts the H_2O_2 generation. The H_2O_2 productivity, at the same applied current of 10 mA, increased with increasing aeration rate, reaching a maximum at 4 vvm. This resulted

in a 54% increase in productivity compared to the non-aerated system, corresponding to 0.84 µM min^{-1} cm^{-2} (**Fig. 6. 2. B**, **Fig. 8. 2**). The observed enhancement in productivity can be attributed to three main factors: an increase in the quantity of dissolved oxygen, an increase in oxygen mass transport to the electrode, and a reduction in the thickness of the electrochemical double layer at the electrode interface due to the turbulent flow introduced by the aeration. Supporting this hypothesis was the increase in both dissolved oxygen concentration and oxygen mass transfer coefficient (k_La) as the flow rate and stirring rate increased (**Fig. 6. 3**). The k_La value exhibited a linear increase from 0.028 min^{-1} to 0.1 min^{-1} at 1 vvm, with an increase in stirring rate from 250 rpm to 1000 rpm, and from 0.028 min^{-1} to 0.061 min^{-1} with an increase in aeration rate from 1 vvm to 4 vvm at a stirring rate of 250 rpm. Furthermore, the turbulent flow at the electrode facilitated the rapid desorption of H_2O_2, thereby reducing the likelihood of deleterious side reactions at the electrode. Although increasing the stirring rate not only enhanced the k_La value but also reduced the mixing time by a factor of 2.8 (**Fig. S6. 8**), subsequent electroenzymatic experiments were still conducted at a stirring rate of 250 rpm to maintain consistency with previous experimental conditions and the same k_La value.

Based on the findings of preceding experiments, the electroenzymatic hydroxylation was performed at an applied current of 10 mA and with an aeration of 1 vvm and 4 vvm, which represented the lowest and highest aeration rates tested here (**Fig. 6. 4**). These experiments aimed to determine whether the observed increase in H_2O_2 productivity could directly enhance the enzymatic productivity and overall system efficiency. During these experiments, the accumulation of H_2O_2 was detected in the range of 35 – 60 µM. It was observed that the initial product formation rate increased to 11.0 µM min^{-1} and 11.5 µM min^{-1} for the experiment conducted at 1 vvm and 4 vvm, respectively, in comparison to the non-aerated system (**Table 8. 1**). Accordingly, the initial product formation rate was found to increase the productivity of the system as well, reaching 1.30 g L^{-1} d^{-1} for 1 vvm and to 1.32 g L^{-1} d^{-1} for 4 vvm. Additionally, the TOF and the TTN increased, reaching as high as 17.1 s^{-1} and 670,000 mol mol^{-1}, respectively (**Table 6. 1**, **Fig. 8. 2**). This enhancement in system efficiency, as evidenced by the elevated TOF and TTN values, is primarily attributed to improved biocatalytic productivity due to the moderate accumulation of H_2O_2, especially during the initial stages of the reaction when enzyme activity was at its highest. As a result, a higher final product concentration was achieved upon complete enzyme deactivation. Despite a 48% increase in TTN at 4 vvm compared to the non-aerated system, no significant improvement in PIs was observed between the systems operated at 1 vvm and 4 vvm. This suggested a potential limitation in the system, where the electrochemical surface area of the electrode was insufficient to fully utilize the available oxygen in the ORR for the H_2O_2 generation.

One of the key benefits of the application of the AiO electrode is its versatile design, with dimensions closely resembling those of a conventional pH probe, enabling convenient integration into existing bioreactors. Accordingly, this allows for the incorporation of multiple AiO electrodes within a single reactor, increasing the surface area-to-volume ratio and addressing the limitation of electrochemical surface area. Two AiO electrodes were integrated into the reactor, doubling the surface-to-volume ratio from 0.055 cm^{-1} to 0.11 cm^{-1}. Despite this increase, the surface-to-volume ratio remained comparable to that of electrochemical systems employed in Chloralkali processes [10]. The concept of a multiple AiO electrodes was initially tested without aeration to compare the PIs with those of a single AiO electrode system under non-aerated condition. The application of two AiO electrodes in the BES at 10 mA, applied at each AiO electrode, resulted in a doubling of the TOF from 7.7 s^{-1} to 15.8 s^{-1} (**Table 6.1**, **Fig. 8. 2**). This increase was attributed to the doubling of the electrochemical surface area, which resulted in a corresponding increase in the concentration of electrochemically generated H_2O_2. Despite the doubling of the TOF, the resulting TTN remained relatively unchanged, exhibiting a value of 480,000 mol mol^{-1} (**Fig. 8. 2**). The slight increase in the TTN indicated a decline in the stability of r*Aae*UPO. The accumulation of H_2O_2 to a concentration of 40 µM during the course of the experiment may have contributed to the decrease in r*Aae*UPO stability (**Fig. S6. 9**). Moreover, the rise in the biocatalytic turnover might potentially enhance the likelihood of a catalase malfunction reaction. Of particular importance was the doubling of radical formation in the multiple AiO electrodes system (**Fig. 6. 5. A**), which was attributed to the increased in the electrode surface area. As a consequence of these factors, the stability of r*Aae*UPO was compromised, as reflected by a 1.2-fold increase in the enzyme deactivation rate compared to the single AiO electrode system. For that reason, the attained final product concentration (also the TTN) was not much higher due to the faster enzyme deactivation rate, despite the increased TOF and productivity. Subsequently, aeration at 1 vvm was introduced into the multiple electrodes system. An aeration rate of 1 vvm was selected over 4 vvm as both aeration rates yielded comparable TTN. Furthermore, the application of 4 vvm aeration rate was deemed too excessive and could introduce a potential safety risk due to a high pressure inside the vessel. The integration of multiple AiO electrodes with 1 vvm aeration in the electroenzymatic hydroxylation at 10 mA (applied to each AiO electrode) (**Fig. S6. 11**) significantly enhanced the catalytic performance, achieving a TOF of up to 20.1 s^{-1} (**Fig. 6. 5. D**, **Fig. 8. 2**), which was also the highest TOF obtained in the multiple electrodes system with aeration. This represents a 52% and a 27% increase compared to the TOF obtained in a single electrode system at 1 vvm and to the multiple AiO electrodes system without aeration (**Fig. 8. 2**), respectively. Furthermore, the TTN reached a value of 660,000 mol mol^{-1}, comparable to that achieved in the single AiO electrode system at 4 vvm. These results indicated that the

application of multiple AiO electrodes, to enhance the electrochemical surface area, and its combination with aeration in electroenzymatic r*Aae*UPO-catalyzed hydroxylation resulted in an increase in the initial product formation rate and the TOF. Nevertheless, this configuration did not necessarily result in an increase in the final product concentration or the TTN.

This suggests that there may be an intrinsic upper limit to the TTN that can be achieved with this type of enzymes, independent of the H_2O_2 concentration and supply. This hypothesis has been proposed previously [106]. Hence, a reduction in the biocatalyst loading would not result in a substantial increase of the TTN, as the productivity of H_2O_2 will exceed its consumption by the enzyme. Consequently, a reduction in H_2O_2 productivity, as observed in the single AiO electrode system, would not lead to an increase in TTN, since the enzyme would become destabilized by other factors such as the reaction with H_2O_2 and radicals. Notably, the highest TTN achieved with this configuration was 700,000 mol mol^{-1} at 5 mA (**Fig. 6. 5. D**). The highest TTN achieved in this study not only falls within the upper range of TTN values reported in the literature for r*Aae*UPO-catalyzed reactions but also represents one of the highest TTN reported to date in BES for r*Aae*UPO-catalyzed electroenzymatic reactions. Consistent with observations from the single AiO electrode system, both TTN and TOF generally decreased with increasing applied current (**Fig. 6. 5. D**), likely due to similar factors—primarily the destabilization of r*Aae*UPO in the presence of H_2O_2 and radicals.

The AiO electrode system exhibited several limitations, including a comparatively low H_2O_2 productivity and TOF, particularly in comparison to GDE-based systems. It is evident that the enhanced oxygen mass transfer facilitated by the GDE's three-phase boundary contributes to its higher H_2O_2 productivity [112,113]. Consequently, the limitations associated with low oxygen solubility and diffusivity in the medium are avoided. Nonetheless, the H_2O_2 productivity in the AiO electrode system still can be potentially increased, apart by optimizing the reaction parameter like stirring rate, aeration rate and applied current, for example by employing surface modification and coating method to the working electrode. Additional carbon materials like carbon nanotubes (CNTs) can be used to coat the surface of the carbon felt [105]. Coating the electrode by CNTs offers not only an enlargement of the surface area, but also a reduction in the overpotential, as has been demonstrated in previous study [105]. Therefore, the formation of radicals at higher potential is minimized, while the H_2O_2 productivity and its selectivity might be increased. Furthermore, a strategy like surface oxidation can be applied for carbon-based electrocatalysts. Chemical methods are employed for the surface oxidation process, for example by using wet method such as the application of high concentration of nitric acid or KOH solution [127]. Moreover, a dry method can also be used to oxidize carbon-based electrodes by mixing the electrocatalyst with polyethylene oxide and carbonizing it at

high temperature [127]. The effect of oxidation treatment on the electrode surface is the introduction of disorder (defect) in the structure of the electrode. The defect is the induction of oxygen-containing functional groups, including C-O-C, C=O, and -COOH, into the catalyst [127]. A positive correlation was observed between the ORR activity and selectivity for H_2O_2 of an electrocatalyst and the increasing content of oxygen-containing functional groups. It was suggested that the defects in the carbon materials could act as reactive sites for oxygen adsorption and potentially its reduction during the electrocatalytic process [62]. In addition, the pressure of the system can be increased to promote mass transfer and oxygen solubility in the medium. Increasing the pressure of the system, for example up to 30 relative bar, proved to be an efficient way to intensify oxygen mass transport, resulting in a two order of magnitude increase in H_2O_2 productivity and its accumulation [128]. Additionally, the concept of the AiO electrode could be expanded in a number of ways. One would be the combination of the AiO electrode with the flow reactor technology to develop an electrochemical flow cell. This combination could provide an alternative scale-up strategy and higher electrode surface-to-volume ratio. The design of flow cells allows for their numbering up or stacking as modular units, with the number of cells increasing as the reaction volume increases. The H_2O_2 productivity could be further optimized by leveraging the additional properties offered by a flow cell, such as excellent heat and mass transfer as well as predictable flow behavior. The research initiative pertaining to this subject is underway and its findings are documented in **11. 4**. These proposed methods to improve the H_2O_2 productivity are only one side of the story, since they will only improve the electrochemical part of the whole BES. In other words, the impact on the electroenzymatic reaction would be the improvement of the TOF. Regarding r*Aae*UPO as a biocatalyst, it would be beneficial to implement a suitable immobilization method to increase the stability not only against H_2O_2, but perhaps also against generated radicals. Thus, the catalyst operational lifetime and the TTN of the electroenzymatic reaction could be improved. One possible immobilization method would be the combination of r*Aae*UPO with an anchor peptide and a spacer [129], so that the enzyme could be immobilized via the anchor peptide on the electrode. This will increase the proximity between the co-substrate generation and the enzymatic reaction, while simultaneously reduce the sterical hindrance. A potential advantage of using a spacer between the r*Aae*UPO and the anchor peptide is that the enzyme would not be directly located on the electrode, thus avoiding the possibility of enzyme deactivation due to the electric field [120]. Most importantly, the possibility of recurrent reactions between r*Aae*UPO and H_2O_2 due to the close proximity and high affinity can also be minimized.

Succeeding the establishment of the concept AiO electrode system as an optimizable platform for H_2O_2-dependent enzymatic reactions, further optimization was pursued to enhance the

efficiency of the system and improve the operational stability and productivity of r*Aae*UPO. While most BES studies utilized a galvanostatic or potentiostatic mode [16,104,105], one inherent limitation of this approach for *in situ* H_2O_2 generation is its constant production rate over time. A constant H_2O_2 productivity could restrict the overall catalytic rate during the initial stage of the reaction when the enzyme is still active. However, as the reaction progresses and the enzyme activity declines due to deactivation, the H_2O_2 productivity will exceed its consumption and accumulate in the medium. The accumulation of H_2O_2 further accelerates the enzyme deactivation via the catalase malfunction reaction. To address this issue, a customized automation program was developed to dynamically control the current supplied to the electrodes. The program utilized the input from the H_2O_2 sensor to ensure a constant H_2O_2 concentration, also referred to as H_2O_2-stat mode, independent of the enzyme activity. In this setup, a commercial GDE was utilized as the cathode, replacing the AiO electrode with the carbon felt cathode. The GDE was selected for this system due to its high oxygen mass transfer and its high selectivity towards H_2O_2. Consequently, this configuration enables a rapid generation of H_2O_2 to a specified concentration, while minimizing deleterious and competing reactions, ensuring a constant H_2O_2 concentration.

To validate the concept of H_2O_2-stat mode, this system was applied in a BES combined with the enzymatic hydroxylation of EBA catalyzed by r*Aae*UPO. The H_2O_2 concentration limits in the H_2O_2-stat mode were set at 0.06 mM, 0.15 mM, 0.20 mM and 0.28 mM. Within the H_2O_2-stat mode, the power supply dynamically adjusted the current sent to the electrodes, thereby adjusting the H_2O_2 productivity to attain and sustain a predetermined H_2O_2 concentration throughout the experiment. As the concentration of H_2O_2-stat limit was increased and more H_2O_2 became available in the medium, the reaction rate also increased, resulting in a higher TOF and productivity. In this regard, the maximum TOF and productivity were 87.5 s^{-1} and 6.9 g L^{-1} d^{-1}, respectively (**Fig. 6. B**; publication chapter 7). However, while a high TOF at elevated H_2O_2 concentrations enhances the reaction rate, it also increases the likelihood of r*Aae*UPO undergoing catalase and catalase malfunction reactions, which accelerate enzyme deactivation. Subsequently, as the enzyme deactivation rates increased, both the experiment duration and final product concentration declined. This trend was also observed in the TTN, which dropped from a maximum of 710,000 mol mol^{-1} at a H_2O_2-stat concentration of 0.15 mM to 570,000 mol mol^{-1} at 0.28 mM. Considering the obtained PIs at various H_2O_2-stat concentration thresholds tested, in this particular system it is advisable that the H_2O_2-stat concentration is set to 0.2 mM. This concentration limit not only facilitated the attainment of comparably high TOF (80.3 s^{-1}) and productivity (6.1 g L^{-1} d^{-1}) but also maintained a competitive TTN (655,000 mol mol^{-1}) (**Fig. 8. 2**), compared to values reported for similar reaction systems on a laboratory-scale.

In addition to the H_2O_2-stat mode, the electroenzymatic experiment in the GDE system was correspondingly conducted in galvanostatic mode to provide a basis for comparison. The maximum TOF attained via both methodologies was comparable, around 80 s^{-1}. Notably, the highest productivity achieved under the galvanostatic method with 10.5 g L^{-1} d^{-1}, exceeded that observed under the H_2O_2-stat mode (**Fig. 8. 2**). The higher productivity observed under the galvanostatic method can be attributed to two main factors: higher H_2O_2 productivity and a greater accumulation of H_2O_2 in the medium. Nevertheless, the continuous increase of H_2O_2 under galvanostatic mode resulted in a more rapid deactivation of r*Aae*UPO. In this context, the maximum TTN obtained under the H_2O_2-stat mode was 10% higher in comparison to the maximum TTN achieved under the galvanostatic mode. When comparing the AiO electrode system with the GDE system under H_2O_2-stat mode, the TOF obtained in the AiO electrode system was about 4.4 times lower, namely 20.1 s^{-1} (**Fig. 8. 2**). Meanwhile, the highest productivity in the AiO electrode system was 1.32 g L^{-1} d^{-1} (**Fig. 8. 2**), which was approximately 5.3 times lower than that in the H_2O_2-stat mode. A lower TOF and productivity obtained by the AiO electrode system were the result of a lower H_2O_2 productivity, which has already been discussed before. Within the AiO electrode system, the highest H_2O_2 productivity reached up to 0.87 µM min^{-1} cm^{-2}, meanwhile the GDE system reached a productivity up to 5.5 µM min^{-1} cm^{-2} (**Fig. 8. 2**). Furthermore, the reaction window for the ORR within the AiO electrode was quite narrow which spanned between 5 mA to 20 mA, or 0.45 mA cm^{-2} to 1.82 mA cm^{-2}. As the applied current was increased further, the productivity decreased and the rate of the deleterious and competing reaction increased, as shown by the non-linear increase of accumulated H_2O_2 concentration over time (**Fig. 3. B**; publication chapter 6, **Fig. 6. 5. B**) and the increasing rate of radical formation (**Fig. 6. 5. A**, **Fig. S6. 10**). On the contrary, GDE showed a wide operating window for the ORR that ranged between 0.8 mA cm^{-2} to 6.4 mA cm^{-2}. Within this operating window the productivity of H_2O_2 exhibited a linear increase with increasing current density and the accumulation of H_2O_2 showed a linear correlation with the experiment time (**Fig. 2. A**; publication chapter 7). Therefore, the final accumulated H_2O_2 concentration within the GDE system could reach up to 2000 µM, while within the AiO electrode system reached only up to 270 µM. These results once again underscore the shortcomings of the AiO electrode system, but more crucially, they illustrate the limitations of utilizing the non-modified carbon felt material as the working electrode. While the concept of the AiO electrode is promising and has been demonstrated to yield competitive results in comparison to other reported systems [43,104,106,121], further optimization of the working electrode through a material science-focused approach could enhance the selectivity of H_2O_2 and reduce the overpotential. In addition to the previously outlined methodology, further methods may be employed to enhance selectivity and productivity. These include surface

treatment with polyethyleneimide, doping with nitrogen [130], and the application of highly porous carbon materials such as Globugraphite [131]. Furthermore, with regard to catalyst efficiency, both systems yielded a comparable TTN, which was approximately 700,000 mol mol^{-1}. The TTN remains a critical metric in this study, as it indicates the suitability and stability of a biocatalyst for a specific process. Thus, it aligns with one of the study's objectives, which is to enhance the stability of H_2O_2-dependent enzymes. The comparable TTN achieved by both systems at a very different TOFs strengthens again the indication that there is an inherent maximum number of turnovers for r*Aae*UPO, independent of extrinsic inactivating factors and H_2O_2 supply [106,132].

Despite the indication of the maximum achievable TTN by r*Aae*UPO, further system optimization was performed to enhance the efficiency. This optimization involved the application of a fed-batch operation mode for the target substrate EBA. It was observed that the r*Aae*UPO activity exhibited a markedly accelerated decline when the EBA concentration approached or fell below its K_M value. This phenomenon can be attributed to the higher affinity of H_2O_2 ($K_{M,\ H_2O_2}$: 1.3 mM [133]) towards r*Aae*UPO and the constant availability of H_2O_2 in the medium, which ultimately results in a catalase malfunction reaction. By maintaining the EBA concentration above its K_M value ($K_{M,\ EBA}$: 2.3 mM [106]), r*Aae*UPO becomes saturated with the substrate, thereby minimizing the probability of multiple reactions occurring solely with H_2O_2. To prevent substrate surplus inhibition above 8 mM (**Fig. S7. 6**), the fed-batch operation mode was preferred over a higher initial EBA concentration. The implementation of a fed-batch operation under H_2O_2-stat mode, at 0.2 mM threshold, improved r*Aae*UPO stability, as demonstrated by a longer operational times and increased final product concentration (**Fig. 7. 1**). Specifically, the operational time increased from 300 min to 420 min, while the final product concentration rose from 7.6 mM to 9 mM, compared to the batch operation mode. Additionally, the TTN improved by 30%, reaching 850,000 mol mol^{-1}. Meanwhile, the TOF and productivity remained consistent with those obtained in batch operation mode, at 67 s^{-1} and 5.12 g L^{-1} d^{-1}, respectively. Throughout the experiment, the EBA concentration gradually increased to 18 mM, despite continuous feed rate adjustments. The accumulation of EBA reduced the enzymatic conversion rate due to substrate inhibition. For example, an accumulation of EBA above 15 mM resulted in a 65% reduction in r*Aae*UPO activity (**Fig. S7. 6**). In this instance, the TOF and productivity as well as the conversion and analytical yield could be maximized if the EBA concentration was maintained at 8 mM, which is also the point at which r*Aae*UPO exhibited its highest activity. Future applications of nuclear magnetic resonance (NMR) could enable real-time monitoring of EBA concentration to maintain the concentration above its K_M value and around 8 mM. The results from the fed-batch operation demonstrated that by maintaining EBA concentrations above its K_M value and exceeding the H_2O_2 concentration

could reduce the probability of r*Aae*UPO being susceptible to catalase malfunction reaction, thus enhancing the r*Aae*UPO operational stability.

The results obtained in this study were reproducible, demonstrating the reliability of the experimental setup. However, several potential sources of error were identified. For instance, errors could arise during the preparation of calibration curves for EBA and HEBA, which were prepared manually by correlating peak areas with known concentrations of these compounds (**Fig. S6. 1**). These errors could occur during the preparation of the stock solutions or the subsequent dilution steps to prepare solutions of varying concentrations. Inaccuracies in this process could affect the determination of the residual EBA concentration or the final HEBA concentration. Similarly, this also applies to the benzene model reaction system involving phenol, hydroquinone, resorcinol and catechol as intermediate and products (**Fig. S5. 2**). Such an error would have an impact on the determination of the molar balance, TOF, TTN, and productivity. A comparable source of error exists for the offline H_2O_2 calibration (**Fig. S6. 3**), as the H_2O_2 solutions were prepared manually from a concentrated stock solution. Error in this step could impact the calibration of the H_2O_2 sensor for online measurements. This is because the H_2O_2 sensor had to be calibrated manually using known H_2O_2 concentrations. These calibration inaccuracies could affect the determination of H_2O_2 concentration in the medium, its productivity, and the H_2O_2 threshold settings in the H_2O_2-stat mode within the GDE system. Furthermore, the initial activity and concentration of r*Aae*UPO for each experiment were determined using the ABTS assay in the presence of EBA (r*Aae*UPO was mixed in the medium with the rest of the reaction components) prior to the start of the experiment. Since r*Aae*UPO reacts with both ABTS and EBA, the presence of EBA could potentially reduce the measured activity and concentration of r*Aae*UPO. This could influence the calculations for TOF and TTN. However, this method was still considered optimal, as it provided an estimation of r*Aae*UPO activity and concentration within the reaction medium. Notably, the higher affinity of r*Aae*UPO for ABTS ($K_{M, ABTS}$: 0.025 mM [134]) compared to EBA supports this assumption. It is important to note that all these small sources of error can combine and multiply when determining PIs. As a result, larger deviations in TOF and TTN are expected, which is around 12 – 31%, compared to other parameters like productivity or conversion, which is between 7 – 20%.

In conclusion, recent advancements in electroenzymatic processes have demonstrated impressive laboratory-scale PIs. For the successful transition from laboratory-scale experiments to technical applications, it is essential to establish standardized benchmarks and PIs. This dissertation represents a significant step in this direction by employing the concept of AiO electrode in an electroenzymatic process for *in situ* H_2O_2 generation, specifically for enzymatic hydroxylation. The results highlight that while the AiO electrode system achieved a

TTN comparable to the best values in the literature, the system's productivity was constrained by H_2O_2 generation. Optimization of the AiO electrode design, including incorporation of porous electrode materials and surface modifications, could potentially enhance the H_2O_2 selectivity and productivity. The simplicity and effectiveness of the electrochemical *in situ* H_2O_2 generation method make it an attractive alternative, reducing r*Aae*UPO deactivation and avoiding common drawbacks such as volume increase, by-product formation, and pH shifts. Furthermore, this dissertation illustrates the critical impact of the H_2O_2 electrogeneration mode on both r*Aae*UPO stability and overall productivity. While galvanostatic mode offers higher productivity at the expense of rapid r*Aae*UPO deactivation, the H_2O_2-stat mode provides superior TTN by preventing excess H_2O_2 accumulation. Even more, the EBA fed-batch operation mode further increases the r*Aae*UPO stability by keeping it saturated by the EBA. The PIs achieved under the H_2O_2-stat mode align with those reported in the literature, with the TTN surpassing all previously reported values for r*Aae*UPO-catalyzed reactions in BES. The versatility of the H_2O_2-stat approach also holds potential for broader applications, including studies on inactivation mechanisms in other H_2O_2-dependent enzymes. Finally, this dissertation underscores the potential of the AiO electrode system as a customizable and scalable platform for H_2O_2-dependent electroenzymatic reactions. Through optimization of the electrode material to enhance the H_2O_2 selectivity and F.E., as well as improvement of the enzyme stability and the TTN, this system could facilitate a successful transition of electroenzymatic processes from the laboratory to the technical scale.

9. Summary

In this chapter, key findings relevant to the objective of this dissertation are summarized as key points. An alternative electrochemical approach for *in situ* H_2O_2 generation is presented, using the All-in-One (AiO) electrode system as an optimizable platform for H_2O_2-dependent enzymatic reactions. The main goal was to integrate the electrochemical *in situ* H_2O_2 generation with the enzymatic hydroxylation, demonstrating a proof of concept for this integrated approach. To enhance the catalytic efficiency and biocatalyst stability, an automation system was developed, employing a real-time feedback from an H_2O_2 sensor to dynamically adjust the electrical output sent to electrodes, ensuring a consistent and low H_2O_2 concentration. The viability of the automation system was validated in a gas diffusion electrode (GDE) system, underscoring its potential to maintain stable reaction conditions. Moreover, this study recommended for the standardization and uniform reporting of performance indicators (PIs) and process parameters in electroenzymatic processes, with the goal of facilitating more accurate qualitative and quantitative comparisons in future research.

- Despite advancements in electroenzymatic processes, a gap remains in the literature regarding the reporting of essential reaction parameter and PIs, limiting objective comparisons across different studies.
    - The key PIs and reaction parameters critical for quantitative analysis in electroenzymatic processes can be categorized into four groups: (i) general reaction engineering PIs, (ii) enzymatic PIs, (iii) electrochemical PIs and (iv) reactor indicators. Each group encompasses various metrics, such as:
        - General reaction engineering PIs: productivity, product concentration, (analytical-) yield, initial product formation rate.
        - Electrochemical PIs and parameter: co-substrate productivity, Faradaic efficiency, cell potential, applied current, current density, geometrical electrode surface area.
        - Enzymatic PIs and parameter: total turnover number, turnover frequency, half-life time, biocatalyst loading, enzyme activity over time.
        - Reactor: electrode surface per reaction volume, reaction volume.
    - Non-quantitative factors such as system scalability, simplicity, alignment with the United Nations Sustainable Development Goals, and application flexibility are essential for a comprehensive evaluation of electroenzymatic processes.
    - The evaluation of processes involving H_2O_2-dependent peroxygenases led to several conclusions: (i) no existing process is yet optimal, (ii) the process with

the rotating-bed reactor with immobilized enzymes and feeding of H_2O_2 showed the best overall performance, and (iii) electrochemical systems require further optimization, particularly regarding product concentration, substrate concentration, and productivity.

- The AiO electrode system was applied for the first time in an electroenzymatic process, with the objective of developing a controllable *in situ* generation of H_2O_2 and establishing an optimizable platform for H_2O_2-dependent reactions.
    - H_2O_2 productivity increased with increasing applied current, reaching a maximum of 0.87 µM min^{-1} cm^{-2} at 25 mA, while the maximum Faradaic efficiency (F.E.) of 60% was achieved at an applied current of 5 mA.
    - Competing and deleterious reactions which include hydrogen evolution reaction, full oxygen reduction to water, radical formation, further redox reactions of formed H_2O_2, and its decomposition, were intensified at higher currents, reducing the F.E., H_2O_2 productivity and H_2O_2 accumulation.
    - The total turnover number (TTN), turnover frequency (TOF) and productivity within bioelectrochemical system (BES) were influenced by the applied current, r*Aae*UPO concentration and r*Aae*UPO stability. At 10 mA, TTN, TOF and productivity reached 450,000 mol mol^{-1}, 7.7 s^{-1} and 0.8 g L^{-1} d^{-1}, respectively.
    - The introduction of aeration improved the H_2O_2 productivity, attributed to the increase in soluble oxygen concentration, oxygen mass transfer to the cathode and reduction in the thickness of the electrochemical double layer, leading to an increase in biocatalytic productivity to 1.30 g L^{-1} d^{-1}, the TOF to 13.2 s^{-1} and the TTN to 650,000 mol mol^{-1}, at 10 mA and 1 vvm.
    - The application of multi-electrode system at 10 mA and 1 vvm achieved a TTN of 660,000 mol mol^{-1}, a TOF of 20.1 s^{-1} and a productivity of 1.18 g L^{-1} d^{-1}. The highest TTN recorded was 700,000 mol mol^{-1} at 5 mA, representing one of the highest TTN value reported for *Aae*UPO-catalyzed electroenzymatic reactions.
    - The combination of a multi-electrode system with aeration improved the initial product formation rate and TOF, but did not significantly increase final product concentration and TTN, indicating a potential intrinsic upper limit for the TTN in r*Aae*UPO-catalyzed reactions.
    - Although H_2O_2 productivity was identified as a limiting factor in the AiO electrode system, the AiO electrode system demonstrated significant potential as an optimizable platform for H_2O_2-dependent enzymatic reactions.
- An automation system was developed to prevent an excessive H_2O_2 accumulation by dynamically regulating the current output based on a real-time feedback from an H_2O_2 sensor. This system maintained a low and consistent H_2O_2 concentration (H_2O_2-stat

mode) throughout the electroenzymatic reaction. This approach was demonstrated in a GDE system, highlighting its potential for maintaining stable H_2O_2 concentration.

- Within H_2O_2-stat mode, the power supply delivered a dynamic current to the electrodes, thereby adjusting the H_2O_2 productivity to its consumption by the enzyme to maintain a constant H_2O_2 concentration, independent of the enzyme activity.
- The H_2O_2-stat concentration threshold influenced the stability of r*Aae*UPO, TTN, TOF and productivity. While both biocatalytic productivity and TOF increased with increasing H_2O_2 concentration threshold, the r*Aae*UPO stability and the TTN decreased, due to the catalase malfunction reaction.
- While the highest biocatalytic productivity of 10.5 g L^{-1} d^{-1} was achieved under galvanostatic mode at a current density of 6.4 mA cm^{-2}, the continuous increase of H_2O_2 led to a more rapid deactivation of r*Aae*UPO.
- The highest TTN of 710,000 mol mol^{-1} and TOF of 87.5 s^{-1} were obtained under H_2O_2-stat mode at concentration limits of 0.15 mM and 0.28 mM, respectively.
- The most favorable outcome was found in the H_2O_2-stat mode at 0.2 mM, where a TTN of 655,000 mol mol^{-1}, a TOF of 80.3 s^{-1} and a productivity of 6.1 g L^{-1} d^{-1} were obtained. The implementation of the fed-batch process improved the r*Aae*UPO stability as verified by the increase of the TTN to 850,000 mol mol^{-1}.
- Both AiO electrode system and GDE system under the H_2O_2-stat mode yielded a comparable TTN of 700,000 mol mol^{-1}. A comparable TTN achieved by both systems at different TOFs strengthens the indication of an inherent maximum number of turnovers for r*Aae*UPO, independent of extrinsic inactivating factors.
- The advantage of the H_2O_2-stat mode lies in its ability to adapt to the changes of the H_2O_2 consumption rate, in accordance to the progress of the reaction, thus, preventing H_2O_2 accumulation and protecting the enzyme from rapid deactivation.

This dissertation effectively demonstrates the application of an electrochemical approach for *in situ* H_2O_2 generation in enzyme catalysis, highlighting the potential of the AiO electrode system as a versatile platform for H_2O_2-dependent enzymatic reactions. In addition, the H_2O_2-stat mode significantly enhanced the efficiency of the electroenzymatic system and biocatalyst stability. This approach enabled precise control and consistent regulation of H_2O_2 concentration throughout the reaction, in accordance to the progress of the reaction.

10. References

[1] Keller A, Belderok A, Douma E, Kuhner S. Chemicals 2035–gearing up for growth. Eur Chem Ind Can Gain Tract Tougher World Roland Berg Strategy Consult GMBH Retrieved From 2015.

[2] Harnisch F, Holtmann D. Electrification of biotechnology: Status quo. In: Harnisch F, Holtmann D, editors. Bioelectrosynthesis, vol. 167, Cham: Springer International Publishing; 2017, p. 1–14. https://doi.org/10.1007/10_2017_41.

[3] Gulliver JS. Transport and fate of chemicals in the environment: selected entries from the Encyclopedia of sustainability science and technology. Springer Science & Business Media; 2012.

[4] Sillanpää M, Ncibi C, Sillanpää M, Ncibi C. Biorefineries: industrial-scale production paving the way for bioeconomy. Sustain Bioeconomy Green Ind Revolut 2017:233–70.

[5] Holtmann D, Harnisch F. Electrification of biotechnology: Quo Vadis? In: Harnisch F, Holtmann D, editors. Bioelectrosynthesis, Cham: Springer International Publishing; 2019, p. 395–411. https://doi.org/10.1007/10_2018_75.

[6] Schröder U, Harnisch F, Angenent LT. Microbial electrochemistry and technology: terminology and classification. Energy Environ Sci 2015;8:513–9. https://doi.org/10.1039/C4EE03359K.

[7] Anastas PT, Warner JC. Principles of green chemistry. Green Chem Theory Pract 1998;29:14821–42.

[8] Krieg T, Hüttmann S, Mangold K-M, Schrader J, Holtmann D. Gas diffusion electrode as novel reaction system for an electro-enzymatic process with chloroperoxidase. Green Chem 2011;13:2686–9. https://doi.org/10.1039/C1GC15391A.

[9] Schmitz LM, Rosenthal K, Lütz S. Enzyme-based electrobiotechnological synthesis. In: Harnisch F, Holtmann D, editors. Bioelectrosynthesis, vol. 167, Cham: Springer International Publishing; 2017, p. 87–134. https://doi.org/10.1007/10_2017_33.

[10] Jüttner K. Technical scale of electrochemistry. In: Bard AJ, editor. Encycl. Electrochem. 1st ed., Wiley; 2007. https://doi.org/10.1002/9783527610426.bard050001.

[11] Matthews MA. Green electrochemistry. Examples and challenges. Pure Appl Chem 2001;73:1305–8.

[12] Halan B, Tschörtner J, Schmid A. Generating electric current by bioartificial photosynthesis. Bioelectrosynthesis 2019:361–93.

[13] Herzog J, Mook A, Guhl L, Bäumler M, Beck MH, Weuster-Botz D, et al. Novel synthetic co-culture of *Acetobacterium woodii* and *Clostridium drakei* using CO_2 and *in situ* generated H_2 for the production of caproic acid via lactic acid. Eng Life Sci 2022;23:e2100169. https://doi.org/10.1002/elsc.202100169.

[14] Hiegemann H, Herzer D, Nettmann E, Lübken M, Schulte P, Schmelz K-G, et al. An integrated 45 L pilot microbial fuel cell system at a full-scale wastewater treatment plant. Bioresour Technol 2016;218:115–22.

[15] Anthony PF, Turner APF. Biosensors: Sense and sensibility. Chem Soc Rev 2013;42:3184–96.

[16] Lütz S, Steckhan E, Liese A. First asymmetric electroenzymatic oxidation catalyzed by a peroxidase. Electrochem Commun 2004;6:583–7. https://doi.org/10.1016/j.elecom.2004.04.009.

[17] Schröder I, Steckhan E, Liese A. *In situ* NAD+ regeneration using 2, 2′-azinobis (3-ethylbenzothiazoline-6-sulfonate) as an electron transfer mediator. J Electroanal Chem 2003;541:109–15.

[18] Kerzenmacher S. Engineering of microbial electrodes. In: Harnisch F, Holtmann D, editors. Bioelectrosynthesis, Cham: Springer International Publishing; 2019, p. 135–80. https://doi.org/10.1007/10_2017_16.

[19] Chidambara Raj CB, Li Quen H. Advanced oxidation processes for wastewater treatment: Optimization of UV/H_2O_2 process through a statistical technique. Chem Eng Sci 2005;60:5305–11. https://doi.org/10.1016/j.ces.2005.03.065.

[20] A. Camblor M, Corma A, Martínez A, Pérez-Pariente J. Synthesis of a titaniumsilicoaluminate isomorphous to zeolite beta and its application as a catalyst for the selective oxidation of large organic molecules. J Chem Soc Chem Commun 1992;0:589–90. https://doi.org/10.1039/C39920000589.

[21] Clerici MG, Ingallina P. Epoxidation of lower olefins with hydrogen peroxide and titanium silicalite. J Catal 1993;140:71–83. https://doi.org/10.1006/jcat.1993.1069.

[22] Kosaka K, Yamada H, Shishida K, Echigo S, Minear RA, Tsuno H, et al. Evaluation of the treatment performance of a multistage ozone/hydrogen peroxide process by decomposition by-products. Water Res 2001;35:3587–94. https://doi.org/10.1016/S0043-1354(01)00087-2.

[23] Hsiao YL, Nobe K. Oxidative reactions of phenol and chlorobenzene with in situ electrogenerated Fenton's reagent. Chem Eng Commun 1993;126:97–110. https://doi.org/10.1080/00986449308936212.

[24] Li H, Quispe-Cardenas E, Yang S, Yin L, Yang Y. Electrosynthesis of >20 g/L H_2O2 from air. ACS EST Eng 2022;2:242–50. https://doi.org/10.1021/acsestengg.1c00366.

[25] Campos-Martin JM, Blanco-Brieva G, Fierro JL. Hydrogen peroxide synthesis: an outlook beyond the anthraquinone process. Angew Chem Int Ed 2006;45:6962–84.

[26] Pan Z, Wang K, Wang Y, Tsiakaras P, Song S. *In-situ* electrosynthesis of hydrogen peroxide and wastewater treatment application: A novel strategy for graphite felt activation. Appl Catal B Environ 2018;237:392–400. https://doi.org/10.1016/j.apcatb.2018.05.079.

[27] Wiley-VCH, editor. Ullmann's Encyclopedia of Industrial Chemistry. 1st ed. Wiley; 2003. https://doi.org/10.1002/14356007.

[28] Edwards JK, Hutchings GJ. Palladium and gold–palladium catalysts for the direct synthesis of hydrogen peroxide. Angew Chem Int Ed 2008;47:9192–8. https://doi.org/10.1002/anie.200802818.

[29] Palmer MJ, Musker AJ, Roberts GT, Ponce de Leon Albarran CA. A method of ranking candidate catalyst for the decomposition of hydrogen peroxide, 2010.

[30] Burek BO, Bormann S, Hollmann F, Bloh JZ, Holtmann D. Hydrogen peroxide driven biocatalysis. Green Chem 2019;21:3232–49. https://doi.org/10.1039/C9GC00633H.

[31] Peter S, Kinne M, Ullrich R, Kayser G, Hofrichter M. Epoxidation of linear, branched and cyclic alkenes catalyzed by unspecific peroxygenase. Enzyme Microb Technol 2013;52:370–6. https://doi.org/10.1016/j.enzmictec.2013.02.013.

[32] Wise CE, Hsieh CH, Poplin NL, Makris TM. Dioxygen activation by the biofuel-generating cytochrome P450 OleT. ACS Catal 2018;8:9342–52. https://doi.org/10.1021/acscatal.8b02631.

[33] Karich A, Kluge M, Ullrich R, Hofrichter M. Benzene oxygenation and oxidation by the peroxygenase of *Agrocybe aegerita*. AMB Express 2013;3:5. https://doi.org/10.1186/2191-0855-3-5.

[34] Park J-B, Clark DS. Deactivation mechanisms of chloroperoxidase during biotransformations. Biotechnol Bioeng 2006;93:1190–5. https://doi.org/10.1002/bit.20825.

[35] Ullrich R, Nüske J, Scheibner K, Spantzel J, Hofrichter M. Novel haloperoxidase from the agaric basidiomycete *Agrocybe aegerita* oxidizes aryl alcohols and aldehydes. Appl Environ Microbiol 2004;70:4575–81.

[36] Karich A, Scheibner K, Ullrich R, Hofrichter M. Exploring the catalase activity of unspecific peroxygenases and the mechanism of peroxide-dependent heme destruction. J Mol Catal B Enzym 2016;134:238–46. https://doi.org/10.1016/j.molcatb.2016.10.014.

[37] Hofrichter M, Kellner H, Pecyna MJ, Ullrich R. Fungal unspecific peroxygenases: Heme-thiolate proteins that combine peroxidase and cytochrome P450 properties. In: Hrycay EG, Bandiera SM, editors. Monooxygenase Peroxidase Peroxygenase Prop. Mech. Cytochrome P450, vol. 851, Cham: Springer International Publishing; 2015, p. 341–68. https://doi.org/10.1007/978-3-319-16009-2_13.

[38] Hofrichter M, Ullrich R. Oxidations catalyzed by fungal peroxygenases. Curr Opin Chem Biol 2014;19:116–25. https://doi.org/10.1016/j.cbpa.2014.01.015.

[39] Godula K, Sames D. C-H bond functionalization in complex organic synthesis. Science 2006;312:67–72. https://doi.org/10.1126/science.1114731.

[40] Molina-Espeja P, Ma S, Mate DM, Ludwig R, Alcalde M. Tandem-yeast expression system for engineering and producing unspecific peroxygenase. Enzyme Microb Technol 2015;73–74:29–33. https://doi.org/10.1016/j.enzmictec.2015.03.004.

[41] Bernhardt R. Cytochromes P450 as versatile biocatalysts. J Biotechnol 2006;124:128–45. https://doi.org/10.1016/j.jbiotec.2006.01.026.

[42] van de Velde F, van Rantwijk F, Sheldon RA. Selective oxidations with molecular oxygen, catalyzed by chloroperoxidase in the presence of a reductant. J Mol Catal B Enzym 1999;6:453–61. https://doi.org/10.1016/S1381-1169(99)00059-X.

[43] Ni Y, Fernández-Fueyo E, Baraibar AG, Ullrich R, Hofrichter M, Yanase H, et al. Peroxygenase-catalyzed oxyfunctionalization reactions promoted by the complete oxidation of methanol. Angew Chem Int Ed 2016;55:798–801. https://doi.org/10.1002/anie.201507881.

[44] van de Velde F, Lourenço ND, Bakker M, van Rantwijk F, Sheldon RA. Improved operational stability of peroxidases by coimmobilization with glucose oxidase. Biotechnol Bioeng 2000;69:286–91. https://doi.org/10.1002/1097-0290(20000805)69:3<286::AID-BIT6>3.0.CO;2-R.

[45] Yoon J, Kim J, Tieves F, Zhang W, Alcalde M, Hollmann F, et al. Piezobiocatalysis: Ultrasound-driven enzymatic oxyfunctionalization of C–H bonds. ACS Catal 2020;10:5236–42. https://doi.org/10.1021/acscatal.0c00188.

[46] Kohlmann C, Lütz S. Electroenzymatic synthesis of chiral sulfoxides. Eng Life Sci 2006;6:170–4. https://doi.org/10.1002/elsc.200620907.

[47] Bormann S, Baraibar AG, Ni Y, Holtmann D, Hollmann F. Specific oxyfunctionalisations catalysed by peroxygenases: opportunities, challenges and solutions. Catal Sci Technol 2015;5:2038–52. https://doi.org/10.1039/C4CY01477D.

[48] Perry SC, Pangotra D, Vieira L, Csepei L-I, Sieber V, Wang L, et al. Electrochemical synthesis of hydrogen peroxide from water and oxygen. Nat Rev Chem 2019;3:442–58.

[49] Tanev PT, Chibwe M, Pinnavaia TJ. Titanium-containing mesoporous molecular sieves for catalytic oxidation of aromatic compounds. Nature 1994;368:321–3.

[50] Yamanaka I, Murayama T. Neutral H_2O_2 synthesis by electrolysis of water and O_2. Angew Chem 2008;120:1926–8.

[51] Hage R, Lienke A. Applications of transition-metal catalysts to textile and wood-pulp bleaching. Angew Chem Int Ed 2006;45:206–22. https://doi.org/10.1002/anie.200500525.

[52] Goor G. Hydrogen peroxide: Manufacture and industrial use for production of organic chemicals. In: Strukul G, editor. Catal. Oxid. Hydrog. Peroxide Oxid., Dordrecht: Springer Netherlands; 1992, p. 13–43. https://doi.org/10.1007/978-94-017-0984-2_2.

[53] Kirk RE, Othmer DF. Kirk-Othmer encyclopedia of chemical technology. Wiley; 1978.

[54] Choi CH, Kwon HC, Yook S, Shin H, Kim H, Choi M. Hydrogen peroxide synthesis via enhanced two-electron oxygen reduction pathway on carbon-coated Pt surface. J Phys Chem C 2014;118:30063–70. https://doi.org/10.1021/jp5113894.

[55] Zhou J, Guo H, Wang X, Guo M, Zhao J, Chen L, et al. Direct and continuous synthesis of concentrated hydrogen peroxide by the gaseous reaction of H_2/ O_2 non-equilibrium plasma. Chem Commun 2005;0:1631–3. https://doi.org/10.1039/B416835F.

[56] Zhao J, Zhou J, Su J, Guo H, Wang X, Gong W. Propene epoxidation with *in-site* H_2O_2 produced by H_2/ O_2 non-equilibrium plasma. AIChE J 2007;53:3204–9. https://doi.org/10.1002/aic.11317.

[57] Choudhary VR, Sansare SD, Gaikwad AG. Direct oxidation of H_2 to H_2O_2 and decomposition of H_2O_2 over oxidized and reduced Pd-containing zeolite catalysts in acidic medium. Catal Lett 2002;84:81–7. https://doi.org/10.1023/A:1021032819400.

[58] Burch R, Ellis PR. An investigation of alternative catalytic approaches for the direct synthesis of hydrogen peroxide from hydrogen and oxygen. Appl Catal B Environ 2003;42:203–11.

[59] Landon P, J. Collier P, J. Papworth A, J. Kiely C, J. Hutchings G. Direct formation of hydrogen peroxide from H_2/ O_2 using a gold catalyst. Chem Commun 2002;0:2058–9. https://doi.org/10.1039/B205248M.

[60] Landon P, J. Collier P, F. Carley A, Chadwick D, J. Papworth A, Burrows A, et al. Direct synthesis of hydrogen peroxide from H_2 and O_2 using Pd and Au catalysts. Phys Chem Chem Phys 2003;5:1917–23. https://doi.org/10.1039/B211338B.

[61] Choudhary VR, Samanta C. Role of chloride or bromide anions and protons for promoting the selective oxidation of H_2 by O_2 to H_2O_2 over supported Pd catalysts in an aqueous medium. J Catal 2006;238:28–38.

[62] Liu Y, Quan X, Fan X, Wang H, Chen S. High-yield electrosynthesis of hydrogen peroxide from oxygen reduction by hierarchically porous carbon. Angew Chem 2015;127:6941–5. https://doi.org/10.1002/ange.201502396.

[63] Samanta C. Direct synthesis of hydrogen peroxide from hydrogen and oxygen: An overview of recent developments in the process. Appl Catal Gen 2008;350:133–49. https://doi.org/10.1016/j.apcata.2008.07.043.

[64] Cassidy KD. Electrosynthesis of hydrogen peroxide in an acidic environment with RuO_2 as a water oxidation catalyst; Silver nanoparticles in zeolite Y: Surface enhanced raman spectroscopic (SERS) studies. The Ohio State University, 2010.

[65] Jones CW. Applications of hydrogen peroxide and derivatives. Royal Society of Chemistry; 1999.

[66] Burek BO, de Boer SR, Tieves F, Zhang W, van Schie M, Bormann S, et al. Photoenzymatic hydroxylation of ethylbenzene catalyzed by unspecific peroxygenase: Origin of enzyme inactivation and the impact of light intensity and temperature. ChemCatChem 2019;11:3093–100. https://doi.org/10.1002/cctc.201900610.

[67] Deurzen MPJV, Seelbach K, Rantwijk F van, Kragl U, Sheldon RA. Chloroperoxidase: Use of a hydrogen peroxide-stat for controlling reactions and improving enzyme performance. Biocatal Biotransformation 1997. https://doi.org/10.3109/10242429709003606.

[68] van Deurzen MPJ, Remkes IJ, van Rantwijk F, Sheldon RA. Chloroperoxidase catalyzed oxidations in *t*-butyl alcohol/water mixtures. J Mol Catal Chem 1997;117:329–37. https://doi.org/10.1016/S1381-1169(96)00259-2.

[69] Grey CE, Rundbäck F, Adlercreutz P. Improved operational stability of chloroperoxidase through use of antioxidants. J Biotechnol 2008;135:196–201. https://doi.org/10.1016/j.jbiotec.2008.03.015.

[70] Santhanam L, Dordick JS. Chloroperoxidase-catalyzed epoxidation of styrene in aqueous and nonaqueous media. Biocatal Biotransformation 2002;20:265–74. https://doi.org/10.1080/10242420290029481.

[71] Holtmann D, Krieg T, Getrey L, Schrader J. Electroenzymatic process to overcome enzyme instabilities. Catal Commun 2014;51:82–5.

[72] I. Perez D, Mifsud Grau M, E. Arends IWC, Hollmann F. Visible light-driven and chloroperoxidase-catalyzed oxygenation reactions. Chem Commun 2009;0:6848–50. https://doi.org/10.1039/B915078A.

[73] Okrasa K, Falcimaigne A, Guibé-Jampel E, Therisod M. Enantioselective synthesis of sulfoxides catalysed by an oxidase–peroxidase bienzymatic system. Tetrahedron Asymmetry 2002;13:519–22. https://doi.org/10.1016/S0957-4166(02)00142-8.

[74] van Rantwijk F, Sheldon RA. Selective oxygen transfer catalysed by heme peroxidases: synthetic and mechanistic aspects. Curr Opin Biotechnol 2000;11:554–64. https://doi.org/10.1016/S0958-1669(00)00143-9.

[75] A. Sheldon R. E factors, green chemistry and catalysis: An odyssey. Chem Commun 2008;0:3352–65. https://doi.org/10.1039/B803584A.

[76] Churakova E, Kluge M, Ullrich R, Arends I, Hofrichter M, Hollmann F. Specific photobiocatalytic oxyfunctionalization reactions. Angew Chem 2011;123:10904–7. https://doi.org/10.1002/ange.201105308.

[77] Churakova E, Arends IWCE, Hollmann F. Increasing the productivity of peroxidase-catalyzed oxyfunctionalization: A Case study on the potential of two-liquid-phase systems. ChemCatChem 2013;5:565–8. https://doi.org/10.1002/cctc.201200490.

[78] Águila S, Vazquez-Duhalt R, Tinoco R, Rivera M, Pecchi G, Alderete JB. Stereoselective oxidation of R-(+)-limonene by chloroperoxidase from *Caldariomyces fumago*. Green Chem 2008;10:647. https://doi.org/10.1039/b719992a.

[79] Paul CE, Churakova E, Maurits E, Girhard M, Urlacher VB, Hollmann F. *In situ* formation of H_2O_2 for P450 peroxygenases. Bioorg Med Chem 2014;22:5692–6. https://doi.org/10.1016/j.bmc.2014.05.074.

[80] Hollmann F, Schmid A. Towards [Cp∗Rh(bpy)(H_2O)]2^+-promoted P450 catalysis: Direct regeneration of CytC. J Inorg Biochem 2009;103:313–5. https://doi.org/10.1016/j.jinorgbio.2008.11.005.

[81] Traube M. Ueber die elektrolytische Entstehung des Wasserstoffhyperoxyds an der Anode. Berichte Dtsch Chem Ges 1887;20:3345–51. https://doi.org/10.1002/cber.188702002250.

[82] Giomo M, Buso A, Fier P, Sandonà G, Boye B, Farnia G. A small-scale pilot plant using an oxygen-reducing gas-diffusion electrode for hydrogen peroxide electrosynthesis. Electrochimica Acta 2008;54:808–15. https://doi.org/10.1016/j.electacta.2008.06.038.

[83] Song C, Zhang J. Electrocatalytic oxygen reduction reaction. In: Zhang J, editor. PEM Fuel Cell Electrocatalysts Catal. Layers Fundam. Appl., London: Springer; 2008, p. 89–134. https://doi.org/10.1007/978-1-84800-936-3_2.

[84] Peralta E, Natividad R, Roa G, Marin R, Romero R, Pavon T. A comparative study on the electrochemical production of H_2O_2 between BDD and graphite cathodes. Sustain Environ Res 2013;23:259–66.

[85] Khataee AR, Safarpour M, Zarei M, Aber S. Electrochemical generation of H_2O_2 using immobilized carbon nanotubes on graphite electrode fed with air: Investigation of operational parameters. J Electroanal Chem 2011;659:63–8. https://doi.org/10.1016/j.jelechem.2011.05.002.

[86] Murayama T, Yamanaka I. Electrosynthesis of neutral H_2O_2 solution from O_2 and water at a mixed carbon cathode using an exposed solid-polymer-electrolyte electrolysis cell. J Phys Chem C 2011;115:5792–9.

[87] Zhou M, Yu Q, Lei L. The preparation and characterization of a graphite–PTFE cathode system for the decolorization of C.I. Acid Red 2. Dyes Pigments 2008;77:129–36. https://doi.org/10.1016/j.dyepig.2007.04.002.

[88] Qiang Z, Chang J-H, Huang C-P. Electrochemical generation of hydrogen peroxide from dissolved oxygen in acidic solutions. Water Res 2002;36:85–94.

[89] Jirkovský JS, Panas I, Ahlberg E, Halasa M, Romani S, Schiffrin DJ. Single atom hot-spots at Au–Pd nanoalloys for electrocatalytic H_2O_2 production. J Am Chem Soc 2011;133:19432–41. https://doi.org/10.1021/ja206477z.

[90] Pinheiro VS, Paz EC, Aveiro LR, Parreira LS, Souza FM, Camargo PHC, et al. Ceria high aspect ratio nanostructures supported on carbon for hydrogen peroxide electrogeneration. Electrochimica Acta 2018;259:865–72. https://doi.org/10.1016/j.electacta.2017.11.010.

[91] Sánchez-Sánchez CM, Bard AJ. Hydrogen peroxide production in the oxygen reduction reaction at different electrocatalysts as quantified by scanning electrochemical microscopy. Anal Chem 2009;81:8094–100. https://doi.org/10.1021/ac901291v.

[92] Pletcher D, Sotiropoulos S. A study of cathodic oxygen reduction at platinum using microelectrodes. J Electroanal Chem 1993;356:109–19. https://doi.org/10.1016/0022-0728(93)80514-I.

[93] Chen S, Kucernak A. Electrocatalysis under conditions of high mass transport rate: Oxygen reduction on single submicrometer-sized Pt particles supported on carbon. J Phys Chem B 2004;108:3262–76. https://doi.org/10.1021/jp036831j.

[94] Félix-Navarro RM, Beltrán-Gastélum M, Salazar-Gastélum MI, Silva-Carrillo C, Reynoso-Soto EA, Pérez-Sicairos S, et al. Pt–Pd bimetallic nanoparticles on MWCNTs: Catalyst for hydrogen peroxide electrosynthesis. J Nanoparticle Res 2013;15:1802. https://doi.org/10.1007/s11051-013-1802-3.

[95] Antonin VS, Parreira LS, Aveiro LR, Silva FL, Valim RB, Hammer P, et al. W@Au nanostructures modifying carbon as materials for hydrogen peroxide electrogeneration. Electrochimica Acta 2017;231:713–20. https://doi.org/10.1016/j.electacta.2017.01.192.

[96] Siahrostami S, Verdaguer-Casadevall A, Karamad M, Deiana D, Malacrida P, Wickman B, et al. Enabling direct H_2O_2 production through rational electrocatalyst design. Nat Mater 2013;12:1137–43. https://doi.org/10.1038/nmat3795.

[97] Marković NM, Adić RR, Vešović VB. Structural effects in electrocatalysis: Oxygen reduction on the gold single crystal electrodes with (110) and (111) orientations. J Electroanal Chem Interfacial Electrochem 1984;165:121–33. https://doi.org/10.1016/S0022-0728(84)80091-1.

[98] Pozzo AD, Palma LD, Merli C, Petrucci E. An experimental comparison of a graphite electrode and a gas diffusion electrode for the cathodic production of hydrogen peroxide. J Appl Electrochem 2005;35:413–9. https://doi.org/10.1007/s10800-005-0800-2.

[99] Wang S, Zhang L, Xia Z, Roy A, Chang DW, Baek J-B, et al. BCN graphene as efficient metal-free electrocatalyst for the oxygen reduction reaction. Angew Chem Int Ed 2012;51:4209–12.

[100] Hasanzadeh A, Khataee A, Zarei M, Zhang Y. Two-electron oxygen reduction on fullerene C60-carbon nanotubes covalent hybrid as a metal-free electrocatalyst. Sci Rep 2019;9:13780.

[101] Park J, Nabae Y, Hayakawa T, Kakimoto M. Highly selective two-electron oxygen reduction catalyzed by mesoporous nitrogen-doped carbon. ACS Catal 2014;4:3749–54. https://doi.org/10.1021/cs5008206.

[102] Gong K, Du F, Xia Z, Durstock M, Dai L. Nitrogen-doped carbon nanotube arrays with high electrocatalytic activity for oxygen reduction. Science 2009;323:760–4. https://doi.org/10.1126/science.1168049.

[103] Lütz S, Vuorilehto K, Liese A. Process development for the electroenzymatic synthesis of (*R*)-methylphenylsulfoxide by use of a 3-dimensional electrode. Biotechnol Bioeng 2007;98:525–34. https://doi.org/10.1002/bit.21434.

[104] Horst AEW, Bormann S, Meyer J, Steinhagen M, Ludwig R, Drews A, et al. Electro-enzymatic hydroxylation of ethylbenzene by the evolved unspecific peroxygenase of *Agrocybe aegerita*. J Mol Catal B Enzym 2016;133:S137–42. https://doi.org/10.1016/j.molcatb.2016.12.008.

[105] Bormann S, van Schie MM, De Almeida TP, Zhang W, Stöckl M, Ulber R, et al. H_2O_2 production at low overpotentials for electroenzymatic halogenation reactions. ChemSusChem 2019;12:4759–63.

[106] Bormann S, Hertweck D, Schneider S, Bloh JZ, Ulber R, Spiess AC, et al. Modeling and simulation-based design of electroenzymatic batch processes catalyzed by unspecific peroxygenase from *A. aegerita*. Biotechnol Bioeng 2021;118:7–16.

[107] Abt M, Franzreb M, Jestädt M, Tschöpe A. Three-phase fluidized bed electrochemical reactor for the scalable generation of hydrogen peroxide at enzyme compatible conditions. Chem Eng J 2023;476:146465. https://doi.org/10.1016/j.cej.2023.146465.

[108] Krieg T, Madjarov J, Rosa LFM, Enzmann F, Harnisch F, Holtmann D, et al. Reactors for microbial electrobiotechnology. In: Harnisch F, Holtmann D, editors. Bioelectrosynthesis, vol. 167, Cham: Springer International Publishing; 2018, p. 231–71. https://doi.org/10.1007/10_2017_40.

[109] Logan BE. Scaling up microbial fuel cells and other bioelectrochemical systems. Appl Microbiol Biotechnol 2010;85:1665–71. https://doi.org/10.1007/s00253-009-2378-9.

[110] Hu H, Fan Y, Liu H. Hydrogen production using single-chamber membrane-free microbial electrolysis cells. Water Res 2008;42:4172–8. https://doi.org/10.1016/j.watres.2008.06.015.

[111] Stöckl M, Lange T, Izadi P, Bolat S, Teetz N, Harnisch F, et al. Application of gas diffusion electrodes in bioeconomy–an update. Biotechnol Bioeng 2023.

[112] Horst AEW, Mangold K-M, Holtmann D. Application of gas diffusion electrodes in bioelectrochemical syntheses and energy conversion. Biotechnol Bioeng 2016;113:260–7. https://doi.org/10.1002/bit.25698.

[113] Stöckl M, Lange T, Izadi P, Bolat S, Teetz N, Harnisch F, et al. Application of gas diffusion electrodes in bioeconomy: An update. Biotechnol Bioeng n.d.;n/a. https://doi.org/10.1002/bit.28383.

[114] Arbter P, Sabra W, Utesch T, Hong Y, Zeng A-P. Metabolomic and kinetic investigations on the electricity-aided production of butanol by *Clostridium pasteurianum* strains. Eng Life Sci 2021;21:181–95.

[115] Utesch T, Zeng A-P. A novel All-in-One electrolysis electrode and bioreactor enable better study of electrochemical effects and electricity-aided bioprocesses. Eng Life Sci 2018;18:600–10.

[116] Kluge M, Ullrich R, Scheibner K, Hofrichter M. Stereoselective benzylic hydroxylation of alkylbenzenes and epoxidation of styrene derivatives catalyzed by the peroxygenase of *Agrocybe aegerita*. Green Chem 2012;14:440–6. https://doi.org/10.1039/C1GC16173C.

[117] Sayoga G, Abt M, Teetz N, Bueschler V, Liese A, Franzreb M, et al. Quantitative and non-quantitative assessments of enzymatic electrosynthesis: A case study of parameter requirements. ChemElectroChem 2023;10:e202300226. https://doi.org/10.1002/celc.202300226.

[118] Sayoga GV, Bueschler VS, Beisch H, Holtmann D, Zeng A-P, Fiedler B, et al. Application of the all-in-one electrode for *in situ* H_2O_2 generation in hydroxylation catalyzed by unspecific peroxygenase from *Agrocybe aegerita*. Mol Catal 2023;547:113325. https://doi.org/10.1016/j.mcat.2023.113325.

[119] Sayoga GV, Bueschler VS, Beisch H, Utesch T, Holtmann D, Fiedler B, et al. Electrochemical H_2O_2-stat mode as reaction concept to improve the process performance of an unspecific peroxygenase. New Biotechnol 2023;78:95–104. https://doi.org/10.1016/j.nbt.2023.10.007.

[120] Poojary M, Roohinejad S, Koubaa M, Barba F, Passamonti P, Jambrak AR, et al. Impact of pulsed electric fields on enzymes 2016.

[121] Bormann S, Burek BO, Ulber R, Holtmann D. Immobilization of unspecific peroxygenase expressed in *Pichia pastoris* by metal affinity binding. Mol Catal 2020;492:110999. https://doi.org/10.1016/j.mcat.2020.110999.

[122] Garcia-Ochoa F, Gomez E. Oxygen transfer rate determination: Chemical, physical and biological methods. Encycl. Ind. Biotechnol. 1st ed., Wiley; 2010, p. 1–21. https://doi.org/10.1002/9780470054581.eib467.

[123] Seelbach K, van Deurzen MPJ, van Rantwijk F, Sheldon RA, Kragl U. Improvement of the total turnover number and space-time yield for chloroperoxidase catalyzed oxidation. Biotechnol Bioeng 1997;55:283–8. https://doi.org/10.1002/(SICI)1097-0290(19970720)55:2<283::AID-BIT6>3.0.CO;2-E.

[124] Kipf E, Koch J, Geiger B, Erben J, Richter K, Gescher J, et al. Systematic screening of carbon-based anode materials for microbial fuel cells with *Shewanella oneidensis* MR-1. Bioresour Technol 2013;146:386–92. https://doi.org/10.1016/j.biortech.2013.07.076.

[125] Knoll MT, Fuderer E, Gescher J. Sprayable biofilm – Agarose hydrogels as 3D matrix for enhanced productivity in bioelectrochemical systems. Biofilm 2022;4:100077. https://doi.org/10.1016/j.bioflm.2022.100077.

[126] Jung S, L. McCrory CC, M. Ferrer I, C. Peters J, F. Jaramillo T. Benchmarking nanoparticulate metal oxide electrocatalysts for the alkaline water oxidation reaction. J Mater Chem A 2016;4:3068–76. https://doi.org/10.1039/C5TA07586F.

[127] Lu Z, Chen G, Siahrostami S, Chen Z, Liu K, Xie J, et al. High-efficiency oxygen reduction to hydrogen peroxide catalysed by oxidized carbon materials. Nat Catal 2018;1:156–62. https://doi.org/10.1038/s41929-017-0017-x.

[128] Pérez JF, Galia A, Rodrigo MA, Llanos J, Sabatino S, Sáez C, et al. Effect of pressure on the electrochemical generation of hydrogen peroxide in undivided cells on carbon felt electrodes. Electrochimica Acta 2017;248:169–77. https://doi.org/10.1016/j.electacta.2017.07.116.

[129] Büscher N, Sayoga GV, Rübsam K, Jakob F, Schwaneberg U, Kara S, et al. Biocatalyst immobilization by anchor peptides on an additively manufacturable material. Org Process Res Dev 2019;23:1852–9. https://doi.org/10.1021/acs.oprd.9b00152.

[130] Iglesias D, Giuliani A, Melchionna M, Marchesan S, Criado A, Nasi L, et al. N-doped graphitized carbon nanohorns as a forefront electrocatalyst in highly selective O_2 reduction to H_2O_2. Chem 2018;4:106–23.

[131] Beisch H, Fiedler B. Nanocarbon aerogels and aerographite. Synth. Appl. Nanocarbons, John Wiley & Sons, Ltd; 2020, p. 247–74. https://doi.org/10.1002/9781119429418.ch8.

[132] Brummund J, Müller M, Schmitges T, Kaluzna I, Mink D, Hilterhaus L, et al. Process development for oxidations of hydrophobic compounds applying cytochrome P450 monooxygenases *in-vitro*. J Biotechnol 2016;233:143–50. https://doi.org/10.1016/j.jbiotec.2016.07.002.

[133] Kluge MG, Ullrich R, Scheibner K, Hofrichter M. Spectrophotometric assay for detection of aromatic hydroxylation catalyzed by fungal haloperoxidase–peroxygenase. Appl Microbiol Biotechnol 2007;75:1473–8.

[134] Molina-Espeja P, Garcia-Ruiz E, Gonzalez-Perez D, Ullrich R, Hofrichter M, Alcalde M. Directed evolution of unspecific peroxygenase from *Agrocybe aegerita*. Appl Environ Microbiol 2014;80:3496–507.

[135] Wise WS. The measurement of the aeration of culture media. Microbiology 1951;5:167–77. https://doi.org/10.1099/00221287-5-1-167.

[136] Wapshott-Stehli HL, Grunden AM. *In situ* H_2O_2 generation methods in the context of enzyme biocatalysis. Enzyme Microb Technol 2021;145:109744. https://doi.org/10.1016/j.enzmictec.2021.109744.

[137] Kern S, Himmelspach A, Grammann K, Thum O, Liese A. Process characterization studies for solvent-free simultaneous epoxidation and transesterification of fatty acid methyl esters. Org Process Res Dev 2016;20:1930–6. https://doi.org/10.1021/acs.oprd.6b00254.

[138] Zhou P, Zhang J, Zhang Y, Liu Y, Liang J, Liu B, et al. Generation of hydrogen peroxide and hydroxyl radical resulting from oxygen-dependent oxidation of *L*-ascorbic acid via copper redox-catalyzed reactions. RSC Adv 2016;6:38541–7. https://doi.org/10.1039/C6RA02843H.

[139] Arbter P, Sinha A, Troesch J, Utesch T, Zeng A-P. Redox governed electro-fermentation improves lipid production by the oleaginous yeast *Rhodosporidium toruloides*. Bioresour Technol 2019;294:122122. https://doi.org/10.1016/j.biortech.2019.122122.

[140] Watts P, Wiles C. Micro Reactors, Flow reactors and continuous flow synthesis. J Chem Res 2012;36:181–93. https://doi.org/10.3184/174751912X13311365798808.

[141] Baxendale IR. The integration of flow reactors into synthetic organic chemistry. J Chem Technol Biotechnol 2013;88:519–52. https://doi.org/10.1002/jctb.4012.

[142] Invitrogen. *Pichia* fermentation process guidelines 2002.

[143] Cino J. High-yield protein production from *Pichia pastoris* yeast: A protocol for benchtop fermentation. Am Biotechnol Lab 1999;17:10–3.

[144] Perz F, Bormann S, Ulber R, Alcalde M, Bubenheim P, Hollmann F, et al. Enzymatic oxidation of butane to 2-butanol in a bubble column. ChemCatChem 2020;12:3666–9.

[145] Perçin Z, Kursula L, Löfgren E, Byström E, Kexel F, Bubenheim P, et al. Intensification of a biocatalytic oxidation under fine bubble aeration in a rotating bed reactor. Biochem Eng J 2024;207:109333. https://doi.org/10.1016/j.bej.2024.109333.

[146] Kolyagin GA, Kornienko VL. Pilot laboratory electrolyzer for electrosynthesis of hydrogen peroxide in acid and alkaline solutions. Russ J Appl Chem 2011;84:68–71. https://doi.org/10.1134/S1070427211010113.

[147] Petrucci E, Da Pozzo A, Di Palma L. On the ability to electrogenerate hydrogen peroxide and to regenerate ferrous ions of three selected carbon-based cathodes for electro-Fenton processes. Chem Eng J 2016;283:750–8. https://doi.org/10.1016/j.cej.2015.08.030.

[148] Panizza M, Cerisola G. Electrochemical generation of H_2O_2 in low ionic strength media on gas diffusion cathode fed with air. Electrochimica Acta 2008;54:876–8.

[149] Sudoh M, Kitaguchi H, Koide K. Electrochemical production of hydrogen peroxide by reduction of oxygen. J Chem Eng Jpn 1985;18:409–14.

[150] Sun Y, Sinev I, Ju W, Bergmann A, Dresp S, Kühl S, et al. Efficient electrochemical hydrogen peroxide production from molecular oxygen on Nitrogen-doped mesoporous carbon catalysts. ACS Catal 2018;8:2844–56. https://doi.org/10.1021/acscatal.7b03464.

[151] Chen JK, Nobe K. Oxidation of dimethylaniline by horseradish peroxidase and electrogenerated peroxide: II . Immobilized enzyme studies. J Electrochem Soc 1993;140:304–8. https://doi.org/10.1149/1.2221042.

[152] Wang K, Zhu Z, Xu D, Li M, Yuan S, Wang H. Highly active and cheap graphite/ polytetrafluoroethylene composite coating cathodes for electrogeneration of hydrogen peroxide. Clean Technol Environ Policy 2022;24:2407–17. https://doi.org/10.1007/s10098-022-02323-z.

[153] Büscher N, Spille C, Kracht JK, Sayoga GV, Dawood AWH, Maiwald MI, et al. Countercurrently operated reactive extractor with an additively manufactured enzyme carrier structure. Org Process Res Dev 2020;24:1621–8. https://doi.org/10.1021/acs.oprd.0c00205.

11. Appendix

This section provides supporting information and additional results to strengthen the argument and key results shown in chapter **5** to **7**, as well as methods used to conduct experiments. The appendix for each chapter are separated in different subsection and titled as such. In addition, results (manuscript, submitted version) on the topic of the integration of the All-in-One electrode in an electrochemical flow cell is documented in subchapter **11.4**.

11.1. Supporting Information to Chapter 5

The materials utilized in the electroenzymatic experiments delineated in subchapter **5.1** were identical to those described in ***2.1. Materials*** (publication in chapter 6). Concurrently, the fermentation process of *P. pastoris* and the production process of his-tagged r*Aae*UPO were conducted in a manner analogous to that described in ***2.2. Production of his-tagged rAaeUPO*** (publication in chapter 6). Unless otherwise indicated, the analytical techniques utilized to quantify r*Aae*UPO activity and H_2O_2 concentration were consistent with those described in ***2.3.1. Determination of enzyme activity*** and ***2.3.2. Determination of H_2O_2 concentration*** (publication in chapter 6), respectively. Simultaneously, the electrochemical setup and the methodology employed in the electroenzymatic experiment were consistent with the procedures outlined in subsections ***2.5. Electrochemical setup*** and ***2.6. Electroenzymatic experiments*** (publication in chapter 6), correspondingly. However, a notable distinction was the utilization of 20 mM benzene as the substrate and 0.05 M citrate/ sodium phosphate pH 5 as the medium.

The following subsection will elaborate on the additional methods employed in the course of these experiments.

11.1.1. Determination of benzene, phenol, hydroquinone, resorcinol and catechol

The HPLC system, Shimadzu Nexera LC-40, with a UV-Vis SPD-40 detector and an Inertsil ODS-P, C18-RP, 5 µm, 100 Å column was employed. Within the reaction system utilizing benzene as the substrate, the intermediate phenol and the products hydroquinone, resorcinol, and catechol were identified and quantified. The specific measurement method for this reaction system is outlined in the table below (**Table S5. 1**). A 100 µL sample was extracted from the

reaction system and combined with 20 µL of a 10% v/v TFA solution. Subsequently, the samples were subjected to a centrifugation step at 4 °C and 13,000 rpm for 4 min. Finally, the supernatant was transferred into an HPLC vial and measured. The retention time of hydroquinone, resorcinol, catechol and phenol were 3.79 min, 6.88 min, 9.15 min and 11.75 min, respectively (**Fig. S5. 1**).

Table S5. 1. *HPLC parameter for the quantification of benzene, phenol, hydroquinone, resorcinol and catechol.*

HPLC system	Detector	Column	Mobile phase (A)	Mobile phase (B)	Gradient of B
Shimadzu Nexera LC-40	UV-Vis SPD-40 at 276 nm	Inertsil ODS-P, C18-RP, 5 µm, 100 Å, at 30 °C	H_2O (0.1% v/v TFA) at 0.7 mL min^{-1}	Acetonitrile (0.095% v/v TFA) at 0.7 mL min^{-1}	0-3 min: 5% 20 min: 100% 25 min: 100% 35 min: 5%

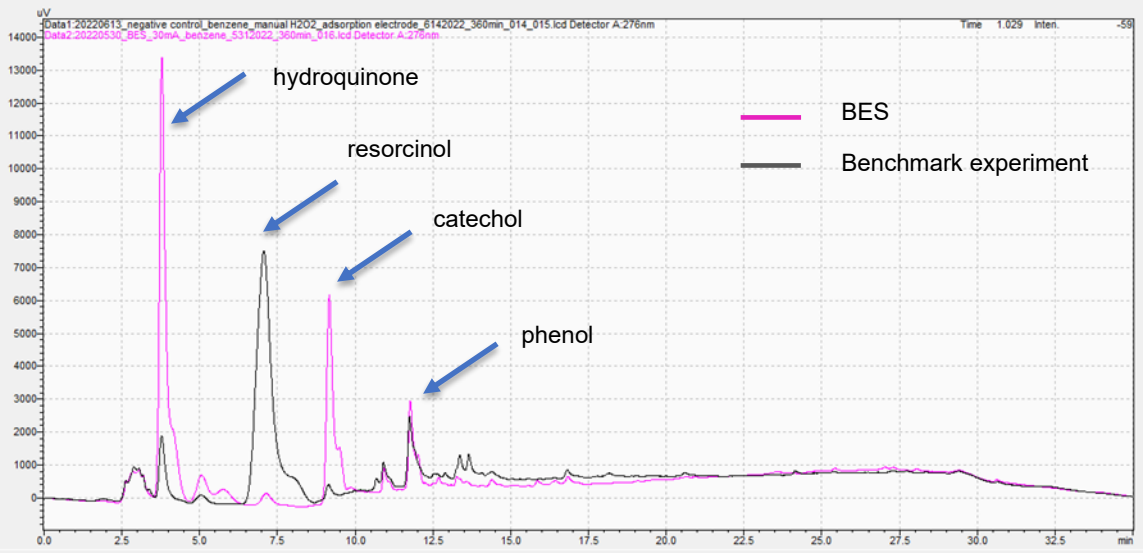

Fig. S5. 1. *Chromatogram from the experiment in the bioelectrochemical system (BES) (pink line) and from the benchmark experiment (manual addition of H_2O_2) with the carbon cloth electrode present in the medium (grey line), obtained after 360 min.*

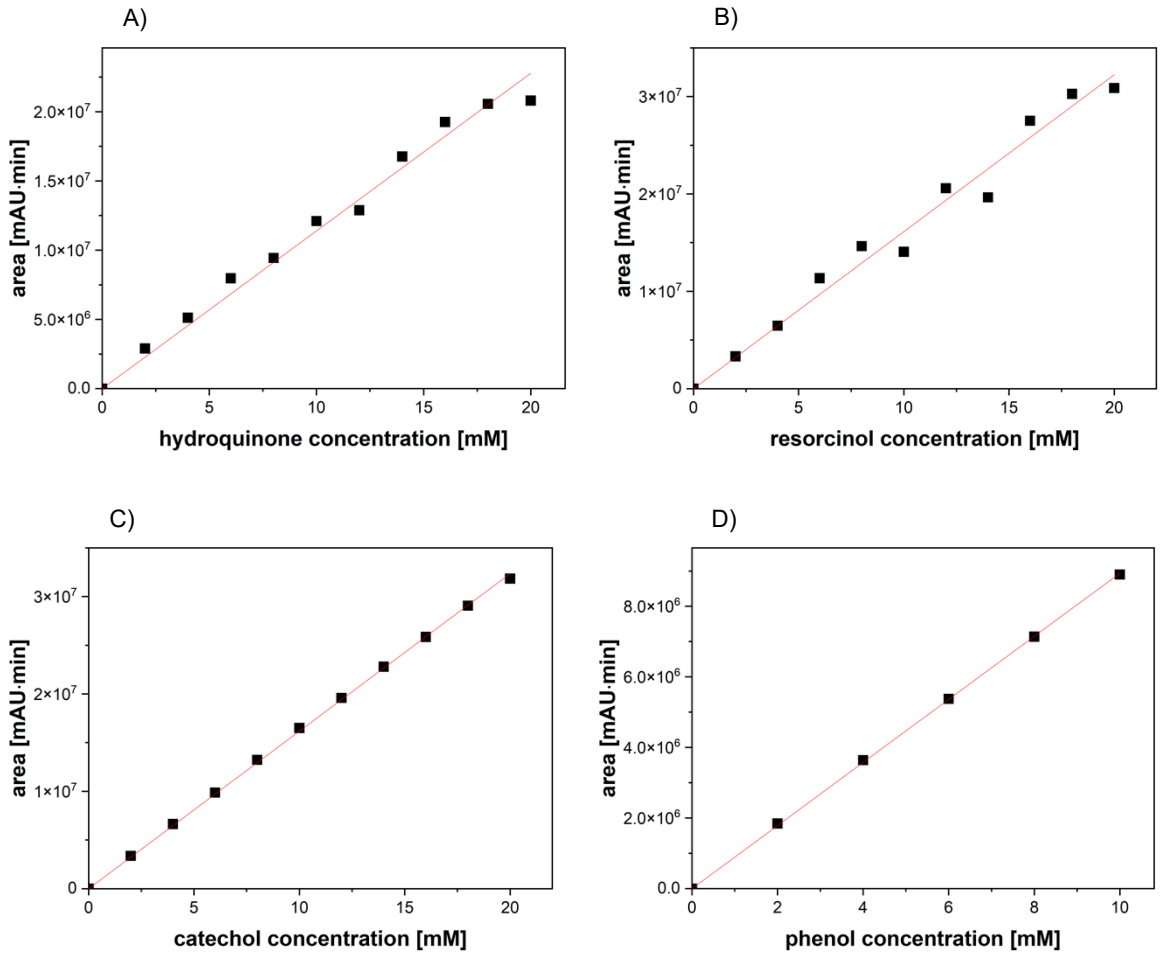

Fig. S5. 2. *Calibration curve of **A**) hydroquinone (y = 1139097.7 · x), **B**) resorcinol (y = 1612306.2 · x), **C**) catechol (y = 1617723.8 · x) and **D**) phenol (y = 893824.5 · x).*

11.1.2. Control experiment with manual feeding of H_2O_2

Instead of being generated *in situ* using the AiO electrode, liquid H_2O_2 (0.245 M) was pumped into the reactor. The medium (200 mL) consisted of 0.05 M citrate/ sodium phosphate buffer pH 5, 20 mM benzene, and 1 U_{ABTS} mL^{-1} (30 nM) r*Aae*UPO. The reaction was initiated by the addition of H_2O_2, with the concentration maintained between 100 and 300 µM. Samples for the analysis of product concentration were collected from the reactor, treated, and prepared according to the methodology outlined in section **11.1.1**. The H_2O_2 concentration was determined using QUANTOFIX Relax from Macherey Nagel, to ensure a quick measurement process.

11.2. Supporting Information to Chapter 6

The materials, analytical methods and electrochemical setup utilized in the electroenzymatic experiments delineated in subchapter **6.1** were identical to those described in the experimental part of the main publication in chapter 6. In the case of the experiment that utilized aeration, the original aeration of the DASGIP system was employed, with a diameter of 0.2 mm. Furthermore, the electroenzymatic experiments conducted with aeration were performed at an air flow rate of 1, 2, or 4 vvm, with all other reaction parameters held constant. In the multiple AiO electrodes system, two identical AiO electrodes were installed in the reactor, with each electrode controlled independently. The electrical current was set for each AiO electrode, resulting in an equal current density as obtained in the single electrode system.

The following subsection will elaborate on the additional methods employed in the course of these experiments.

11.2.1. Determination of oxygen productivity at the anode

The oxygen generation at the anode of the AiO electrode was determined in a 250 mL DASGIP reactor comprising of 200 mL 0.1 M KP_i pH 7 buffer. The anodic oxygen generation was conducted at an applied current between 10 mA and 60 mA, at 250 rpm and at a temperature of 22 ± 1 °C. To reduce the likelihood of oxygen reduction reaction during the oxygen generation at the anode (*A*: 4.24 cm^2), the carbon felt cathode was substituted with a titanium wire (*A*: 1.59 cm^2). The dissolved oxygen concentration in the medium was determined using an oxygen sensor (Mettler Toledo, InPro6860i, Ohio, United States of America). Prior to initiating the experiment, the medium was sparged with N_2 until no oxygen was detected by the sensor. The experiment was initiated by activating the power supply, and the subsequent increase in the oxygen concentration was monitored for a period of 5 min.

11.2.2. Determination of oxygen mass transfer coefficient (k_La) in the bioelectrochemical system with an aeration

The oxygen mass transfer coefficients (k_La) within the BES equipped with an aeration system were determined at an air flow rate between 1 vvm and 4 vvm and a stirring rate between 250 rpm and 1000 rpm via the gassing out method. Subsequent to sparging the medium with N_2 (until no oxygen was detected), the aeration was turned on and the dissolved oxygen

concentrations were quantified by an oxygen sensor. Each experiment was conducted for a period of 5 min, with the dissolved oxygen concentration (C_t) monitored at regular intervals. The theoretical maximum dissolved oxygen concentration (C^*) in a 0.1 M KP_i pH 7 buffer (15.6 g_{salt} kg_{water}^{-1} salinity) at an atmospheric pressure and at a temperature of 22 ± 1 °C is 245 µM. The k_La values were calculated from the slope of the difference in the natural logarithm of C* and Ct (ln (C^*-C_t)) over time [122,135].

11.2.3. Determination of superoxide and hydroxyl radical concentration

A nitro blue tetrazolium (NBT) assay and a terephthalic acid (TA) assay were employed to estimate the concentration of electrochemically generated superoxide and hydroxyl radicals, respectively [45]. The assay was prepared by dissolving either 20 µM NBT or 300 µM TA in 0.1 M KP_i pH 7 buffer. The electrochemical formation rate of the radicals was determined through an experiment conducted in manner similar to that described for the determination of H_2O_2 productivity. Samples were periodically collected from the medium and analyzed photometrically to quantify either the residual NBT concentration or the 2-hydroxyterephthalic acid (HTA) concentration, which is the product of the reaction between TA and hydroxyl radical. The superoxide concentration was calculated with the aid of the prepared calibration curves (**Fig. S6. 12**), via the converted NBT concentration (measured at 259 nm). The hydroxyl radical concentration was calculated via the formation of the HTA, which was measured at excitation wavelength of 315 nm and emission wavelength of 430 nm (Infinite M Nano+, Tecan, Männedorf, Switzerland).

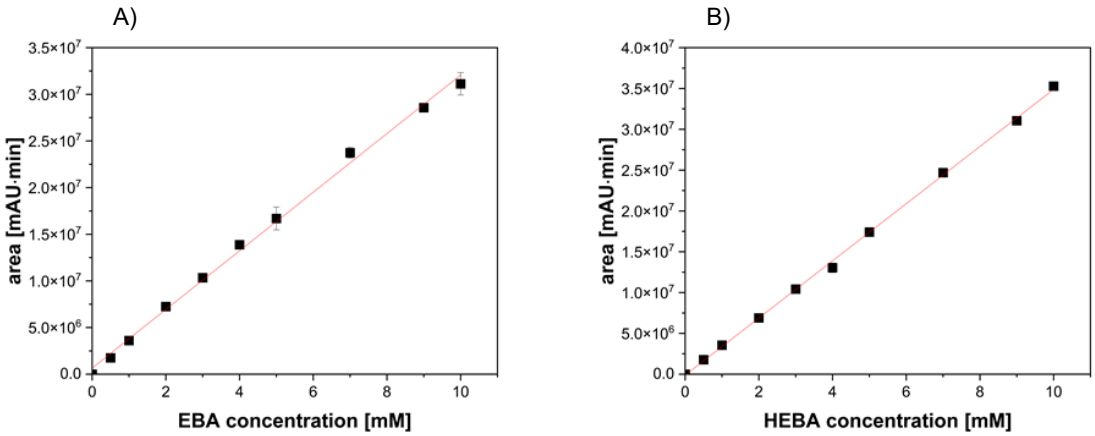

Fig. S6. 1. *Calibration curve of the **A**) substrate 4-ethylbenzoic acid (EBA) and the **B**) product 4-(1-hydroxyethyl)benzoic acid (HEBA). The chromatography analysis was carried out at 35 °C using a binary gradient of 0.1% v/v of trifluoroacetic acid (TFA) in H_2O and 0.095% v/v TFA in acetonitrile (ACN) at a flow rate of 0.5 mL min^{-1}. A gradient for ACN was applied as follow: 0 min: 35%, to 7 min: 80%, to 9 min: 35%, to 10 min: 35%. EBA and HEBA were detected at 237 nm. Sample preparation: a 20 µL sample was taken out from the reactor and mixed with 80 µL 3% v/v TFA in H_2O, followed by a centrifugation at 13,000 rpm and 4 °C for 4 min. Biological duplicates were performed. EBA: y = 655,208.9 + 3,142,507.5 · x and HEBA: y = -177,822.13 + 3,501,602.5 · x.*

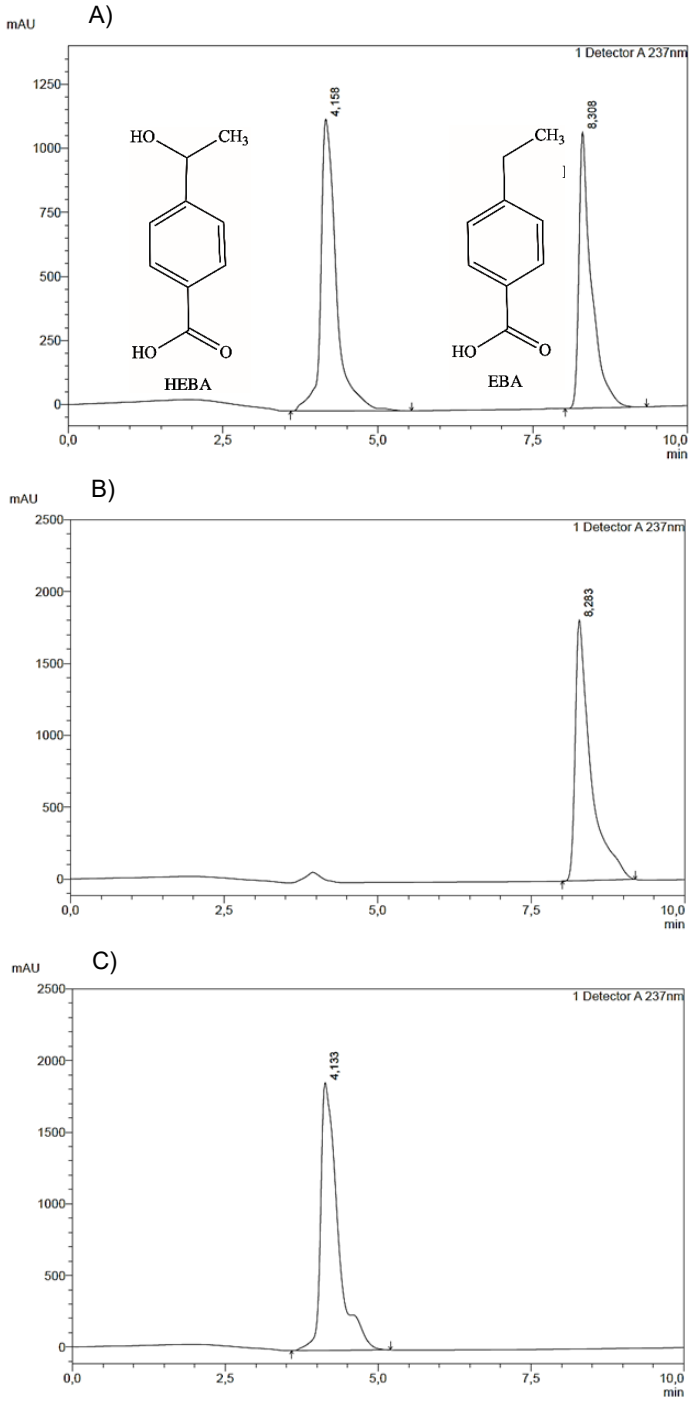

***Fig. S6. 2. A**) Representative chromatogram of the substrate 4-ethylbenzoic acid (EBA) and the product 4-(1-hydroxyethyl)benzoic acid (HEBA) from the electroenzymatic experiment. Retention time of EBA: 8.3 min, and HEBA: 4.2 min. **B**) Chromatogram from the authentic substrate and **C**) the authentic product from the calibration curves.*

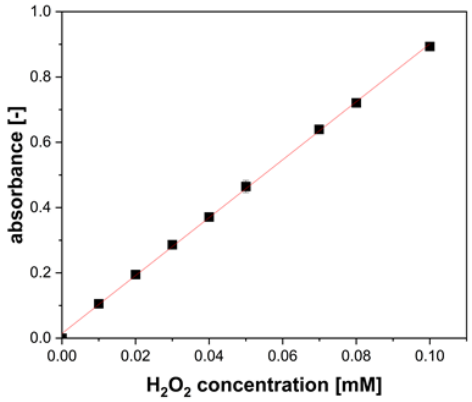

Fig. S6. 3. *Calibration curve of hydrogen peroxide (H_2O_2). Samples were measured using the iodide method. The assay (1 mL) contained the H_2O_2 sample, iodide reagent (0.4 M potassium iodide, 0.05 M NaOH, 10^{-4} M ammonium molybdate) and 0.5 M potassium hydrogen phthalate in a ratio of 4:3:3 and was measured at 351 nm in technical duplicates. Biological duplicates were performed. y = 9.0859 · x.*

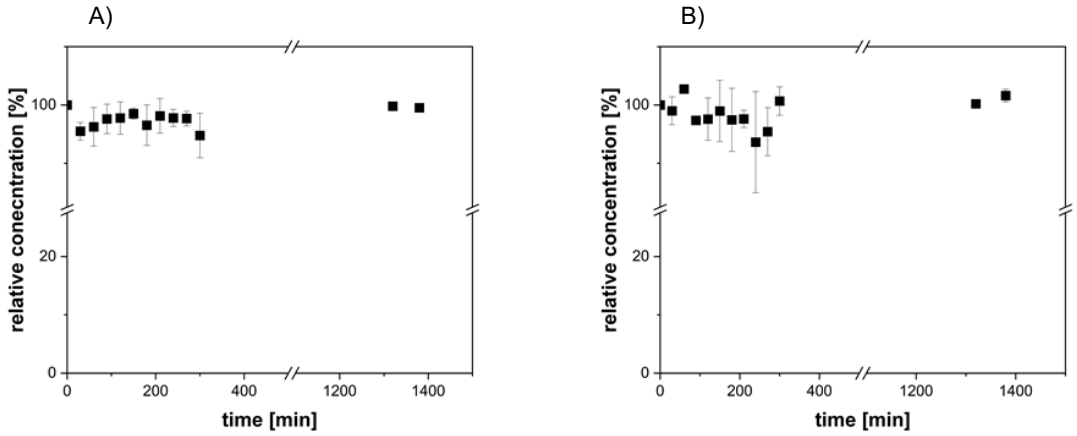

Fig. S6. 4. *Adsorption test of the substrate 4-ethylbenzoic acid (EBA) and the product 4-(1-hydroxyethyl)benzoic acid (HEBA) on the electrode surface. Relative concentration of **A**) EBA and **B**) HEBA as a function of the incubation time. Reaction condition: 200 mL 0.1 M KP_i pH 7, 8 mM EBA or 5 mM HEBA, 250 rpm, temperature: 22 ± 1 °C. Technical duplicates were performed.*

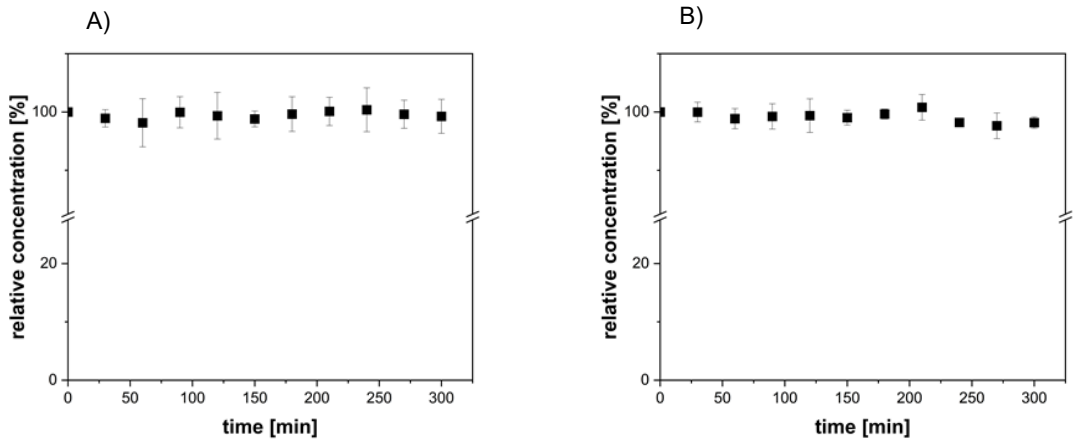

Fig. S6. 5. *Electrochemical stability test of the substrate 4-ethylbenzoic acid (EBA) and the product 4-(1-hydroxyethyl)benzoic acid (HEBA) at 10 mA. Relative concentration of* ***A****) EBA and* ***B****) HEBA as a function of the incubation time. Reaction condition: 200 mL 0.1 M KP$_i$ pH 7, 8 mM EBA or 5 mM HEBA, 250 rpm, temperature: 22 ± 1 °C. Technical duplicates were performed.*

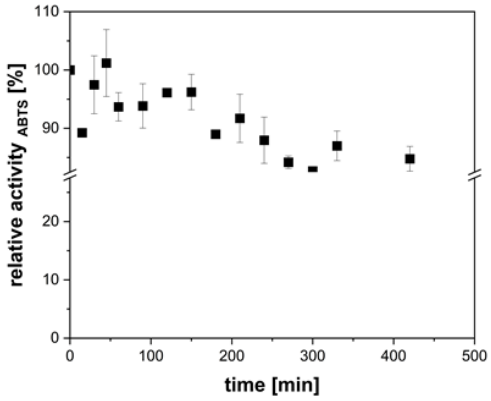

Fig. S6. 6. *Adsorption test of the recombinant unspecific peroxygenase from Agrocybe aegerita(rAaeUPO) on the electrode surface. Relative activity of rAaeUPO as a function of the incubation time. Reaction condition: 200 mL 0.1 M KP$_i$ pH 7, 250 rpm, temperature: 22 ± 1 °C, 100% relative activity corresponds to 1 U_{ABTS} mL^{-1} (30 nM), the initial activity. Technical duplicates were performed.*

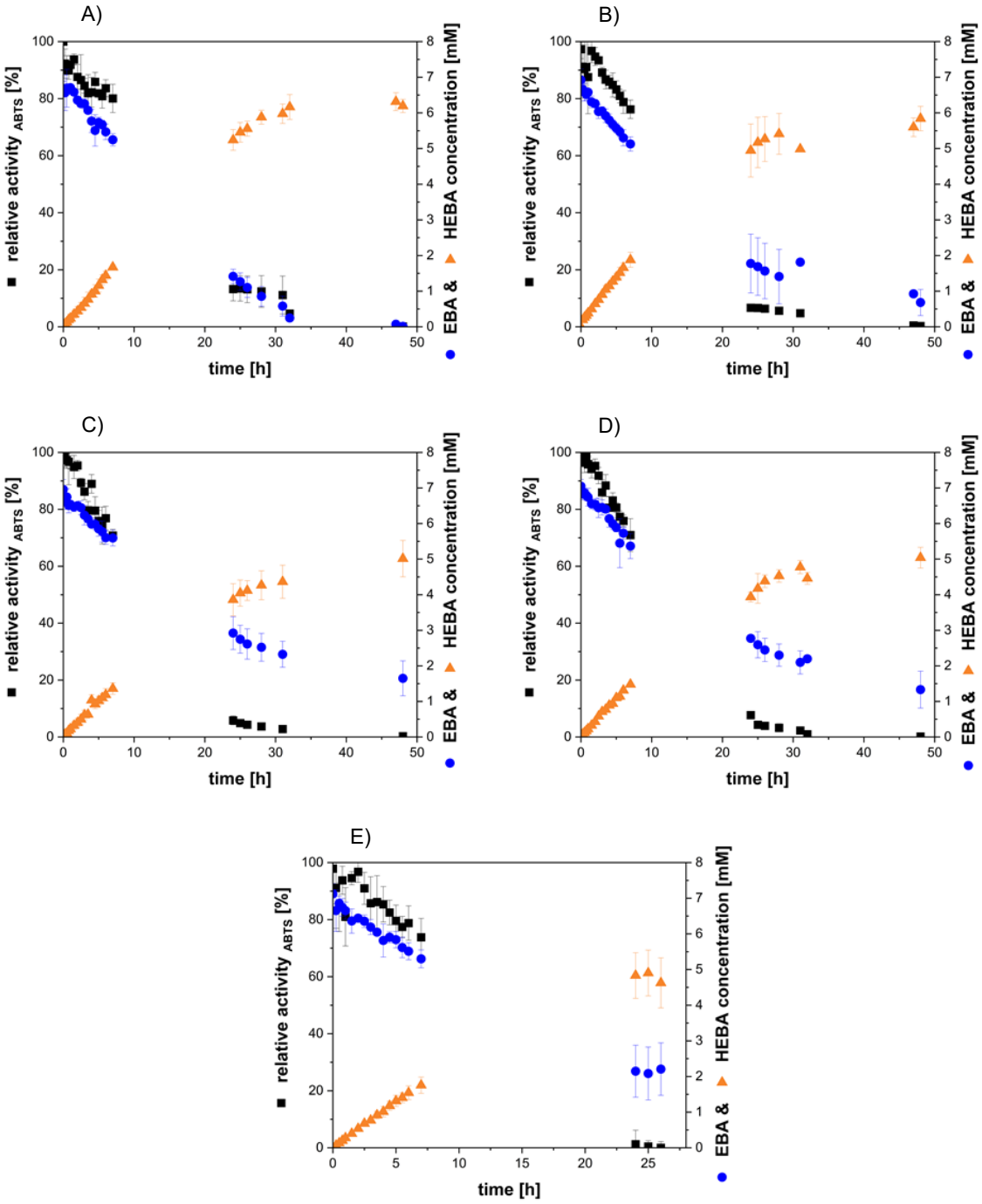

Fig. S6. 7. *Hydroxylation of 4-ethylbenzoic acid (EBA) to 4-(1-hydroxyethyl)benzoic acid (HEBA) catalyzed by the recombinant unspecific peroxygenase from Agrocybe aegerita (rAaeUPO) in an All-in-One (AiO) electrode system with in situ hydrogen peroxide (H_2O_2) generation at **A**) 5 mA, **B**) 15 mA, **C**) 20 mA, and **D**) 25 mA. Reaction condition: 200 mL 0.1 M KP_i pH 7, 8 mM EBA, 1 U_{ABTS} mL^{-1} (30 nM) rAaeUPO, 250 rpm, temperature: 22 ± 1 °C. Biological duplicates were performed. **E**) Hydroxylation of EBA catalyzed by rAaeUPO in an AiO electrode system with in situ H_2O_2 generation at 10 mA & 0.3 U_{ABTS} mL^{-1} (10 nM) rAaeUPO. Other parameter was identical. Biological triplicates were performed.*

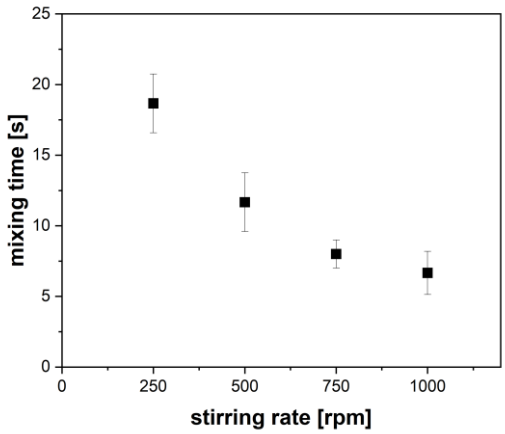

Fig. S6. 8. *Mixing time inside the bioelectrochemical system as a function of stirring rate. Parameter: 200 mL demineralized H_2O, addition of 5 M NaCl into the medium, temperature: 22 ± 1 °C, the distribution and homogeneity of the salt in the solution was measured by the detection of solution's conductivity. The time takes until the potential reached the constant value is defined as the mixing time.*

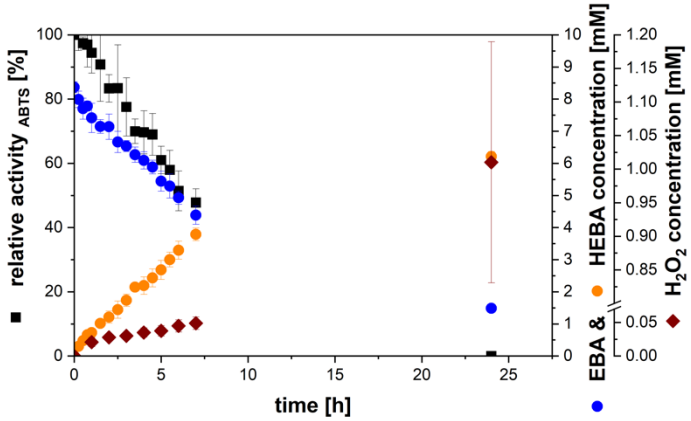

Fig. S6. 9. *Hydroxylation of 4-ethylbenzoic acid (EBA) to 4-(1-hydroxyethyl)benzoic acid (HEBA) catalyzed by the recombinant unspecific peroxygenase from Agrocybe aegerita (rAaeUPO) in the two All-in-One (AiO) electrodes system with in situ hydrogen peroxide (H_2O_2) generation. Reaction condition: 200 mL 0.1 M KP_i pH 7, 8 mM EBA, 0.3 U_{ABTS} mL^{-1} (10 nM) rAaeUPO, 250 rpm, temperature: 22 ± 1 °C, 10 mA was applied to each of the AiO electrode. Biological duplicates were performed.*

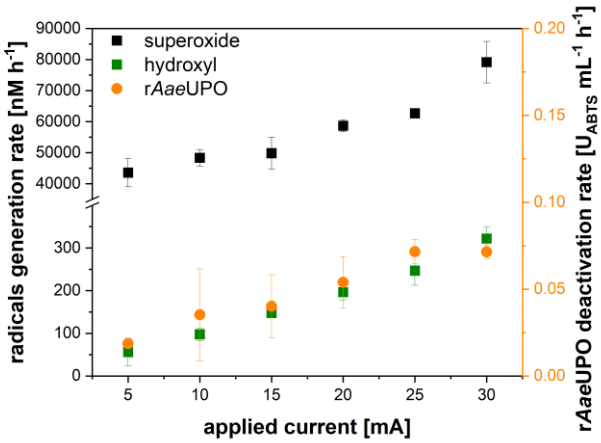

Fig. S6. 10. *Formation rate of superoxide and hydroxyl radicals, and deactivation rate of rAaeUPO in an All-in-One electrode system. Reaction condition: 200 mL nitro blue tetrazolium or terephthalic acid assay in 0.1 M KP$_i$ pH 7, 250 rpm, temperature: 22 ± 1 °C. rAaeUPO deactivation rates were determined from electroenzymatic experiments. Biological duplicates were performed.*

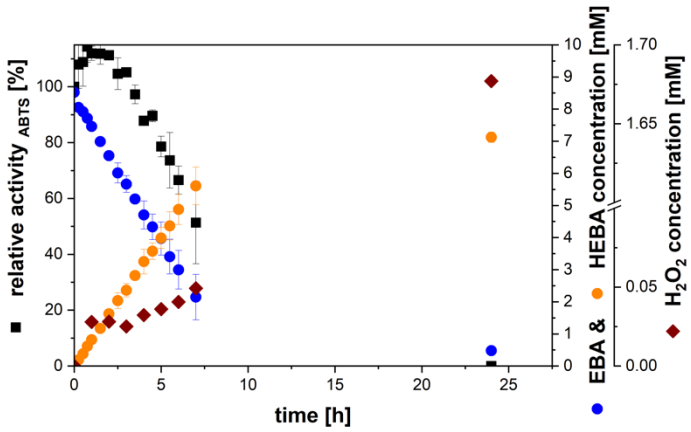

Fig. S6. 11. *Hydroxylation of 4-ethylbenzoic acid (EBA) to 4-(1-hydroxyethyl)benzoic acid (HEBA) catalyzed by the recombinant unspecific peroxygenase from Agrocybe aegerita (rAaeUPO) in the two All-in-One (AiO) electrodes system with in situ hydrogen peroxide (H_2O_2) generation and 1vvm aeration. Reaction condition: 200 mL 0.1 M KP$_i$ pH 7, 8 mM EBA, 0.3 U_{ABTS} mL^{-1} (10 nM) rAaeUPO, 250 rpm, temperature: 22 ± 1 °C, 10 mA was applied to each of the AiO electrode. Biological duplicates were performed.*

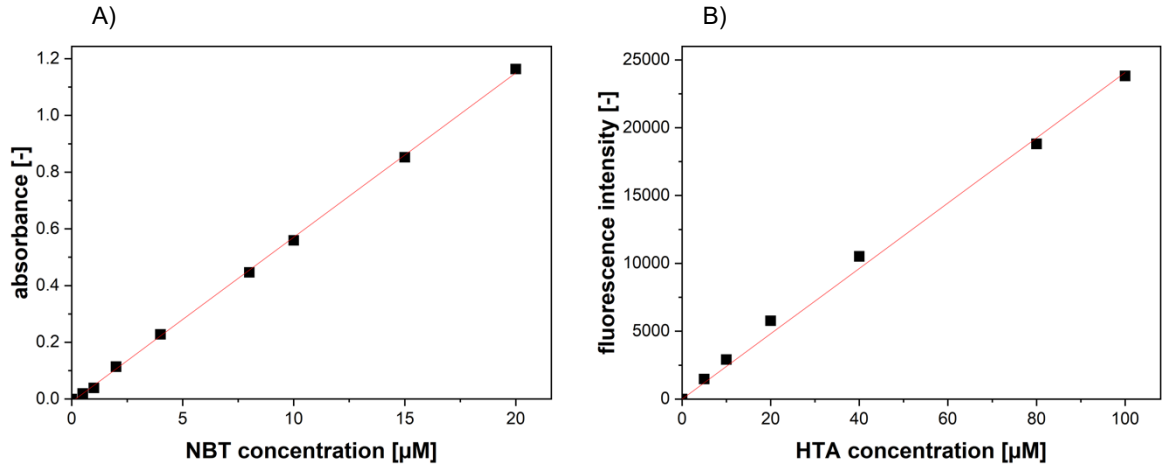

Fig. S6. 12. A*) Calibration curve of nitro blue tetrazolium (NBT). 20 µM NBT stock solution was prepared in 0.1 M KP_i pH 7 buffer and the NBT concentration was measured photometrically at 259 nm. y = 0.0573 · x.* ***B****) Calibration curve of 2-hydroxyterephthalic acid (HTA). 300 µM HTA stock solution was prepared in 0.1 M KP_i pH 7 buffer and the HTA concentration was measured photometrically at an excitation wavelength of 315 nm and an emission wavelength of 430 nm. y = 240.71 · x.*

11.3. Supporting Information to Chapter 7

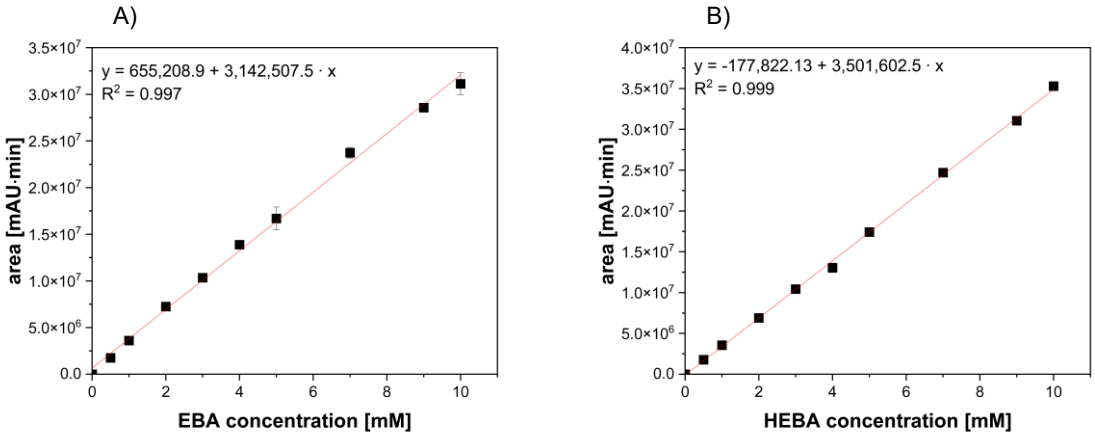

Fig. S7. 1.*Calibration curve of the* ***A****) substrate 4-ethylbenzoic acid (EBA) and the* ***B****) product 4-(1-hydroxyethyl)benzoic acid (HEBA). The chromatography analysis was carried out at 35 °C using a binary gradient of 0.1% v/v of trifluoroacetic acid (TFA) in H_2O and 0.095% v/v TFA in acetonitrile (ACN) at a flow rate of 0.5 mL min^{-1}. A gradient for ACN was applied as follow: 0 min: 35%, to 7 min: 80%, to 9 min: 35%, to 10 min: 35%. EBA and HEBA were detected at 237 nm. Sample preparation: a 20 µL sample was taken out from the reactor and mixed with 80 µL 3% v/v TFA in H_2O, followed by a centrifugation at 13,000 rpm and 4 °C for 4 min. Biological duplicates were performed. EBA: y = 655,208.9 + 3,142,507.5 · x and HEBA: y = -177,822.13 + 3,501,602.5 · x.*

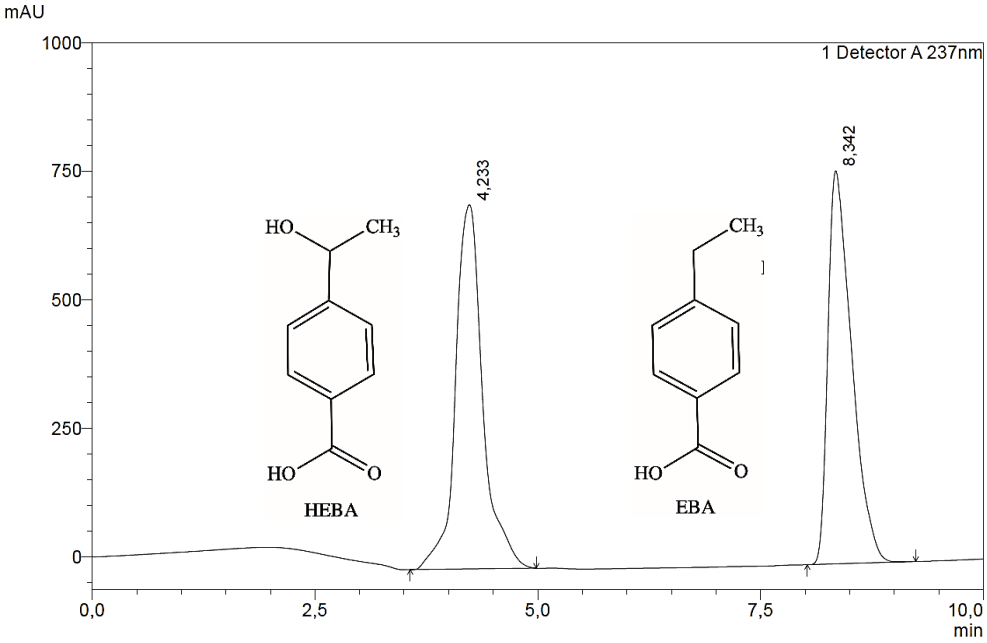

Fig. S7. 2. *Representative chromatogram of the substrate 4-ethylbenzoic acid (EBA) and the product 4-(1-hydroxyethyl)benzoic acid (HEBA) from the electroenzymatic experiment. Retention time of EBA: 8.3 min and HEBA: 4.2 min.*

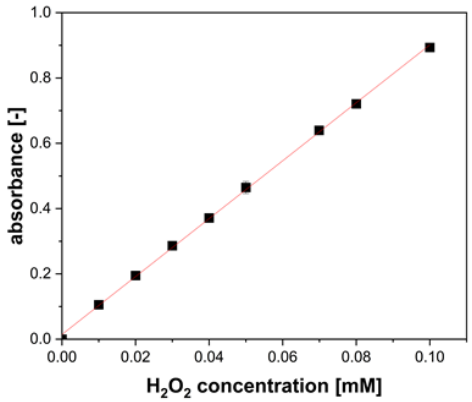

Fig. S7. 3. *Calibration curve of hydrogen peroxide (H_2O_2). Samples were measured using the iodide method as described in the experimental section. Duplicates were performed.*

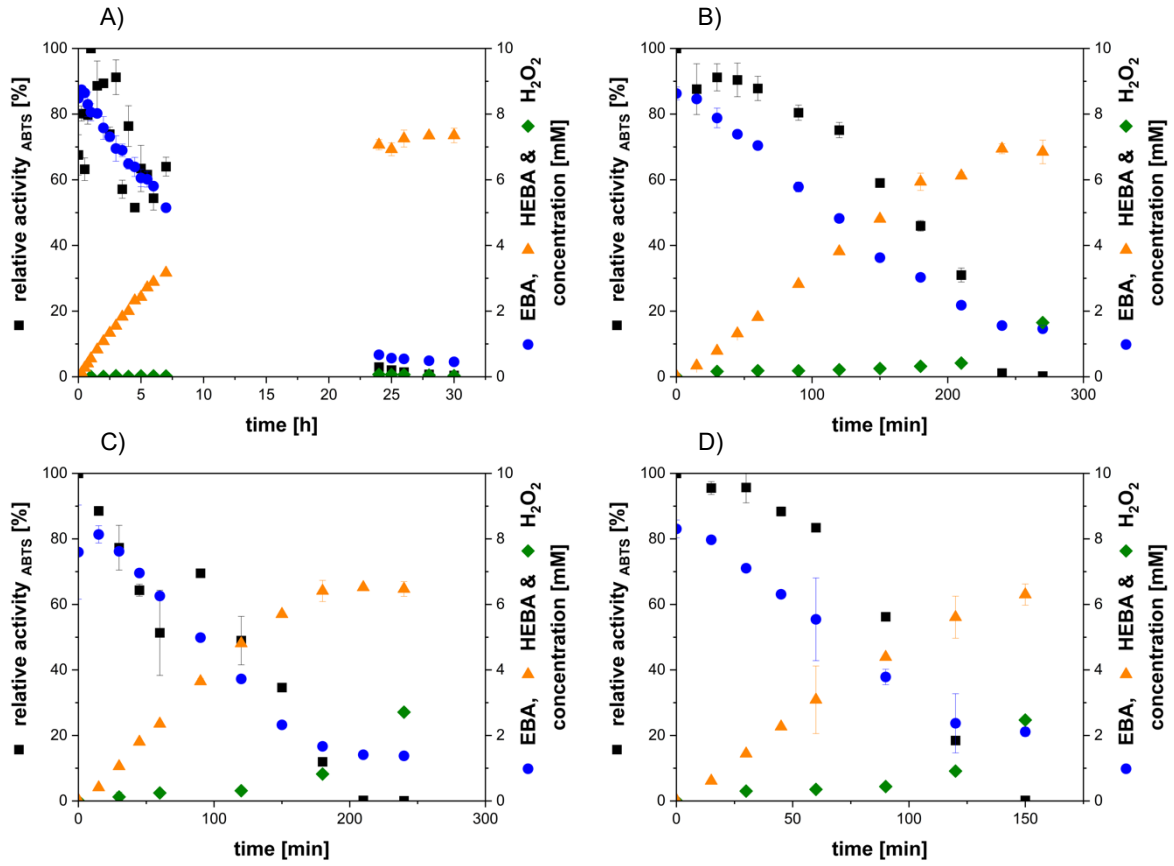

Fig. S7. 4. *Hydroxylation of EBA catalyzed by rAaeUPO in a GDE system with in situ H_2O_2 generation at **A**) 1.6 mA cm^{-2}, **B**) at 3.2 mA cm^{-2}, **C**) at 4.8 mA cm^{-2} and **D**) at 6.4 mA cm^{-2}. Reaction condition: 200 mL 0.1 M KP_i pH 7, 8 mM EBA, 10 nM rAaeUPO, 250 rpm, temperature: 22 ± 1 °C. EBA: 4-ethylbenzoic acid, HEBA: 4-(1-hydroxyethyl)benzoic acid.*

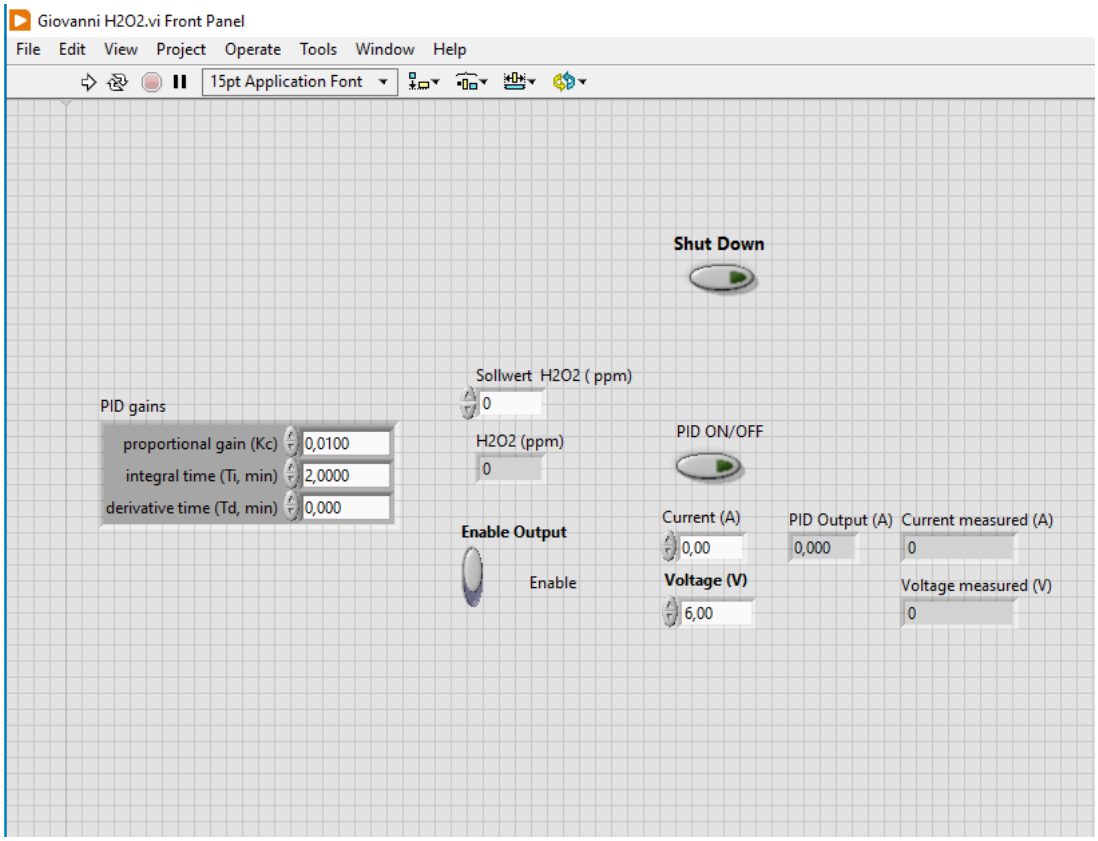
Giovanni H2O2.vi Front Panel
File Edit View Project Operate Tools Window Help
15pt Application Font
Shut Down
Sollwert H2O2 (ppm)
0
PID gains
proportional gain (Kc) 0,0100
integral time (Ti, min) 2,0000
derivative time (Td, min) 0,000
H2O2 (ppm)
0
PID ON/OFF
Enable Output
Enable
Current (A)
0,00
PID Output (A)
0,000
Current measured (A)
0
Voltage (V)
6,00
Voltage measured (V)
0

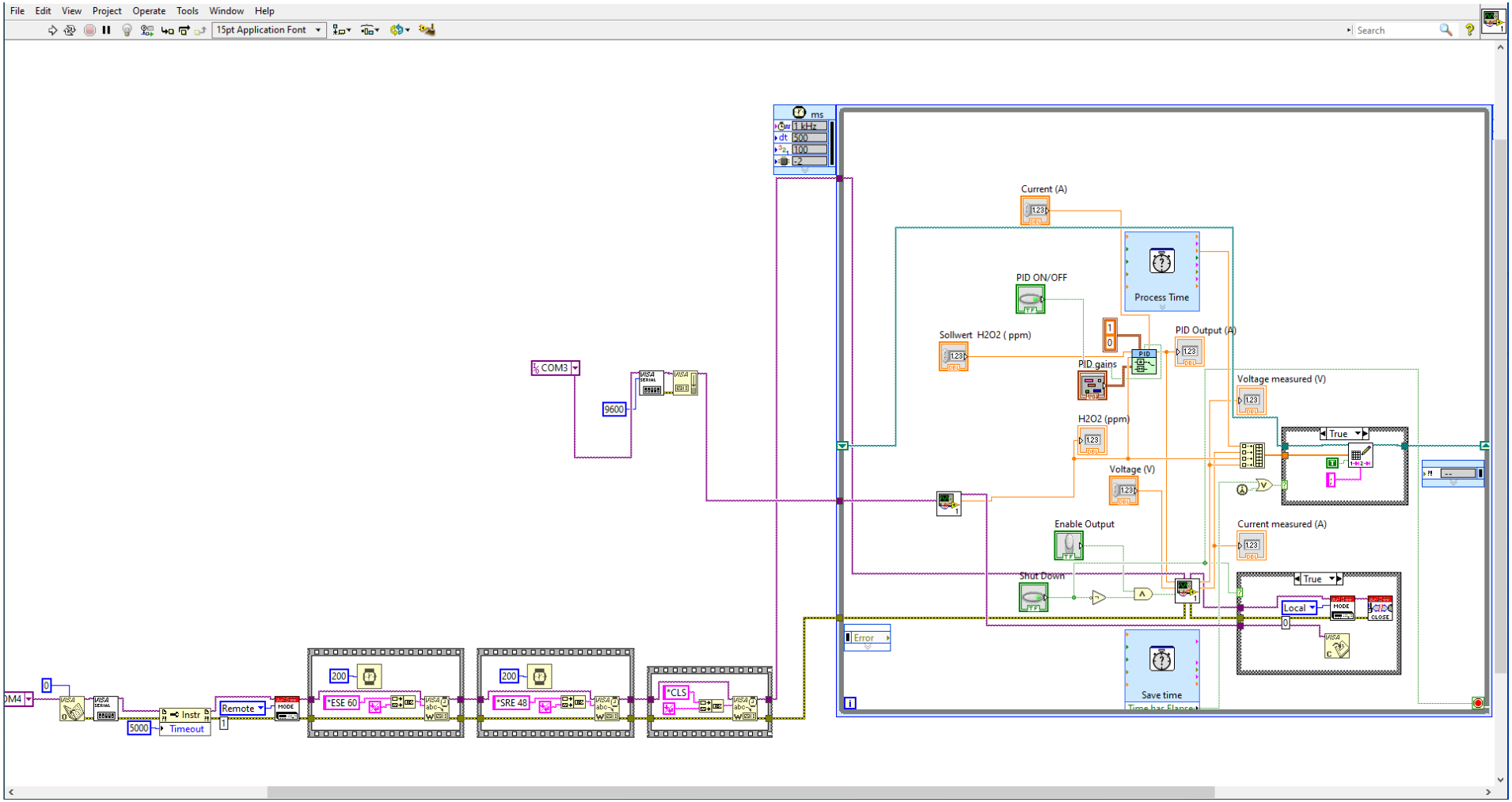

***Fig. S7. 5. A**) Interface (front panel) of the automation program in the LabVIEW 2021 SP1 software. **B**) The corresponding block diagram of the automation program. (DOI: https://doi.org/10.15480/882.14298; Handle: https://tore.tuhh.de/handle/11420/53140).*

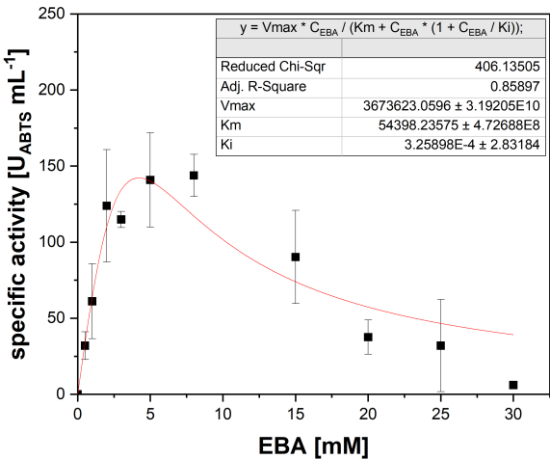

Fig. S7. 6. *Free rAaeUPO specific activity as a function of 4-ethylbenzoic acid (EBA) concentration. Reaction condition: total reaction volume of 1 mL (0.1 M KP_i pH 7), 2 mM H_2O_2, 1 U_{ABTS} mL^{-1} (30 nM) rAaeUPO, 1000 rpm, at 30 °C and 3 min. The reaction was started by adding the rAaeUPO and sample was taken every 30 s.*

11.4. Integration of the All-in-One Electrode in an Electrochemical Flow Cell for *in situ* Hydrogen Peroxide Supply in Hydroxylation Mediated by Immobilized Unspecific Peroxygenase

Giovanni V. Sayoga[a], Victoria S. Bueschler[a], Hubert Beisch[b], Bodo Fiedler[b], Daniel Ohde[a], Andreas Liese[a]

[a]Institute of Technical Biocatalysis, Hamburg University of Technology, Denickestraße 15, 21073 Hamburg, Germany
[b]Institute of Polymers and Composites, Hamburg University of Technology, Denickestraße 15, 21073 Hamburg, Germany

(Submitted to the Journal of *Electrochemistry Communications* on 22nd December 2024)

11.4.1. Abstract

Hydrogen peroxide (H_2O_2) is a strong oxidizing agent that is commonly employed in chemical synthesis. Nevertheless, its utilization as a cosubstrate in biocatalytic reactions remains limited due to the deactivating effect on biocatalysts at an elevated concentration. An electrochemical synthesis of H_2O_2 represents an attractive approach, offering a controllable *in situ* generation of H_2O_2 without producing complex by-products. The objective of this study is to demonstrate

the feasibility of the *in situ* electrogeneration of H_2O_2 using the All-in-One (AiO) electrode within a flow reactor technology. Integrating a bioelectrochemical system (BES) into a flow reactor technology, such as a flow cell, presents an alternative strategy for scale-up. In this study, the *in situ* generation of H_2O_2 is coupled with the hydroxylation of 4-ethylbenzoic acid catalyzed by the immobilized recombinant unspecific peroxygenase from *Agrocybe aegerita* (r*Aae*UPO) within a complete BES under batch and fed-batch operation modes. The electrochemical flow cell facilitates a controllable H_2O_2 generation by adjusting experimental parameters such as current density, aeration rate and residence time. The flow cell BES equipped with the AiO electrode yielded a catalytic productivity as high as 1.24 ± 0.02 mM h^{-1} (4.95 ± 0.1 g L^{-1} d^{-1}), a total turnover number of r*Aae*UPO up to 3.38 · 10^5 ± 702 mol mol^{-1} and a turnover frequency up to 8.34 ± 0.14 s^{-1}.

11.4.2. Introduction

Hydrogen peroxide (H_2O_2) finds its extensive application across diverse industrial sectors, particularly in chemical synthesis [19–21], environmental remediation [22,23] and energy conversion [24]. Despite its eco-friendly attributes, owing to its environmentally benign nature with water being its sole degradation product [25], current large scale production methods, such as the anthraquinone oxidation (AO) process, pose sustainability challenges [25,26]. The AO process involves multistep-reactions, is energy-intensive and generates waste, which has detrimental impact on the environment [26,27]. Moreover, the handling and storage of bulk H_2O_2 entail safety risks and significant costs [28], which is unjustifiable given that only certain industries require the use of concentrated H_2O_2 [25,29]. In light of these challenges, ongoing research focuses on alternative, cleaner synthesis routes for H_2O_2 [48]. This aspect is further supported considering that H_2O_2 also can be used as a cosubstrate in a variety of industry-relevant biocatalytic reactions [30], offering green alternative to conventional chemical processes [136], such as epoxidation [31,137], decarboxylation [32] and hydroxylation [33]. Nonetheless, the full technical implementation of H_2O_2 in biocatalytic reactions is still limited, mainly due to H_2O_2 deactivating biocatalysts rapidly at excess concentrations [30,34].

$$O_2 + 2H^+ + 2e^- \rightarrow H_2O_2 \qquad \textbf{(S8.1)}$$

A direct *in situ* electrosynthesis of H_2O_2 through the oxygen reduction reaction (ORR) (equation (**Eq.**) **S8.1**) at an electrode surface emerges as an appealing strategy to mitigate the irreversible enzyme deactivation [107]. This approach not only prioritizes environmental sustainability by eliminating the need for additional chemicals [47], but also facilitates precise and controllable H_2O_2 supply, thereby circumvents the risk of excessive H_2O_2 accumulation [107]. In contrast to the manual or sensor-controlled feeding of H_2O_2, *in situ* electrosynthesis

of H_2O_2 maintains a constant reaction volume and prevents high local H_2O_2 concentrations [46,123]. Furthermore, it circumvents the formation of complex by-products (*e.g.,* gluconic acid) [103] and the necessity to employ additional enzymes (*e.g.,* glucose oxidase) [74] or chemicals (*e.g.,* L-ascorbic acid) to generate H_2O_2 *in situ* [138]. Additionally, its application in bioelectrochemical system (BES) facilitates a nearly CO_2 neutral chemical synthesis with an exceptional selectivity, especially through the combination of renewable energy, green biocatalysts and sustainable resources [11,117]. The electrochemical *in situ* H_2O_2 generation, utilizing various electrodes materials, has been already combined with biocatalytic reactions [8,71,106]. Specifically, this approach has been applied in the selective oxidation of thioanisole catalyzed by chloroperoxidase (CPO) [16], the synthesis of bromolactone mediated by vanadium CPO [105], and the hydroxylation of ethylbenzene catalyzed by the recombinant unspecific peroxygenase from *Agrocybe aegerita* (r*Aae*UPO) [104].

Initially developed for the *in situ* generation of hydrogen within anaerobic fermentations [13,115,139], the All-in-One (AiO) electrode, integrates both counter and working electrodes into a single cylindrical structure [115]. This design enables seamless integration into conventional bioreactors, effectively transforming regular bioreactors into a BES [13,115]. The implementation of the AiO electrode within an electroenzymatic process using free enzyme in a stirred tank reactor was already established [118]. Although a numbering-up approach of these electrodes could offer a higher electrode surface to volume ratio in a larger reaction volume [115], an alternative scalable strategy could be realized using flow reactors, which was not yet explored. Continuous flow synthesis in a flow reactor technology has gained an attention from the chemistry community, especially, due to its excellent heat and mass transfer, predictable flow behavior and suitability for sequential reactions with different substrates, thus, exhibiting high degree of reaction control [140,141]. Integrating a flow reactor technology such as flow cell into a BES, particularly for *in situ* cosubstrate generation, presents an alternate scale-up strategy. Flow cells can be numbered-up or stacked as modular units, with the number of cells increasing as the reaction volume increases. This not only combines the benefits of flow reactor technology, but also achieves a higher electrode surface to reaction volume ratio, which is important for BES.

In this study, the AiO electrode was integrated into a flow cell to generate the cosubstrate H_2O_2 *in situ*. The electrochemical flow cell with the integrated AiO electrode was connected and circulated through an enzyme reactor where the enzyme-catalyzed reaction took place, establishing an overall circulation loop reactor (**Fig. S8. 1**). As a model reaction, the *in situ* electrosynthesis of H_2O_2 was combined with the hydroxylation of 4-ethylbenzoic acid (EBA) to 4-(1-hydroxyethyl)benzoic acid (HEBA) catalyzed by immobilized r*Aae*UPO. r*Aae*UPO is of

interest due to its high stability and ability to perform selective oxyfunctionalizations without the need for expensive electron donors like NAD(P)H [38,40,134]. The immobilization was realized by covalently bound r*Aae*UPO on polymer carriers and contained inside the SpinChem® magnetic rotating bed reactor (MagRBR). Immobilization of enzymes is reported to enhance the operational stability and simplify the separation from the reaction medium [129]. In this case, the separation was further simplified by only removing the SpinChem® MagRBR. The main objective of this research was to establish the proof of concept of the *in situ* electrogeneration of H_2O_2 using the AiO electrode within a flow cell of a circulation loop reactor. The study characterized the *in situ* H_2O_2 electrogeneration and its combination with the hydroxylation reaction catalyzed by immobilized r*Aae*UPO under different current densities. Furthermore, key performance indicators from electroenzymatic processes were determined.

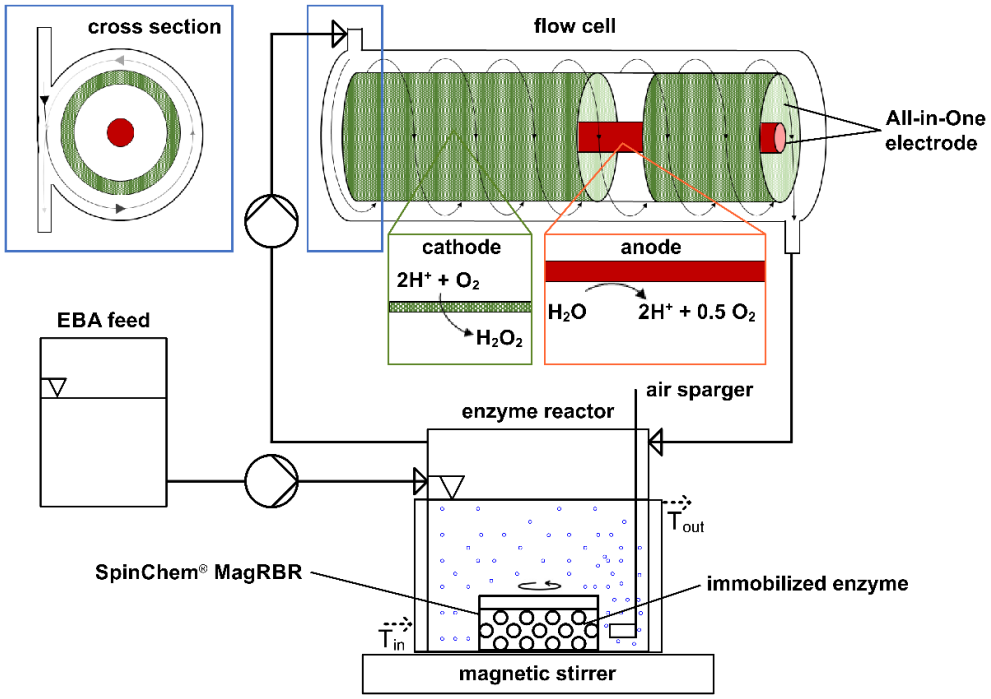

Fig. S8. 1. *Illustration of a differentially operated electrochemical flow cell equipped with the All-in-One (AiO) electrode for in situ supply of H_2O_2 in a circulation loop reactor. The electrochemical flow cell is operated in a circulation through the enzyme reactor for the electroenzymatic hydroxylation of 4-ethylbenzoic acid (EBA) to 4-(1-hydroxyethyl)benzoic acid (HEBA) catalyzed by immobilized recombinant unspecific peroxygenase from Agrocybe aegerita (rAaeUPO). The immobilized rAaeUPO are contained inside the SpinChem® magnetic rotating bed reactor (MagRBR), located inside the enzyme reactor.*

11.4.3. Experimental

11.4.3.1. Materials

2,2'-Azino-bis(3-ethylbenzothiazoline-6-sulfonic acid) (ABTS) (≥98%) was purchased from TCI (Eschborn, Germany). HEBA (≥97%) was purchased from BLD Pharm (China). Zeocin was purchased from InvivoGen (Toulouse, France). Other chemicals were purchased from

Carl Roth (Karlsruhe, Germany) or Sigma Aldrich (Steinheim, Germany) in a purity ≥98%. Carbon felt electrode (area weight: 250 g m^{-2}, thickness: 2.5 mm, surface area (Brunnauer-Emmet-Teller method): 0.4 m^2 g^{-1}) was purchased from SGL Carbon (Sigracell®, Wiesbaden, Germany). Platinized titanium rod electrode (diameter (*d)*: 3 mm) was purchased from METAKEM (Usingen, Germany).

11.4.3.2. Production of his-tagged r*Aae*UPO

The *Pichia pastoris* (X33) pre-culture, able to express recombinant protein r*Aae*UPO-PaDa-I-C6His (Prof. Holtmann, Karlsruhe Institute of Technology, Germany), was inoculated overnight in 50 mL buffered complex glycerol (BMGY) medium with 0.0175 mM Zeocin at 200 rpm, 30 °C [142]. The fermentation was conducted in a 1.5 L DASGIP bioreactor system (Eppendorf, Hamburg, Germany) and following the protocol described in [142]. Deviations from the original protocol are elaborated in the following. The fermentation was started with a batch phase by inoculating 500 mL basal salt medium (390.3 mM phosphoric acid, 6.8 mM calcium sulfate, 104.4 mM potassium sulfate, 60.5 mM magnesium sulfate heptahydrate, 73.6 mM potassium hydroxide, 434.3 mM glycerol) with the pre-culture. Following the depletion of the initial glycerol, the glycerol fed-batch phase was initiated (feed rate: 13.7 – 68.4 mmol h^{-1}) and maintained for 24 h. Subsequently, the methanol fed-batch phase was started (feed rate: 0 – 148.2 mmol h^{-1}) to induce the overexpression of r*Aae*UPO and continued for 120 h. The dissolved oxygen (DO) content and temperature were set at 30% and 30 °C, respectively. To maintain a constant DO, the stirring rate (400 – 1200 rpm) and aeration rate (30 – 60 L h^{-1} ≙ 1 vvm) were regulated by the system. Ammonia solution (13.3 M) was added to maintain the pH at 5. The feeding profile of glycerol and methanol were controlled based on DO levels and set as described in [143]. The biomass was separated via centrifugation (Beckmann J2HS, Beckmann Coulter, California, USA) at 5000 rpm for 2 h at 4 °C. The supernatant-containing r*Aae*UPO was sterile-filtered (0.22 µm, DURAPORE, Merck Millipore, Massachusetts, USA) and concentrated by ultrafiltration (10 kDa molecular weight cut off, Minimate TFF Capsule, Pall, New York, USA). r*Aae*UPOs were diafiltrated and concentrated in 0.1 M potassium phosphate (KP_i) buffer, pH 7.

11.4.3.3. Analytical methods

11.4.3.3.1. Quantification of enzyme activity

The ABTS assay was performed in a photometer (Genesys 180, Thermo Scientific, Massachusetts, USA) at 420 nm and at a room temperature for 1 min as technical duplicates. The assay consisted of 750 µL 0.1 M Na_2HPO_4/ 0.1 M citric acid buffer pH 4.4, 100 µL 3 mM

ABTS, 50 µL 40 mM H_2O_2 and 100 µL enzyme sample solution (unknown activity and concentration). The enzyme was added last to start the reaction. The measurement was started after properly mixing the complete reaction mixture by pipetting up and down 5 times. In the case of the measurement with immobilized r*Aae*UPO, the assay was conducted with 10 mg carrier containing immobilized r*Aae*UPO, 850 µL buffer and mixed with a vortex mixer. The absorbance was monitored for 1 or 10 min. The r*Aae*UPO activity and concentration were calculated as follow [144]:

$$v = \frac{slope\ of\ the\ absorbance\ [min^{-1}] \cdot 10\ (100\ \mu L\ enzyme\ sample\ in\ 1\ mL\ volume)}{36\ [mM^{-1}\ cm^{-1}] \cdot 1\ cm} \quad \textbf{(S8.2)}$$

$$c_{rAaeUPO} = v \cdot \frac{(k_m + C_{ABTS})}{k_{cat} \cdot C_{ABTS}} \cdot 1000 \quad \textbf{(S8.3)}$$

Where v is the r*Aae*UPO ABTS activity [U_{ABTS} mL^{-1}] (or [U_{ABTS} $g^{-1}_{carrier}$] for immobilized enzyme, with a carrier concentration of 0.25 $g_{carrier}$ mL^{-1} (factor 10 in **Eq. S8.2** is disregarded for the activity calculation due to the absence of the dilution effect when the immobilized enzyme was used)), C_{ABTS} is the ABTS concentration in the assay [µM], $c_{rAaeUPO}$ is the concentration of r*Aae*UPO [µM], k_m is the Michaelis-Menten parameter (50 µM) [40] and k_{cat} is the catalytic rate constant (546 s^{-1} ≙ 32,760 min^{-1}) [40].

11.4.3.3.2. Quantification of H_2O_2 concentration

The assay contained 400 µL sample, 300 µL iodide reagent (0.4 M potassium iodide, 0.05 M NaOH, 10^{-4} M ammonium molybdate) and 300 µL 0.5 M potassium hydrogen phthalate [85]. The mixture was measured directly at 351 nm and at a room temperature in technical duplicates. Calibration curves (10 µM to 100 µM) were prepared using diluted H_2O_2 solutions (**Fig. S8. 9**) (lower detection limit of 10 µM).

11.4.3.3.3. Quantification of 4-ethylbenzoic acid (EBA) and 4-(1-hydroxyethyl)benzoic acid (HEBA)

The chromatography analysis (Nexera LC-40 HPLC system, Shimadzu, Kyoto, Japan) was carried out at 35 °C using a binary gradient of 0.1% v/v (13.06 mM) of trifluoroacetic acid (TFA) in H_2O and 0.095% v/v (12.4 mM) TFA in acetonitrile (ACN) at a flow rate of 0.5 mL min^{-1}. A gradient for ACN was applied as follow: 0 min: 35%, to 7 min: 80%, to 9 min: 35%, to 10 min: 35%. EBA and HEBA were detected at 237 nm (UV-Vis SPD-40 detector, Shimadzu, Kyoto, Japan) and had retention times of 8.4 min and 4.3 min (Inertsil ODS-P, C18-RP, 5 µm, 100 Å column, GL Science, Japan), respectively (**Fig. S6. 2**). For the sample preparation, a 20 µL

sample was mixed with 80 µL 3% v/v (391.8 mM) TFA in H_2O, followed by a centrifugation (Biofuge Fresco, Heraeus, Hanau, Germany) at 13,000 rpm and 4 °C for 4 min. The supernatant was transferred to an HPLC-vial and measured as described. Calibration curves (1 mM to 8 mM) were prepared using authentic standards (**Fig. S8. 8**). All measurements were done in technical duplicates.

11.4.3.4. r*Aae*UPO immobilization

The epoxy resins (10 g) (Lifetech ECR 8285 [epoxy/ butyl methacrylate]; 400-600 Å, Purolite, King of Prussia, USA) underwent three equilibration cycles in a 1 M KP_i buffer at pH 7, with a resin to buffer ratio of 1:1 w/v, using an overhead shaker at 80 rpm and 22 °C for 10 minutes each time. Separately, the r*Aae*UPO was diluted, also with 1 M KP_i buffer pH 7, to reach a final activity of 20 U_{ABTS} mL^{-1} in a total volume of 40 mL. The epoxy resin and the r*Aae*UPO were combined in a 50 mL falcon tube to achieve a final resin to buffer ratio of 1:4 w/v. The mixture was incubated on an overhead shaker at 80 rpm and 22 °C for 18 h, followed by static incubation at the same condition for an additional 20 h. Washing steps were conducted three times using 40 mL of 0.01 M KP_i buffer pH 7, following the equilibration cycle protocol. The resulting immobilized enzyme was stored in a 0.1 M KP_i buffer pH 7 and kept at 4 °C. The activity and concentration of the immobilized enzyme used for calculations in this study were determined based on the measured activity and their corresponding concentrations, as described in section *11.4.3.3.1*.

11.4.3.5. Electrochemical setup

Electrochemical and electroenzymatic experiments were conducted in a circulation loop reactor consisting of electrochemical flow cell (made out of a polyether ether ketone (PEEK) material) and an enzyme reactor with a total working volume of 50 mL. The flow cell has an inner diameter of 12.4 mm and a length (*l*) of 65 mm, with a volume of 7.8 mL without the AiO electrode installed or 1.7 mL with the AiO electrode installed (**Fig. S8. 2**). To induce a circular flow inside the flow cell, inlet and outlet (*d*: 1.5 mm) flows were tangentially directed into and out of the flow cell. The AiO electrode (*l* within the flow cell: 62 mm, *d* within the flow cell: 12 mm, M20x1.5 thread to connect the AiO electrode into the flow cell) was fitted with the carbon felt as the working electrode (cathode) (*A*: 8.3 cm^2) and integrated into the flow cell (**Fig. S8. 2**). A platinized titanium rod (*A*: 4.24 cm^2) was used as the counter electrode (anode) and located inside the AiO electrode scaffold. A perforated cylindrical separator with an outer diameter of 9 mm and thickness of 1 mm was used to separate the cathode and anode (**Fig. S8. 2**). Water electrolysis takes place at the anode generating O_2 and H^+ molecules *in situ*. These molecules diffuse from the anode towards the cathode, where O_2 is reduced at the

surface of the cathode to react with H^+ to H_2O_2, which subsequently used as co-substrate for the enzymatic hydroxylation inside the SpinChem® MagRBR. The SpinChem® MagRBR (*d*: 19.5 mm, *h*: 13.7 mm, SpinChem AB, Umeå, Sweden) contained the immobilized enzyme and was located inside the enzyme reactor (**Fig. S8. 1**).

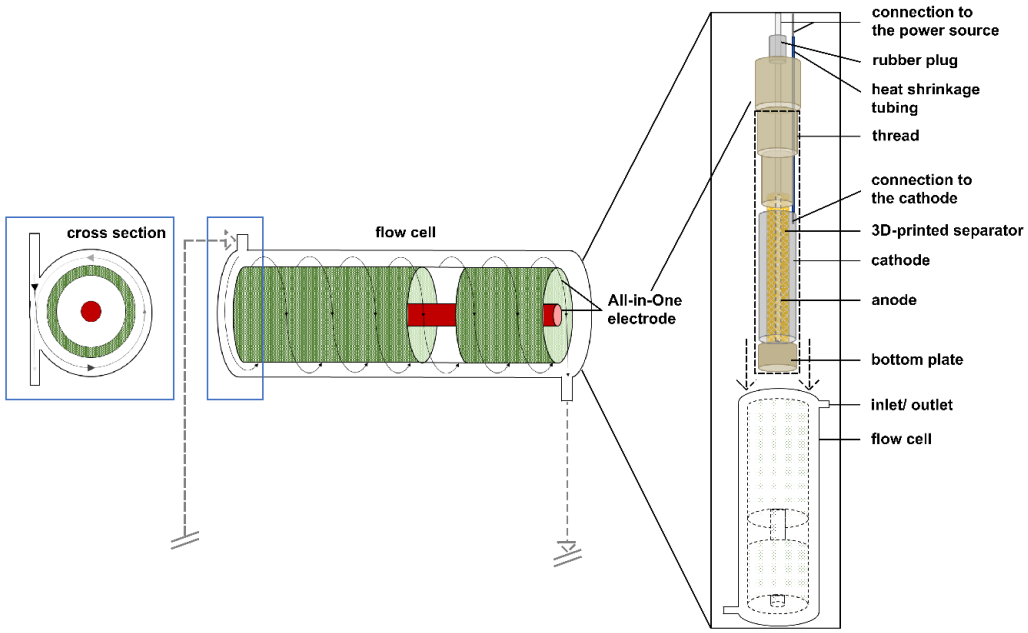

Fig. S8. 2. *Illustration of the electrochemical flow cell equipped with the All-in-One (AiO) electrode for the in situ electrochemical generation of H_2O_2. Dimensions, volumes and technical descriptions are delineated in the text.*

11.4.3.6. Electroenzymatic experiments

Experiments were operated either as batch or fed-batch (EBA feed). Unless otherwise stated, the reaction medium contained 50 mL 0.1 M KP_i pH 7, 8 mM EBA and 0.8 g (40 nM, 1.4 U_{ABTS} $g^{-1}_{carrier}$) carrier containing immobilized r*Aae*UPO contained inside the SpinChem® MagRBR. The enzyme reactor was sparged with air at 4 vvm using a porous sintered frit sparger [145] (microbubble generator, *d*: 13 mm, *l*: 25 mm) having an average pore diameter of 5 µm. A circulation flow rate of 24 mL min^{-1} was pumped through the flow cell (resulting residence time in the flow cell (τ_{FC}): 0.07 min) and the enzyme reactor (resulting residence time in the enzyme reactor (τ_{ER}): 2.01 min). In the case of fed-batch operation, 200 mM EBA solution was fed at a rate of either 0.008, 0.012 or 0.016 mmol h^{-1} (40, 60 or 80 µL h^{-1}). The EBA feed was started after 90 min. The SpinChem® MagRBR speed was set to 1000 rpm. Galvanostatic experiments were performed at a current density between 0.61 mA cm^{-2} and 3.64 mA cm^{-2} (Keithley 2231a-30-3 DC power supply, Tektronix, Oregon, USA). Samples for the measurement of EBA, HEBA, H_2O_2 concentration, and r*Aae*UPO activity were taken periodically from the enzyme reactor. Each experiment was conducted at 22 ± 1 °C and stopped after 24 h, and performed in duplicates.

The total turnover number (TTN) is defined as the quotient of the final product concentration once the enzyme was deactivated ($C_{HEBA,t=end}$) and the applied enzyme concentration ($C_{rAaeUPO}$) (**Eq. S8.4**). Meanwhile, the turnover number (TON) is described as the quotient of the product concentration at a specific time (at 60 min) before the enzyme was deactivated ($C_{HEBA,t=60\ min}$) and the applied enzyme concentration (**Eq. S8.5**). The turnover frequency (TOF) refers to the TON per unit time and were calculated from the initial part (≤15% conversion, 60 min) of the experiment where the product formation was linear (**Eq. S8.6**).

$$TTN = \frac{C_{HEBA,t=end}\ [mol]}{C_{rAaeUPO}\ [mol]} \quad \textbf{(S8.4)}$$

$$TON = \frac{C_{HEBA,t=60\ min}\ [mol]}{C_{rAaeUPO}\ [mol]} \quad \textbf{(S8.5)}$$

$$TOF = \frac{TON}{3600\ s} \quad \textbf{(S8.6)}$$

The H_2O_2 productivity was determined at current densities between 0.61 mA cm^{-2} and 3.64 mA cm^{-2}, within the same setup under abiotic condition and performed in duplicates. The Faradaic efficiency (F.E.) describes how much energy is consumed for the formation of H_2O_2 or the formation of side products, and was determined as follow [8].

$$F.E. = \frac{n \cdot F \cdot C_{H_2O_2} \cdot V}{Q\ (\int_{t=0}^{t=t} I(constant)dt)} \quad \textbf{(S8.7)}$$

Where *n* is the number of transferred electron (2), *F* is the Faraday constant (96,500 C mol^{-1}), $C_{H_2O_2}$ is the accumulated H_2O_2 concentration in the medium [M], *V* is the volume of the reaction medium [L] and *Q* is the total charge [C], which was calculated by integrating the applied current over time.

11.4.4. Results and discussion

In order to validate the feasibility of *in situ* electrogeneration of H_2O_2 using the AiO electrode within a flow reactor technology, it was first necessary to characterize the productivity of H_2O_2 in dependence of current density, aeration rate and liquid residence time. Subsequently, the *in situ* H_2O_2 generation within the flow cell was combined with the enzymatic hydroxylation reaction under batch and fed-batch operation modes catalyzed by the immobilized r*Aae*UPO to establish a BES.

11.4.4.1. *in situ* electrogeneration of H_2O_2 within the electrochemical flow cell system

The AiO electrode, equipped with a carbon felt cathode, was integrated into a flow cell and applied in a circulation loop of an enzyme reactor, as illustrated in **Fig. S8. 1**. Prior to starting the electroenzymatic hydroxylation reaction, a characterization study was done to evaluate the AiO electrode's ability to generate H_2O_2 *in situ*, especially, within a flow cell of a circulation loop reactor. This assessment was conducted in an abiotic environment, without the addition of biocatalyst and substrate EBA. **Fig. S8. 3** illustrates the specific productivity, the Faradaic efficiency (F.E.), and the resulting cell potential in relation to current density.

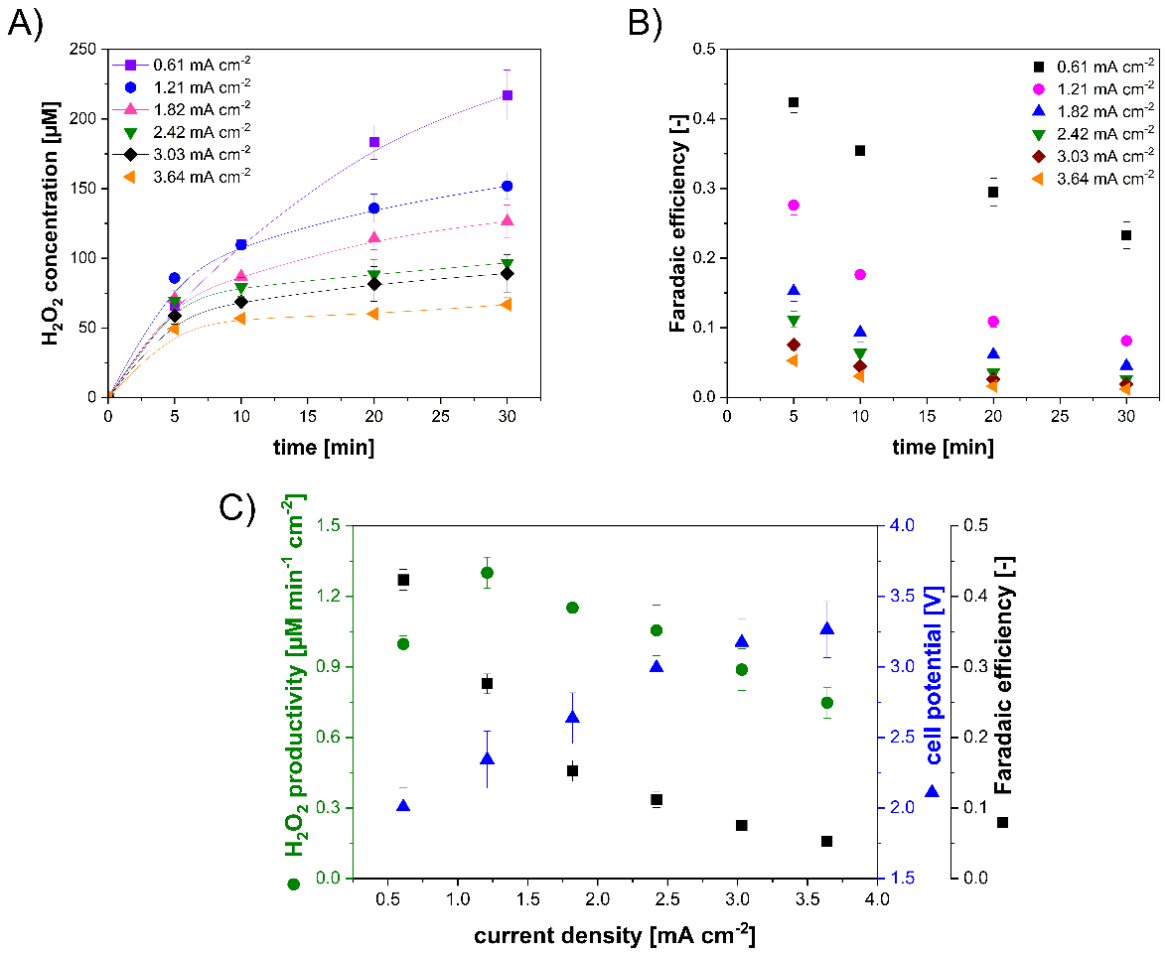

***Fig. S8. 3. A**) H_2O_2 concentration as a function of time at different current densities. **B**) Faradaic efficiency (F.E.) as a function of time at different current densities. **C**) Specific H_2O_2 productivity, resulting cell potential and F.E. (t: 5 min) as a function of current density. Conditions: carbon felt working electrode (8.3 cm^2), platinized titanium counter electrode (4.24 cm^2), 50 mL 0.1 M KP_i pH 7, at 22 ± 1 °C, 1000 rpm, circulation flow rate: 24 mL min^{-1} (resulting τ_{FC}: 0.07 min and τ_{ER}: 2.01 min) and 4 vvm. Duplicates were performed. Depicted lines serve as a visual aid.*

As depicted in **Fig. S8. 3. A**, the H_2O_2 concentration exhibits a gradual increase over time across all applied current densities and eventually reaching a maximum value of approximately

217 µM after 30 min at 0.61 mA cm^{-2}. Although an increasing trend is still observed between 20 and 30 min, the H_2O_2 generation rate had already declined, indicating that the H_2O_2 accumulation is approaching an asymptotic trend. This steady-state condition arises when the generation rate of H_2O_2 (**Eq. S8.1**) is equivalent to the rate of: (1) its reduction at the cathode (**Eq. S8.8**), which occurs due to the accumulation of H_2O_2 at the working electrode, or its competing reactions such as (2) oxidation at the anode (**Eq. S8.9**), (3) hydrogen evolution reaction (**Eq. S8.10**) or (4) full reduction of oxygen to water (**Eq. S8.11**) via the four-electron reduction mechanism [146,147]. Extending the reaction time would not necessarily lead to a significant increase in the accumulation of H_2O_2 concentration.

$$H_2O_2 + 2H^+ + 2e^- \rightarrow 2H_2O \quad \textbf{(S8.8)}$$

$$H_2O_2 \rightarrow 2H^+ + O_2 + 2e^- \quad \textbf{(S8.9)}$$

$$2H^+ + 2e^- \rightarrow H_2 \quad \textbf{(S8.10)}$$

$$O_2 + 4H^+ + 4e^- \rightarrow 2H_2O \quad \textbf{(S8.11)}$$

An increase in the applied current density from 0.61 mA cm^{-2} to 1.21 mA cm^{-2} leads to an increase in the productivity of H_2O_2 from 0.99 µM min^{-1} cm^{-2} to 1.30 µM min^{-1} cm^{-2} (**Fig. S8. 3. C**). However, a further increase of the applied current density above 1.21 mA cm^{-2} leads to a decrease of the H_2O_2 productivity. This trend can also be observed for the accumulation of the H_2O_2 concentration, as already shown in **Fig. S8. 3. A**. The decrease in both productivity and accumulation of H_2O_2 with increasing applied current can be explained by the increasing rate of competing reactions mentioned earlier. Prior studies also reported a similar observation, where the rate of competing reactions are increasing with an increase in the applied current density [85,128], one literature even reported an increased rate of competing reactions already at a current density of 0.38 mA cm^{-2} [84]. In the meantime, the cell potential shows a linear increase from 2.0 V to 3.3 V as the current density is increased.

The F.E, depicted in **Fig. S8. 3. B**, is decreasing over time, for all applied current density. This behavior occurs because in the beginning of the experiment, the concentration of H_2O_2 in the medium and at the electrode was zero. Thus, the decomposition rate of H_2O_2 was equally zero. As the electrolysis progresses, the H_2O_2 concentration in the medium and at the electrode increases, and, at the same time, the rate of its decomposition and side reactions become more pronounce and relevant. Of particular significance are the cathodic reduction of H_2O_2 and the complete reduction of oxygen to water. In other studies, comparable F.Es. from electrochemical systems equipped with a carbon based electrode are reported, which ranges between 0.18 and 0.57 [84,107,148]. Considering the achieved H_2O_2 productivity and the F.E. (**Fig. S8. 3. C**), the optimal electrochemical operation window would be between 0.61 –

1.21 mA cm^{-2}. This interval represents the compromise point between the highest H_2O_2 productivity and the highest F.E. within the investigated range of current density. The specific electrode area in this study corresponds to 0.17 cm^{-1}, which is comparable to electrochemical cells such as chloralkali cells and is lower than fluidized-bed cells or porous flow through cells, which typically ranges between 10 – 100 cm^{-1} [10].

Given that the H_2O_2 generation by the AiO electrode occurs within the flow cell, the oxygen availability may pose a limiting factor that could affect the H_2O_2 productivity. Since the *in situ* oxygen generation takes place at the anode, the lack of rigorous stirring in a flow cell could impact the oxygen distribution and mass transfer towards the cathode. Furthermore, it is important to note the electron balance during the process: for every H_2O_2 molecule generated at the cathode (**Eq. S8.1**), only half an oxygen molecule is generated at the anode (**Eq. S8.12**). This imbalance may exacerbate the oxygen limitation. To address these subjects, the *in situ* H_2O_2 electrogeneration was tested at 1.21 mA cm^{-2}, while varying the aeration rate inside the enzyme reactor and the liquid residence time inside the flow cell (τ_{FC}), by varying the circulation flow rate. In this way, the influence of these parameter on the productivity of the H_2O_2 was determined.

$$H_2O \rightarrow 2H^+ + \frac{1}{2}O_2 + 2e^- \qquad \textbf{(S8.12)}$$

In the previous experiments, the enzyme reactor was sparged with an aeration rate of 4 vvm to supply additional oxygen to the cathode for the electrosynthesis of H_2O_2. While increasing the aeration rate by a factor of three did not further increase the initial productivity (see **Fig. S8. 11** for the full data set) and the accumulation of H_2O_2 concentration, completely eliminating the aeration in the enzyme reactor led to a decrease in both productivity, from 1.30 µM min^{-1} cm^{-2} to 0.53 µM min^{-1} cm^{-2}, and H_2O_2 accumulation after 30 min, from 152 µM to 69 µM (**Fig. S8. 4. A** & **C**). This difference can be attributed to the stoichiometry of the electrochemical reactions. Since only half an oxygen molecule is generated at the anode, while a full oxygen molecule is required at the cathode for H_2O_2 formation, the anode reaction must occur twice to generate one oxygen molecule. Introducing additional aeration compensates for this oxygen deficit, preventing oxygen limitation at the cathode and enabling unrestricted H_2O_2 formation. Consequently, with sufficient oxygen supply, the productivity doubled, aligning with theoretical expectation. It can be concluded, that under chosen experiment conditions the oxygen availability is one of the limiting factors. Thus, it is beneficial to introduce an aeration into the enzyme reactor to supply additional oxygen molecules to the cathode for the generation of H_2O_2. The concern regarding the oxygen availability, especially due to its solubility and diffusivity towards the electrode, during the electrosynthesis of H_2O_2 was also

expressed in former studies [88,149]. In a conventional stirred tank reactor with 3D carbon-based electrode, this limitation is normally being resolved by sparging air or pure oxygen and rigorous mixing [98,150]. The absence of an increase in the H_2O_2 productivity following an increase in the aeration rate by a factor of three in this case can be attributed to two factors: (1) the maximum oxygen solubility in the enzyme reactor (0.25 mM at room temperature and atmospheric pressure [47]) could have been reached, and (2) oxygen mass transport limitation from the enzyme reactor towards the cathode in the flow cell has been encountered, given that the aeration and the cathodic reduction of oxygen are separated. Therefore, not only the current density and the aeration rate are of the essence for the H_2O_2 electrogeneration, but also the τ_{FC} (determined by the circulation flow rate).

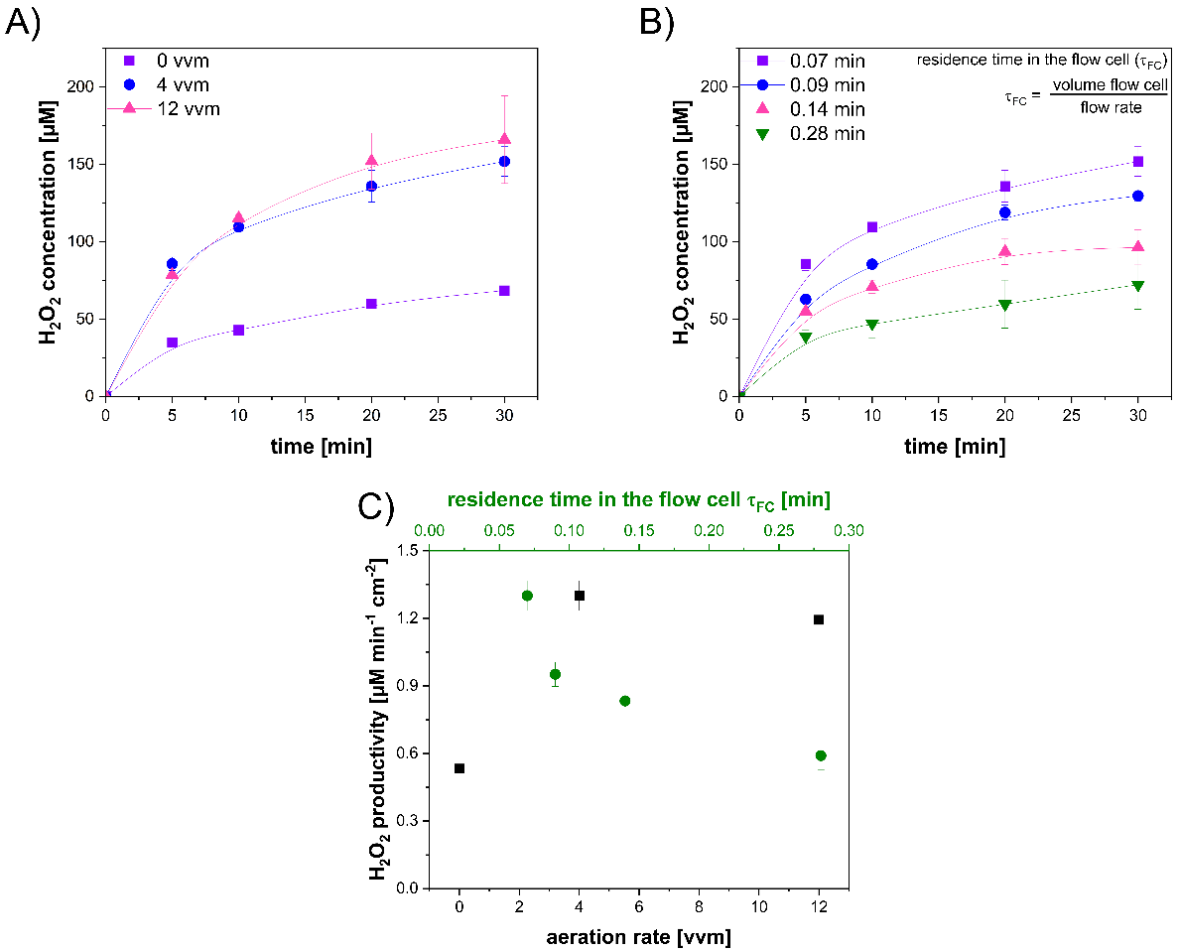

***Fig. S8. 4. A**) H_2O_2 concentration as a function of time at different aeration rates. **B**) H_2O_2 concentration as a function of time at different residence times in the flow cell (τ_{FC}). τ_{FC} of 0.28, 0.14, 0.09 and 0.07 min correspond to circulation flow rates of 6, 12, 18 and 24 mL min^{-1}, respectively. **C**) Specific H_2O_2 productivity as a function of aeration rate and as a function of τ_{FC} (independent from each other). Conditions: carbon felt working electrode (8.3 cm^2), platinized titanium counter electrode (4.24 cm^2), 1.21 mA cm^{-2}, 50 mL 0.1 M KP$_i$ pH 7, at 22 ± 1 °C, 1000 rpm, circulation flow rate: 24 mL min^{-1} (resulting τ_{FC}: 0.07 min and τ_{ER}: 2.01 min) (if the τ_{FC} was not varied) and 4 vvm (if the aeration rate was not varied). Duplicates were performed. Depicted lines serve as a visual aid.*

As previously mentioned, although the aeration rate inside the enzyme reactor was increased, the oxygen molecules had to diffuse towards the cathode inside the flow cell. The oxygen mass

transfer towards the cathode in this instance is defined by the circulation flow rate, which carries the dissolved oxygen from the enzyme reactor to the cathode in the flow cell. By adjusting the circulation flow rate through the flow cell, thus also the residence time in the flow cell (τ_{FC}), the mass transfer of the dissolved oxygen to the cathode can be influenced. As shown in **Fig. S8. 4. B** & **C**, the accumulation and the productivity of H_2O_2 is increasing with a decrease in the τ_{FC} (increase in the circulation flow rate), at the same aeration rate. By decreasing the τ_{FC} from 0.28 min to 0.07 min (increasing the flow rate from 6 mL min^{-1} to 24 mL min^{-1}), the productivity and the accumulation of H_2O_2 after 30 min increase from 0.59 µM min^{-1} cm^{-2} to 1.30 µM min^{-1} cm^{-2} and from 72.3 µM to 151.9 µM, respectively. Nevertheless, the increase in the productivity and the accumulation cannot be attributed solely due to the increase in the oxygen mass transfer to the cathode, but also due to a faster desorption of formed H_2O_2 from the cathode surface owing to an increase of the flow rate. The Reynolds (Re) number at the highest flow rate tested in this study is 84.73 (Re < 2300), meaning that the flow is still in the laminar region (**Eq. S8.13** and **Eq. S8.14**). Because of a faster H_2O_2 desorption from the electrode surface, further redox reactions of H_2O_2 are minimized, leading to a higher H_2O_2 accumulation and measured productivity in the medium. Correspondingly, the F.E. after 30 min increased from 0.04 at a τ_{FC} of 0.28 min (circulation flow rate: 6 mL min^{-1}) to 0.08 at a τ_{FC} of 0.07 min (circulation flow rate: 24 mL min^{-1}). Additionally, the decrease of the circulation flow rate (increase in the τ_{FC}) leads to a potentially thicker electrochemical double layer at the interface of the cathode and the medium. Thus, increasing the resistance of the electron transfer, which is reflected by the increase in the resulting cell potential from 2.34 V to 2.71 V, at the same current density of 1.21 mA cm^{-2}. In return, the increase of the resulting cell potential favors the full reduction of oxygen and reduction of H_2O_2 to water. The influence of the flow rate and the τ_{FC} on the H_2O_2 productivity and its accumulation at a lower current density, such as at 0.61 mA cm^{-2} (**Fig. S8. 12**), is less apparent due to the fact that at lower current density, the mass transport phenomena are not the limiting factor for the H_2O_2 productivity, but rather controlled by the applied current (current determines the H_2O_2 productivity). At the same time, the rate of competing reactions like further redox reaction of formed H_2O_2, full reduction of oxygen to water and hydrogen evolution reaction is less prominent. In this instance, the H_2O_2 productivity and its accumulation is increased by a factor of 1.5 by decreasing the τ_{FC} from 0.28 min to 0.07 min (increasing the circulation flow rate from 6 mL min^{-1} to 24 mL min^{-1}). As illustrated in **Fig. S8. 4. C**, the maximum obtained specific H_2O_2 productivity indicates that the *in situ* electrogeneration of H_2O_2 within this setup is optimal when an aeration rate of 4 vvm and a τ_{FC} of 0.07 min are employed.

An experiment with a flow rate exceeding 24 mL min^{-1} (τ_{FC}: 0.07 min) was not conducted due to the pump reaching its maximum flow rate. One potential strategy for further enhancing the electrochemical productivity of H_2O_2 is the application of high pressure within the system. This approach has been demonstrated to enhance the solubility of oxygen and its mass transfer, thereby also increasing the productivity of H_2O_2 [128]. Overall, the H_2O_2 productivity generated by the AiO electrode in a flow cell obtained in this study is comparable to the reported productivities in the literature [84,85,151,152], particularly when the AiO electrode system is employed in a stirred tank reactor [118]. Following the characterization study of *in situ* electrosynthesis of H_2O_2, the *in situ* supply of H_2O_2 was combined with the enzymatic hydroxylation reaction to establish a BES.

11.4.4.2. Electroenzymatic hydroxylation of 4-ethylbenzoic acid (EBA)

After the characterization of the H_2O_2 electrosynthesis in a flow cell of the circulation loop reactor, the electrochemical and the biocatalytic systems were combined to form a BES for the hydroxylation of EBA to HEBA, catalyzed by immobilized r*Aae*UPO. EBA was selected as the model substrate over benzene or ethylbenzene due to its higher solubility in aqueous solution [121]. Additionally, its application eliminates the potential formation of by-products or subsequent reactions that could affect reaction selectivity [33].

Immobilized biocatalysts are often used both in a lab or in an industrial application [129]. General advantages of enzyme immobilization are, among others, increase of enzyme operational stability and ease of recovery from the reaction medium [153]. In this specific case, a direct immobilization of r*Aae*UPO on the surface of the electrode was an attractive option, because, then, the electrode does not only supply the cosubstrate H_2O_2, but also works as a carrier for the enzyme. Furthermore, this approach would increase the proximity between the enzyme and the cosubstrate, potentially increasing the efficiency of the biocatalytic reaction. However, a direct immobilization of r*Aae*UPO on the electrode surface led to a faster deactivation (**Fig. S8. 13**). A faster deactivation could be attributed to the following factors: (1) the r*Aae*UPO reacted directly with the formed H_2O_2 and radicals such as superoxide and hydroxyl radical on the electrode, and (2) a possible diffusion limitation of the EBA into the pores, where the r*Aae*UPO was immobilized, prompted further reactions only between r*Aae*UPO and H_2O_2, thus, leading to a catalase malfunction reaction. In this contribution, an alternative immobilization strategy was employed, involving the covalent binding of r*Aae*UPO onto an epoxy resins carrier. The carrier was then placed within the SpinChem® MagRBR, which was positioned inside the enzyme reactor of the circulation loop reactor (**Fig. S8. 1**).

The immobilization of r*Aae*UPO on the Lifetech ECR 8285 epoxy resins carrier resulted in an immobilization yield of 85.2% and an activity yield of 1.75%, with a measured activity of 1.4 ± 0.3 U_{ABTS} $g^{-1}_{carrier}$. The calculated activity loss, derived from residual r*Aae*UPO activities in the supernatant following the immobilization process and washing steps, was less than 3.0 U_{ABTS} mL^{-1} (**Table S8. 4**). The theoretical activity of immobilized r*Aae*UPO on the carrier based on the immobilization yield was 68.2 U_{ABTS} $g^{-1}_{carrier}$. In this study, the immobilization efficiency was calculated by dividing the measured immobilized enzyme activity by the theoretical immobilized enzyme activity, resulting in an efficiency of 2.05%. A low activity yield and immobilization efficiency despite a high immobilization yield could indicate the presence of steric hindrance and mass transport limitation during the activity assay in the photometer. This is despite the fact that the reaction mixture and the immobilized enzyme were mixed with a vortex mixer prior to the measurement. Furthermore, despite the carrier underwent three washing cycles after the immobilization step, with a maximum of 3.0 U_{ABTS} mL^{-1} removed, there remained the possibility of multilayer adsorption of the enzyme on the carrier.

Electroenzymatic experiments were performed for 24 h at various current densities between 0.61 mA cm^{-2} and 3.64 mA cm^{-2} in a batch operation mode. The reaction medium consisted of 8 mM EBA and 0.8 g of carrier containing immobilized r*Aae*UPO, contained within the SpinChem® MagRBR. H_2O_2 was generated *in situ* by the AiO electrode inside the flow cell. The dissolved H_2O_2 was then circulated through the enzyme reactor, where the hydroxylation occurred. The concentrations of EBA, HEBA and H_2O_2 during the experiments were measured and are depicted in **Fig. S8. 5**.

To monitor the potential of enzyme leaching, samples were withdrawn from the medium at a specific frequency in order to measure the r*Aae*UPO activity via the ABTS assay. The ABTS assays indicated that r*Aae*UPO activity was not detected in the reaction medium supernatant, suggesting that the immobilized r*Aae*UPO was not detached from the carrier. As illustrated in **Fig. S8. 5**, the productivity and the accumulation of H_2O_2 during the electroenzymatic hydroxylation reaction are dependent on the current density. At lower current density such as 0.61 mA cm^{-2} (**Fig. S8. 5. A**), the H_2O_2 productivity was lower. However, the H_2O_2 concentration was gradually increasing over time and accumulated to 0.7 mM after 7 h, and higher than 1.5 mM after 24 h. In contrast, at higher current density such as 1.82 mA cm^{-2} and 2.42 mA cm^{-2} (**Fig. S8. 5. C** & **D**), the H_2O_2 productivity was comparably faster and the H_2O_2 concentration accumulated to a concentration around 1.1 mM after 7 h. Albeit, this concentration did not significantly increase after 24 h. It is important to note that in **Fig. S8. 5. C** and **D**, the final H_2O_2 concentrations are lower than the preceding measurement points. The discrepancy was caused by the inlet tubing of the flow cell inside the enzyme reactor being

drawn into the vortex above the SpinChem® MagRBR. This resulted in a mixture of air and liquid being sucked into the flow cell, forming a slug flow that impeded the H_2O_2 generation due to the disruption of the continuous liquid flow by gas bubbles at the cathode. Simultaneously, the existing H_2O_2 in the enzyme reactor was consumed during the hydroxylation process, further contributing to the observed reduction in the concentration. At the highest tested current density of 3.64 mA cm^{-2} (**Fig. S8. 5. F**), the productivity of H_2O_2 decreased, with the H_2O_2 concentration fluctuating around 0.3 mM. As previously discussed, the observed decline in both H_2O_2 productivity and its accumulation can be attributed to the increasing rate of the H_2O_2 decomposition and competing reactions. After 24 h and for each experiment, the immobilized r*Aae*UPO was deactivated. This was confirmed by the ABTS assay, which was performed using 10 mg of the carrier taken from within the SpinChem® MagRBR. The relevant performance indicators from the electroenzymatic experiments such as TTN, TOF, catalytic productivity and final HEBA concentration are summarized in **Table S8. 1**.

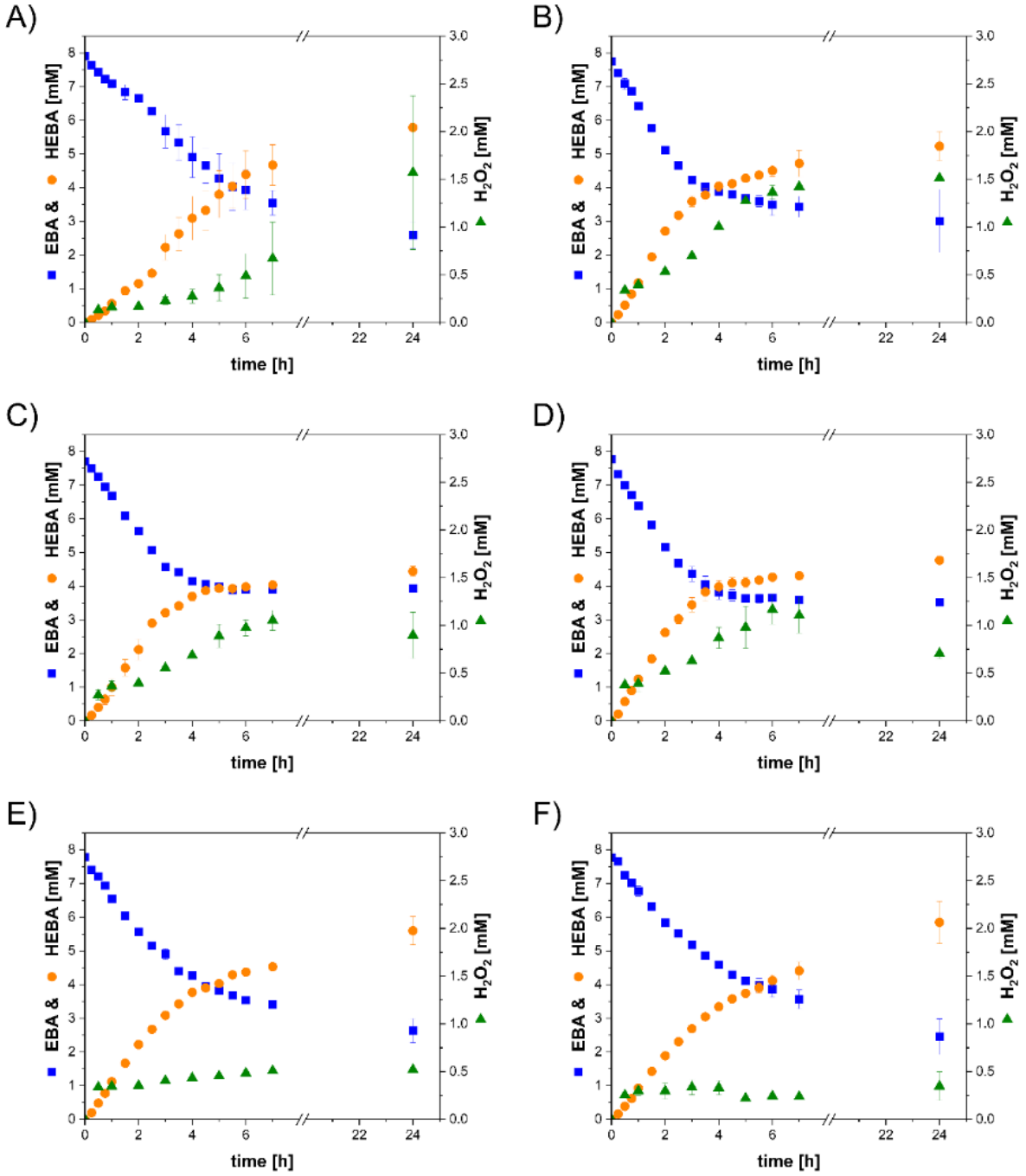

Fig. S8. 5. *Hydroxylation of EBA catalyzed by immobilized rAaeUPO in a circulation loop reactor equipped with the All-in-One electrode for in situ H_2O_2 generation at **A**) 0.61 mA cm^{-2}, **B**) 1.21 mA cm^{-2}, **C**) 1.82 mA cm^{-2}, **D**) 2.42 mA cm^{-2}, **E**) 3.03 mA cm^{-2} and **F**) 3.64 mA cm^{-2}. Conditions: 50 mL 0.1 M KP$_i$ pH 7, 8 mM EBA, 0.8 g carrier (40 nM rAaeUPO), 1000 rpm, circulation flow rate: 24 mL min^{-1}(resulting τ_{FC}: 0.07 and τ_{ER}: 2.01 min), 4 vvm and at 22 ± 1 °C. EBA: 4-ethylbenzoic acid, HEBA: 4-(1-hydroxyethyl)benzoic acid. Duplicates were performed.*

Table S8. 1. *Summary of total turnover number (TTN), turnover frequency (TOF), catalytic productivity and final concentration of HEBA determined from electroenzymatic experiments in the circulation loop reactor equipped with the All-in-One electrode at various current densities.*

Current density [mA cm^{-2}]	Catalytic productivity [mM h^{-1}]	Final HEBA concentration [mM]	TOF [s^{-1}]	TTN [mol mol^{-1}]
0.61	0.56 ± 0.07	5.79 ± 0.03	3.77 ± 0.45	$1.40 \cdot 10^5$ ± 840
1.21	1.18 ± 0.02	5.23 ± 0.43	7.91 ± 0.07	$1.26 \cdot 10^5$ ± 10,458
1.82	1.24 ± 0.11	4.44 ± 0.15	6.74 ± 1.64	$1.07 \cdot 10^5$ ± 3,623
2.42	1.24 ± 0.02	4.77 ± 0.09	8.34 ± 0.14	$1.15 \cdot 10^5$ ± 2,143
3.03	1.12 ± 0.02	5.60 ± 0.42	7.53 ± 0.15	$1.35 \cdot 10^5$ ± 10,194
3.64	0.92 ± 0.01	5.85 ± 0.63	6.23 ± 0.04	$1.41 \cdot 10^5$ ± 15,225

Within an electroenzymatic system, particularly utilizing peroxygenases and peroxidases, the productivity and the accumulation of H_2O_2 inside the medium determine not only the biocatalytic productivity but also the enzyme stability. A higher and faster accumulation of H_2O_2 within the medium will result in a higher degree of enzyme saturation with the H_2O_2. This, in turn, will result in a higher biocatalytic rate ($K_{M,\ H2O2}$: 0.79 – 1.8 mM [36,40,106]) and TOF, reaching a maximum of 8.34 ± 0.14 s^{-1}. Simultaneously, the higher the accumulation of H_2O_2 and the catalytic rate, the higher the probability of r*Aae*UPO undergoing an unproductive catalytic cycle, such as a catalase reaction. Even a catalase malfunction reaction occurs more frequently, which leads to an enzyme deactivation. The aforementioned reaction and its mechanism have been previously proposed [36]. The catalase malfunction reaction can be attributed to the subsequent reactions between the intermediate compound I, which is formed after the resting state of r*Aae*UPO binds with the first H_2O_2 molecule, and a further H_2O_2 molecule instead of with the substrate EBA. The reaction of the intermediate compound I with the second H_2O_2 molecule yields the intermediate compound II. Subsequently, compound II is susceptible to further reactions with additional H_2O_2, resulting in the formation of compound III. The formation and the presence of compound III would ultimately result in the heme-bleaching of r*Aae*UPO. This is because if the compound III were to be exposed to additional H_2O_2, it would form free radicals, which would cause heme-destruction and result in the irreversible deactivation [36,106]. Additionally, the deactivation due to the degradation of heme is inevitable and correlated directly with the product formation [103]. The catalase and catalase malfunction reactions are intensified at lower concentrations of EBA, given that the reported K_M value of EBA, which is 2.3 mM [106], is higher than the K_M value of H_2O_2. Under these conditions, applying or achieving during the course of a reaction EBA concentrations close or below its K_M value not only diminishes the catalytic rate but also promotes the catalase malfunction reaction due to the continuous presence of H_2O_2. Consequently, this leads to an accelerated r*Aae*UPO deactivation as the H_2O_2 productivity and its accumulation increase. As a result, the final concentration of HEBA is reduced. This phenomenon is evident in the

observation that at the highest TOF of 8.34 ± 0.14 s^{-1}, one of the lowest final HEBA concentration (4.77 ± 0.09 mM) and also one of the lowest TTN of 1.15 · 10^5 ± 2,143 mol mol^{-1} are obtained (**Table S8. 1**). Conversely, at the lowest TOF of 3.77 ± 0.45 s^{-1}, one of the highest TTN values is obtained, corresponding to 1.40 · 10^5 ± 840 mol mol^{-1}. Additional control experiments, in which the substrate or product were circulated for 7 h through the circulation loop reactor, revealed no substantial adsorption of substrate or product on the electrode surface, tubing or PEEK material (**Fig. S8. 10**). Furthermore, the mass transport of the liquid into and out of the SpinChem® MagRBR was impeded by the carrier loading and the surface roughness, leading to an incomplete utilization of the immobilized enzyme. This was confirmed by reducing the carrier loading by 50% (0.4g) (**Fig. S8. 14**). Under the same reaction conditions at 1.21 mA cm^{-2}, the catalytic rate achieved with the reduced carrier was 0.79 mM h^{-1}, which corresponded to 67% of the rate observed with full carrier loading (0.8 g). This rate exceeded the expected value of 0.59 mM h^{-1}, suggesting that the enzyme's activity was not fully utilized in the higher carrier loading scenario

As discussed in section ***11.4.4.1***, in addition to the current density, the residence time in the flow cell (τ_{FC}) (determined by the circulation flow rate) could affect the productivity and the accumulation of H_2O_2 during the experiment. Therefore, after the initial establishment of a BES using the integrated flow cell in a circulation loop reactor, the influence of the residence time on the electroenzymatic hydroxylation was also investigated.

11.4.4.3. Evaluation of different residence times and fed-batch operation mode on electroenzymatic hydroxylation

Once the implementation of the AiO electrode in a BES, specifically in a flow cell of the circulation loop reactor, was established, the next step was to evaluate the effect of the residence time on the electroenzymatic hydroxylation. This investigation was accomplished by employing different circulation flow rates within the pump's limits, which resulted in varying residence time in both flow cell (τ_{FC}) and enzyme reactor (τ_{ER}).

Electroenzymatic hydroxylation at different residence times was performed at 0.61 mA cm^{-2} because, based on previous results, this current density delivered one of the highest final HEBA concentration and TTN (**Table. S8. 1**), as well as the highest F.E. in this study (**Fig. S8. 3. C**). The tested circulation flow rates were 6 mL min^{-1}, 12 mL min^{-1} and 18 mL min^{-1}, which corresponded to τ_{FC} of 0.28 min, 0.14 min and 0.09 min, and to τ_{ER} of 8.05 min, 4.03 min and 2.68 min, respectively. The results from this investigation are shown in **Fig. S8. 6**. Simultaneously, the corresponding performance indicators are listed in **Table S8. 2**.

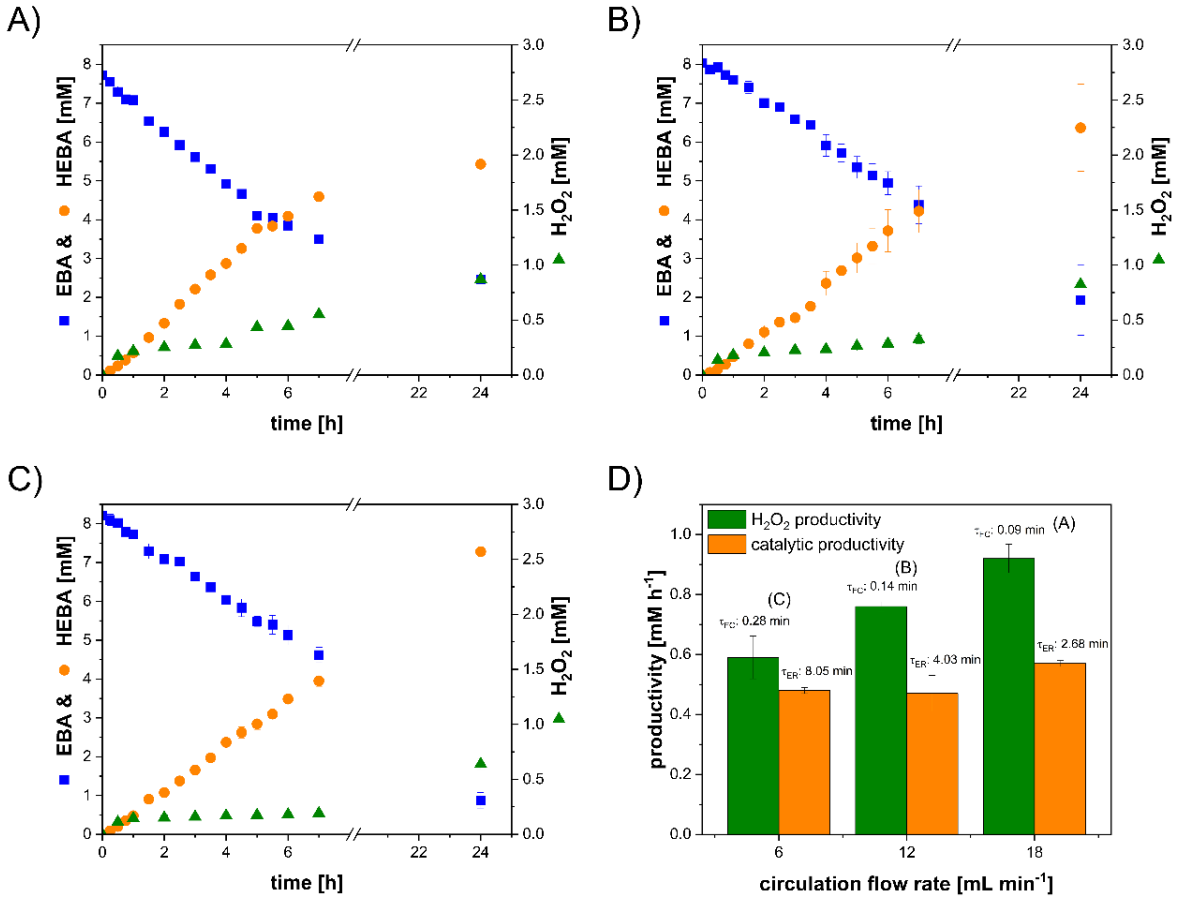

Fig. S8. 6. *Hydroxylation of EBA catalyzed by immobilized rAaeUPO in a circulation loop reactor equipped with the All-in-One electrode for in situ H_2O_2 generation at **A**) a circulation flow rate of 18 mL min^{-1} (resulting τ_{FC}: 0.09 min and τ_{ER}: 2.68 min), **B**) a circulation flow rate of 12 mL min^{-1}(resulting τ_{FC}: 0.14 min and τ_{ER}: 4.03 min) and **C**) a circulation flow rate of 6 mL min^{-1} (resulting τ_{FC}: 0.28 min and τ_{ER}: 8.05 min). **D**) Specific H_2O_2 productivity and catalytic productivity as a function of circulation flow rate (depicted τ_{FC} and τ_{ER} are the corresponding resulting residence time in the flow cell and enzyme reactor based on the set circulation flow rate). Conditions: 50 mL 0.1 M KP$_i$ pH 7, 8 mM EBA, 0.8 g carrier (40 nM rAaeUPO), 1000 rpm, 0.61 mA cm^{-2}, 4 vvm and at 22 ± 1 °C. EBA: 4-ethylbenzoic acid, HEBA: 4-(1-hydroxyethyl)benzoic acid. Duplicates were performed.*

Table S8. 2. *Summary of total turnover number (TTN), turnover frequency (TOF), catalytic productivity and final concentration of HEBA determined from electroenzymatic experiments in the circulation loop reactor equipped with the All-in-One electrode at various residence times, at 0.61 mA cm^{-2}.*

τ_{FC} (τ_{ER}) [min]	Catalytic productivity [mM h^{-1}]	Final HEBA concentration [mM]	TOF [s^{-1}]	TTN [mol mol^{-1}]
0.28 (8.05)	0.48 ± 0.01	7.28 ± 0.05	3.24 ± 0.09	$1.76 \cdot 10^5$ ± 1,213
0.14 (4.03)	0.47 ± 0.06	6.37 ± 1.12	3.14 ± 0.44	$1.54 \cdot 10^5$ ± 27,234
0.09 (2.68)	0.57 ± 0.01	5.43 ± 0.04	3.85 ± 0.04	$1.31 \cdot 10^5$ ± 970

τ_{FC}: resulting residence time in the flow cell. τ_{ER}: resulting residence time in the enzyme reactor. τ_{FC} of 0.28 min, 0.14 min and 0.09 min correspond to circulation flow rates of 6 mL min^{-1}, 12 mL min^{-1} and 18 mL min^{-1}, respectively. τ_{ER} of 8.05 min, 4.03 min and 2.68 min correspond to circulation flow rates of 6 mL min^{-1}, 12 mL min^{-1} and 18 mL min^{-1}, respectively.

As shown in **Fig. S8. 6**, the apparent accumulation of H_2O_2 decreases as the τ_{FC} increases (circulation flow rate decreases). At the highest τ_{FC} tested, 0.28 min (circulation flow rate:

6 mL min^{-1}), the accumulation of H_2O_2 was less than 0.2 mM after 7 h. Consequently, with lower productivity and accumulation of H_2O_2 in the medium, the operational stability of r*Aae*UPO was higher, resulting in higher final HEBA concentration and TTN (**Table S8. 2**). The highest final concentration of HEBA and TTN in this regard were 7.28 ± 0.05 mM and $1.76 \cdot 10^5$ ± 1,213 mol mol^{-1}, respectively. Although a trend was observed for the TOF, with a slight increase as the τ_{FC} decreased, this change was not substantial. The resulting TOF from all the experiments were close to each other, and this can be explained by the fact that the experiments were run at a concentration of H_2O_2 well below its reported K_M value ($K_{M,\ H2O2}$: 0.79 – 1.8 mM [36,40,106]) to make a substantial difference in the catalytic rate. Furthermore, **Fig. S8. 6. D** shows the catalytic productivity and the specific H_2O_2 productivity (in the absence of simultaneous biocatalytic reaction) as a function of the circulation flow rate. Consistent with previous observations (**Fig. S8. 4. C**), H_2O_2 productivity increases with higher circulation flow rates or shorter residence time. This enhancement is attributed to improved oxygen mass transfer rate to the cathode, faster desorption of formed H_2O_2 from the cathode and thinner electrochemical double layer at the cathode interface. Although the catalytic productivity follows a similar trend, it is consistently around 19 – 38% lower than their corresponding H_2O_2 productivity, leading to a H_2O_2 accumulation in the medium over time. This difference indicates that, in this specific system and under selected conditions, the catalytic productivity in the enzyme reactor is the rate limiting step, rather than the H_2O_2 productivity. This contrasts with the BES employing free r*Aae*UPO [118], where the H_2O_2 productivity was the limiting factor. A lower catalytic productivity observed in this study could be explained by two main reasons. First, the application of immobilized r*Aae*UPO likely reduces the enzyme activity compared to free enzymes due to steric hindrance or mass transport limitations of either the substrate EBA or the co-substrate H_2O_2. Second, the resulting τ_{ER} might still be too low, meaning that there was insufficient residence time in the enzyme reactor for the biocatalytic reaction to fully proceed and consumed the formed H_2O_2. To offset the imbalance between the H_2O_2 productivity and the catalytic productivity the τ_{ER} could be increased by increasing the volume of the enzyme reactor while keeping the τ_{FC} constant, applying a lower circulation flow rate (resulting in higher τ_{FC} and τ_{ER}) to further reduce the H_2O_2 productivity, or by increasing the applied enzyme concentration. In summary, these results suggest that applying a low current density in combination with a low circulation flow rate, resulting in high τ_{FC} and τ_{ER}, is beneficial for minimizing H_2O_2 accumulation in the reaction medium and achieving a high TTN. However, it is important to note that this combination also results in relatively low TOF and F.E., primarily due to reduced oxygen mass transfer to the cathode, slower desorption of the generated H_2O_2, and an increased thickness of the electrochemical double layer, as previously discussed.

Under current operating conditions, the TTN of r*Aae*UPO in the hydroxylation of EBA was limited by the initial EBA concentration and the concentration of r*Aae*UPO, which were 8 mM and 40 nM, respectively. To increase the efficiency of the system and the TTN, the experiment could be performed with a higher initial EBA concentration. However, the activity of r*Aae*UPO decreases at an EBA concentration higher than 8 mM due to substrate surplus inhibition (**Fig. S7. 6**). Therefore, the electroenzymatic experiment was conducted under an EBA fed-batch operation mode. By continuously feeding highly concentrated EBA solution (200 mM) into the medium, the concentration of EBA could be maintained well above its K_M value ($K_{M,\,EBA}$: 2.3 mM [106]). This may not only increase the catalytic rate, it may also minimize the catalase malfunction reaction. Given the high concentration of EBA employed in the fed-batch operation mode, the reaction volume increased only by a maximum of 1.7 mL. The increase in reaction volume resulting from the feeding was counterbalanced by the sampling and volume loss due to evaporation caused by sparging, which were subsequently taken into account for the calculation of the concentrations. The results for the electroenzymatic hydroxylation of EBA under the EBA fed-batch operation mode are depicted in **Fig. S8. 7**.

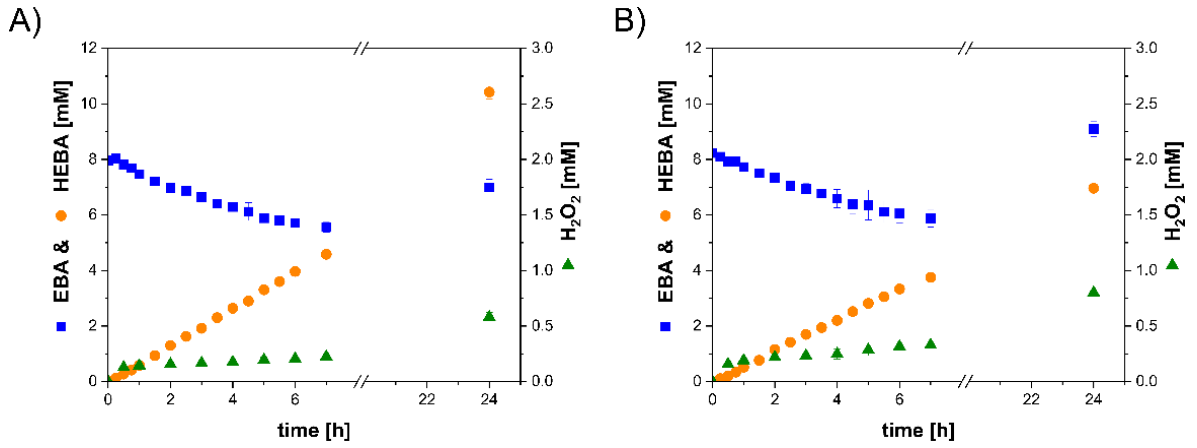

Fig. S8. 7. *Hydroxylation of EBA catalyzed by immobilized rAaeUPO in a circulation loop reactor equipped with the All-in-One electrode for in situ H_2O_2 generation.* ***A****) Fed-batch operation mode with 0.8 g carrier (40 nM rAaeUPO).* ***B****) Fed-batch operation mode with 0.4 g carrier (20 nM rAaeUPO). Conditions: 50 mL 0.1 M KP$_i$ pH 7, 8 mM EBA, 1000 rpm, circulation flow rate: 6 mL min^{-1} (resulting τ_{FC}: 0.28 min and τ_{ER}: 8.05 min), 0.61 mA cm^{-2}, 4 vvm, 200 mM EBA stock solution and at 22 ± 1 °C. EBA: 4-ethylbenzoic acid, HEBA: 4-(1-hydroxyethyl)benzoic acid. Duplicates were performed.*

EBA feeding was started after 90 min of the start of the reaction. To avoid an accumulation of EBA way above 8 mM, the feeding rate was set to 0.008 – 0.016 mmol h^{-1} (0.16 – 0.32 mM h^{-1}), which was lower than the actual catalytic rate determined from previous experiment (**Fig. S8. 6. C**). The fed-batch operation mode was able to maintain the EBA concentration between 6 mM and 9 mM during the whole duration of the experiment. Nevertheless, the EBA concentration was increasing near the end of the experiment because the activity of the enzyme was decreasing and correspondingly, the EBA conversion rate as well. The

continuous supply of substrate EBA increased the catalytic productivity by 20.8%, from 0.48 ± 0.01 mM h^{-1} (**Table S8. 2**) to 0.58 ± 0.02 mM h^{-1} (**Table S8. 3**). At the same time, the final HEBA concentration and the TTN obtained under the fed-batch operation mode were elevated to 10.43 mM ± 0.24 mM and 2.53 · 10^5 ± 5,887 mol mol^{-1}, respectively, in comparison to the batch operation mode. To further enhance the catalyst efficiency, an electroenzymatic experiment was conducted using half of the catalyst loading, corresponding to 0.4 g. This approach was supported by the observation that by adjusting the current density and the residence time, the accumulation of H_2O_2 could be maintained at approximately 0.2 mM (**Fig. S8. 6. C**, **Fig. S8. 7. A**). Thus, despite the reduced catalyst loading, the enzyme stability could be conserved for a longer time.

Table S8. 3. *Summary of total turnover number (TTN), turnover frequency (TOF), catalytic productivity and final concentration of HEBA determined from electroenzymatic experiments in the circulation loop reactor equipped with the All-in-One electrode under fed-batch operation mode, and at various catalyst loading.*

Catalyst loading [g]	Catalytic productivity [mM h^{-1}]	Final HEBA concentration [mM]	TOF [s^{-1}]	TTN [mol mol^{-1}]
0.4	0.51 ± 0.05	6.96 ± 0.01	6.94 ± 0.70	3.38 · 10^5 ± 702
0.8	0.58 ± 0.02	10.43 ± 0.24	3.93 ± 0.15	2.53 · 10^5 ± 5,887

The reduction in the catalyst loading resulted in a 12% decline in catalytic productivity, from 0.58 ± 0.02 mM h^{-1} to 0.51 ± 0.05 mM h^{-1}. As a consequence of the reduced catalyst loading, the H_2O_2 consumption rate decreased, resulting in a higher accumulation of H_2O_2 within the medium, reaching approximately 0.3 mM after 7 h. In addition to the reduced catalyst loading, the higher accumulation of H_2O_2 also led to a faster enzyme deactivation. Accordingly, the final concentration of HEBA was lower, at 6.96 ± 0.01 mM. Nevertheless, the obtained TTN using 50% less catalyst loading was 33% higher, with a value of 3.38 · 10^5 ± 702 mol mol^{-1}. It is possible that a further reduction in catalyst loading may not necessarily increase the TTN substantially. This is because the rate of H_2O_2 production may exceed the rate of enzymatic conversion of H_2O_2, resulting in a higher accumulation.

A TTN value of 3.38 · 10^5 ± 702 mol mol^{-1} is comparable to those reported in the literature from BES using electrochemical generation of H_2O_2 [8,104,106,119], including to the system with the AiO electrode employed in a stirred tank reactor [118], and exceeds the TTN obtained in the system employing manual addition of H_2O_2 [121]. In comparison to a system employing an enzymatic cascade for *in situ* generation of H_2O_2, the TTN achieved here is 28% lower. However, to realize such an enzymatic cascade, five different enzymes, NAD^+ as a cofactor, and methanol as a sacrificial electron donor were required [43]. In terms of the TOF, a TOF of 8.34 ± 0.14 s^{-1} is approximately 14 times lower than the TOF reported in a gas diffusion electrode (GDE) system [106]. This is due to the lower H_2O_2 productivities achieved in this

system in comparison to those observed in GDE-based systems [8,71,104,106]. Nonetheless, both system's productivity and TOF could be enhanced by implementing numbering-up or modular stacking of the flow cell to increase surface to volume ratio, as well as surface modification of the cathode to increase the H_2O_2 selectivity.

11.4.5. Conclusions

The AiO electrode was successfully integrated within an electrochemical flow cell to enable the electrochemical *in situ* generation of H_2O_2. The feasibility of this concept was validated through an electroenzymatic hydroxylation catalyzed by immobilized r*Aae*UPO, utilizing H_2O_2 as the cosubstrate. Electroenzymatic experiments under batch and fed-batch operation modes were performed. The results indicated that within a flow cell, not only do current density, cell potential and aeration rate significantly influence H_2O_2 productivity and its accumulation, but the residence time (flow rate) is also critical. This is because the aforementioned parameters influence the reaction rate of competing reactions, availability of oxygen in the medium, mass transfer of oxygen towards the cathode, desorption of formed H_2O_2 from the cathode and thickness of electrochemical double layer. Moreover, the containment of the carrier within the SpinChem® MagRBR facilitated a simple separation of the biocatalyst from the reaction medium. The study achieved a TTN comparable to the best values reported in the literature within a BES. Within the system, the electrochemical *in situ* generation of H_2O_2 proved to be an effective method for minimizing biocatalyst deactivation by ensuring a controllable supply of H_2O_2 and preventing its excessive accumulation. This implementation demonstrates the potential for flow reactor technology in BES to facilitate alternative scale-up strategies, such as numbering-up or modular stacking. This aspect will be investigated further in a subsequent study, in which the flow cell will be operated continuously, either in a plug flow mode or in a continuous stirred tank reactor mode. Further optimization of the flow cell BES is ongoing, particularly regarding H_2O_2 productivity and Faradaic efficiency (F.E.). Potential enhancements include surface modification approaches, such as coating with carbon nanotubes, surface oxidation and thermal treatment. Additionally, the system's applicability could be broadened by employing industrially relevant model reactions, such as the oxidation of 5-(hydroxymethyl)furfural to 2,5-furandicarboxylic acid. This study demonstrates that the integration of the AiO electrode within flow reactor technology is not only feasible but also offers a promising alternative scalable strategy. It provides a reliable platform for H_2O_2-dependent enzymatic reactions, paving the way for further advancements in the field.

11.4.6. Supporting Information

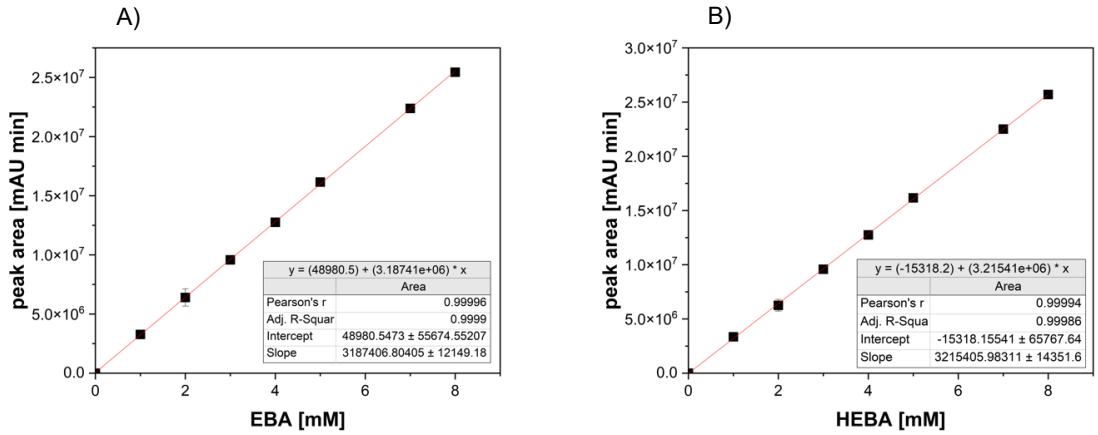

Fig. S8. 8. *Calibration curve of the **A**) substrate 4-ethylbenzoic acid (EBA) and the **B**) product 4-(1-hydroxyethyl)benzoic acid (HEBA) using the described HPLC method.*

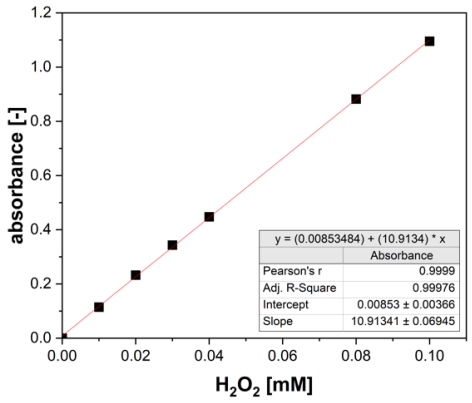

Fig. S8. 9. *Calibration curve of hydrogen peroxide (H_2O_2) using the described colorimetric assay.*

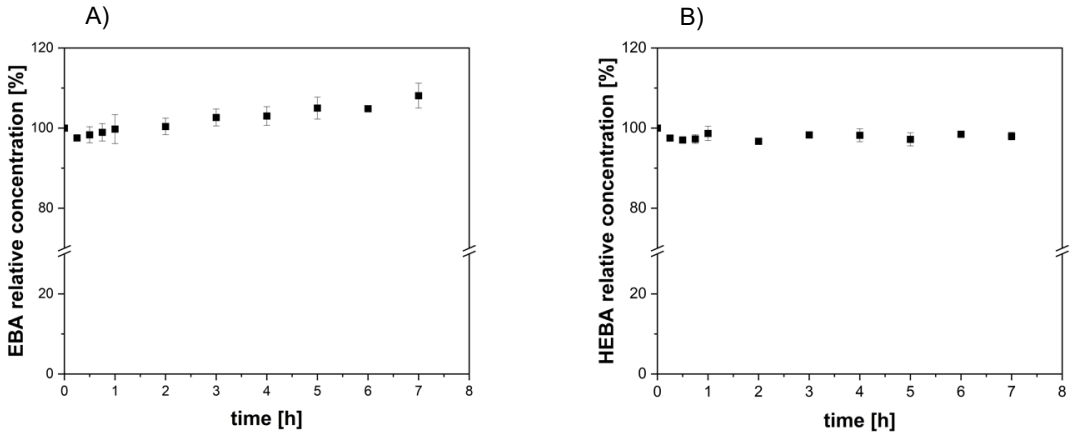

Fig. S8. 10. *Adsorption test of the substrate 4-ethylbenzoic acid (EBA) and the product 4-(1-hydroxyethyl)benzoic acid (HEBA) on the material surface (electrode, tubing and polyether ether ketone surface) in a circulation loop reactor. Shown are the relative concentrations of* ***A****) EBA and* ***B****) HEBA as a function of the incubation time. Conditions: 8 mM EBA or HEBA in 50 mL 0.1 M KP$_i$ pH 7, 1000 rpm, circulation flow rate: 24 mL min^{-1} (resulting τ_{FC}: 0.07 and τ_{ER}: 2.01 min), at 22 ± 1 °C. EBA or HEBA solution was circulated through the flow cell and the enzyme reactor under the aforementioned conditions.*

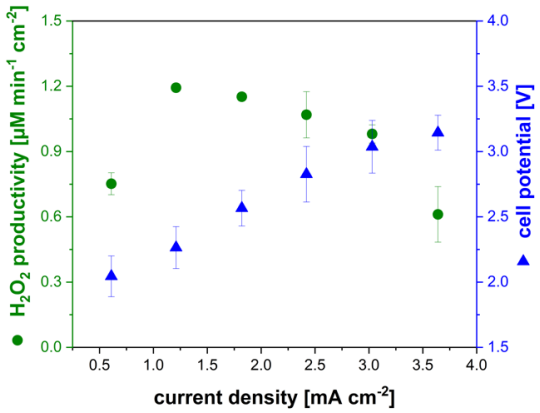

Fig. S8. 11. *Specific H_2O_2 productivity and the resulting cell potential as a function of current density. Conditions: carbon felt working electrode (8.3 cm^2), platinized titanium counter electrode (4.24 cm^2), 50 mL 0.1 M KP$_i$ pH 7, at 22 ± 1 °C, 1000 rpm, circulation flow rate: 24 mL min^{-1} (resulting τ_{FC}: 0.07 and τ_{ER}: 2.01 min) and 12 vvm. Biological duplicates were performed.*

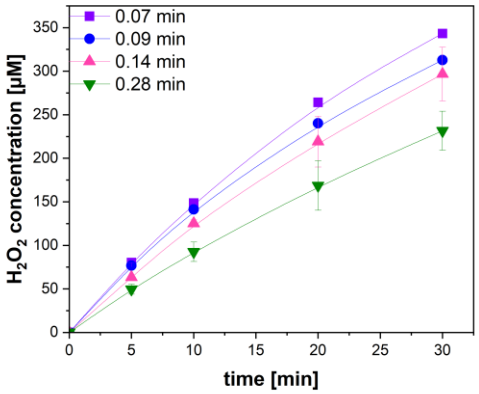

Fig. S8. 12. *H_2O_2 concentration as a function of time at different residence times in the flow cell (τ_{FC}). τ_{FC} of 0.28, 0.14, 0.09 and 0.07 min correspond to circulation flow rates of 6, 12, 18 and 24 mL min^{-1}, respectively. Conditions: carbon felt working electrode (8.3 cm^2), platinized titanium counter electrode (4.24 cm^2), 50 mL 0.1 M KP$_i$ pH 7, 0.61 mA cm^{-2}, at 22 ± 1 °C, 1000 rpm and 4 vvm. Biological duplicates were performed.*

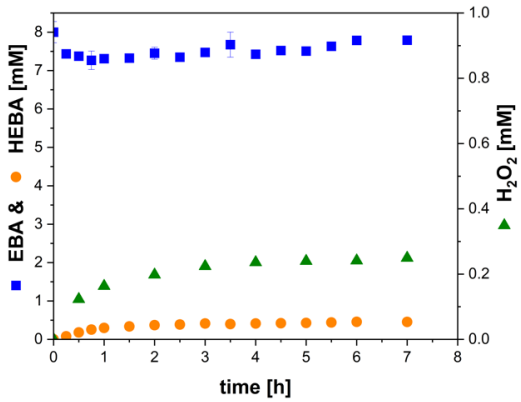

Fig. S8. 13. *Hydroxylation of 4-ethylbenzoic acid (EBA) to 4-(1-hydroxyethyl)benzoic acid (HEBA) catalyzed by the immobilized unspecific peroxygenase from Agrocybe aegerita (rAaeUPO) in a circulation loop reactor equipped with the All-in-One (AiO) electrode for in situ hydrogen peroxide (H_2O_2) generation at 0.61 mA cm^{-2}. Enzyme immobilization: carbon felt electrode (8.3 cm^2) was incubated in a 0.1 M KP$_i$ pH 7 solution containing 1.1 U_{ABTS} mL^{-1} rAaeUPO in a falcon tube, and placed on an overhead shaker at 4 °C for 16 h. The rAaeUPO activity in the supernatant after the immobilization was 0.75 U_{ABTS} mL^{-1} and in the wash fraction was 0.004 U_{ABTS} mL^{-1}. Conditions: 50 mL 0.1 M KP$_i$ pH 7, 8 mM EBA, 0.61 mA cm^{-2}, 4 vvm, 1000 rpm, circulation flow rate: 24 mL min^{-1} (resulting τ_{FC}: 0.07 and τ_{ER}: 2.01 min), at 22 ± 1 °C.*

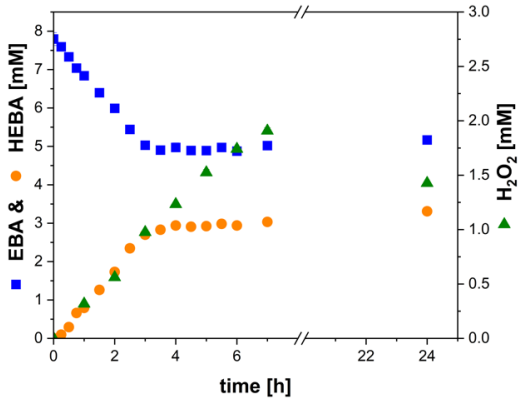

Fig. S8. 14. *Hydroxylation of 4-ethylbenzoic acid (EBA) to 4-(1-hydroxyethyl)benzoic acid (HEBA) catalyzed by the immobilized unspecific peroxygenase from Agrocybe aegerita (rAaeUPO) in a circulation loop reactor equipped with the All-in-One (AiO) electrode for in situ hydrogen peroxide (H_2O_2) generation at 1.21 mA cm^{-2}. The rAaeUPO was covalently immobilized on epoxy resins and contained inside a SpinChem® MagRBR. Conditions: 50 mL 0.1 M KP_i pH 7, 8 mM EBA, 1.21 mA cm^{-2}, 0.4 g carrier (20 nM, 1.4 U_{ABTS} g^{-1}$_{carrier}$), 1000 rpm, circulation flow rate: 24 mL min^{-1} (resulting τ_{FC}: 0.07 and τ_{ER}: 2.01 min), at 22 ± 1 °C.*

Table S8. 4. *Summary of the activity measurement of rAaeUPO in the supernatant before and after the immobilization process, including the washing steps.*

Purolite Lifetech ECR 8285				
Before immobilization [U_{ABTS} mL^{-1}]	After immobilization [U_{ABTS} mL^{-1}]	1st wash [U_{ABTS} mL^{-1}]	2nd wash [U_{ABTS} mL^{-1}]	3rd wash [U_{ABTS} mL^{-1}]
20 ± 1	0.004 ± 0.002	0.86 ± 0.29	1.38 ± 0.042	0.71 ± 0.02
Immobilization yield of 85.2%				

Determination of Reynolds (*Re*) number

$$Re = \frac{d \cdot D \cdot v}{\mu} \quad \textbf{(S8.13)}$$

With:

d: density of water (1000 kg m^{-3})

D: pipe diameter (inner diameter of separator, 6 mm)

μ: dynamic viscosity of water (0.001002 Pa·s)

v: flow velocity (0.024 L min^{-1} = 0.01415 m s^{-1}, 0.006 L min^{-1} = 0.00354 m s^{-1})

$$Re\ (0.024\ \frac{L}{min}) = \frac{1000\frac{kg}{m^3} \cdot 6{\cdot}10^{-3} m \cdot 0.01415\frac{m}{s}}{0.001002\ Pa{\cdot}s} = 84.73 \quad \textbf{(S8.14)}$$

$$Re\ (0.006\ \frac{L}{min}) = \frac{1000\frac{kg}{m^3} \cdot 6{\cdot}10^{-3} m \cdot 0.00354\frac{m}{s}}{0.001002\ Pa{\cdot}s} = 21.19 \quad \textbf{(S8.15)}$$